The Dissertation Committee for Pinaki Ghosh Certifies that this is the approved version of the following dissertation:

Effective Mobility Control Mechanisms for EOR processes in Challenging Carbonate Reservoirs

Committee:

Kishore K. Mohanty, Supervisor

David DiCarlo

Kamy Sepehrnoori

Keith P. Johnston

Charles Werth

Effective Mobility Control Mechanisms for EOR processes in Challenging Carbonate Reservoirs

by

Pinaki Ghosh

Dissertation

Presented to the Faculty of the Graduate School of

The University of Texas at Austin

in Partial Fulfillment

of the Requirements

for the Degree of

Doctor of Philosophy

The University of Texas at Austin

May 2019

Dedication

To my loving and supportive parents and my loving sister who all have been part of this amazing journey

Acknowledgements

I would like to acknowledge and express my deepest gratitude to Dr. Kishore Mohanty for his constant support and guidance throughout my research. I am grateful to him for giving me the freedom to explore diverse research areas and expand my knowledge in EOR processes. I appreciate his sincerity, humbleness and compassion for others. I would also like to extend my sincerest thanks to Dr. Gary Pope for his guidance and valuable input on my research work. My dissertation committee members Dr. David DiCarlo, Dr. Charles Werth and Dr. Keith P. Johnston also have offered patient guidance, and their inputs and comments have made this dissertation better.

It was an honor to work with Dr. Upali Weerasooriya on the new surfactant development technology at CPGE. His energy and enthusiasm in surfactant chemistry have always been a motivation for me. I am grateful to him for all the discussions and knowledge on surfactant chemistry. I appreciate his support in providing recommendations for my summer internship jobs during my PhD program at UT Austin.

My deepest appreciation for my family who have always encouraged me to pursue my dreams and aspirations. I am thankful to my parents for always being supportive of my decisions and their relentless prayers and sacrifices for my well-being. I am also thankful to my amazing sister, Gargi for her constant encouragement and support in my journey as a graduate student. I am thankful to my brother-in-law, Sujan for his support and help especially during my surgery time that helped me recover fast and get back on my feet. I

believe without the help of my sister and brother-in-law the recovery process could have been very difficult. I thank God for blessing me with such a wonderful and loving family.

My special thanks to Jith Liyanage and Eric Dao for all the help and knowledge with my experimental work, Nadeeka Upamali for helping with phase behavior and surfactant synthesis, and other current and previous research staff in the lab including Leonard Chang, Jonathan Drivers, Himanshu Sharma, Shashvat Doorwar, Krishna Panthi, Chammi Miller, Haofeng Song, Lauren Churchwell and Bahar Koparal. I would also like to thank my undergraduate research assistants Angel Zepada and Gildardo Bernal for their hard work and dedication along the way that guaranteed me to finish the work on time. I also would like to thank the Stephane Jouenne from Total E&P for his support and guidance in the collaborative work on my research work. Many thanks to my colleagues Chris Britton, Stephanie Adkins, Pearson Suniga, Eric Trine, and Dan Glushko from Ultimate EOR Services and Heesong Koh, Soma Chakraborty, Christabel Tomla and Lirio Quintero from Baker Hughes for their valuable guidance during my internships.

I thank Barbara Messmore for managing our research group and her administrative support and providing me the necessary assistance when required. I want to thank the UT PGE staff members for their help, especially Daryl Nagard, Glen Baum and Gary Miscoe for assisting me with experimental setups and Amy Stewart for assisting me with all the administrative process.

Finally, I would like to acknowledge the funding sources that supported me financially throughout my Ph.D. at the University of Texas at Austin. These include the John and Kelli Weinzierl Endowed Presidenial Fellowship (2017 & 2018).

Abstract

Effective Mobility Control Mechanisms for EOR processes in Challenging Carbonate Reservoirs

Pinaki Ghosh, PhD

The University of Texas at Austin, 2019

Supervisor: Kishore K Mohanty

Mobility control mechanisms are key to the success of any enhanced oil recovery processes due to their ability to provide favorable mobility ratio of the injected fluids, thus improving the sweep efficiency during the process. This work is focused on developing effective mobility control mechanisms in challenging carbonate reservoirs that are typically high temperature and high salinity and low permeability formations. The first half of the dissertation is focused on investigating novel foam technology using anionic and cationic surfactants to improve the gas enhanced oil recovery process. Typically, gas injection processes suffer from poor volumetric sweep efficiency due to viscous fingering, channeling, and gravity override. Foam helps to improve the sweep efficiency of the gas floods significantly by reducing the mobility of the gas by orders of magnitude, blocking

the high permeability channels and diverting fluids to the bypassed lower permeability channels.

Carbonate reservoirs, which are typically oil-wet heterogeneous and low permeability, pose additional challenges for an effective foam EOR process. Crude oils destabilize foam rapidly and the thin oil film on oil-wet rock surfaces makes in-situ foam generation difficult as well. Hence, wettability alteration from oil-wet to water-wet using a surfactant was one of the necessary mechanisms for in-situ foam stability. Low permeability of the carbonates makes strong foam generation challenging due to higher entry capillary pressure in small pore throats that exceeds the critical capillary pressures usually. On the other hand, low interfacial tensions (IFT) of the surfactant formulations helps to lower the entry pressure and stabilize the foam better. This work demonstrated the benefits of two different chemical systems – one that includes use of anionic surfactants for low IFT formulations and the other that includes blends of cationic, non-ionic and zwitterionic surfactants for non low IFT formulations in combination with wettability alteration and foaming to improve oil recovery in oil-wet carbonates after a secondary gas flood process.

The second half of the dissertation is focused on developing a novel polymer treatment protocol for successful injection in low permeability carbonate reservoirs through mechanical shear degradation and aggressive filtration tests. The behavior of shear degradation of high molecular weight polymers of different chemistry in varying brine salinities performed with a laboratory blender at a constant speed and varying shearing times followed an exponential decay until a steady state was obtained. Master curves for

degraded viscosity predictions were developed to estimate the degraded viscosity of any given polymer in any brine salinity at any given shearing time, given the shearing speed was kept constant. A superimposed master curve for the degradation for all kinds of polymers investigated was established to predict the rate of degradation at any given time. A robust approach of comparison of polymer size distribution from dynamic light scattering (DLS) method and pore throat distribution from mercury injection capillary pressure (MICP) was established for injection qualification of high molecular weight polymers in low permeability carbonates.

A novel class of hydrophobically modified acrylamides, also known as associative polymers, were investigated as an alternative to conventional HPAMs and synthetic polymers for injection in low permeability carbonates. The thermo-thickening properties of the associative polymers at elevated temperatures and salinities (with high divalent ions) and higher resistance to shear degradation makes them promising for carbonate reservoirs in comparison to HPAMs, where high polymer dosages are required due to significant viscosity loss in shear degradation. The apparent high viscosities generated from high resistance factors during flow in porous media for associative polymers can be advantageous for optimization of polymer dosage in chemical EOR processes. This work demonstrated a significant potential for application of associative polymers as an effective mobility control agent in carbonate reservoirs, especially in low permeability formations.

The novel polymer treatment method for low permeability reservoirs was combined with the development of alkaline-surfactant-polymer (ASP) and surfactant-polymer (SP) technology for improvement of oil recovery in carbonates. The successful polymer

transport in low permeability carbonates showed great potential for application of chemical EOR processes like ASP and SP in tight formations. Development of robust SP technology for high temperature and high salinity reservoirs also showed promising results in phase behavior experiments and coreflood experiments. This work demonstrated the benefits of SP technology with optimization of surfactant formulation and coreflood design for lower surfactant retention and higher oil recovery, thus making the process economical.

Table of Contents

Tables

List of Figures

Chapter 1: Introduction

The first chapter of this thesis discusses the motivation for application of enhanced oil recovery techniques in carbonate reservoirs and the potential challenges in secondary injection processes like waterflood and gasflood. It also emphasizes the importance of foam and polymer injection as a mobility control mechanism, coupled with reduction of interfacial tension in presence of surfactants, in carbonate reservoirs which leads to incremental oil recovery. Finally, it provides the working principle for this research along with the research objectives of this thesis and an overview of the remaining chapters.

1.1 MOTIVATION FOR APPLICATION OF EOR IN CARBONATES

More than 60% of the oil reserves and 40% of the gas reserves worldwide are estimated to be in carbonate reservoirs (Schlumberger Market Analysis, 2007). **Figure 1.1** shows a map of distribution of carbonate reservoirs across the world. Typically, most of these carbonate oil reservoirs are believed to be oil-wet or mixed-wet and highly heterogeneous compared to sandstones which are predominantly water-wet. Many carbonate reservoirs have low permeability (about 10 mD) and most are naturally fractured. The oil-wettability originates from negatively charged carboxylic ions in the oil adhering to the carbonate mineral surface which has a positive zeta potential (Seethepalli et al, 2004). Carbonate rocks typically have a complex pore structure and the heterogeneity exists in all scales- in the pores, in the grains, and in the textures. The average recovery factor (the ratio of recoverable oil to the volume of oil originally in place) during secondary processes in carbonate reservoirs is low (typically <35%) due to heterogeneity and complexity in the

pore structure (Schlumberger, 2007). Additionally, in some reservoirs due to heterogeneity and natural fractures, water-flooding has been reported to have recovery factors as low as 10% (Montaron, 2006). This unrecovered oil is classified as either “remaining” or “residual” oil. The remaining oil after secondary recovery processes is either residual oil trapped in the swept portion of the reservoir or oil bypassed in the unswept portions of the reservoir. Hence the target oil reserves for enhanced oil recovery process in carbonates are significant. These oil reserves increase with increasing heterogeneity and mobility ratio between the displacing (water/gas) and displaced (oil) fluids.

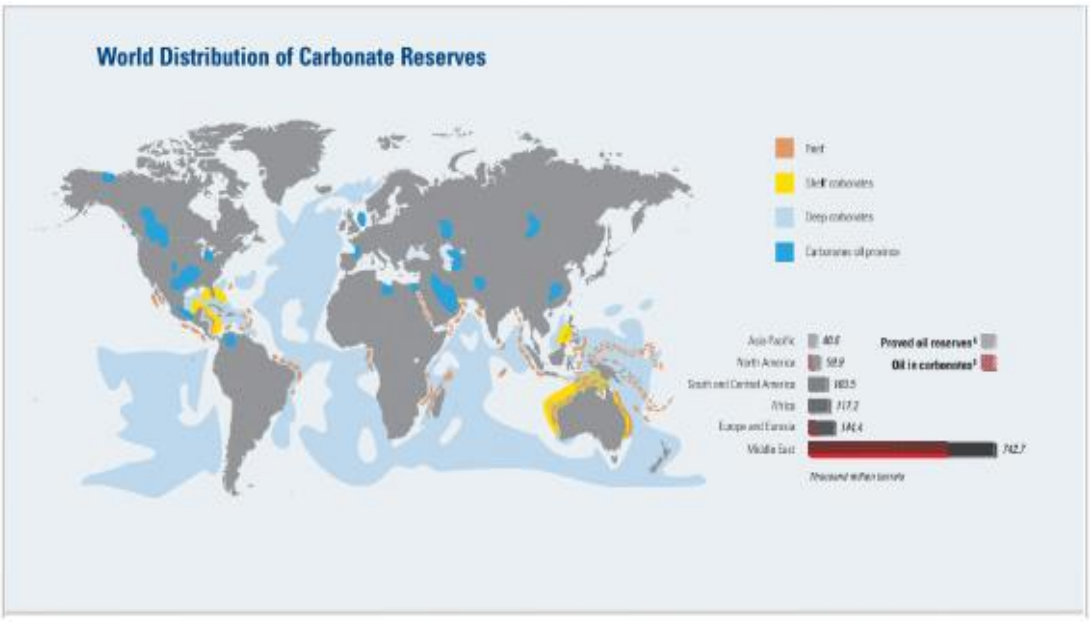

Figure 1.1. World distribution of carbonate reservoirs (Schlumberger Market Analysis, 2007)

Water injection is a proven secondary recovery process applied to both sandstone and carbonate reservoirs. This method is very effective in light to medium gravity crude oils since it is easy to inject into oil-bearing formations, cheap, readily available, requires

lower capital investment and operating cost. Hence, water flood is an economical method to increase oil production. But for reservoirs with high heterogeneity and natural fractures, water flood can be challenging due to early breakthrough and channeling. The importance of sweep efficiency cannot be understated in oil recovery.

Gas injection is a proven enhanced oil recovery method, especially for light oil reservoirs and significantly improves the displacement efficiency and reduces the residual oil saturation, especially under miscible reservoir conditions. For immiscible operating conditions, the main challenge for gas injection EOR processes is to improve the sweep efficiency, mainly for heterogeneous reservoirs, hence the need for mobility control.

1.2 POTENTIAL CHALLENGES IN WATER INJECTION PROCESSES

The typical recovery during waterflood processes can vary between 40 to 50% original oil in place for sandstones, and lower for carbonate reservoirs (Satter et al., 2008). Hence, a significant amount of oil is left unrecovered in these reservoirs. Most of these carbonate reservoirs are oil-wet and contain natural fractures. Waterflooding can be inefficient in recovery because the capillary pressure curve is predominantly negative, and heterogeneity (and the connected fractures) lead to early breakthrough and low recoveries. This requires the use of mobility control mechanism to improve the sweep efficiency of these heterogeneous carbonate reservoirs and wettability alteration mechanism to alter the wettability of the rock surface from oil-wet to water-wet and convert the capillary pressure curve towards more positive, thus increasing oil recovery.

1.3 POTENTIAL CHALLENGES IN GAS INJECTION PROCESSES

Gas injection is a proven technology for improved oil recovery (Stalkup, SPE Monograph, ~1984), but the potential challenges for application in carbonate reservoirs are - viscous instability, channeling, and gravity override. Viscous instability is the result of the differences in viscosity of the displacing fluid (gas) and the displaced fluid (oil and water). Channeling is due to the heterogeneity where flow through higher permeable regions only results in bypassing of a significant amount of oil in the lower permeable regions. Gravity override is caused by the density difference between gas and the displaced fluid (oil and water) which leads to the segregation of gas to the upper part of reservoirs. These challenges contribute to a poor sweep efficiency of the displacing fluid leaving behind a significant amount of remaining oil and results in lower oil recovery, as shown in **Figure 1.2**. Mobility control is needed to improve sweep efficiency of the carbonate reservoirs to achieve higher oil recovery.

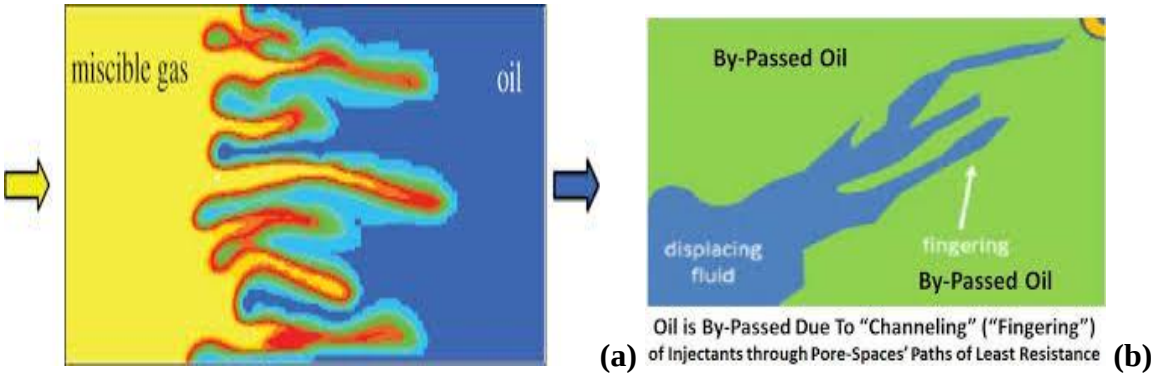

(a) **(b)**

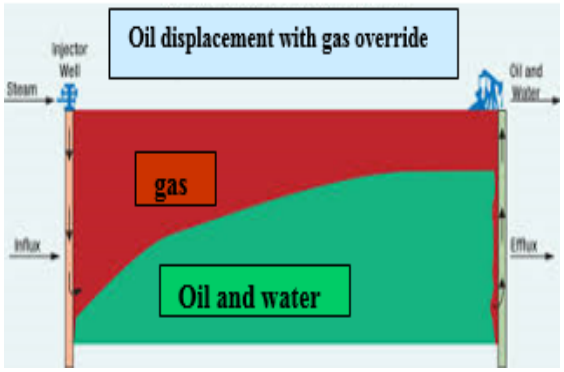

(c)

Figure 1.2. Potential Challenges in Gas Injection: (a) Viscous instability (b) Fingering (c) Gravity Override

1.4 MOTIVATION FOR APPLICATION OF POLYMERS IN CARBONATES

Polymers are the most common mobility control agents used in the oil industry (Abidin et al., 2012; Jennings et al., 1971; Gogarty, 1967). Addition of polymer to the injected water increases its viscosity which leads to enhanced mobility control and stability, thus reducing the viscous fingering and diverting the displacing fluid to previously bypassed regions in the reservoir during a waterflood. This leads to a significant improvement in the sweep efficiency of the process. **Figure 1.3** shows how a decrease in mobility ratio can improve the areal sweep efficiency during a typical polymer flood.

Polymer floods are often not employed in carbonate rocks due to poor injectivity. Poor injectivity might be a result of incompatibility between the injection brine and the polymer, incompatibility between the formation brine and the polymer, low permeability, and due to contamination in the surface facilities (Caenn et al, 1989). Hence literature studies have recommended that for successful polymer injection it is necessary to have reservoirs with a permeability of at least 50 mD (Lyons and Plisga, 2011), whereas most of the carbonate tend to have permeabilities lower than 50 mD. In addition, carbonate reservoirs often contain hard brine which reduces polymer viscosity and increases adsorption. Also, the wide distribution of pore throat sizes in carbonate reservoirs makes it challenging for the large sized polymer molecules to transport easily. The small pore throats can lead to plugging and bypassing of a significant amount of oil in the reservoir, leading to lower oil recovery. Typically, most of the carbonate reservoirs have high temperature and high salinity which negatively affects the stability of the polymers. Conventional HPAM molecules would be unsuitable for application under these conditions due to hydrolysis and precipitation in presence of divalent ions in the brine.

Biopolymers (e.g., Scleroglucan and Schizophyllan) and recently developed specialty synthetic polymers for high temperature and high salinity reservoirs seem to have potential for application in polymer flooding for carbonate reservoirs. Recent studies have shown great potential application of Scleroglucan polymer as an alternative to synthetic polymers in higher permeability carbonate reservoirs with extreme high salinity (Jensen et al., 2018; Shoaib and Quadri, 2016), and studies are ongoing on modification of the polymer molecule to be able to inject in lower permeability formations. Novel methods of

mechanical shearing and aggressive filtration technique have also shown promising future for application of polymer flooding in lower permeability carbonate formations, where polymer molecular size distribution can be tailor designed to achieve successful transport in porous media (Ghosh et al., 2018). An alternative technology of using hydrophobically modified water-soluble polymers, also known as associative polymers, have shown great potential as a mobility control agent in moderate temperatures below 70 ^{o}C but at very high salinity brines (Wang et al., 1999; Seright et al., 2011; Kang et al., 2017). The high resistance factors generated with the use of associative polymers can provide more economical solution for polymer EOR processes. Hence, these breakthroughs in research of enhanced oil recovery techniques have enabled promising future of polymer injection in carbonate reservoirs, but more work and better understanding of the novel polymers are required for development of robust polymer technology targeted for challenging carbonate reservoirs.

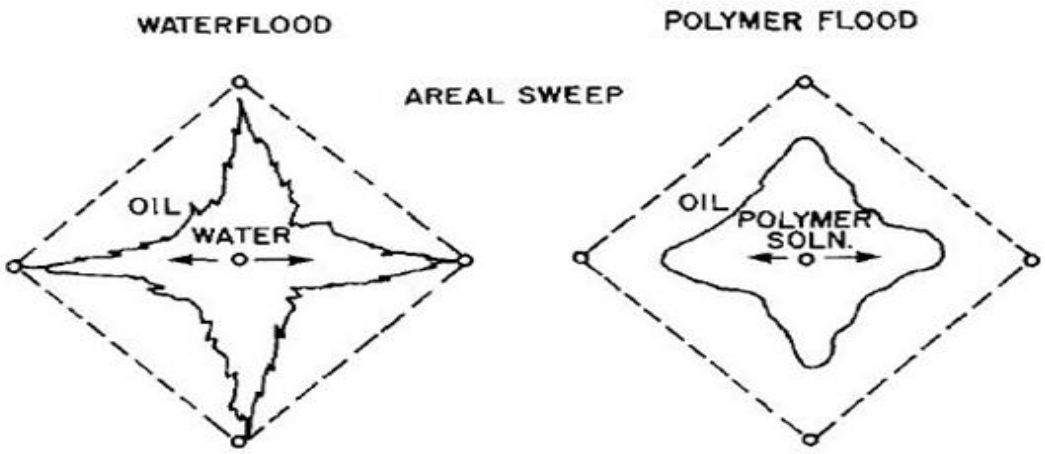

Figure 1.3. Areal sweep schematic of a polymer flood for mobility control (Caenn et al, 1989).

1.5 MOTIVATION FOR APPLICATION OF FOAM IN CARBONATE RESERVOIRS

The challenges for gas injection processes have been long recognized and the possible solutions, such as water alternating gas (WAG) injection and simultaneous injection of water and gas (SWAG), are beneficial for relatively homogeneous reservoirs (Surguchev et. al., 1996). For heterogeneous carbonate reservoirs, a better mobility control mechanism and conformance control through the formation of foam can be helpful. Foam greatly reduces gas mobility, the reduction increases with increasing permeability, thereby mitigating the disadvantages of reservoir heterogeneity, low gas viscosity and low gas density (ref). Foams are also used to divert acid flow in matrix well stimulation treatments (Gdanski, 1993) and to divert liquid or gas flow in environmental remediation processes (Hirasaki and Miller, 1997). The chemicals used to generate foam are used in low concentrations and are relatively inexpensive. The shear thinning nature of foam provides good injectivity near injection wellbore and leads to more effective mobility control in far-wellbore regions at lower shear rates. There are two modes of foam injection - continuous co-injection of gas and liquid (containing surface active agents) or injection of alternating slugs of liquid and gas. **Figure 1.4** shows schematic description how foam flooding helps to address the challenges of gas injection and increases the sweep efficiency in three scenarios: gravity override, viscous fingering, and channeling through high permeability zones. Foam technology also shows promising potential in conformance control for heterogeneous systems (Wassmuth et al., 2005; Haugen et al., 2014; Srivastava et al., 2010; Li et al., 2011).

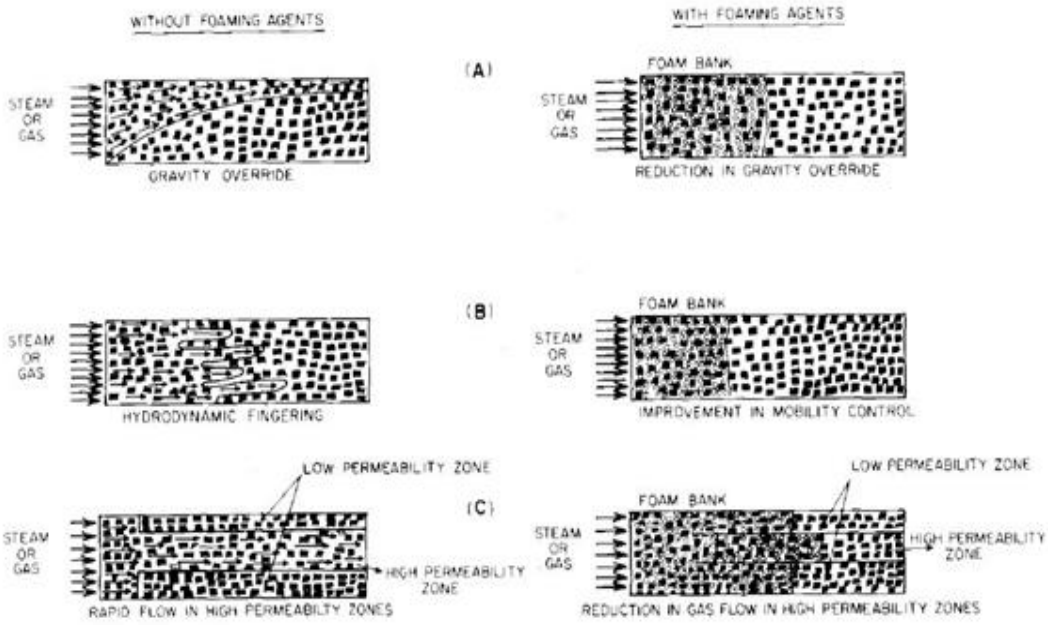

Figure 1.4. Schematic of possible effects of foam on gas transport in porous media (Sharma and Shah, 1989).

Literature studies have reported that the best foam process to reduce gravity override is the injection of a large slug of surfactant followed by a large slug of gas, described as surfactant alternating gas (SAG) process, injected at a constant, maximum-allowable injection pressure (Faisal, 2009; Kloet, 2009; Xu and Rossen, 2004). The injection rate is adjusted to maintain this maximum allowable injection pressure in this process. The injection rate to maintain the maximum pressure was found to be nearly constant for a strong foam and increasing with time for a weaker foam regime (Boeije and Rossen, 2013). Some researchers have reported that multiple-slug processes result in extremely poor injectivity of surfactant slugs near injection well whereas, others have suggested that injection of small multiple-slugs can lead to higher oil recovery and higher pressure drop in porous media (Lawson and Reisberg, 1980). In addition, foam injection

shows promising potential for application in high salinity (containing significant number of divalent ions) and high temperature carbonates due to its high thermal stability. Foam injection also does not suffer severe injectivity issues in low permeability reservoirs which is an advantage over the use of polymers for carbonate reservoirs. Use of engineered nanoparticles and amphoteric foaming agents are one of the several ways to stabilize foams at harsh conditions of high salinity and high temperature present in carbonate reservoirs for a longer period (Zhang, 2011; Fuseni et al., 2014; Singh and Mohanty, 2014).

1.6 WORKING PRINCIPLE

The challenges for application of any enhanced oil recovery methods in carbonate reservoirs are: oil-wetness, natural fractures and wide variation in permeability in combination with extreme high salinity and high concentrations of divalent ions. The oil-wetness and the mixed-wetness of the carbonate reservoirs can be altered using wettability altering surfactant solutions. The severity of heterogeneity of the carbonate reservoirs can be reduced using mobility control agents like foam and polymer to divert the injected fluids into the lower permeable regions and improve the sweep efficiency. In addition, temperature and salinity tolerant surfactants that help to provide low interfacial tension (IFT) formulation can improve oil recovery through reduction of capillary forces. Hence the working principle is the incorporation of the synergistic effect of surface-active agents with low IFT and wettability alteration capability along with mobility control mechanisms like foam and polymer injection.

1.7 RESEARCH OBJECTIVES

The goal of this research was to explore novel methods to improve the oil recovery in challenging carbonate reservoirs, i.e., in high temperature and high salinity reservoirs with wide variation in permeability, especially in tight carbonates. First, systematic study was performed to investigate the best performing surfactant formulations under different reservoir conditions targeting low IFT and wettability alteration capabilities. Second, different mobility control mechanisms through the injection of polymer and foam were studied in detail. The purpose of this research was to push the limits of enhanced oil recovery techniques in heterogeneous carbonate reservoirs through novel polymer pretreatment processes and specialty chemicals that can significantly improve the potential of polymer injection and investigate the lower permeability constraints for foam injection to obtain favorable mobility control in oil-wet porous media.

The first part of the research was to investigate the mechanisms of improving incremental oil recovery in low permeability oil-wet carbonate rocks through generation of foam – in combination with low IFT and wettability altering anionic surfactant formulation. The purpose was to inject alternating surfactant-gas slugs to create in-situ foam that reduces the relative permeability of gas and mobility ratio and diverts the fluids to bypassed regions in the reservoir. The experiments were performed to replicate matured carbonate reservoirs that have been gas flooded for about 30 years and have a large gas cap on the top. Henceforth, tertiary recovery processes were performed using foam to further increase the oil recovery after gas injection in these mature carbonate reservoirs. Another novel technique was developed to incorporate the synergistic effect of wettability alteration

and foaming using cationic surfactants to improve the sweep efficiency in oil-wet carbonates and increase the oil recovery. Aqueous stability, phase behavior experiments, wettability alteration (contact angle and spontaneous imbibition experiments) and bulk foam tests were performed to screen the surfactant solutions for this study. Single phase foam experiments (with no crude oil) were performed with varying foam quality and foam injection velocity in outcrop Texas Cream limestones to determine the foam strength in the porous medium and determine the optimum foam injection parameters. The efficiency of incremental oil production, after secondary gas injection processes, was investigated in each of these experiments with anionic and cationic surfactants developed for foam EOR processes.

The second part of the research was focused on investigating the application of polymer as mobility control in combination with ultra-low IFT surfactant formulations for challenging carbonate reservoirs – low permeability formations and high temperature and high salinity reservoirs. A novel method was developed to mechanically shear degrade the high molecular weight polymers and tailor the molecular weight distribution for successful injection in low permeability formations depending on the pore throat distribution of the porous medium. Systematic study was performed to study the impact of variable shear degradation in combination with aggressive filtration through smaller filter papers on reduction of polymer molecular size distribution (based on dynamic light scattering method). The polymer size was compared with the pore throat distribution obtained from mercury injection capillary pressure (MICP). Alternatively, associative polymers were also investigated for application in low permeability carbonate reservoirs with moderate

temperatures and high salinity as a mobility control agent. The high resistance factors generated at low concentrations with associative polymers showed great potential for economic EOR processes compared to shear degraded polymers. Experiments were also performed to develop the application of surfactant-polymer (SP) technology for high salinity reservoirs containing high concentrations of divalent ions. Specialty synthetic polymers were investigated to understand the surfactant brine compatibility under these harsh reservoir conditions.

1.8 DESCRIPTION OF CHAPTERS

The second chapter provides a literature review on the theories of mobility control mechanisms like foam generation and coalescence, and polymer injection. The literature review emphasizes the importance of mobility control in heterogeneous carbonate reservoirs to improve the sweep efficiency and increase the oil production through EOR processes. Also, this chapter provides background information on cationic and anionic surfactant properties, specialty synthetic polymers and associative polymers that have promising potential for EOR application in carbonates.

The third chapter discusses the materials, equipment and methodology used to perform the screening tests in selection and development of an optimum chemical formulation for a suitable EOR process. For foam injection and polymer injection processes, the screening criteria vary significantly and have been outlined in this chapter to provide a detailed understanding of the steps and processes performed in developing the EOR technology for application in carbonate reservoirs.

The fourth chapter is the introduction of the results for one of the EOR technology developed using foam injection in low permeability oil-wet carbonate formations. This chapter includes detailed investigation of the performance of low IFT, wettability alteration and foaming surfactants using anionic surfactants in improving incremental oil production over a secondary gas injection process. The chapter also includes comparative study on the performance of a good foaming agent with no wettability alteration in oil-wet carbonates.

The fifth chapter discusses the use of novel cationic surfactants to explore the synergistic effect of wettability alteration and foaming ability to improve oil recovery in oil-wet low permeability carbonate reservoirs. It emphasizes the benefits of blending cationic and zwitterionic surfactants in improving the foam strength and compatibility with formation brine containing significant number of divalent ions. The better compatibility of cationic surfactants with high salinity brine containing significant number of divalent ions in comparison to anionic surfactants was one of the key motivations for this study.

The sixth chapter introduces the novel technique of polymer pretreatment using mechanical shear degradation of high molecular weight polymers to tailor the molecular weight distribution for successful injection in low permeability formations. This chapter provides detailed insight into the novel approach developed for polymer processing to successfully extend polymer (P), alkali-surfactant-polymer (ASP) and surfactant-polymer (SP) processes to these challenging formations. This study was also extended to different polymer molecules (with different polymer chemistry) to enhance future polymer EOR technology for challenging reservoir conditions.

The seventh chapter discusses the application of novel associative polymers as a mobility control agent in low permeability carbonate reservoirs. This study was emphasized to understand the polymer rheology of associative polymers with varying molecular weight and hydrophobicity at moderate temperature (60 ^{o}C) and high salinity. The high resistance factors generated with low concentrations of polymer showed great potential for economical polymer EOR application in challenging carbonates compared to shear degraded polymer where huge viscosity loss was observed.

The eighth chapter discusses the application of ASP process for a low permeability carbonate formation. This scope of work includes the application of the novel polymer technology developed in Chapter 6 for incremental oil production. It also includes the surfactant and polymer compatibility with formation brine and the effect of use of a chelating agent for preventing any precipitation in presence of alkali. In addition, a simpler SP process was developed under similar reservoir conditions to perform a comparative study on the performance of ASP and SP processes.

The nineth chapter discusses the application of SP processes for challenging carbonate reservoirs – high salinity and high temperature conditions. This study provides detailed information on developing better surfactant-polymer compatibility under harsh conditions. Specialty synthetic polymers have been explored for application in combination with surfactants for improving oil production. In addition, a complete analysis of robust coreflood design of SP processes for challenging carbonate reservoirs has been provided as a part of this study.

The final chapter discusses the conclusions reached from the experiments and suggestions for future work to further develop more robust EOR technology for application in challenging carbonate reservoirs.

Chapter 2: Literature Review

This chapter provides a brief background on the fundamental principles of foam and polymer as mobility control mechanisms. It is important to note, that not all aspects of foam will be covered in this section. The aspects relating to the viability of foam for chemical Enhanced Oil Recovery (EOR), however, will be addressed in this chapter. This chapter will include the basic understanding of foam, in addition to the application of foam in chemical EOR especially for low permeability formations. In addition, this chapter discusses the fundamentals of polymer rheology and transport properties and modifications necessary for injection in low permeability carbonates. A brief discussion on the chemistry and structure of the surfactants used in chemical EOR applications is also provided, since it is an integral part of any EOR processes.

2.1 INTRODUCTION

2.1.1 Foams in EOR Applications

Gas injection is an established enhanced oil recovery (EOR) technique (Taber et al., 1997). The type of gases injected can include hydrocarbon components like methane, propane and enriched gases, and non-hydrocarbon components like carbon dioxide, nitrogen and flue gas. They are typically injected into oil reservoirs that have been previously waterflooded. Currently in U.S. CO_2 EOR projects alone contribute to 280,000 barrels of oil per day production, which is only 3% of the domestic oil production (Enick et al., 2012). These gas injection processes have high microscopic sweep efficiency under miscible (first or multi contact) conditions with the crude oil (Orr et al., 1982). On the other

hand, for immiscible processes the adverse mobility ratio caused due to low density and viscosity of gas leads to viscous fingering and gravity override, leaving a significant part of the reservoir unswept (Lake and Venuto, 1990). In case of carbonate reservoirs, reservoir heterogeneity and oil-wetness also contribute to poor sweep efficiency (Koval, 1963).

Due to the wide variation in heterogeneity of carbonate reservoirs from pore scale to reservoir scale, foam is considered to mitigate the sweep efficiency problems associated with gas injection processes (Kovscek et al., 1994; Rossen et al., 2010). Foam helps to improve both the displacement and sweep efficiency by reducing the gas mobility through immobilization or trapping a large fraction of the gas in the reservoir and increasing the apparent viscosity of the gas (Hirasaki and Lawson, 1985). The concept of foam as a mobility control agent was first proposed by Boud and Holbrook (1958). Since then, there have been several field tests, e.g., carbon dioxide foam flood (Chou et al., 1992), steam foam flood (Patzek, 1996), and foam assisted water-alternating-gas injection (Blaker et al., 2002). Foam formulations have been improved lately by including ultra-low interfacial tension (Wang and Mohanty, 2014) and nanoparticles (Singh and Mohanty, 2015a). Many studies in the past have addressed foam flow in sandstones, but few studies have been reported on foam flow in carbonate rocks (Singh and Mohanty, 2016; Das et al., 2016). There are two challenges for foams to survive in low permeability carbonate rocks. The foams have to deal with low permeability and oil-wettability of carbonate rocks.

2.1.2 Polymers in EOR Applications

Waterflood is one of the most commonly used EOR technique in both sandstone and carbonate reservoirs due to its low cost and easy availability. The success of the waterflood process is significantly dependent on the oil properties and the reservoir properties. Waterflood recovery in the low permeability carbonate reservoirs are low because of oil wettability, heterogeneity and low waterflood throughput due to low permeability (Sharma and Mohanty, 2013). Recent studies have shown that low salinity waterflood can be very effective in incremental oil production, especially in carbonates. If the reservoir temperature is high (above 70 ºC), lowering the salinity of the brine, or modifying the brine composition such as adding sulfate ion, can change the wettability of some carbonate rocks and reduce the residual oil saturation (Yousef et al., 2011; Strand et al., 2006).

Polymers are the most common mobility control agents used in the oil industry. They help in increasing the viscosity of the injected water and improve mobility control, thus reducing the channeling in heterogeneous reservoirs and improving the sweep efficiency. The first polymer flood was conducted in the early 1960s (Pye, 1964; Sandiford, 1964; Mungan et al., 1966; Gogarty, 1967). For field scale application, a typical injection sequence includes a brine preflush, polymer flood, fresh water buffer flood and the drive water flood (Lake et al., 2015). Conventional polymers such as hydrolyzed polyacrylamide has limited thermal stability in high salinity/hardness and high temperature environment. Variants of polyacrylamides (e.g., NVP-AM/AMPS) have been developed for higher temperature applications (Kulawardana et al., 2012; Dupuis et al., 2017; Gaillard et al.,

2015), but at the expense of higher cost. Biopolymers like Xanthan gum, Scleroglucan and Schizophyllan are also suitable for high temperature and high salinity reservoirs, but limited to high permeability reservoirs (Leonhardt et al., 2014; Huang and Sorbie, 1993; Jensen et al., 2018). Some recent work has been published on injection of synthetic polymers in tight carbonates through modification of high molecular weight polymers by shear degradation; but at the cost of significant viscosity loss (Levitt et al., 2011; Bennetzen et al., 2014).

2.2 BASIC CONCEPTS OF FOAM

2.2.1 Foam Theory

Foam is defined as a dispersion of gas bubbles in a continuous liquid phase where the gas flow paths have been made discontinuous by thin liquid films called lamellae (Gauglitz et al., 2002; Schramm and Wassmuth, 1994). These lamellae are defined as a thin liquid film with interfaces on both sides of the liquid phase. Surfactants in the aqueous phase help to stabilize the gas dispersion in the liquid phase and generate foam (Kovscek and Radke, 1994), which can improve conformance in gas-injection improved oil recovery (Schramm, 1994; Rossen, 1996), acidizing (Smith et al., 1969; Gdanski, 1993) and environmental remediation (Hirasaki et al., 2000; Mamun et al., 2002). The dispersion of the gas phase in foam can also be stabilized using nanoparticles. The scope of this study is restricted to the application of surfactant stabilized aqueous foams. The foam rheology in a porous medium is quite different than that in bulk. In porous medium, the foam is a two-phase fluid system where the continuous regeneration and collapse of the foam lamellae is

an essential mechanism of foam transport, as shown in **Figure 2.1 (a)**. On the other hand, bulk foam, defined as dispersion of gas in a liquid phase without the presence of porous medium, is contained on the bottom of the bulk foam by a liquid phase and on the top by a gas phase as shown in **Figure 2.1 (b)**, which is a 2D interface of a bulk foam system.

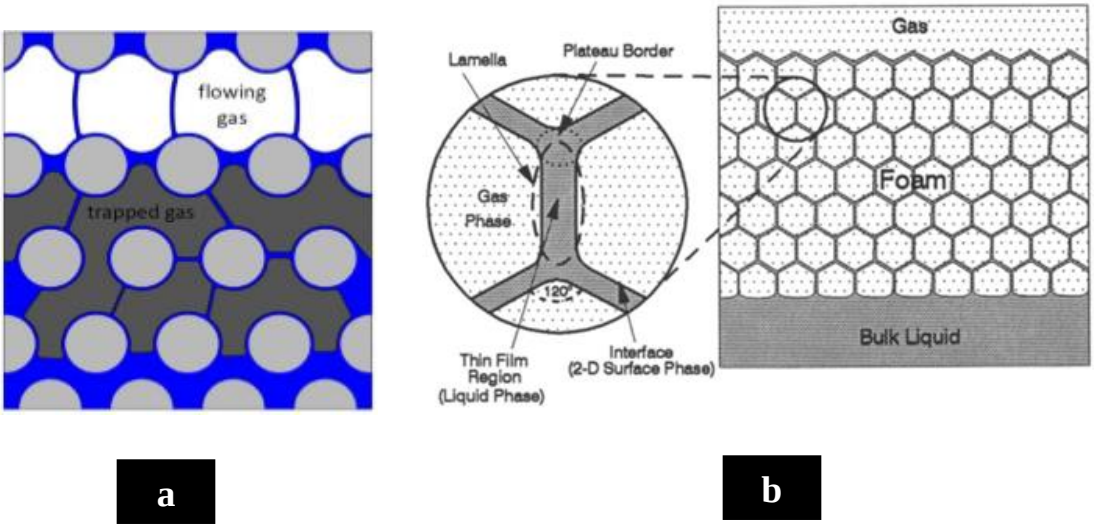

Figure 2.1. (a) Schematic of foam flow in porous media (Almajid and Kovscek, 2016) (b) Schematic of a bulk foam system (Schramm, 1994)

2.2.2 Foam Properties

Foams in bulk or porous media can be categorized based on the following three properties: texture, quality and rheology.

2.2.2.1 Foam Texture

The bubble size distribution of the foam is often classified as the foam texture. It plays a significant role in understanding the foam strength and its ability to provide mobility control in porous medium. It determines the generation of foam as bulk foam or as a chain of bubbles separated by an individual lamella, the number of lamellae per unit

length of capillary, and the radius of curvature of the gas-liquid interface (Hirasaki and Lawson, 1985). Ettinger and Radke (1992) were the first researchers to quantify the role of bubble size in foam flow in porous media. They proposed a 1D population balance model where bubbles sizes were calculated based on the lamellae generation and collapse processes. Nguyen (2000) have suggested that finer bubble sizes result in more stable foam. It is believed that with finer foam texture, foam provides better resistance to flow in rock matrix and reduces mobility of gas significantly (Falls, 1988; Kovscek and Radke, 1994). Bulk foam with a broad gas bubble size distribution is found to be less stable because of the gas diffusion from small to large gas bubbles. Bulk foam is formed when the capillary radius is larger than the equivalent radius of the bubble and individual lamellae are formed when the capillary radius is smaller compared to the radius of the bubbles (Hirasaki and Lawson, 1985). Friedmann (1991) found that bubble size and bubble size distribution range decrease with an increase in surfactant concentration and increase in system pressure. Foam texture depends on the type of surfactant, pore network, and foam quality.

2.2.2.2 Foam Quality

Foam quality is defined as the gas volume percentage within foam at a specified pressure and temperature. The in-situ foam quality present during foam flow in porous media changes spatially as a function of time until steady state is achieved. Hence, most of the experiments report the injection foam quality which can be controlled under laboratory conditions. In the bulk phase, foam quality is expressed by the following equation,

$$\text{Foam quality (\%)} = \frac{\text{gas volume}}{(\text{gas volume}+\text{liquid volume})} \text{ X } 100 \qquad (2.1)$$

In coreflood experiments, foam quality is defined as the following equation,

$$\text{Foam quality (\%)} = \frac{\text{gas injection rate}}{(\text{gas injection rate} + \text{liquid injection rate})} \text{ X } 100 \qquad (2.2)$$

Bulk foam having high foam quality is referred to as “dry foam” (Schramm, 1994). Researchers have reported evidence of two different foam flow regimes: high quality, where foam mobility increases with increases in foam quality and foam shows shear thinning properties, and low-quality regime, where foam mobility decreases with increase in foam quality and foam shows shear thickening properties. High foam quality leads to the reduction of mobility due to discontinuous gas bubbles in the liquid films. Hence, an optimum foam quality is determined from the intersection of the high and low foam quality regions. This optimum foam quality, where transition happens from low to high quality regime, is dependent on the surfactant type, type of gas used for generating foam, properties of the porous media, surfactant concentration, salinity and temperature. The effect of foam quality to change the radius of curvature of the liquid, an important variable in the thickness of the liquid film wetting the solid and affecting the resistance to flow, is significant at high qualities (Hirasaki and Lawson, 1985). Foam qualities can exceed 97%. Studies have shown that foam is unstable below quality 40% and above 95% quality; not much research has been done at these extreme low- and high-quality values (Bullen, 1976; Chang, 1998; Hutchins, 2005).

2.2.2.3 Foam Rheology

This study is focused on understanding the behavior of foam flow in the porous media and the impact of its petro physical properties like increased viscosity of the fluids

during the transport processes. Foams are typically shear thinning fluids whose viscosity decreases with increasing shear rate in the high-quality regime (Marsden, 1965). Due to technical challenges it is difficult to measure absolute foam viscosity directly. Hence, the term "apparent foam viscosity" has been derived, which can be obtained from Darcy's law. The apparent foam viscosity varies with rock permeability non-linearly and approaches asymptotic values at both high and low permeabilities, with viscosity being higher for high permeability rocks (Lee, 1991). Foam mobility, ease with which foam flows in a porous medium, is defined as the ratio of the effective permeability to apparent viscosity. In porous media, the apparent foam viscosity depends on the bubble size. The flow resistance tends to increase with decrease in foam bubble size due to increase in the foam apparent viscosity (Hirasaki and Lawson, 1985). Falls (1988) suggested that the apparent gas viscosity increases by an order of magnitude when the ratio of bubble size to average pore size decreases by two-fold.

2.2.3 Foam Generation Mechanisms

Foam generation in porous medium is governed by the operating conditions such as pressure gradient, and pore network in the reservoir. As the fractional flow of gas is increased, the capillary pressure increases (along with gas saturation) but reaches a limiting or "critical" capillary pressure, above which foam lamella starts breaking and gas mobility increases without the change in gas saturation (Rossen and Gauglitz, 1990; Ransohoff and Radke, 1988). The critical capillary pressure varies with surfactant type and concentration, gas flow rate and porous medium permeability (Khatib et al., 1988; Falls et al., 1988; Rossen, 1990). These studies were conducted in porous media of permeability greater than

a Darcy. Limited number of studies are available on foam in low permeability porous media. Raza et al. (1970) reported that the ability of foam to provide flow resistance is greater in high permeability porous media than in low permeability media. Siddiqui et al. (1997) suggested that the important factors governing the foam flow in low permeability sandstones are bubble-size and pressure drop which are functions of flow rate. Very high-pressure gradients (>1000 psi/ft) were generated in these experiments which are not feasible in fields.

Studies have shown that the ability of foam to control gas mobility is greater in high permeability porous media than in low permeability media (Raza, 1970). The key to understanding the performance of foam flow in porous media is based on two concepts: limiting capillary pressure (Pc*), defined as the gas-water capillary pressure above which foam coalescence and lamella rupture are rapid, and minimum pressure gradient (∇p^{min}), defined as the pressure gradient necessary for mobilization of the liquid lamellae and foam generation (Rossen and Gauglitz, 1990). Pc* is dependent on the gas flow rate, liquid saturation, absolute permeability and the surfactant. For higher permeability porous media, Pc* typically decreases with increase in permeability (Kovscek and Radke, 1993). In low permeability rocks, the entry gas-water capillary pressure is high; thus, the capillary pressure would be expected to be higher than Pc*. Thus, foam coalescence is expected to be high leading to coarse or very weak foam. Researchers have emphasized the importance of critical injection velocity or pressure gradient ∇p^{min} in porous medium for transition from “coarse” foam to “strong” foam. The minimum pressure gradient ∇p^{min} scales with $k^{-1/2}$ (where k is the permeability of the porous medium), and dependent on the surfactant

type, surfactant concentration and surface tension of the gas and surfactant used for foam generation (Gauglitz et al., 2002). Hence, low permeability porous media requires a higher ∇p^{min} for mobilization of foam lamellae. Again, in reservoirs, pressure gradients available are limited, often less than 5 psi/ft away from well bores. Thus, applied pressure gradients would be lower than the ∇p^{min}, leading to unstable foam flow. The type of gas used for generation of foam also plays an important factor in the determination of ∇p^{min} with CO_2 generating lower liquid-gas interfacial tension compared to nitrogen, methane and flue gases. Researchers have suggested that the important factors governing the foam flow in low permeability porous media are bubble-size and pressure drop which are functions of flow rate (Siddiqui et al., 1997). For foam applications in low permeability formations, both high Pc* and ∇p^{min} make it difficult for good foam stability which leads to higher rates of foam coalescence at lower liquid saturations. Kahrobaei et al. (2017) suggested that ∇p^{min} required to transition from coarse foam to strong foam is independent of flow rate, surfactant concentration and foam quality; but the critical velocity for the transition is dependent on the foam quality. These past studies suggest that for low permeability (~10 mD) cores, foam is very difficult to generate and propagate. It is possible that a few lamellae, stabilized by surfactants, can block flow in some pores and help divert the fluids to improve the displacement efficiency.

The foam generation and propagation in the porous media depend on the continuous generation of the foam lamellae. The three main mechanisms governing foam generation in porous media are snap-off, lamella division, and leave behind. Recently, Liontas et al.

(2013) proposed two new mechanisms of in-situ foam generation in microfluidic channels defined as bubble pinch-off. These mechanisms are detailed in the subsequent sections.

2.2.3.1 Snap-Off

Snap-off is a process of creating several discontinuous gas bubbles of smaller size from a larger gas film at the pore throats. It is one of the most important mechanisms for foam generation in porous media (Morrow, 1990; Ransohoff and Radke, 1988). The necessary conditions for snap-off to occur in porous media are that the body-to-throat ratio must be larger than two (Roof, 1970), the capillary pressure must be low, and the liquid saturation must be high (Falls, 1988). Snap-off occurs when the capillary pressure is larger than the entry pressure, and gas enters the pore body, as seen in **Figure 2.2**. The bubbles formed by snap-off are not stable in the absence of the surfactant, and tend to coalesce quickly, forming a continuous gas phase.

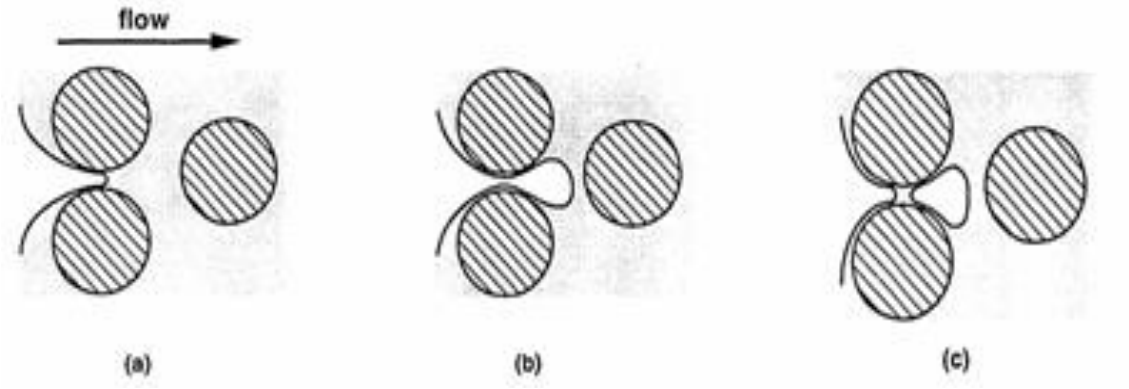

Figure 2.2. Mechanism for foam generation via snap-off (Kovscek and Radke, 1994).

According to Chambers and Radke (1990), snap-off in porous media can be classified into three types: pre-neck, neck snap-off, and rectilinear snap-off. Pre-neck snap-off is caused due to complete blockage of a pore throat by a gas bubble. Neck snap-off,

also known as roof snap-off, occurs during a drainage displacement due to the negative capillary pressure which drives the liquid in the pore body to flow into the pore throat. This mechanism is an artifact of a sharp permeability contrast in presence of moderate water fraction in the porous media. Rectilinear snap-off most likely occurs in relatively long and straight pores, which is a similar mechanism to neck snap-off. In addition to snap-off, lamella division is another important mechanism for foam generation in porous medium.

2.2.3.2 Lamella Division

Lamella division is the process of creation of new lamellae from an existing lamella. This occurs when the lamella is stretched around a branch point, as seen in **Figure 2.3**. The creation of lamellae by lamellae division requires the static lamellae in pore throats to be displaced by a sufficient pressure gradient. One of the necessary criteria for lamella division to occur is that the bubble size should be equal to or greater than the size of the pore throat in the porous media (Chambers and Radke, 1990). Researchers have suggested that a minimum velocity or pressure gradient should be exceeded for foam generation (Rossen and Gauglitz, 1990). The frequency of lamellae division is a function of density of flowing bubbles, gas velocity, bubble sizes, branch points, and capillary pressure (Falls, 1988).

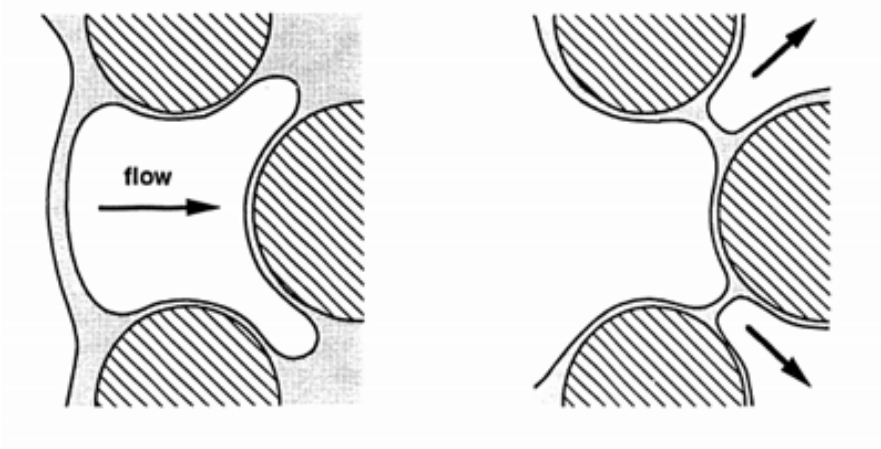

Figure 2.3. Schematic of lamella division mechanism (a) flow of a gas bubble through a pore throat (b) branching of lamella to create new lamellae (Kovscek and Radke, 1994).

2.2.3.3 Leave Behind

The snap-off and lamellae-division results in the formation of disconnected gas bubbles, thus reducing the gas mobility. Hence, these two mechanisms contribute to the formation of strong foam. Unlike snap-off and lamella division which generate lamellae parallel to the flow, leave-behind generates lamellae perpendicular to the flow. Leave behind lamellae occur when a continuous gas phase invades a surfactant laden region, thus causing weak foam (Dicksen et al., 2002). These lamellae are stationary and block parts of the pore network to gas flow reducing the gas-phase relative permeability (Friedmann et al., 1991; Nguyen, 2000). These stationary films dominate gas-mobility reduction at low velocities and discrete bubbles dominate the reduction at high injection rates (Ransohoff and Radke, 1988). As two gas menisci converge downstream, a lens is left behind, and it may drain to a lamella, as seen in **Figure 2.4**.

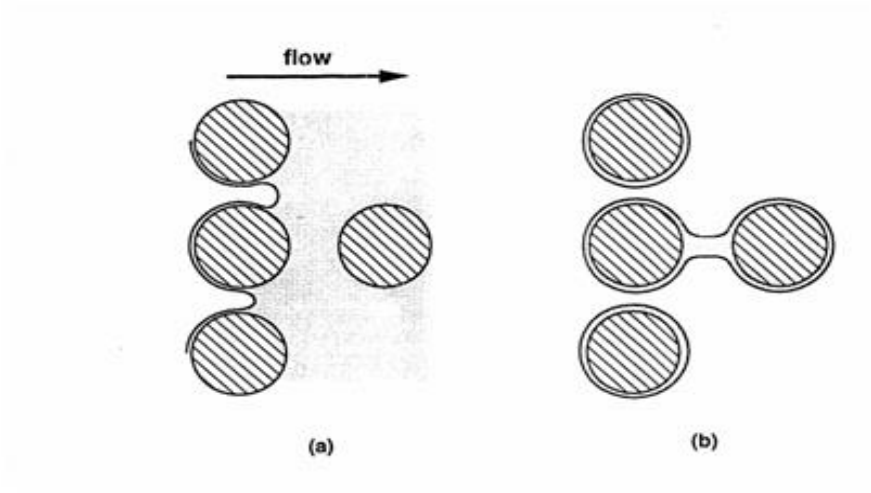

Figure 2.4. Schematic of leave-behind mechanism (a) two gas bubbles invading liquid phase (b) creation of new lamella (Kovscek and Radke, 1994).

2.2.3.4 Bubble Pinch-off

Liontas et al. (2013) conducted foam flow experiments in microfluidic channels. The pre-generated foam was injected into the device, and a visual observation of the foam flow was monitored using high-speed imaging. Two new pinch-off mechanisms were reported for bubble generation: neighbor-wall pinch-off, which occurs when a bubble entering the pore throat is pinched between a neighboring bubble and the curved wall of the pore throat (**Figure 2.5 (a)**), and neighbor-neighbor pinch-off , resulted when a bubble is pinched between two neighboring bubbles approaching the constriction (**Figure 2.5 (b)**).

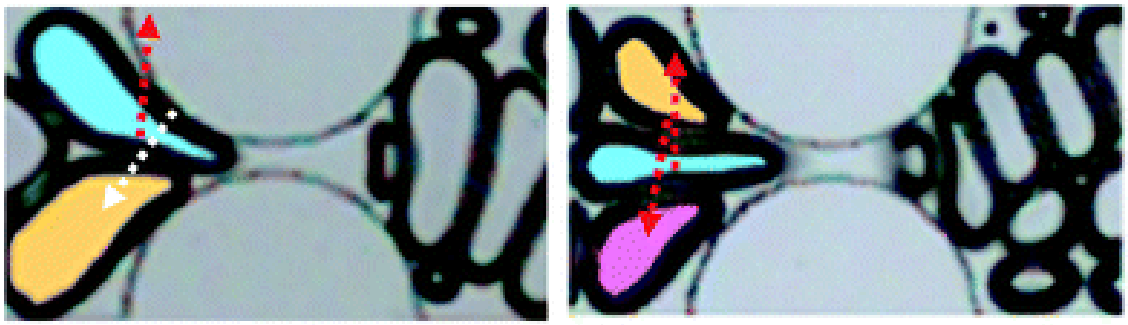

Figure 2.5. Bubble pinch-off mechanisms (Liontas et al., 2013)

2.2.4 Foam Destruction Mechanisms

The half-life can vary from seconds to years, but thermodynamically foams are always unstable (Bergeron, 1997). Chambers and Radke (1990) suggested two main mechanisms of lamellae destruction or coalescence: capillary suction and gas diffusion.

2.2.4.1 Capillary Coalescence

Thin foam lamellae are thermodynamically unstable. The stability of these lamellae is governed by the balance of the attractive and repulsive intermolecular forces. Capillary coalescence is one of the primary mechanisms for foam destruction. This phenomenon is based on the important concept of disjoining pressure (π) introduced first by Derjaguin (1940). This pressure is defined as the difference in the thermodynamic equilibrium pressure applied to the surfaces and the pressure in the bulk phase. Disjoining pressure is a function of film thickness where a positive value of π implies net repulsive forces and a negative value of π implies net attractive forces. **Figure 2.6** shows the typical behavior of disjoining pressure as a function of lamella thickness for a bulk foam system. A higher capillary pressure is required to balance the disjoining pressure, which increases with the

decrease in lamella thickness until it reaches a critical lamella thickness (h_c) as shown in **Figure 2.6**. Beyond this point, the lamella is no longer stable, and it collapses.

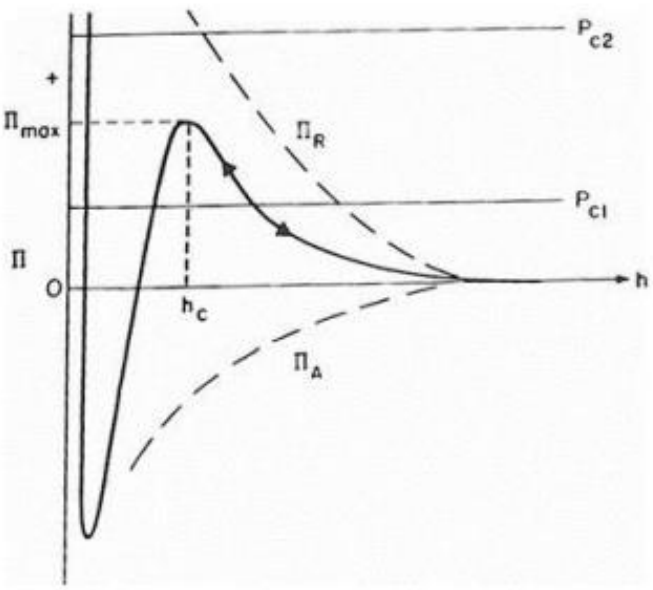

Figure 2.6. Typical disjoining pressure π isotherm (solid line), resultant of attractive π and repulsive π contributions (dashed lines) (Chambers and Radke, 1990)

A similar analogy of the critical disjoining pressure, an artifact of bulk foam lamellae, to foam flow in porous media is the concept of limiting capillary pressure, P_c*. **Figure 2.7** shows a description of the nature of P_c* as a function of liquid saturation, Sw. The diagram shows that with increase in gas fractional flow, the liquid saturation decreases, and the foam breaks abruptly at S_w* corresponding to a P_c*. Also, for a fixed water saturation (S_w*) with increase in gas fractional flow, there is an increase in the bubble sizes as observed by Khatib et al. (1988).

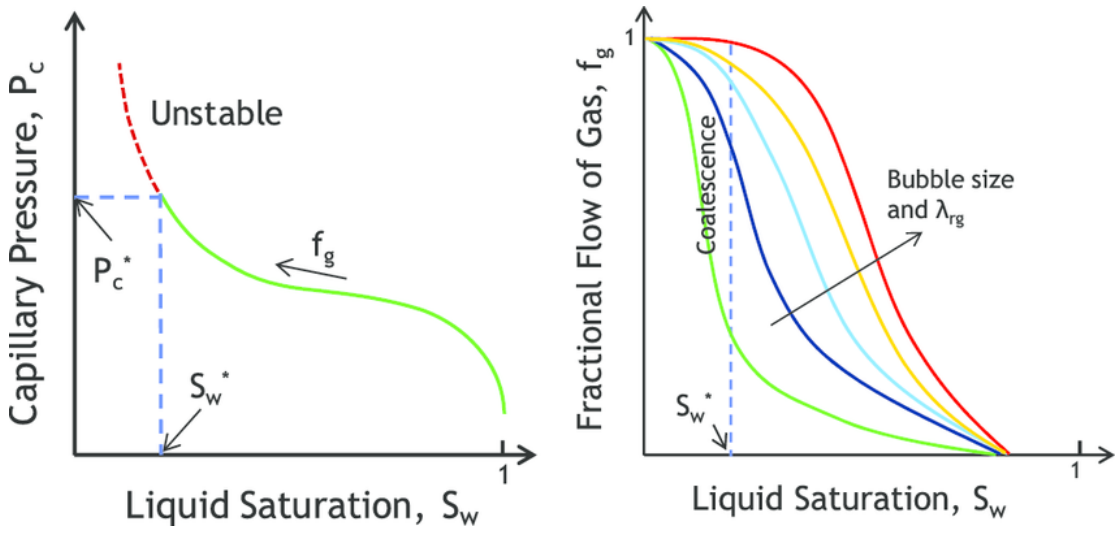

Figure 2.7. Sketch of capillary pressure as a function of liquid saturation (left) and fractional flow of gas as a function of liquid saturation (Farajzadeh et al., 2015; Khatib et al., 1988)

2.2.4.2 Gas Diffusion

One of the other predominant mechanism of foam destruction is gas diffusion. This mechanism is more enhanced in bulk or static foam such as trapped foam in porous media. Based on Young-Laplace equation, smaller bubbles tend to have higher pressure and higher chemical potential compared to larger bubbles. Hence, there is a potential gradient that results in mass transfer from smaller bubbles to larger bubbles. This leads to continuous growth of larger bubbles and shrinkage of smaller bubbles in bulk foams, which is often referred as Ostwald Ripening in bulk foam literature (Tcholakova et al., 2011).

2.2.4.3 Negative Effect of Crude Oil

Typically, crude oils have a detrimental effect on foam stability and generation in porous media. Several experiments performed in the past have demonstrated the negative impact of oil on foam stability (Arnaudov et al., 2001; Hdjiiski et al., 2001; Vikingstad et

al., 2005; Farajzadeh et al., 2010a; Andrianov et al., 2012). The degree of this effect on foam destabilization depends on the oil-, surfactant-, and aqueous-phase compositions (Farajzedah, 2012). A qualitative analysis of the stability or instability of bulk foams in the presence of oil depends on the spreading (S), entering (E), and bridging coefficients (B) of the gas/surfactant/oil interactions which are defined as follows:

$$S = \gamma_{S/G} - \gamma_{S/O} - \gamma_{O/G} \quad (2.3)$$

$$E = \gamma_{S/G} + \gamma_{S/O} - \gamma_{O/G} \quad (2.4)$$

$$B = \gamma_{S/G}^{\ 2} + \gamma_{S/O}^{\ 2} - \gamma_{O/G}^{\ 2} \quad (2.5)$$

where $\gamma_{S/G}$, $\gamma_{S/O}$ and $\gamma_{O/G}$ are the interfacial tensions between surfactant-gas, surfactant-oil and oil-gas respectively.

Researchers have suggested the following values for these coefficients to ensure better foam stability in the presence of oil, i.e., S<0 which would imply less affinity of the crude oil to spread at the interface, E<0 which signifies that the crude oil have less tendency to enter the gas-water interface, and B<0 which implies low tendency of the crude oil to form a bridge between two bubbles (Denkov, 2004). Foam in porous media behaves significantly different from bulk (Mannhardt et al., 2000; Bergeron et al., 1993). Also, Schramm and Novosad (1992) suggested use of lamella number, L, as an indication of the ability of the crude oil to imbibe into the foam lamellae from micromodel experiments. The stability of the foam can be classified into three categories: Type A for L<1, most stable foam, Type B for 1<L<7, moderate foam, and Type C for L>7, unstable foam; but researchers have suggested contradictory results in bulk foam and foam flow in porous

media (Bergeron et al., 1993; Vikingstad et al., 2005; Andrianov et al., 2012; Jones et al., 2016). In cases of low-IFT foams, foams can exist after displacement of oil. Despite the destabilization impact of crude oil on foam, studies have shown a significant mobility factor reduction due to the presence of foam in zones previously occupied by oil (Zhang et al., 2000).

2.2.4.4 Effect of Rock Wettability on Foam Properties

Wettability indicates the affinity of the rock to different fluids; it affects several parameters such as fluid distribution, relative permeabilities, capillary pressure, and residual oil saturation (Du and Malmaison, 1990; Anderson, 1987). It is a function of rock mineralogy, fluid composition, saturation history, and reservoir temperature. Schramm et al. (1996) reported decreased efficiency of foam in oil-wet or intermediate-wet porous media than in water-wet media due to foam-oil interactions. Wettability of carbonate rocks can be altered from oil-wet to water-wet by using anionic surfactants (Seethepalli et al., 2004; Zhang et al., 2006; Sharma and Mohanty, 2013), cationic surfactants (Austad and Milter, 1997; Strand et al., 2003) or non-ionic surfactants (Gupta and Mohanty, 2010; Alvarez et al., 2014). The choice of surfactant depends on the reservoir properties like the crude oil, reservoir mineralogy, brine composition and temperature (Mohan et al., 2011; Adibhatla and Mohanty, 2008). Wettability can also be altered by low salinity water injection at high reservoir temperature (Tang and Morrow, 1997; Yousef et al., 2011; Mahani et al., 2015).

Oil wettability and presence of crude oil (Schramm et. al., 1992) have a negative impact on the foam strength. Yu and Wardlaw (1986) reported that for surfaces with contact angle (with respect to aqueous phase) greater than about 70^{o}, snap-off does not occur in throats. This signifies that it is crucial to alter the wettability of oil-wet systems to water-wet for foam generation. Haugen et al. (2012) conducted foam flow experiments in fractured, oil-wet limestone cores and observed that in-situ foam generation in the fractures via co-injection of gas and surfactant was inefficient and large pore volumes (>100 PV) of pre-generated foam was necessary to recover oil. This is primarily due to the negative effect of crude oil on foam generation and foam stability. Experimental studies have demonstrated the detrimental impact of oil on foam stability (Arnaudov et al., 2001; Hadjiiski et al., 2001; Vikingstad et al., 2005; Farajzadeh et al., 2012). The effect of the presence of oil on foam destabilization depends on the oil-, surfactant-, and aqueous-phase compositions (Farajzedah et al., 2012). The foam rheology in the presence of oil depends on the spreading, entering, and bridging coefficients of the gas/surfactant/oil interactions, oil emulsification and pinch-off.

2.2.5 Other Factors Affecting Foam Stability

Foam stability also depends on other factors like temperature, surfactant concentration, salinity, and presence of solid particles. Researchers have found that foam stability decreases with increasing temperature (Kapetas, 2015; Chen et al., 2012; Spirov et al., 2012) due to increase in the drainage rate and rapid foam destruction. At low concentrations typically below critical micelle concentration (CMC), the interfacial tension

decreases with increase in surfactant concentration and helps to stabilize the foam. At high surfactant concentrations significantly above CMC, increase in surfactant concentration increases foam stability due to ordered microstructure formation in the lamellae (Nikolov et al., 1986). The effect of salinity on foam stability is dependent on the type of surfactant, salinity, concentration and the presence of divalent ions. Above the critical micelle concentration, foam stability is relatively insensitive to pH change (Liu, 2005). The presence of solid particles can either be beneficial or detrimental to foam stability. If the particles are not water-wet, they gather at the interfaces in the foam, enhancing the mechanical stability of the lamellae. Dispersed particles can also influence the stability by enhancing the bulk viscosity, and thus, increasing the stability (Schramm, 1994).

Formation brines in most carbonate reservoirs have a significant amount of divalent ions. The impact of divalent ions on surfactant adsorption (Yekeen et al., 2017), lamellae drainage (Angarska et al., 1997) and foam rheology has been studied in the past. The anionic surfactant adsorption is high on carbonates in the presence of divalent ions (and in absence of alkali) and may be economically impractical. Thus, the use of cationic and cationic/zwitterionic surfactants for foam applications in carbonate formations needs to be explored.

2.2.6 Application of Foam in Enhanced Oil Recovery

Foam has a great potential for application in porous media as an enhanced oil recovery mechanism due to its ability to reduce the mobility of gases inside the reservoirs and increase the sweep efficiency of the processes. This mobility reduction is an effect of the reduction of the relative permeability of the gas phase, and the factors affecting these

properties have been described in the previous sections. The mobility reduction factor also depends on different foam injection strategies in the reservoirs as discussed later in details.

2.2.6.1 Mobility Reduction

Gas injection is a widely used enhanced oil recovery mechanism, but the low viscosity of gas results in early gas breakthrough, poor sweep efficiency, viscous fingering, and channeling that result in low oil recovery, in the order of 10 to 20% (Lee, 1991). Due to low viscosity, gases tend to have higher mobility than oil and water which leads to gravity override and channeling through oil in rocks. This decreases the amount of oil being contacted by gas and leads to early gas breakthrough, causing poor sweep efficiency. Mobility ratio, M, is defined as the mobility of the displacing phase, gas, divided by the mobility of the displaced phase, oil, as seen in the equation below:

$$M = \frac{k_{rg}\mu_o}{k_{ro}\mu_g} \tag{2.6}$$

The efficiency of the gas displacement process can be improved significantly with the reduction of the mobility ratio. The mobility ratio can be decreased by increasing the gas viscosity or decreasing the relative permeability of gas, both of which can be achieved through foam generation. Foam decreases the relative permeability of gas by blocking the pores through which the gas can flow and also diverts flow from higher permeability zones to lower permeability unswept zones. Since foam is a dispersion of discontinuous gas in a liquid film, foam also increases the apparent viscosity of the gas phase. In addition, foam helps to improve oil recovery by reduction of the capillary forces due to lower interfacial tensions generated in the presence of surfactants in the aqueous phase.

2.2.6.2 Injection Strategies: Surfactant-Alternating-gas (SAG) vs. Co-injection

Primarily there are two different injection strategies for foam injection in the porous media. Foam can either be injected in alternating slugs of surfactant solution and gas, or co-injected together with gas and surfactant formulation pre-generated in surface facilities. Co-injection is more desirable than an alternating injection when foam is needed near wellbore in a heterogeneous reservoir to ensure that both gas and liquid enter the same zones. Generally, gas mobility is reduced more during the co-injection than the surfactant-alternating-gas (SAG) injection (Farajzedah, 2012). For steam-foam injections, it is less practical to sequentially inject surfactant and gas in alternating slugs because the steam depletes the top section due to gravity segregation. Hence, it is critical to co-inject surfactant, steam, and a non-condensable gas during the steam foam process. Co-injection processes tend to have higher injection well pressure due to loss of injectivity which could fracture the injection well, thus rendering such a process impractical for field scale application (Shan and Rossen, 2004). High injection pressure in steady co-injection process helps to trigger foam generation in layered media, but no significant impact in homogeneous packs (Li and Rossen, 2005).

On the other hand, the significance of snap-off as one of the primary mechanisms of lamella mobilization and generation implies that an alternating surfactant and gas injection strategy may be more beneficial than co-injection. Previous studies (Li and Rossen, 2005) and several field trial experiments (Blaker et al., 2002; Skauge et al., 2002) have shown SAG injection is more preferable than co-injection because it minimizes contact between water and gas in surface facilities and piping. This can be important in

preventing corrosion, typically when the gas is CO_2 because it can lead to formation of acid upon contact with water (Mattews, 1989). The benefit of SAG injection is the improvement in the injectivity of the displacing water from the near-well region during the gas injection, since foam weakens and gas mobility rises (Shi and Rossen, 1998). Researchers have suggested that a SAG process performed at fixed, maximum injection pressure provides better control against gravity override in homogeneous reservoirs than either continuous foam injection or a fixed-rate injection process (Shan and Rossen, 2004). The injection of gas at maximum pressure helps to partially reverse the effects of gravity slumping of surfactant during injection of the liquid. Several researchers have reported that SAG with fewer larger slugs gives a better sweep efficiency compared to many smaller slugs due to a coupling between gravity segregation and surfactant propagation (Shan and Rossen, 2004; Faisal, 2009; Kloet, 2009). However, Lawson and Reisberg (1980) in their study showed that smaller slugs in alternating gas and surfactant injection leads to additional oil recovery due to higher pressure drop. Hence, a lot of ambiguity is prevalent in the literature studies on the best injection strategies for optimal foam performance in the porous media.

2.2.7 Foaming Surfactants

The surfactants comprise of both hydrophilic portion (“head”) and a hydrophobic portion (“tail”)with straight or branched hydrocarbons. The functional groups in the head can be cationic, anionic, zwitterionic or non-ionic in nature. Due to the amphiphilic nature, the surfactant can adsorb at the gas-water interface, which makes them an ideal candidate to stabilize strong foam. The adsorption of surfactant on the interface helps to lower the interfacial tension between aqueous and gas/oil phase that further improves the oil recovery

process. At low surfactant concentrations, the surfactant molecules are dispersed in the bulk liquid phase as monomers. However, above a critical surfactant concentration, the surfactant molecules aggregate to form spherical structures, which are known as micelles (Miller and Neogi, 1985). Depending on the degree of hydrophobicity (or hydrophilicity), the surfactant molecules partition in aqueous or gas/oil phase.

Researchers have shown that the chain length of the hydrophobic part of the surfactant plays an important role in the determination of the kinetic migration to the interfaces and the ensuing surface activity, as suggested by the extent of phase delay and foam stability (Beneventi et al., 2001). Surfactants with branched hydrophobe have shown higher surface activity and hence lowers the interfacial tension significantly at the oil and water interface (Zhang et al., 2000; Lu et al., 2014). On the other hand, for foaming application, a straight hydrophobe surfactant is preferred due to its ability to provide higher viscosity and slower drainage rate (Lu et al. Hence for developing low IFT foaming application, the choice of an optimum surfactant formulation can be challenging - low IFT prefers branched hydrophobe and foaming requires straight hydrophobe. Several studies have shown blend of surfactants with both branched and linear hydrophobes can provide a good synergy for these applications. (Ma et al., 2017; Bera et al., 2013). Foaming ability and foam stability tend to decrease with increase in salinity and show low values at the optimal salinity (Bergeron et al., 1993; Li et al., 2011; Srivastava et al., 2009; Wang et al., 2001). In most of studies where foaming and low IFT are combined, the formulation is mostly optimized for low-IFT, but not for foam performances, and the evidence of foam (e.g. by estimation of a mobility reduction) is often poor in these studies. However,

promising results are obtained by adding alkali to a surfactant, with both foaming and low-IFT occurring simultaneously (Zhang et al., 2000). Use of alkali leads to dissolution & precipitation in carbonate reservoirs in presence of divalent ions in the formation brine. Alternatively, a strong chelating agent like ethylenediaminetetraacetic acid (EDTA) is used in combination with alkali to keep the divalent ions in solution and prevent precipitation.

2.3. BASIC CONCEPTS OF POLYMER

Waterflooding does not generally have a stable displacement for medium to heavy crude oils (and therefore has a low overall sweep efficiency) because of low fluid viscosity and reservoir heterogeneity. Much of the unrecovered oil is unswept. Water soluble polymers are often used to – 1) viscosify the displacing fluid in EOR and reduce the mobility ratio from waterflooding; 2) reduce the effective permeability and improve sweep efficiency, thus recovering most of the remaining oil from previously bypassed channels. Chemical EOR processes target at increasing the viscosity of the injected fluids (by adding polymers) and reducing interfacial tension (IFT) (by adding surfactants/alkali) to improve oil production beyond waterflooding. Anionic surfactants can be used to generate ultra-low IFT between crude oil and aqueous phase by creating microemulsions with suitable surfactants and alkali system, thus mobilizing a significant amount of residual oil after waterflood. Alkali-polymer (AP), Alkali-surfactant-polymer (ASP) and surfactant-polymer (SP) flooding are popular EOR techniques to reduce Sor. The conventional understanding is that polymer flooding itself cannot reduce Sor, because most polymers do

not reduce IFT and typical reservoir rates (~1 ft/day) do not result in high enough viscous forces (even for viscous polymers) to overcome strong capillary forces.

The first polymer floods were conducted in the early 1960s (Pye, 1964; Sandiford, 1964; Mungan et al., 1966; Gogarty, 1967). All reservoirs are not suitable candidates for polymer flooding; hence, polymer screening is an important step in the development of a polymer flood. Some of the critical screening criteria for polymer flooding are: (1) reservoir temperature, (2) formation-water salinity, (3) divalent contents, (4) clay content, (5) oil viscosity and (6) formation permeability (Sheng et al., 2015). Polymer flooding has been established as an effective EOR process for both mature and immature reservoirs. Several field applications in sandstones and higher permeability reservoirs illustrate the ability to successfully mix and inject high quality polymer solutions for IOR such as Total in Dalia (Morel et al., 2008), several Canada operators in Pelican Lake, Canada (Delamaide et al., 2014) and Cairn India in Mangala, India (Pandey et al., 2012). Most of these applications have used conventional HPAM polymers which are constrained to low salinity and temperature. But there are limited projects for polymer flooding in low permeability carbonates due to serious injectivity issues and thermal stability problems in high temperature and high salinity reservoirs (Han et al., 2013; Levitt et al., 2013).

2.3.1 Mobility Ratio and Capillary Desaturation Curves

2.3.1.1 Mobility Ratio

The mobility ratio (M) is defined as the ratio of the mobility (λ) of the displacing fluid to the displaced fluid and defined as follows:

$$M = \frac{\lambda_{displacing\ fluid}}{\lambda_{displaced\ fluid}} = \frac{\frac{krw}{\mu w}}{\frac{kro}{\mu o}} \quad (2.7)$$

where krw and kro are the relative permeability of the displacing (e.g. water) and displaced (e.g. oil) phases respectively, and μw and μo are viscosities of the displacing and displaced fluids, respectively. For a stable displacement to occur, a favorable mobility ratio (<1) is necessary (**Figure 2.8(a)**), which improves sweep efficiency and oil recovery. A displacement with an unfavorable mobility is unstable, and results in viscous fingering and significant amount of unswept bypassed oil (**Figure 2.8(b)**).

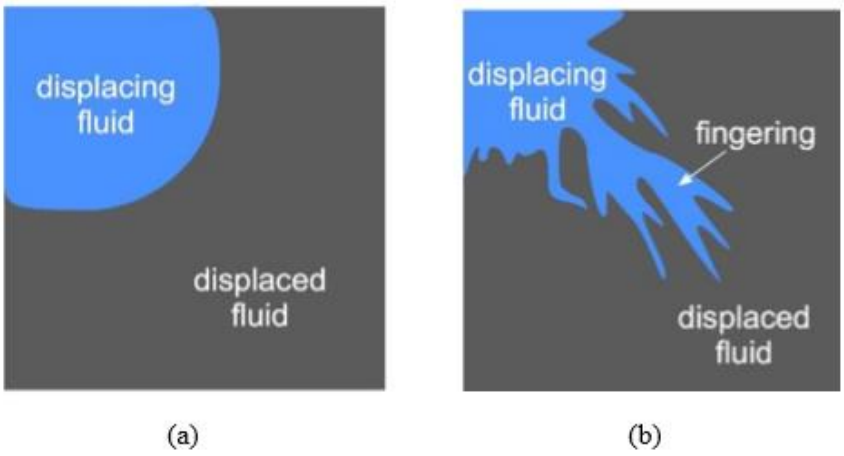

Figure 2.8. (a) Stable displacement during polymer flooding with M < 1 and (b) unstable displacement with viscous fingering for M>1 (Qi, 2018)

2.3.1.2 Capillary Desaturation Curve

Capillary number (Nc) is a dimensionless number, defined as the ratio of viscous forces to capillary forces as shown in the equation below in equation 2.8:

$$\mathrm{Nc}, 1 = \frac{\mu_w * \mathrm{u}}{\sigma} \quad (2.8)$$

where u is the Darcy flow velocity and σ is the interfacial tension between the displaced and displacing fluids. Capillary number can also be defined as shown in equation 2.9 (Brownell and Katz, 1947; Stegemeier, 1977):

$$\mathrm{Nc}, 2 = \frac{k\nabla\varphi}{\sigma} \qquad (2.9)$$

where k is the single-phase permeability to brine, and ∇Φ is the local pressure gradient. In flow experiments through porous media, equation 2.9 is primarily used and is believed to be the more fundamental definition.

Reduction of residual oil after a waterflood is one of the key motivations for application of EOR processes. Researchers have suggested that the residual oil saturations remain constant below a critical $N_{c,\,crit}$, but decreases rapidly above the critical capillary number $N_{c,\,crit}$, as shown in **Figure 2.9**. The **Figure 2.9** below is commonly known as the capillary desaturation curve (CDC) and is key to the design of any EOR processes. The CDC and critical capillary number vary by rock type. Pore size distribution, average pore size, the ratio of pore-body to throat size and wettability significantly affect the critical capillary number. Hence, understanding of the porous media properties and its pore network is key to estimation of the accurate $N_{c,\,crit}$. The curve below shows lower $N_{c,\,crit}$ for wide pore distribution (similar to heterogeneous carbonate reservoirs) and gradual change in residual oil saturation with increasing N_c. On the other hand, higher $N_{c,\,crit}$ is observed for a narrow pore size distribution (similar to homogeneous sandstone reservoirs) with rapid change in residual oil saturation with increasing N_c beyond the critical capillary number.

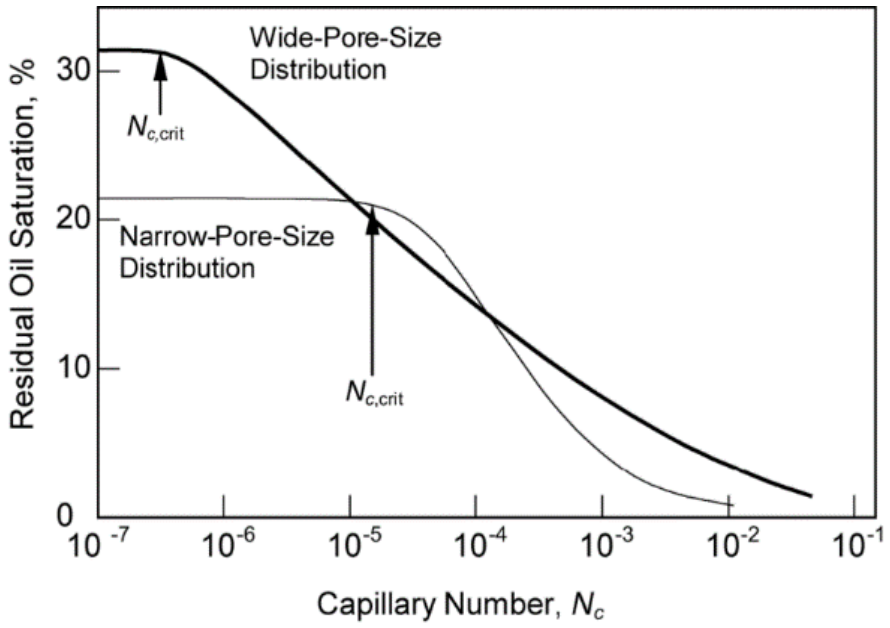

Figure 2.9. Capillary Desaturation curve for carbonate (wide pore size distribution) and sandstone (narrow pore size distribution) reservoirs

For waterflood processes at typical field rates, the capillary number is well below the critical capillary number; hence, it must be increased by two or three orders of magnitude to exceed the critical capillary number in order to reduce residual oil (Wreath, 1989). From equation 2.9, increasing pressure gradient or decreasing interfacial tension between oil and water can increase the capillary number. At a constant injection velocity as waterflood, viscous polymers can provide a higher-pressure gradient (and therefore higher capillary number) but these capillary numbers are still well below the critical capillary number. For carbonate reservoirs with small pore sizes and low permeability, a practical way to increase the capillary number is reducing interfacial tension including the use of surfactants in aqueous phase or other wettability alteration techniques.

2.3.2 Polymer Structures

The most commonly used polymer in enhanced oil recovery is partially-hydrolyzed polyacrylamide, a co-polymer of acrylamide and acrylic acid (Sorbie, 1991). A typical commercial product is synthesized from mixtures of both monomers (~70% acrylamide, 30% acrylic acid) using radical chain growth polymerization chemistry (**Figure 2.10**). The HPAM molecule is a double helix structure with less rigidity (unlike xanthan), which allows the molecules to both stretch out and relax when sheared. The final molecular weight of the polymer is a function of the number of monomers added during the synthesis process.

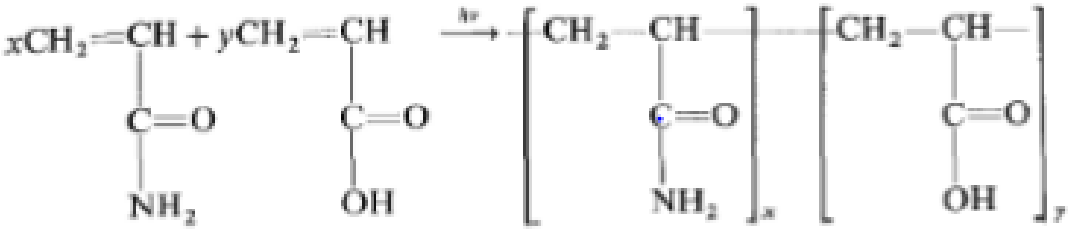

Figure 2.10. Radical copolymerization of HPAM molecules (Sorbie, 1991)

At high temperature and high salinity conditions, the conventional HPAM undergoes thermal degradation and precipitation (Davison and Mentzer, 1982). The rate of hydrolysis of HPAM is enhanced at higher temperatures, results in increase of the polyacrylic acid in the backbone that is very sensitive to hardness and leads to polymer precipitation at higher salinities (Abbas et al., 2013). Also, the coil conformation of HPAM molecules makes them extremely sensitive to ionic environments (Zaitoun and Potie, 1983;

Wu et al., 2012). As a result, use of HPAM becomes challenging at elevated temperature and salinity conditions, which is a common occurrence for most of the carbonate reservoirs.

The incorporation of the anionic monomer 2-Acrylamido-2-Methylpropane Sulfonate (AMPS) gives increased tolerance to divalent ions (Levitt and Pope, 2008), but this monomer does not protect the acrylamide against thermal hydrolysis (Moradi-Araghi et al., 1987). Also, the tolerated Ca^{2+} ion concentration is typically less than 2000 ppm for a polymer containing 20-30% AMPS monomer, which is still well below the Ca^{2+} concentration found in some high-saline carbonate reservoirs. The incorporation of N-Vinyl Pyrrolidone (n-VP) effectively protects the acrylamide groups against thermal hydrolysis. Earlier stability tests on n-VP/AM co-polymers in a weight ratio of 50:50 have shown this polymer to have long term stability in seawater at 120°C (Doe et al., 1987). Recent studies have been published on the stability of a n-VP/AM co-polymer in controlled aerobic conditions which showed polymer stability in presence of 200 ppb of O_2 at a temperature of 120°C in a 50 g/l NaCl brine without the need of protective additives (Gaillard et al., 2010).

Polymer manufacturers have been successful in developing specialty synthetic polymers which are tolerant to high temperature and high salinity conditions. They are typically co-polymers of acrylamide and acrylamide-tertio-butyl sulfonate (ATBS) or ter-polymers of acrylamide, acrylamide-tertio-butyl sulfonate (ATBS) and N-vinyl pyrrolidone (NVP). Acrylamido-TertButyl-Sulfonate (ATBS) is known to provide an improved tolerance to high temperature and high salinity reservoirs (Gaillard, 2015; Vermolen, 2011). The improved chemistry of the polymer products has shown great

potential in changing the future of polymer flooding applications in challenging reservoirs conditions worldwide; but at the expense of increased manufacturing costs. The availability of the monomers is key to the pricing of these products**. Figures 2.11** and **2.12** shows the co-polymer and ter-polymer structures for the specialty synthetic polymers.

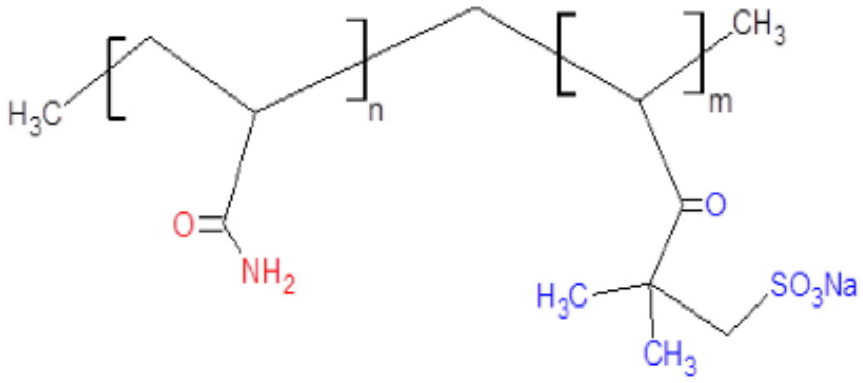

Figure 2.11. Co-polymers of ATBS and acrylamide

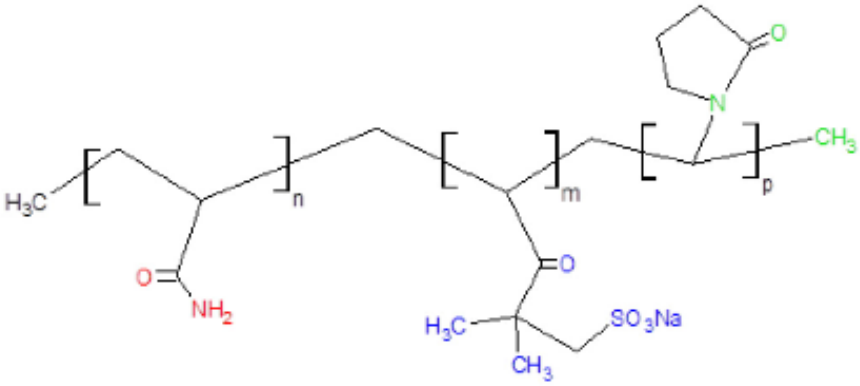

Figure 2.12. Ter-polymer of acrylamide, ATBS and NVP

A novel class of hydrophobically modified water-soluble polymers, also known as associative polymers (AP), containing a small number of hydrophobic, water-insoluble monomers along the polymer backbone have also been developed for polymer flooding applications (Dupuis et al., 2012; Taylor and Nasr-El-Din, 1998; Dupuis et al., 2011).

These polymers constitute of a hydrophilic long chain backbone in combination with small number of hydrophobic groups localized either randomly along the chain or at the chain ends (Lara-Ceniceros et al., 2007). The hydrophobic groups form intramolecular and intermolecular associations that result in three-dimensional network and helps to increase the viscosity of the polymer solution at lower concentrations, especially beyond the critical association concentration (Caram et al., 2006). These polymers do not simply rely on the viscosifying properties due to molecular weight, but additionally on intermolecular hydrophobic interactions of the polymer chains, as shown in **Figure 2.13**. Researchers have suggested that these polymers are less sensitive to salinity variation and usually hydrophobic interactions are enhanced in presence of divalent ions, thus making it a promising candidate for high salinity carbonate reservoirs (Reichenbach-Klinke et al., 2011).

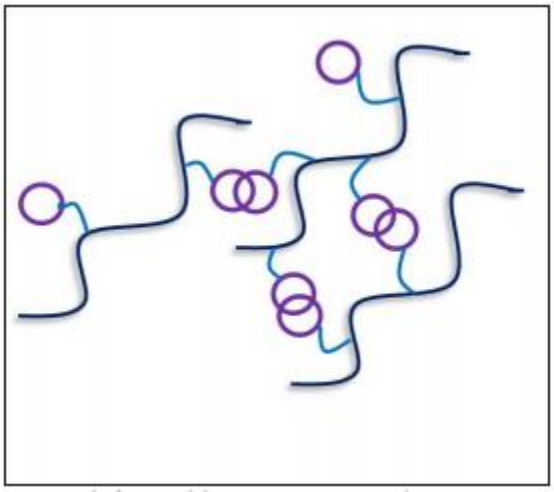

Figure 2.13 Sketch of polymer network formed by associative polymers (Reichenbach-Klinke et al., 2015)

Thermo-associative polymers are a special class of this type of materials. They contain certain chemical entities like polyalkylene oxide or N-isopropylacrylamide, which increases their hydrophobicity with temperature. Hence, they have a lower critical solution temperature (LCST) beyond which they become water insoluble. The functional principle of these type of polymers is outlined in **Figure 2.14** below. With increasing temperature, the hydrophobicity of the thermo-sensitive groups is enhanced, and the intermolecular interaction is strengthened (L'Alloret et al., 1997).

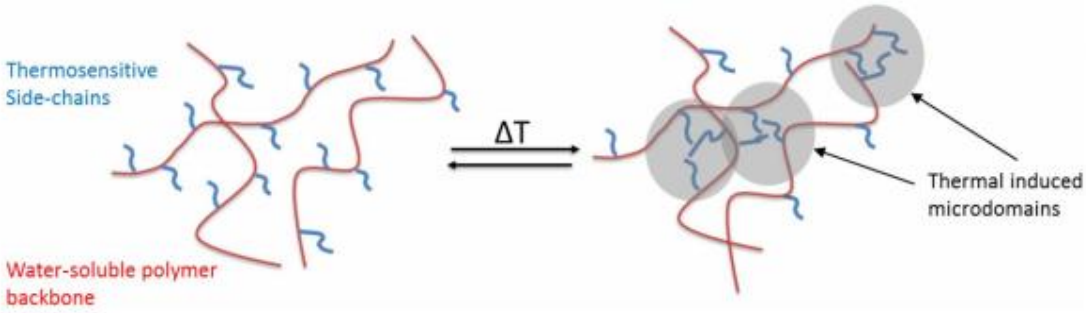

Figure 2.14 Structure and working principle of thermo-associative polymers (Reichenbach-Klinke et al., 2018)

Viscosity and elasticity are two important rheological properties of polymer products, both increase with increasing molecular weight. With the current polymer manufacturing techniques, a varying degree of sulfonated polyacrylamides with wide range of MW can be synthesized for use in EOR applications. The high MW polymers have longer chains and larger hydraulic diameters in aqueous solutions than low MW polymers. However, high MW polymers also have injectivity limitations in low permeability rocks/reservoirs due to ground injectivity supply and bigger molecular size than pore throats.

2.3.3 Polymer Rheology

2.3.3.1. Shear Thinning Behavior

Most of these polymer molecules are loose and coiled in presence of ions in aqueous phase; they are entangled and orient themselves randomly. Shear forces align these molecules in the direction of flow, thus, losing viscosity with increasing shear forces, as shown in **Figure 2.15**. Based on the viscoelastic nature of the polymers and the molecular weight, at very high shear rates a shear thickening effect is also observed which can be explained due to enhanced interactions between polymer chains, thus providing increasing viscosity at higher shear forces. The bulk rheology of polymer solutions shows a Newtonian plateau (at low shear rates), shear thinning region (at intermediate shear rates) and shear thickening behavior (at very high shear rates).

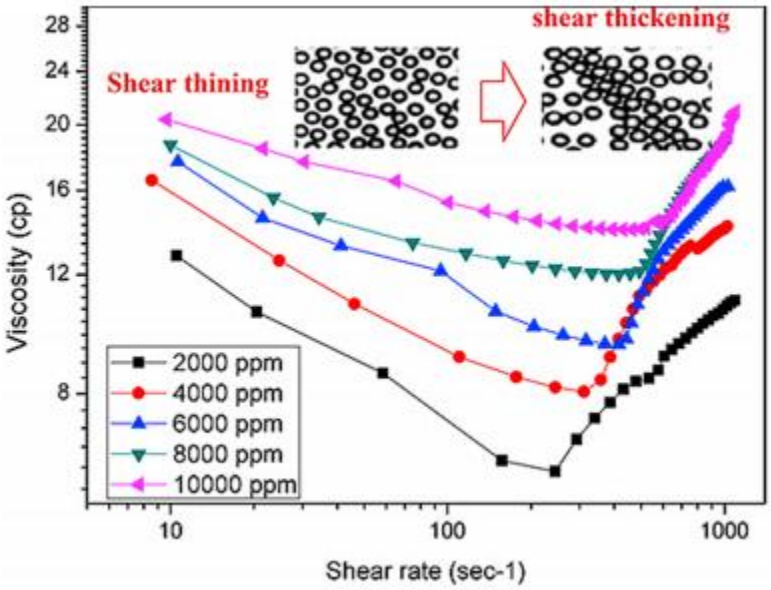

Figure 2.15 Shear rheology of viscoelastic polymer at varying polymer concentrations (Kumar and Mandal, 2017)

Polymer viscosity is a function of shear rates, and few published empirical models like power law (Ostwald, 1925) and Carreau models (Carreau, 1972; Bird et al., 1987) capture the polymer rheology accurately. The power law is the simplest and widely used in the oil and gas industry and is described as shown below:

$$\mu_{app} = K\dot{\gamma}^{n-1} \quad (2.10)$$

where K and n are the power law coefficient (Pa-s^n) and shear thinning index (dimensionless) respectively. These are the fitting parameters for viscosity data obtained from rheometer steady sweep test measurements. The Carreau model accounts for the Newtonian plateaus at low and high shear rates, which is given by,

$$\mu(\dot{\gamma}) \doteq \mu_\infty + (\mu_0 - \mu_\infty)[1 + (\lambda\dot{\gamma})^2]^{n-1/2} \quad (2.11)$$

where μ_0 and μ_∞ are viscosities are zero and infinity shear rates, and n is the same fitting parameter as in the power law model.

The viscosity estimation from polymer concentration can be calculated from polymer's intrinsic viscosity [η], which is a measure of its size in solution relative to its mass and has dimensions of L^3/M. For a dilute suspension, effective viscosity can be calculated by Stokes equation,

$$\eta = \eta_2 (1 + (5/2) * \phi + \ldots] \quad (2.12)$$

where ϕ is the volume fraction of the particles in the system, given by the hydrodynamic volume of the polymer coils as

$$\phi = (c / M)\, N_A\, V_h \quad (2.13)$$

where c is the polymer concentration in solution, M is the molecular weight of the polymer and Vh is the hydrodynamic volume occupied by the polymer.

The specific and intrinsic viscosities are derived as follows:

$$\eta_{sp} = (5/2)\ (c/M)\ N_A\ V_h \qquad (2.14)$$

$$[\eta] = \phi_0\ \alpha_n{}^3 (< R_g{}^2 >^{3/2} /M) \qquad (2.15)$$

where ϕ_0 is a constant which depends on the distribution of segments within the coil and a value of $3.67*10^{24}$ /mol is appropriate for Gaussian coils and Rg is the radius of gyration for the polymer molecule. The above equation can be rearranged to obtain the Flory-Fox equation as below:

$$[\eta] = \phi_0 \frac{Rg^3}{M} \qquad (2.16)$$

Alternatively, the intrinsic viscosity can be estimated from the molecular weight of the polymer solution using the Mark Houwink equation as shown below:

$$[\eta] = K\ M^a \qquad (2.17)$$

where a is a constant between 0.5 and 0.8. Calibration of the constants K and a for any polymer in a given solvent at a given temperature allows determination of the molecular weight of the polymer sample.

Intrinsic Viscosity Determination

The relationship between specific viscosity and intrinsic viscosity is defined by a power series, which when truncated to second degree term results in Huggins equation as shown below:

$$\eta sp / c = [\eta] + k_H\ [\eta]^2\ c \qquad (2.18)$$

The constant k_H is defined as Huggins constant and has values ranging from 0.3 in good solvents to 0.5 in poor solvents.

Alternatively, intrinsic viscosity can also be estimated from relative viscosity for dilute solutions where the specific viscosity is much less than 1, which is defined by Kraemer equation,

$$\ln (\eta_r) / c = [\eta] c + k_K [\eta]^2 c \quad (2.19)$$

A plot of the inherent viscosity, extrapolated to zero concentration, results in the intrinsic viscosity.

On the other hand, associative polymers exhibit double shear thinning behavior, with high hydrophobic content and high molecular weight polymers, with intermediate flat plateau. This is a result of the transition from intramolecular to intermolecular interactions with increasing shear forces (Reichenbach-Klinke et al., 2016). These polymers exhibit a thermothickening effect, which is more pronounced at higher associative content and higher molecular weight. The critical associative content necessary for enhanced polymer network formation was inversely proportional to the MW of the polymers. The elevated viscosity measurements observed in higher salinity brines (higher ionic strength) is dependent on complete charge screening (CCS) and most of these polymers show an initial decrease in viscosity with increase in salinity and then increase in viscosity beyond a certain critical salinity (Viken et al., 2018). The hydrophilic-lipophilic balance (HLB) of the polymers affect the intermolecular interactions and polymer rheology at high shear rates. At elevated salinity conditions, associative polymers have been found to behave more like a viscous fluid than an elastic fluid due to loss of polymer network connectivity, even

though the hydrophobic interactions are enhanced at higher salinities. Thermo-associative polymers exhibit higher storage modulus (G') at higher temperatures due to increased elastic properties compared to loss modulus (G") (Reichenbach-Klinke et al., 2018).

2.3.3.2. Shear Degradation of Polymers

High molecular weight polymers are prone to irreversible shear degradation, which is commonly observed in the laboratory and in the field. During field scale applications, shear degradation can occur at the surface facilities, chokes and valves and perforations. Morel et al. (2008) reported 50% viscosity loss due to mechanical degradation for a high molecular weight HPAM in seawater through a field choke. Mechanical degradation has been studied in laboratory cores and blenders. Degradation in cores occur at extremely high rates, analogus to flow near wellbore region. This behavior of polymer solutions can prove to be beneficial for improvement of polymer filterability (or transport) through small pores for injection in low permeability formations.

Mechanical degradation of polymers leads to scission of polymer backbone chains and formation of two radical species. The critical shear forces to initiate the breakage is dependent on the bond energy, hence polymer chemistry affects the shear degradation mechanism of these polymers. Shear flow is a result of both rotation and extensional flow. During turbulent flow or locally accelerated flow through contractions, valves and porous media, the extensional component of the velocity gradient is more predominant. Due to chain extension and hydrodynamic forces exerted on the stretched chains, beyond a critical strain rate the polymer chains starts to rupture. The critical strain rate depends on the chemistry of the polymer chain and varies inversely with molecular weight of the polymers

(Hunkeler et al., 1996; Nguyen & Kausch, 1988). The degradation was a strong function of fluid velocity in the orifice and was related to the energy accumulated during the deformation process. Vanapalli et al. (2006) suggested a model for polymer degradation in turbulent flow that describes the dependency of molecular weight on critical strain rate for rupture in stagnation points and transient experiments.

Mechanical degradation technique is an effective tool to probe the molecular weight distribution of polymers and vary the polymer concentrations and brine salinities. Polymer injection in low permeability formations has been getting a lot of impetus recently. Hence, limited research is available on the comparative study of polymer degradation mechanism under different polymer concentrations and salinity conditions. Also, the effect of polymer chemistry on the rheological properties of two polymers of varying molecular weight needs to be conducted for better understanding of the underlying mechanisms. Although, several researchers have published the enhanced shear degradation in presence of high salt concentrations, especially divalent ions (Maerker, 1975; Noik et al., 1995; Zaitoun et al., 2012). The possible mechanisms could be chemically enhanced cleavage or reduction of elastic modulus of polymer solutions in presence of divalent ions, but no definitive conclusions have been observed. The elastic modulus is primarily responsible for sharp extensional flows that seems to be an important cause of degradation processes. Zaitoun et al. (2012) reported that at low salinity and hardness, modified HPAMs exhibit higher resistance to mechanical degradation at equal solution viscosity.

The observed loss of viscosity as a function of time spent by the polymer solutions in a blender or number of passes through a valve appears to be asymptotic in time

empirically. This suggests that the degradation process results in a critical molecular weight of the polymer beyond which no further degradation can be observed (Jouenne et al., 2015; Mansour et al., 2014). The higher the shear rate and higher the shearing time, the lower the asymptotic viscosity plateau is. In this scope of work, polymer solutions have been shear degraded in a laboratory blender to improve filterability through small sized pores. The shear degradation mechanism also showed reduction of polydispersity of the molecular size distribution, with breakage of the high MW tails of the polymer chains primarily, as shown in **Figure 2.16**.

On the other hand, associative polymers are more shear resistant than the conventional HPAM and the sulfonated PAMS. The primary reason being the difference in the structure of these molecules. Shear degradation leads to the scission of the heavy polymer backbone which is the primary reason of viscosifying properties for HPAMs and sulfonated PAMs, but associative polymers rely more on the associative polymer network for their higher viscosity than on the molecular weight. Shear degradation possibly breaks the weak intermolecular network but – in contrast to high molecular weight synthetic polymers – the polymer backbone remains intact (Reichenbach-Klinke et al., 2011). Hence, even with the breakage of the polymer network a lower reduction in viscosity is observed for associative polymers compared to HPAMs for a similar weight polymer in a similar brine salinity.

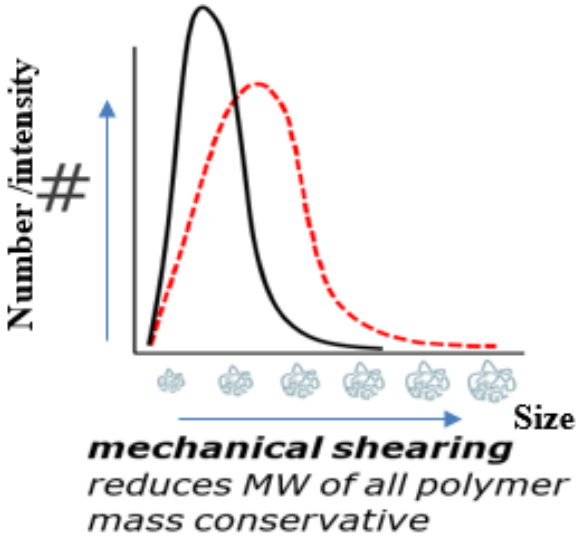

Figure 2.16 Modification of polymer size distribution and reduction of polydispersity during mechanical degradation in blender treatment (Driver, 2017)

2.3.3.3. Polymer Filtration

Polymer filtration is a standard screening criterion in the laboratory and in the field to qualify a polymer solution for injection in porous media. Filtration at the field scale helps to remove large microgels and impurities from the polymer solutions, whereas in the laboratory filtration is used to remove microgel and fine tailoring of the molecular weight distribution of monodisperse polymer, as shown in **Figure 2.17**. The UT filtration ratio test has been widely used as a standard procedure in the oil and gas industry for decades but is inflexible due to the requirement of the fixed volumes of solution filtered during each experiment. Dana Wreath in his master's thesis reported that the filtered volume of polymer solution is a linear function of the square root of the time (Wreath, 1989). Hence, a careful treatment of the plugging characteristics of the polymer filtration through filter papers was performed by Jonathan Driver in his master's thesis (Driver, 2017). He reported multi stage

plugging in filter papers, where resistance of the filter increases linearly with increasing filtered volume (first stage) and thereafter the rate of plugging (or loss of permeability) is accelerated (second stage). Based on Darcy's law, an equivalent plugging parameter β was developed to describe the linear plugging region which is illustrated in the equations below,

$$t = aV^2 + bV + c, \quad \beta = 2a/b \tag{2.20}$$

where t is the cumulative filtration time and V is the cumulative filtered volume of the polymer solution. Here β quantifies the loss in permeability in the linear plugging regime. Thus, a modified filtration ratio FR_β was estimated from the plugging parameter, analogus to the UT filtration ratio, as shown below:

$$FR_\beta = \frac{1+ \beta*190\ mL}{1+ \beta*70\ mL} \tag{2.21}$$

This simple relation gives excellent experimental agreement with the standard filtration ratio for filtration ratio between 1 and 2. Beyond the estimated filtration ratio of 2, the plugging characteristics were found to be at the second stage, where accelerated plugging is more prevalent. Thereafter, the estimated filtration ratio is an under prediction compared to the true filtration ratio because the linear plugging assumption is not valid.

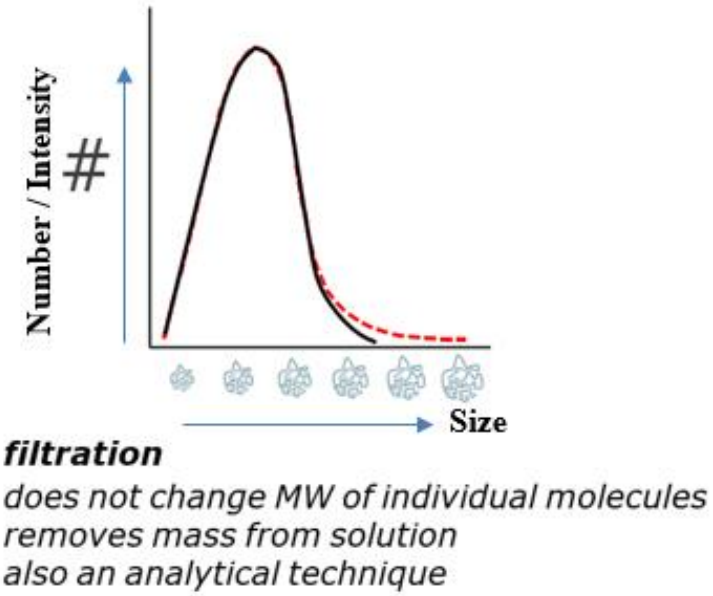

Figure 2.17 Fine modification of polymer size distribution during filtration through small sized filter papers (Driver, 2017)

2.3.3.4. Polymer Size Analysis

Polymer functionality is defined by its molecular weight (MW), molecular size and structure, MW distribution and the degree of cross linking and chain branching. A polymer's molecular weight is determined by the monomer and the number of monomers in the molecule. Hence, the distribution shape and the average MW influence the properties of a polymer. The general distribution of polymer MW is shown in **Figure 2.18**. Mn, Mw and Mz are the number averaged MW, weighted average MW, and molecular weight contributed primarily from the high MW chains of the molecule respectively. Molecular size, like MW, is a defining property of most polymers and impacts the rheological behavior directly. Several techniques like dynamic light scattering (DLS), multi-angle light scattering (MALS), and static light scattering (SLS) in combination with intrinsic viscosity

(IV) can be applied to estimate the polymer size distribution, as shown in equation 2.19. Each of these methods provide different size parameters for molecular size measurement. The hydrodynamic radius (Rh) from the scattered light intensity is estimated using DLS method, the radius of gyration (Rg) for larger molecules is estimated from SLS method, and the relation between intrinsic viscosity, MW and hydrodynamic radius (Rh) can be obtained from SLS method in combination with IV measurements. The difference between these parameters is a function of the molecular density and shape of the polymer molecule.

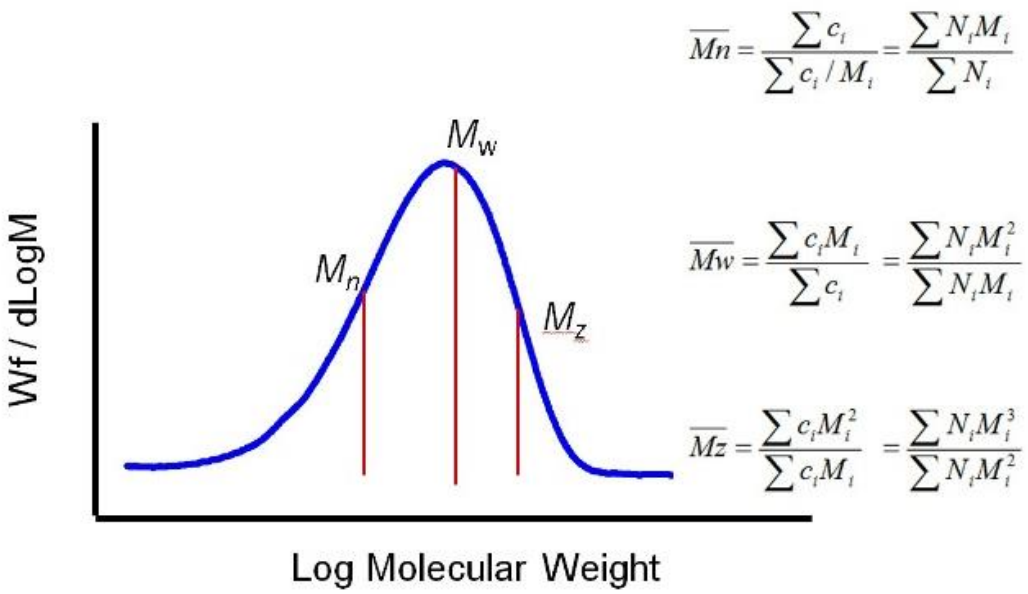

Figure 2.18 Average molecular weight of polymers using different moments of the distribution.

$$[\eta]\, M = 10/3\ \pi .\ R_h^3 \qquad (2.22)$$

The polydispersity index (I), ratio of the weight averaged molecular weight (Mw) and number averaged molecular weight (Mn), is a measure of the width of the molecular weight distribution. Irreducible polydispersity of the synthesized polymer is the primary

reason of plugging in flow through porous media, even though the nominal (average) size of the polymers indicate otherwise. The polydispersity index (I) is a function of the polymerization mechanism, where it can vary from 5 to 20 for addition polymerization, and the reactor type where the index I can vary between 1.5 and 2.

Celis et al. (2008) suggested the use of multiwavelength UV-Vis spectroscopy method to measure the droplet size and distribution of polymer solutions and emulsions which were fast, highly reproducible and applicable to the characterization of the dispersion system. The particle size determined by batch dynamic light scattering (DLS) gives an average size value based on one detector angle (90^{o}) and is a fast and simple way to determine the hydrodynamic radius of polymer molecules (Hinterwirth et al., 2013; Carro et al., 2010). Makan et al. (2016) suggested use of field flow fractionation (FFF) technique, coupled with multiple detectors, to determine size distributions of emulsions. The hydrodynamic radii (Rh) obtained from a DLS measurement of a diluted solution can be converted to radius of gyration (Rg), assuming spherical emulsion particles for these polymer solutions. The calculated Rg was obtained from the relationship Rg = 0.775 times the Rh obtained from DLS measurements (Frankema et al., 2002; Thielking and Kulickle, 1996). The results obtained from FFF technique and DLS measurements agreed with each other with the difference of the effect of hydration shells which is accounted in DLS measurements (Kato et al., 2012; McGrath, 2007).

2.3.4 Flow in Porous Media

Flow of viscous polymer solutions in complex porous media like carbonates can be challenging and complicated. All polymer solutions are non-Newtonian fluid, and viscosity

changes with shear rate. Hence, a better understanding of the polymer fluid flow in porous media can improve the polymer flooding sweep efficiency and maximize oil recovery.

Polymer retention in porous media increases with molecular weight of the polymer, clay content and decreasing permeability of the reservoir rocks. The retention also depends on the anionic and cationic charge of the polymer groups. The primary mechanisms of polymer retention in porous media can be classified as – adsorption, mechanical entrapment and hydrodynamic retention (Sorbie, 2013). Adsorption is a result of interaction between polymer chains and rock surfaces such as Van der Waals attraction, electrostatic interaction and hydrogen bonding. Mechanical entrapment resulting from the trapping of large polymer molecules in small pore throats is quite significant in low permeability rocks (Szabo, 1975; Dominguez & Willhite, 1977). Increase in hydrodynamic retention (laboratory scale artifact) was observed with increasing injection rate, but not a significant factor in field-scale polymer floods. Several researchers recognized the risks of polymer injection in low permeability rocks due to plugging and injectivity issues, but also suggested that the pore structure of the porous medium in more crucial than the actual permeability (Martin, 1974; Dann et al., 1982).

The mobility reduction from polymer flooding through porous media can be estimated by resistance factor, permeability reduction factor and residual resistance factor (Jennings et al., 1971). Resistance factor (RF) is the ratio of the mobility of the brine to that of the polymer flood and permeability reduction (Rk) is the permeability reduction in presence of polymer due to adsorption of polymer at the pore throats. Residual resistance factor (RRF) is a measure of the irreversible adsorption and mechanical entrapment of the

polymer in the porous media and signifies loss of polymer molecules during the experiment.

$$\text{RF} = \frac{\lambda w}{\lambda p} = \frac{{}^{kw}/_{\mu w}}{{}^{kp}/_{\mu p}} \tag{2.23}$$

$$\text{Rk} = \frac{kw}{kp} \tag{2.24}$$

$$\text{RRF} = \frac{\nabla P\ (after\ polymer\ flood)}{\nabla P\ (before\ polymer\ flood)} \tag{2.25}$$

where λw and λp are the mobilities of the brine and polymer solutions, kw and kp are the effective permeability during brine flood and polymer flood respectively, μw and μp are the viscosities of the brine and polymer solution respectively.

Injection of high MW polymer solutions in low permeability heterogeneous porous media can be challenging and difficult due to the wide pore size distribution which can result in significant fraction of pore throats smaller than or equal to polymer average hydrodynamic radius estimated from the molecular weight distribution. Hence, plugging of viscous polymer and losing injectivity at the field scale is a common occurrence for tight formations. An alternative approach for low permeability rocks can be injection of low molecular weight polymers with no injectivity issues but use of higher dosage of polymer concentration to meet viscosity requirements negatively affects the economics. However, injection of high molecular weight polymer in a low permeability core with no plugging was reported by Fletcher et al. (2008). Hydrolyzed polyacrylamides (HPAM) polymers have shown to be sensitive to mechanical degradation and significant viscosity loss due to irreversible scission of polymer backbones. Researchers have reported studies on the

improvement of polymer injectivity due to shear degradation near the wellbore (Seright, 1983; Sorbie & Roberts, 1984). Sorbie (2013) suggested that shear degraded polymers would be beneficial for improved injectivity in low permeability reservoirs with reduced retention, but further work would be required at the laboratory and field scale to understand more realistically the consequences of shear degradation near the wellbore on polymer injectivity. Recent researchers have reported successful polymer flooding applications in low permeability oil-wet carbonate cores with no plugging problems (Bennetzen et al., 2014), comprehensive review of the challenges of chemical EOR application in low permeability reservoirs (Delamaide et al., 2014). Recently, Jouenne et al. (2018) performed polymer stability studies after successive mechanical degradation events and developed a model to predict the viscosity loss as a function of different path dependent degradation steps.

Several researchers have reported significantly higher resistance factors with associative polymer injection in porous media (compared to estimations from viscosity measurements) in contrast to synthetic polymers (Maia et al., 2009; Seright et al., 2011; Dupuis et al., 2011). The spatial restrictions during flow in porous media enforce hydrophobic interactions to be significant at lower concentration than in bulk. The higher in-situ viscosity is a result of these flow induced interactions and not multilayer adsorption (or permeability reduction) (Viken et al., 2017). Recent studies have suggested ability of associative polymers to reduce residual oil saturations in porous media due to hydrophobic interactions between polymer molecule and crude oils (Reichenbach-Klinke et al., 2016; Askarinezhad et al., 2017). Despite these advantages limited field applications of

associative polymers have been reported due to non-ideal behavior and limited solubility of polymers (Han et al., 2006; Zhou et al., 2008). Evidence of unusually high residual resistance factors (RRF) have been observed in porous media with injection of associative polymers due to reversible and irreversible retention; but with shear degradation the RRFs can be reduced significantly (Han et al., 2018). The retention of associative polymers is dependent on the concentration, type of polymer, molecular weight, brine salinity, and amount of associative content (Reichenbach-Klinke et al., 2013). The hydrophobic associations constantly form, break and reform due to thermal fluctuations and changes in shear and extension flow fields. Hence favorable injectivity can be obtained due to shear thinning behavior and mechanical degradation at high shear rates (near injection wellbore) and prove to be more effective with higher resistance factors (RFs) at low shear rates deeper into the formation (Reichenbach-Klinke et al., 2015). Thermo-associative polymers have shown higher storage modulus over loss modulus at elevated temperatures and higher salinities due to enhanced elastic properties, which helped to generated higher RF at higher temperatures and at low injection velocities in porous media (Reichenbach-Klinke et al., 2018). Hence, improvement in chemistry of water-soluble associative polymers, that are stable at elevated temperatures and cost efficient, can change the future of polymer flooding applications in carbonates.

Some researchers have suggested that the high resistance factors generated during injection of associative polymers are a result of irreversible retention and permeability reduction. Evidence of two polymer fronts – first that contained most of the injected polymer and the second that resulted from permeability reduction was reported in the

literature (Reichenbach-Klinke et al., 2016). This study also reported weakened polymer network in presence of crude oils, resulting in lower resistance factors, which was a function of the amount of associative content in a given polymer. The interaction between hydrophilic surfactants and hydrophobic polymer monomers negatively affect the thermo-thickening properties as well.

2.4. ALKALI-SURFACTANT-POLYMER / SURFACTANT-POLYMER PROCESSES

Chemical floods can be applied in a variety of reservoir conditions. Alkali-surfactant-polymer/surfactant-polymer (ASP/SP) floods can improve the oil recovery from carbonate reservoirs. Alkali interact with organic acids in the oil to form soap in situ and reduce anionic surfactant adsorption (Liu et al., 2018). Surfactants along with soaps lower the interfacial tension between oil and water. Polymers provide mobility control and increase sweep efficiency. But there are several challenges to the application of ASP/SP floods in low permeability carbonates, such as transport of polymers in low permeability carbonates, effect of divalent ions on surfactants and alkali, geochemical reactions with the minerals, pore-scale heterogeneity and oil-/mixed-wettability.

Initial development of chemical flooding was directed primarily for sandstone reservoirs (Healy and Reed, 1977; Nelson and Pope, 1978). Many ASP field tests have confirmed that the waterflood residual oil can be displaced by the use of alkaline-surfactant-polymer floods (Huh, 1979; Falls et al., 1994). Particularly, the ASP field test in the Daqing field recovered about 20% additional OOIP after waterflood (Shutang and

Qiang, 2010). Recent research has led to the development of the surfactant systems which are suitable for carbonate environment (Levitt et al., 2006; Adibhatla and Mohanty, 2008). There are many new salinity and hardness tolerant surfactants that can be used in carbonate reservoirs (Han et al., 2013; Lu et al., 2013; Lu et al., 2014).

Use of alkali in addition to surfactant and polymer in chemical flooding was first suggested by Nelson et al. (1984); it raises pH and forms soap if the oil has organic acids. Sodium carbonate is a common alkali for sandstone reservoirs because it raises the pH to about 11 and does not dissolve silica, unlike sodium hydroxide. Alkali reduces anionic surfactant adsorption by reducing the positive surface charge on clay edges and calcites (Hirasaki et al., 2008). Alkali are often used with soft injection brines because they can interact with divalent ions present in brine and precipitate minerals. The main challenge for ASP application in carbonate reservoirs, containing high salinity and high divalent ions concentration, is produced liquid treatment process due to scaling, erosion and strong emulsification caused by alkali. The scaling in a reservoir could block up the pore throat of reservoir, damage oil-bearing layer, and affect well's liquid production capability (Youyi et al., 2013). Many carbonate reservoirs contain small amounts of gypsum or anhydride. These minerals can dissolve, and calcium can interact with sodium carbonate to precipitate calcium carbonate. Therefore, alternative alkalis have been studied such as sodium metaborate (Sharma et al., 2015; Panthi et al., 2016) and ammonia (Southwick et al., 2016; Sharma et al., 2016). If the injection brine has a small amount of divalent ion, the precipitation of minerals can be avoided if the divalent ions can be chelated. Chelating agents such as EDTA (Panthi et al., 2016) and polyacrylic acids (Shamsijazeyi et al., 2013)

have been used in the injection brines to avoid calcium carbonate precipitation but can also lead to severe formation damage for carbonate rocks. Hence, recently more research has been performed on developing SP formulations for reservoirs with high concentration of divalent ions due to increasing concern of severe scale formation and injectivity losses during polymer floods in ASP projects (Han et al., 2013; Wu et al., 2014; Kazempour et al., 2013).

Many carbonate rocks often contain high salinity and high hardness brines and are at high temperatures which is challenging for most conventional surfactants and polymers. Heterogeneity and complex mineralogy of these reservoirs affect surfactant phase behavior and polymer stability adversely, if not designed properly. However, recently a few studies have been performed in carbonate reservoirs (Carlisle et al., 2014; Sharma et al., 2016; Maubert et al., 2018; Jabbar et al., 2017). Surfactant polymer (SP) flooding has been gaining attention due to the complications associated with alkali use in fields. There are still many challenges associated with SP flooding in high temperature-high salinity/hardness (HTHS) carbonate reservoirs. It is difficult to obtain ultra-low interfacial tension (IFT) and aqueous stability in the HTHS environment (Wang et al., 2008). The oil and brine compositions control the surfactant phase behavior. Some recent work has shown promising potential of ultra-low IFT surfactant formulations in HTHS conditions in absence of alkali (Das et al., 2018), and alternative use of switchable amine surfactants for HTHS reservoirs for CO2 foam applications (Cui et al., 2016). Due to high salinity and high hardness environment encountered in SP floods, the effect of surfactant dilution and surfactant interaction with divalent cations on phase behavior becomes critical. In

particular, conventional anionic and non-ionic surfactants cannot be used for carbonate reservoirs with HTHS due to aqueous and thermal stability issues (Zhang et al., 2005; Wu et al., 2007; Kalfoglou, 1977). Conventional polymers such as hydrolyzed polyacrylamide has limited stability in HTHS environment. The key to successful SP flooding is to develop low cost and high efficiency specialty surfactants and polymers tolerant of high temperature and high hardness. Another challenge for SP application is high retention of surfactants in carbonate reservoirs in the absence of alkali. Recent studies have shown potential application of SmartWater flooding combined with the surfactant-polymer process to increase oil recovery in carbonates (Wang et al., 2018). This novel method exploits the benefits through wettability alteration, improved microscopic sweep efficiency and displacement efficiency.

2.4.1 Surfactants with ultra-low IFT for ASP/SP Processes

Formulations for ASP/SP processes can include surfactants, co-solvents and alkalis. The hydrophilic portion of the surfactant molecule is the hydrophile and the lipophilic portion of the molecule is the hydrophobe. The salts of fatty acid (R-COONa) are simple surfactants, where the alkyl chain (R) is the hydrophobe tail, the carboxylate group (COO-) is the hydrophile. The anionic surfactants have been primarily used in this dissertation for the development of ultra-low interfacial (IFT) surfactant formulations. The three most common anionic head groups are sulfonates (SO3-), sulfates (SO4-) and carboxylates (COO-).

Sulfonates are commonly used surfactants in chemical EOR applications due to chemical stability at elevated temperatures and range of pH of interest to EOR. Olefin

sulfonates are produced by the sulfonation of alkenes. Internal olefin sulfonates are produced by the sulfonation of alkenes where the double bond is randomly positioned along the molecule. The carbon number distribution and degree of branching can vary in the sulfonates as well. IOS surfactants have a twin-tailed structure.

Modern sulfate and carboxylate surfactants used for EOR applications are alcohol alkoxy sulfates and alcohol alkoxy carboxylates. Usually, a block of propylene oxide (PO) groups, followed with a block of ethylene oxide (EO) groups separate the alcohol from the head group. The PO and EO groups contribute towards the hydrophilic lipophilic balance of the surfactants and provides a tool for gradual transition with varying number of EO and PO groups. The hydrolytic stability of ethoxy-sulfate surfactants depends on the temperature and pH of the solution (Adkins et al., 2010; Talley, 1988). Sulfates are not recommended at reservoir temperature above 65 ^{o}C unless used under high alkaline conditions. On the other hand, carboxylates are more thermally and chemically stable to harsh reservoir conditions with high salinity and high temperatures.

The hydrophobe structures can be categorized into multiple types like slightly branched C_{13} tridecyl alcohol (TDA), bent hydrophobe C_{18} oleyl alcohol, mid-point branched Guerbet alcohols with carbon number ranging from 16 to 32 carbons, short hydrohobe like ethoxy-hexanol C_8 and no hydrophobe like methoxy C_1. Aromatic hydrophobes like tristyrylphenol (TSP) have been identified to be very effective for high acid number crude oils for ultra-low IFT behavior with high affinity for resins and asphaltenes (Liyanage et al., 2012).

Co-solvents used in chemical EOR are typically short chain aliphatic alcohols such as sec-butyl alcohol (SBA) and iso-butyl alcohol (IBA), aromatic alcohols like phenols. Alcohol ethoxylates and alcohol propoxylates are recently developed co-solvents that are more effective at lower concentrations (Sahni et al., 2010; Upamali et al., 2016). Co-solvents help or prevent any macroemulsion formation and reduce the time for equilibration of the microemulsions (Bourrel and Schechter, 1988). They also help to reduce the microemulsion viscosity but negatively affect the IFT between surfactant formulation and crude oils (Fortenberry et al., 2015, Jang et al., 2016; Tagavifar et al., 2016). Co-solvents at times increase the aqueous stability of the surfactant formulation especially in presence of polymers. In theory, surfactant migrates to the micellar interface whereas the co-solvent partitions between the oil, brine and interface. The distinction between surfactants and co-solvents is not always clear cut.

Chapter 3: Experimental Setup and Methodology

Core flood experiments were conducted to investigate the performance of the EOR technologies developed for application in carbonate reservoirs. Several iterations of experiments were performed with variation of design parameters to optimize the formulations and achieve the best performance. This chapter provides a description of fluid preparation and measurement methods, experimental apparatus, chemicals, and data analysis performed to complete the study.

3.1 MATERIALS

This sub-section discusses the chemicals used to investigate their performance in the development of novel EOR technologies for carbonate reservoirs through coreflood experiments.

3.1.1 Chemicals

Common salts such as sodium chloride (NaCl), sodium sulfate (Na_2SO_4), calcium chloride (as $CaCl_2.2H_2O$) and magnesium chloride (as $MgCl_2.6H_2O$) were obtained from Fisher Scientific. Ethylenediaminetetraacetic sodium salt (EDTA-Na_4) was used as received from Sigma Aldrich and solution prepared in DI water. Anhydrous sodium carbonate (Na_2CO_3) and sodium hydroxide (NaOH) were obtained from Fischer Chemicals and solutions were prepared in DI water. In addition, chemicals like potassium permanganate ($KMnO_4$), potassium dichromate ($K_2Cr_2O_7$), sodium bicarbonate ($NaHCO_3$), and cyclohexane were also obtained from Fisher Chemicals for special use in treatment of crude oil. Specialty chemicals like sodium hydrosulfite ($Na_2S_2O_4$), obtained

from Fisher Chemicals, and N,N'-Diethylthiourea, obtained from Sigma Aldrich, were used for thermal protection of polymers at high temperatures. Lab grade, methane gas (CH_4) and nitrogen gas (N_2), obtained from Praxair, were used for gas injection processes. High purity argon gas (Ar), obtained from Praxair, was used for polymer filtration and deoxygenation of injected fluids. Organic solvents like toluene, chloroform, methanol, and iso-propanol, all obtained from Fischer Scientific, were used for core cleaning purposes during the experiments. Lab grade sodium hypochlorite (bleach), obtained from Fischer Scientific, was used to break polymer solutions during sample preparation for effluent analysis and during core cleaning process. Light mineral oil, obtained from Fischer Scientific, was used to displace aqueous solutions in the glass columns during coreflood experiments.

3.1.2 Crude Oil

Several crude oil samples were used for experiments in this study. The crude oil samples obtained from different reservoirs across the world were investigated in developing novel EOR technologies under various reservoir conditions. For core flood experiments with oil present, four different types crude oil types, Crude A, B, C, and D were used whose properties are reported in **Table 3.1**. Note that the crude oil D was prepared by the dilution of crude oil C with 15 vol% cyclohexane. Each of these crude oils were used to age the carbonate cores for their respective reservoirs and make them oil-wet/intermediate wet. The same crude oils were also used for phase behavior and wettability alteration experiments in the screening process of the chemical formulations.

Table 3.1: Crude Oil Properties

Oil	Reservoir Temperature (°C)	Viscosity (cP) @ Reservoir Temp	Density (g/mL)
Crude A	60	12.6	0.89
Crude B	80	8.3	0.89
Crude C	40	6.8	0.87
Crude D (crude C +15 vol% cyclohexane)	40	7.2	0.87

3.1.3 Surfactants

Several anionic, cationic, non-ionic, and zwitterionic surfactants have been investigated in this study to explore their potential in EOR applications at various reservoir conditions. Anionic surfactants like Alfoterra S23-7S-90 with 89% active content (received from Sasol), alpha olefin sulphonate (AOS_{C14-16}) with 38.86% active components (obtained from Stepan), internal olefin sulfonates (Enordet O332, O242, O342) obtained from Shell Chemicals, alkyl propoxy ethoxy carboxylates and alkyl propoxy ethoxy sulfates (where alkyl group includes C_8, C_{12-13}, C_{18}, C_{16-32} and tristyrlphenol) prepared in-house at UT laboratory were investigated for low interfacial tension (IFT) properties with the crude oil. Non-ionic surfactants like Tergitol NP-10, Triton CG-110, Triton CG-650, and Triton CG-50 (obtained from Dow Chemical), cyclic glucamide 810 and cyclic glucamide C12/14 (obtained from Clariant Oil Services) were explored for their good aqueous stability and foaming abilities. Cationic surfactants like

dodecyltrimethylammonium bromide (DTAB) and cetyltrimethylammonium bromide (CTAB) (obtained from Sigma-Aldrich), alkyl dimethyl benzyl ammonium chloride (BTC 8358) obtained from Stepan, cocoalkylmethyl [polyoxyethylene (15)] ammonium chloride (Ethoquad C/25) obtained from Akzonobel, and in-house synthesized cationic gemini GC 580 were explored for wettability alteration application on oil-wet carbonate surface. Zwitterionic surfactants like lauryl betaine (LB) and cocoamidopropyl betaine (obtained from Solvay), and cocoamidopropyl hydroxysultaine (obtained from Harcros Chemicals) were explored for good foaming properties and tolerance to high salinity and high temperature conditions. In addition, alcohols like isobutanol-ethoxy (IBA-5EO, IBA-1PO-5EO) and Phenol-ethoxy (Phenol-5EO) prepared in-house at UT laboratory and triethylene glycol monobutyl ether (TEGBE) obtained from Sasol were explored to improve the performance of the screening tests in low IFT chemical formulations. Preliminary tests like aqueous stability, phase behavior, wettability alteration, bulk foam experiments, and foam flow experiments with no crude oil were used to screen the surfactant formulations used in developing an EOR technology for application in carbonates. The molecular structures of the most common surfactant molecules are shown below in **Figures 3.1 and 3.2**.

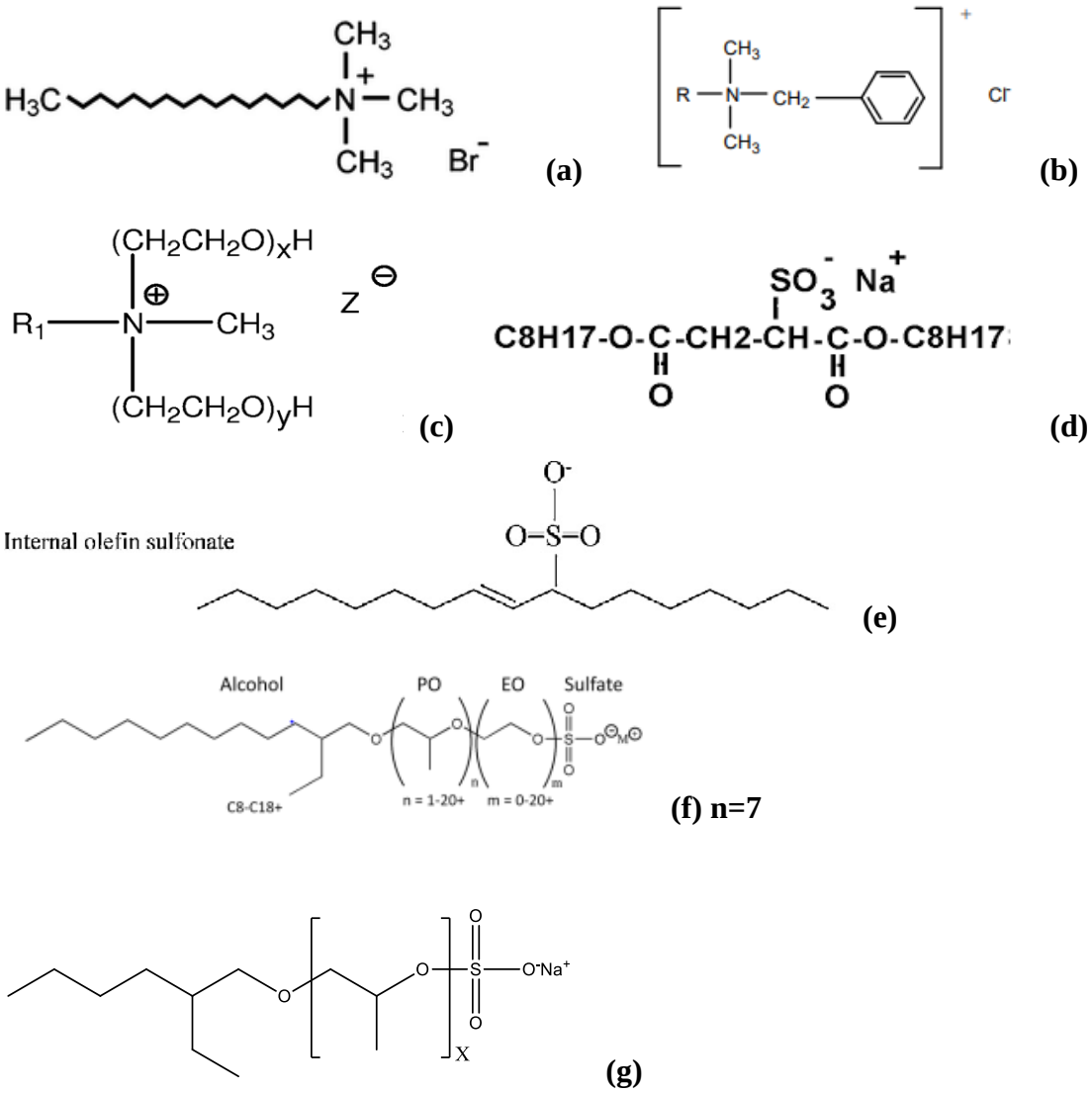

Figure 3.1. Surfactant structures for (a) DTAB (b) BTC-8358 (c) Ethoquad C/25 (d) AOSC14-16 (e) Internal Olefin Sulfonate (f) Alfoterra S23-7S-90 (g) Ethoxyhexanol-xPO-SO4

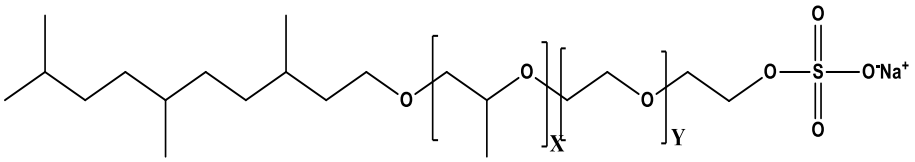

(a)

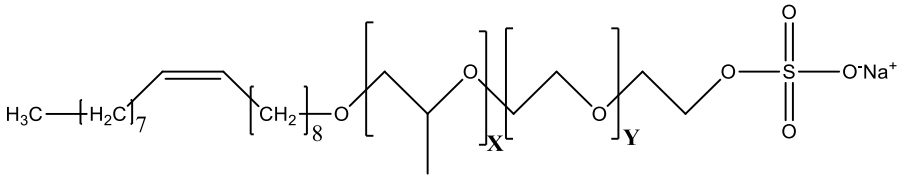

(b)

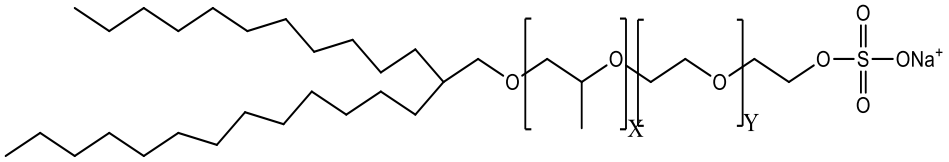

(c)

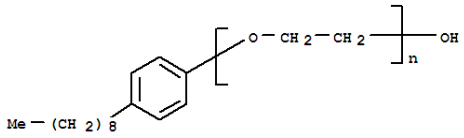

(d)

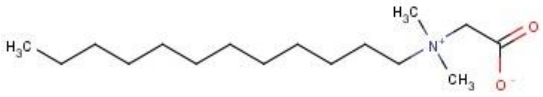

(e)

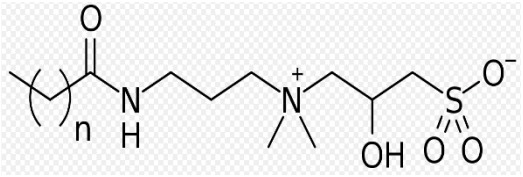

(f)

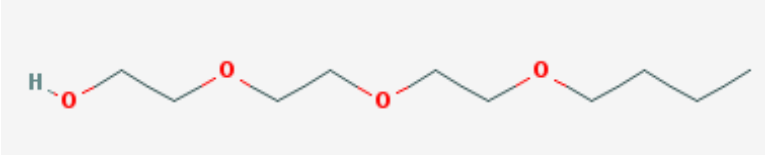

(g)

Figure 3.2. Surfactant structures for (a) TDA-xPO-yEO-SO4 (b) Oleyl-xPO-yEO-SO4 (c) Guerbet-xPO-yPO-SO4 (d)Tergitol NP-10 (e) Lauryl betaine (f) Cocoamidopropyl hydroxysultaine (g) TEGBE

3.1.4 Core Samples

Outcrop and reservoir limestone cores were used for the experiments in investigating the performances of the chemical formulations developed. At first, the chemical formulations were tested in outcrop limestone cores of similar permeability and lithology to the reservoir field cores to screen the best performing surfactant formulations. Then, the optimum surfactant formulations were tested in reservoir field cores to investigate the performance under reservoir conditions.

For single phase experiments (with no crude oil) the cores were vacuum saturated with injection brine and brine permeability was measured for each core. Chemical solutions were injected after the full characterization of the cores and effluent analysis was performed to infer useful information from the experiment.

For oil displacement experiments, the outcrop cores were first vacuum saturated with injection brine, then brine permeability was measured, and finally saturated with dead crude oil by displacement method. In case of reservoir field cores, the cores were initially saturated with a fixed amount of formation brine under vacuum followed by the injection of crude oil. This method was implemented to achieve high initial oil saturation in heterogeneous porous media. Oil permeability was measured in presence of initial oil saturation at the reservoir temperature in each of the cores. Finally, the oil saturated cores were aged at high temperature for about 3-4 weeks to make them oil-wet or intermediate-wet.

For spontaneous imbibition experiments, similar procedure to oil saturation of outcrop limestone cores was followed. The oil saturated limestone core was aged for about

4-5 weeks to make it oil-wet. The aged oil-wet carbonate core was then cut into multiple pieces for use in spontaneous imbibition experiments. For estimation of the oil recovery, each plug of the saturated core was assumed to have similar average oil and water saturation as the whole core.

3.1.5 Formation and Injection Brine

Formation and injection brine compositions were obtained from reservoir water analysis reports. Most of the carbonate reservoirs contain formation and injection brine with significant number of divalent cations. The brines were prepared with calcium chloride dihydrate, magnesium chloride hexahydrate, anhydrous sodium sulphate, and sodium chloride, obtained from Fischer Scientific^{TM} with purity greater than 99%. All brines used in this work were filtered with 0.45 microns filter paper.

3.1.6 Polymers

Various types of polymer molecules were used in this work to meet different reservoir conditions. Conventional HPAM polymers like Flopaam 3130s, 3230s and 3330s (obtained from SNF) and Aspiro P4211 and Aspiro P4251 (obtained from BASF) were used for low temperature carbonate reservoirs. Sulfonated polymers like AN125, AN125 MPM, AN125 SH, AN125 VHM, AN132, and AN132 SH (obtained from SNF), Aspiro P5421X (obtained from BASF) were investigated for use in high temperature and high salinity reservoirs. Associative polymers like DP/MM2282, DP/MM 2292, Superpusher B192 (obtained from SNF), and DP 21051 (obtained from BASF) were investigated for low permeability formations and high salinity reservoirs. Specialty synthetic polymers like

SAV 10, SAV 10 XV, and SAV 55 (obtained from SNF) were investigated for application in harsh reservoir conditions, i.e., temperatures greater than 90 ^{o}C and high salinity brines with high divalent ion content.

Conventional HPAM polymer samples (supplied as powders) were mixed in DI water to prepare a stock solution of 1 wt% (10,000 ppm) with magnetic stirrer at 250 rpm for 24 hours followed with an overhead mixer at 500 rpm for about 4 hours to achieve complete hydration of the powder samples. Sulfonated polymers, associative polymer and specialty synthetic polymers were prepared in synthetic sea water (TDS~ 45,000 ppm) and DI to prepare a stock solution of 1 wt% (10,000 ppm) with magnetic stirrer at 250 rpm for 24 hours followed with an overhead mixer at 500 rpm for about 4 hours to achieve complete hydration of the powder samples.

3.2 CHARACTERIZATION OF SURFACTANT FORMULATIONS

3.2.1 Aqueous Stability

Aqueous stability tests were performed using 20 mL clear glass vials kept in an oven that can be changed to various temperatures based on different reservoir conditions. This is the first screening test performed on the surfactants to investigate the solubility of the chemicals in the aqueous phase at the reservoir salinity and temperature. The surfactant concentration, brine salinity (including the level of hardness) and presence of alkali and polymer affects the aqueous stability of surfactant solutions at various temperature. The chemical stability of the polymers and surfactants needs to be verified before use of any sample for consistent results. The recommended shelf life for polymers are about 1 year

and surfactants about 2 years. A surfactant and brine solution is considered aqueous stable if the solution is clear, homogeneous, and contains only one phase. Slight hazy, cloudy or surfactant solutions containing precipitates might leads to phase trapping and surfactant loss through adsorption on rock surfaces. Sample aqueous stability results are shown in **Figure 3.3**. The results show tubes that are cloudy (a) and contain precipitates (b), hence not aqueous stable; and a tube that has a clear aqueous stable (c) solution. Blends of surfactants were investigated to study the synergistic effect in the improvement of the performance of the surfactant solutions. The aqueous stability samples were monitored in the oven for longer duration to observe any change in aqueous stability, especially at high temperature. Additional experiments were performed to investigate the effect of polymer on aqueous stability and surfactant-brine-polymer compatibility of the surfactant solutions at the reservoir temperatures.

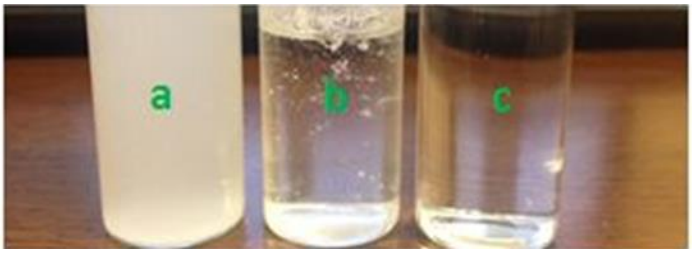

Figure 3.3. Sample aqueous stability result shows (a) a solution that is cloudy, (b) a sample that has a precipitate, and (c) a sample that is aqueous stable**.**

3.2.2 Phase Behavior Experiments

Microemulsion phase behavior experiments were performed to develop surfactant formulations that generated microemulsions with the highest solubilization ratio and lowest interfacial tension (IFT). These experiments included systematic variation of salinity,

surfactant structures and concentrations in injection brine to determine the optimum salinity with various oil concentrations for a given reservoir temperature. The total surfactant concentration in these experiments vary from 0.2-1 wt% depending on the project requirement. At times, the surfactant formulation includes cosolvents to help in the equilibration of the chemicals and reduce the viscosity of the microemulsions, but it also negatively affects the IFT of the formulation developed. These experiments help in the determination of the optimum surfactant formulations with cosolvents, if any, for chemical EOR processes.

The phase behavior experiments may include alkali like Na_2CO_3 or NaOH which depends on the EOR technology being developed, i.e., either alkali-surfactant-polymer (ASP) or surfactant-polymer (SP). For ASP chemical formulation, soda ash (Na_2CO_3) is typically used as the salinity variable in the phase behavior experiments and requires the use of a chelating agent ethylenediaminetetraacetic acid tetrasodium Salt (EDTA-4Na) to prevent any precipitation for injection brine containing divalent ions in presence of alkali. The phase behavior experiments can be described as Winsor type I, type II, and type III with variation in salinity. The salinity at which equal volumes of oil and water are solubilized in the microemulsion is defined as the optimal salinity.

All the phase behavior experiments (without polymer) were performed in 5 ml pipettes with different volumes of surfactant solution and crude oil to vary the water-oil-ratio (WOR). On the other hand, phase behavior experiments with polymer were performed in 10 ml pipettes for better handling of fluids and more mixing head space with viscous polymer solutions. After mixing the samples with surfactant solution and crude oil

vigorously for the initial few days, the pipettes were equilibrated at the reservoir temperature in the oven. The samples in each pipette were prepared with varying salinity to generate Winsor Type I, II and III samples. The level of the aqueous solution in each pipette was recorded before the addition of the crude oil and the fluid interfaces in the phase behavior experiments were recorded periodically, at intervals from 1 day to several months apart, as deemed necessary to observe equilibration. Occasionally, formation of viscous gels or microemulsions required continuous shaking for a longer period. The equilibrated fluid interfaces were recorded to estimate the volume of oil and water solubilized and calculate the interfacial tension.

A theoretical relationship between solubilization ratio and IFT developed by Huh (1979) predicted that the IFT (ɣ) is inversely proportional to the square of the solubilization ratio (σ):

$$\gamma = \frac{C}{\sigma^2}, \qquad (3.1)$$

where C is approximately 0.3 dynes/cm and the solubilization ratio (σ) is defined as the volume of oil or water solubilized divided by the volume of surfactant on a 100% active basis. Measurement of solubilization ratio from phase behavior experiments is a more accurate and effective method to estimate IFT with surfactant formulation and crude oil than measuring IFT directly using an equipment. According to Huh equation, a solubilization ratio of 10 or more corresponds to an IFT of 0.003 dynes/cm or lower.

For non-ultra-low IFT surfactant formulations, estimation of IFT from phase behavior experiments is not feasible due to the absence of microemulsions. Alternatively, the pendant drop method was used to measure the IFT between oil and aqueous solution

for low IFT surfactants using a Rame-hart goniometer as shown in **Figure 3.4**. The surfactant solution and crude oil were mixed and allowed to equilibrate at the reservoir temperature. An oil droplet was held in the aqueous phase and the axisymmetric shape analysis of the droplet was performed by DROPimage Advanced software, which calculates the IFT by fitting the drop profile with the Young-Laplace equation using a contour-fitting algorithm. The surfactant solution was maintained at the reservoir temperature by using heating pads at the bottom of the glassware containing the surfactant solution and controlling the temperature with constant voltage supply.

Figure 3.4. A snapshot of the Rame Hart Goniometer (left) and voltmeter used to control the temperature of the heating pads (right)

Working Principle of Rame-hart Goniometer

The interfacial tension between surfactant solution and crude oil was measured using a pendant drop method in the goniometer. Since the oil phase is lighter than the external aqueous phase, an upright pendant was used. After equilibration of the solutions at the reservoir temperature, a drop of crude oil large enough to be stable was equilibrated for 10 minutes. A schematic of the pendant drop method can be seen in **Figure 3.5**. The goniometer estimates about 10 measurements of the surface tension, calculated from shape

factor, radius of curvature, contact angle, area, volume etc. over 10 seconds, to generate a mean value of the surface tension for the given fluid system. The surface tension of the hanging drop was calculated using the Young-Laplace equation,

$$P = \sigma * \left(\frac{1}{r_1} + \frac{1}{r_2}\right) \quad (3.2)$$

The average surface tension was recorded. For each sample, this process was performed five times to reduce error from drop size variations.

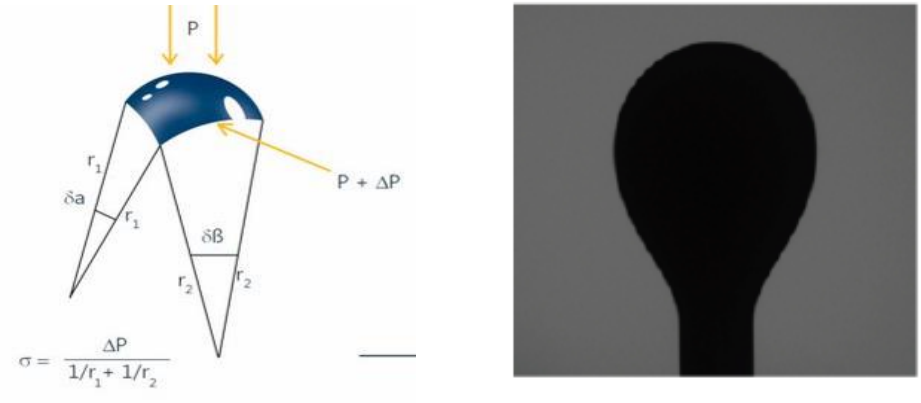

Figure 3.5. Schematic of surface tension measurements. Image obtained at http://www.kruss.de/services/education-theory/glossary/pendant-drop/.

3.2.3 Preliminary Wettability Alteration Studies

3.2.3.1 Contact Angle Experiments

Contact angle experiment, a qualitative screening experiment performed to investigate the wettability altering capabilities of the surfactant formulations, was performed on calcite plates similar in mineralogy to carbonate cores. The first step was to polish these calcite plates by a 600-mesh diamond grinding plate to make the surface - smooth and free from any contamination. Second, the polished plates were immersed in formation brine for 24 hours to achieve equilibration with the calcite surface and the ions

present in the brine, and then aged in the crude oil at high temperatures (higher than reservoir temperature) for 3-4 weeks. The next step was to ensure the oil-wetness of these aged calcite plates in the injection brine at reservoir temperature. Finally, the plates were immersed in different surfactant formulations inside an optical cell and kept at reservoir temperature for 24 hours to observe the change of wettability of the aged calcite chips. Zoomed images of the oil droplets on the plate were captured and contact angles were measured using an image analysis software. Accurate measurements of the small droplet sizes (<0.5 mm) in some formulations could not be obtained in this experiment. An alternative method to measure the change of contact angle of the oil on the calcite surface was performed using the goniometer to determine the change of the wettability of the calcite surface with time.

3.2.3.2 Spontaneous Imbibition Experiments

The wettability altering ability of a surfactant solution is further quantified by static imbibition experiments performed in optical cells. Aged oil-wet carbonate core plugs were put into imbibition cells containing injection brine overnight at the reservoir temperature. A minimal amount of oil produced during this step was a verification of initial oil-wetness of the aged carbonate core. Then the injection brine was replaced by a surfactant solution in the imbibition cell, as shown in **Figure 3.6**. A good wettability altering and low IFT surfactant solution was able to imbibe into the rock matrix by lowering the capillary entry pressure and equal volume of crude oil was displaced towards the top of the imbibition cell. The volume of oil collected was monitored for over a period and spontaneous imbibition experiments lasted from several days to several months. The rate of imbibition

of the surfactant solution into the core was dependent on the degree of low interfacial tension generated with crude oil and wettability altering capabilities based on the type of surfactant in the solution.

Figure 3.6. An imbibition cell used for spontaneous imbibition tests

3.2.4 Bulk Foam Stability

3.2.4.1 Equipment and Methodology

Bulk foam tests were performed as an initial qualitative screening experiment to investigate the foaming ability of various surfactant formulations used in oil-displacement experiments. These experiments were performed at the reservoir temperature. Two different apparatus were used for this experiment. For low temperatures, the setup consisted of transparent graduated cylinder made of acrylic (diameter: 3 cm, length: 23 cm), a rubber cork to seal the top of the cylinder with a stainless-steel sparging frit (pore size 2 μm) connected at the bottom as shown in **Figures 3.7 (a)** and **3.7 (b)**. The sparging frit, representative of the pore throats in the porous media, was used to disperse gas in the surfactant formulation. Nitrogen at a constant pressure of 5-10 psi was injected into the

bottom of the cylinder containing 30 mL of surfactant solution. The gasflow was stopped, after a significant volume of bulk foam was generated in the cylinder. After equilibration at the reservoir temperature, the decay of foam height (above the liquid phase) was measured as a function of time. Half-life, measured as the time required to reduce the foam volume to half its original volume, was observed for each surfactant solution. Each experiment was repeated at least two times and average half-lives were reported. For measurement of foam stability in the presence of oil, a similar procedure was followed. Before the gas was injected into the surfactant solution to generate foam, a small amount of crude oil (approximately 2-3 ml) was inserted at the interface to uniformly mix with the foam generated as shown in **Figure 3.7 (b)**. The foam decay in presence of crude oil was measured as a function of time to investigate the destabilizing effect of crude oil on foam half-life. For bulk foam tests at high temperature, a closed setup was used for the experiments as shown in **Figure 3.7 (c).** The setup, made of polycarbonate column, consisted of a pressure gauge to monitor the system pressure generated by the gas cap at the top of the column, a sparging frit to disperse the gas inside the surfactant solution and a separate entry point to inject the crude oil into the system for studies of foam half-life in presence of crude oil. The polycarbonate column was calibrated for volume with a manual scale to monitor the volume changes during the experiment. This setup was necessary to prevent any evaporation of surfactant solution at higher temperatures and perform experiments with high accuracy.

(a)


(b)

(c)

Figure 3.7. A snapshot of the experimental setup for bulk foam stability at low temperatures (a) no oil present (b) with oil present and at (c) high temperatures

3.2.5 Polymer Procedures

3.2.5.1 Storage

Conventional partially hydrolyzed polyacrylamide (HPAM), sulfonated PAM polymers, and hydrophobically modified associative polymers were received as a powder and stored at room temperature in vacuum containers to avoid any absorption of moisture into the polymer from the environment, which can lead to degradation of the polymer samples and inaccurate mass measurements in polymer sample preparation. Batch numbers and dates of polymer samples were catalogued for quality tracking.

3.2.5.2 Polymer Rheology

Conventional HPAM polymer stocks were prepared with 1 wt% in DI water. For complete hydration of the polymer solutions, all stock solutions were mixed overnight for 24 hours with magnetic stir bar at 250 rpm followed with 4 hours of overhead mixing at 500 rpm. The prepared stock solutions were diluted to the target concentration with the

injection brine to study the filterability of the polymer solutions. Various samples of different polymer concentration were prepared to investigate the effect of viscosity/polymer concentration on the filtration properties. Inert argon gas at 15 psi was used to perform the filtration process using hydrophilic polycarbonate membranes of 90 mm diameter size (obtained from Sterlitech). Hydrophilic polycarbonate membranes were preferably used compared to cellulose membranes from Millipore due to a well-defined pore size and higher maximum operating temperature of 140 ^{o}C. A schematic representation of the microstructure of the membranes and pore size distribution of the filter papers are shown in **Figure 3.8**. Different sizes of filter paper were used during this step based on the application and permeability of the porous media.

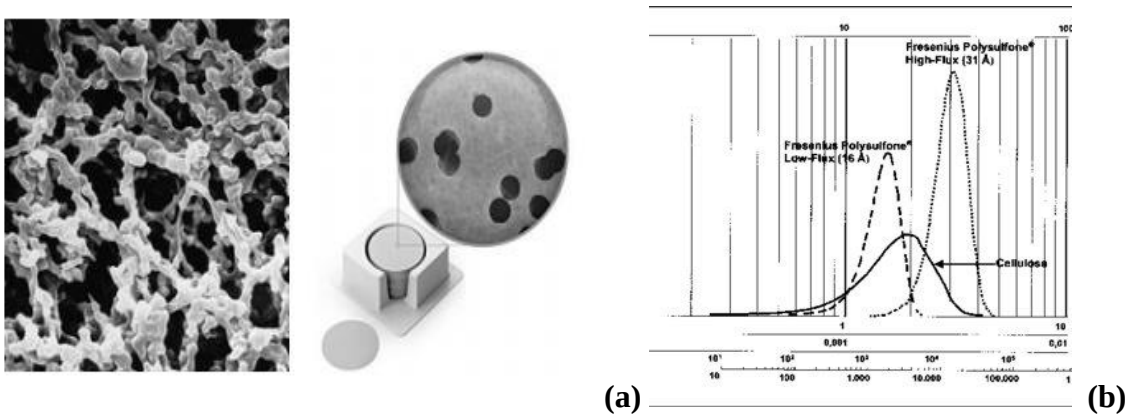

Figure 3.8. (a) Cellulose (left) and polycarbonate (right) filter microstructures (b) pore size distribution of cellulose and polysulfone membranes

Filtration was performed at a constant pressure maintained by a mechanical regulator on the argon tank, as shown in **Figure 3.9**. The pressure at the gauge needs to be monitored during the experiment to ensure that it is stable. After the polymer solution was poured into the OFITE stainless steel bell filter, the head pressure was applied. The filtered

polymer solution was collected in a graduated cylinder with elapsed time recorded for every incremental 10 mL of the solution; the volume varied in size depending on the volume of polymer to be filtered and the aggressiveness of the plugging anticipated. For a standard filtration test, greater than 200 mL of filtered solution is required, and the filtration ratio is defined as the ratio of the 180-200 mL and 60-80 mL interval times.

$$\text{F.R.} = \frac{t_{200\ mL} - t_{180\ mL}}{t_{80\ mL} - t_{60\ mL}} \quad (3.3)$$

Figure 3.9. Polymer Filtration Setup with OFITE filter bell and graduated cylinder

The standard filtration ratio test requires F.R. < 1.2 measured at 15 psig on 1.2-micron filter paper. But this value was generalized for polymer injections in sandstones and high permeability formations to represent their larger pore throats. For applications in low permeability formations, filtration tests were performed at lower sized filter papers to provide a more accurate representation of the pore throat sizes. The standard filtration ratio was calculated based on the full filtration volume of 200 mL of the solution. Alternatively,

a generalized method was developed for any volume of filtered solution by fitting the full volume time course to a second order polynomial to extract the plugging coefficient, β, as a ratio of the quadratic and linear coefficients of the fit (Driver, 2017). Note, this method ignores any non-linear plugging towards the end of the filtration. The plugging coefficient was translated into a β-estimated filtration ratio, $F.R._{\beta}$, even if the standard filtration ratio was not recorded. Based on Darcy's law, $F.R._{\beta}$ has been estimated for the filter paper of varying pore size using β, defined as the plugging parameter. The correspondence between F.R. and $F.R._{\beta}$ was very close for F.R. < 2.0 as shown in **Figure 3.10**.

$$t = aV^2 + bV + c \quad (3.4)$$

$$\beta = \frac{2*a}{b} \quad (3.5)$$

$$F.R._{\beta} = \frac{1+ \beta*190}{1+ \beta*70} \quad (3.6)$$

where t = filtration time, V= filtered volume; a, b, c = constant positive coefficients

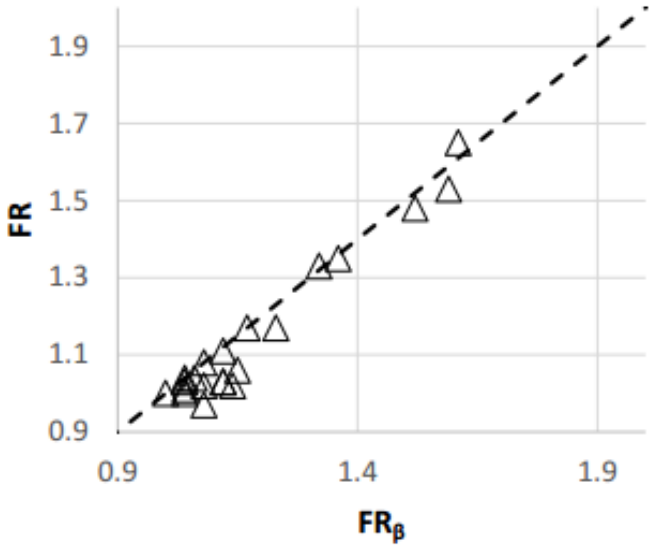

Figure 3.10. Comparison of UT filtration ratio (F.R.) and β estimated filtration ratio ($F.R._{\beta}$)

All HPAM, sulfonated polymer and associative polymer solutions that were used in core flood experiments were filtered at 15 psig head pressure. The filtered solutions were then characterized in a rheometer (obtained from TA Instruments AR G2) for its elastic properties and shear thinning properties with variation of shear rate varying from 0.01 to 100 s^{-1}.

Sulfonated and associative polymers, stock prepared with 1 wt% in sea water (TDS ~ 45,000 ppm), were diluted to the target concentrations with the injection/formation brine and surfactants to study the filtration properties of the solution. A similar procedure was followed for measuring the $F.R._{\beta}$ as mentioned above. In addition, thermal stability tests were performed on these polymer solutions to investigate their temperature tolerance and salinity tolerance at higher temperatures. Multiple solutions of varying polymer concentration and salinity were prepared in sealed glass containers, after removal of any dissolved oxygen from the solution, aged at the reservoir temperature and monitored for a longer period.

3.2.5.3 Polymer Pretreatment and Processing

A novel method was developed to tailor the molecular size distribution of the high molecular weight polymer molecules for successful transport through low permeability formations. Polymer solutions can be shear degraded using any number of devices, including overhead mixers, pumps/valves and orifices, and more commonly laboratory blenders. Hence, each device must be calibrated for the duration of shearing (or the number of passages for a valve) and the shearing strength i.e. speed setting or flow rate for better

quality control. All these mechanical degradation steps are additive and cumulative in the final characterization of the polymer solutions.

For laboratory studies, the polymer stock solutions with 1 wt% polymer concentration was mechanically sheared in a Waring industrial blender at 18,000 rpm for varying amounts of time to achieve the desired shear degradation. The temporal decay of the Newtonian plateau viscosity was plotted and interpolated to target a particular viscosity in future batches. The best practice would be to choose a shearing device and speed setting that requires relatively long shearing time (~ 1 min) to degrade the polymer solutions by the desired amount. Studies have shown that this process is significantly dependent on the total mass of the polymer stock solution used during the shear degradation. Hence, mass of the polymer solution in the blender was standardized to 200 g per batch, as the shearing time is essentially shared within the volume of the blender between solution near the blades and that lies above the blades. Other factors that play a significant role in the mechanical shear degradation process are polymer type or molecular weight, concentration, salinity, hardness, or degree of hydrolysis. Thus, an optimization process is essential to standardize this process for comparative study between different polymer molecules. All the shear degradation experiments were performed at ambient temperature. This shear degradation technique helps to break the high molecular weight chains and reduce the polydispersity of the polymer samples, thus improving the injectivity in tight formations, as shown in **Figure 2.16**. Samples were taken out at every shearing time to estimate the viscosity loss, modified size distribution using DLS and to investigate the filtration properties of the shear degraded samples through small sized filter papers.

Samples were prepared from the sheared stock solution with varying polymer concentration in the target brine to study the effect of shearing time on polymer filtration through filter papers. Each of the samples with different concentrations of polymer underwent a series filtration test to investigate the filtration properties along with their elastic properties. For applications in low permeability formations (< 30 mD), successive filtration was performed at 15 psig starting at 0.4 microns filter paper and then the product of each step was used to perform the next filtration. The series filtration was performed with 0.4, 0.2, 0.1, 0.2 and 0.4 microns sequentially. This strategy was effectively designed to study the filtration properties through small pore throats (approximately 0.1 microns) and its effect on tailor designing the polymer molecular size distribution, as shown in **Figure 2.17**. Small samples were taken out between each filtration steps to further investigate any possible viscosity loss during aggressive filtration and re-modification of polymer size distribution.

3.2.6 Rheological Measurements

3.2.6.1 Rheometer

The AR G2 Magnetic Bearing Rheometer from TA Instruments was used for the measurement of the bulk rheological properties (**Figure 3.11**). This instrument is specially equipped with low torque performance important for characterization of lightly structured materials. This equipment is designed for fluid rheology testing both in dynamic and steady state conditions. During the measurements, the motor generates either a dynamic or steady shear strain deformation, and the transducer detects the responded torques. A temperature-

controlled water circulation apparatus maintains the sample temperature as specified by the user on a Peltier Plate Temperature system.

In this study, a standard plate geometry of 40 mm diameter with 2^{o} cone was used on a flat plate for polymer solutions both dynamic and steady state tests with a sample size of 2 ml in volume. In addition, an insulating thermal cover was used to prevent vaporization of samples at high temperatures.

In the dynamic measurements, the rheometer measures the strain and torque, which allows for calculation of storage modulus (G') and loss modulus (G''). During the steady state process, rotational rate, torque and normal force can be measured, which can provide estimation of viscosity as a function of shear rate. Two different types of dynamic measurements were performed to measure the polymer rheological properties: dynamic strain sweep test and dynamic frequency sweep test. The steady state flow sweep rate is used for polymer viscosity measurements with varying shear rates.

Figure 3.11. TA Instruments AR-G2 rheometer (left) and standard geometry and thermal insulation cover (right)

Viscosity measurements of the polymer samples were taken at every step to record the viscosity loss due to shear degradation. Each measurement was taken at 25 ^{o}C using an AR-G2 rheometer in the shear rate range 0.01 – 100 s^{-1}. Shear viscosity measurements at ultra-low shear rates were used to estimate the intrinsic viscosity and predict the modified MW of the shear degraded polymer stock using Mark Howink relationship. The degradation of polymer solution corresponding the extent of viscosity loss, η_{loss} was calculated using the following expression,

$$\eta_{loss} = \frac{\eta_0 - \eta_{deg}}{\eta_0 - \eta_{solvent}} \; X \; 100 \qquad (3.7)$$

where η_0 is the viscosity of the non- degraded solution, $\boldsymbol{\eta_{deg}}$ is the viscosity of the degraded solution, and $\boldsymbol{\eta_{solvent}}$ is the water viscosity (taken as 1 cP at 25 ^{o}C). Because of

poor sensitivity of the viscometer at low shear rates, measurements at 10 s^{-1} (more representative of the shear rates experienced in porous media flow) were taken as a reference.

3.2.6.2 Dynamic Light Scattering Method

Dynamic light scattering (DLS) is a technique that can be used to determine the molecular size distribution of small particles in suspension or polymers in solution. Under the scope of DLS, temporal fluctuations can be analyzed by means of the intensity or photon auto-correlation function (also known as photon correlation frequency). DelsaNano C is a photon correlation spectroscopy (PCS) instrument, which determines particle size by measuring the rate of fluctuations in laser light intensity scattered by particles as they diffuse through a fluid (**Figure 3.12**). This equipment was used to characterize the different polymer solutions to study the effect on their molecular size distribution through mechanical shear degradation and series filtration process. The DelsaNano series is capable of measuring particles as small as 6 Angstrom and as large as 7 microns with molecular weight as small as 267 Dalton in a concentration range from 0.001% to 40%.

The observed intensity of the scattered light is a result of the interference of the light reflected by each element; hence, for particles in motion the fluctuations in time of the scattered light will be observed. Due to random Brownian motion the scattered intensity fluctuations are random as well. The fluctuations are rapid for smaller sized particles and slower for larger particles and can be analysed using the autocorrelation function. The calculation of the autocorrelation function $g^{(2)}(\tau)$ is one of the ways to analyze random intensity fluctuations and is expressed as follows:

$$g^{(2)}(\tau) = \frac{<I(t).\ I(t+\tau)>}{<I(t)>^2} \quad (3.8)$$

where $g^{(2)}(\tau)$ is the normalized intensity autocorrelation function, I(t) is the intensity detected at time t, τ is the delay time, $< I(t) >^2$ is the normalization factor, and < > is the time average.

For particles in Brownian motion, the normalized intensity autocorrelation function $g^{(2)}(\tau)$ is a sum of exponential functions. Hence, it can be estimated from single exponential function $g^{(1)}(\tau)$ by using the Siegert relationship:

$$g^{(2)}(\tau) = | g^{(1)}(\tau) |^2 + 1 \quad (3.9)$$

The single exponential function $g^{(1)}(\Gamma)$ can be calculated from the following expressions:

$$g^{(1)}(\Gamma) = B.\ \exp(-\Gamma\ \tau) \quad (3.10)$$

$$\Gamma = Dq \quad (3.11)$$

where B is a constant dependent on instrumental parameters, Γ is the decay constant proportional to the diffusion coefficient, D is the diffusion coefficient and q is the magnitude of the scattering vector.

For small particles the autocorrelation function is a rapidly decaying exponential function with a large decay constant, whereas for large particles the exponential decays more slowly. For a mixture of particles (polydisperse), the intensity fluctuations will vary due to different diffusion coefficients; therefore, autocorrelation function will be a sum of the exponentials with different decay constants:

$$g^{(1)}(\Gamma) = B\ \Sigma\ (A\ \exp(-\Gamma\ \tau) \quad (3.12)$$

where A is the relative intensity of the light scattered by a particle with decay constant Γ and is related to relative amount of such particles. For monodisperse particles, the logarithm of $g^{(1)}(\tau)$ will become a straight line and for polydisperse samples, the logarithm of $g^{(1)}(\tau)$ will exhibit a curvature line.

Initial tests were run at varying polymer concentrations between 200 and 1000 ppm of FP 3330s to study the effect of polymer concentration on aggregate formation and its effect on polymer size distribution. Polymer aggregates at higher concentrations seemed to interfere with the signal response and hence 500 ppm was chosen as the standard concentration for all polymer samples henceforth. Each shear degraded stock sample and samples taken between each filtration steps were diluted to 500 ppm in their respective brines to estimate the polymer size distribution using DelsaNano analyzer. The photon correlation spectroscopy (PCS) directly measures intensity (weighted) distributions as intensity histograms. The software delivers reports with normalized intensity distribution (interpreted as normalized size distribution), cumulative intensity distribution (interpreted as cumulative size distribution), and volume and number distribution. Hence, normalized intensity distribution from DLS was used to infer useful knowledge on polymer size distribution and modification of MW distribution due to shear degradation. Multiple runs were also performed for each sample to ensure repeatability and reproducibility of the data generated from the software. All these size analysis measurements were also performed at ambient temperature.

Figure 3.12. DelsaNano C Particle Analyzer used for DLS measurement

3.2.6.3 Mercury Injection Capillary Pressure (MICP)

Pore throat distribution of the low permeability carbonate rocks was obtained through mercury injection test where drainage and imbibition experiments were performed to estimate the porosity of the core sample and incremental fraction of each pore throat diameter. Different carbonate core samples of similar permeability were found to have very different pore throat distribution depending on the pore network and the heterogeneity of the core samples. The incremental PV and cumulative PV estimations during the test provides an insight on the fraction of pores below a critical pore throat diameter. Finally, a normalized saturation plot is obtained from the incremental PV measurements to compare the pore throat distribution to the polymer size distribution obtained using DLS method. A polymer sample with minimum overlap between the polymer size distribution and the pore throat distribution was found to be the necessary condition for successful injection in low permeability carbonate cores.

3.3 COREFLOOD SETUP AND CORE PREPARATION

3.3.1 Core Preparation

Mostly all limestone cores used for core flood experiments were 1.5 inches in diameter and 12 inches long, with an exception in few of the reservoir core flood experiments. The outcrop core samples were dried in an oven at a high temperature overnight before use. The dry weight, length and diameter were measured before laminating with a FEP heat shrink tubing (Geophysical Supply Company, Houston, TX) to prevent fluids from flowing out of the core along the length of the core. The core was then placed in the core holder, and an overburden pressure of at least 700 psi was applied; higher for high reservoir working pressure.

3.3.2 Coreflood Equipments

Hastelloy Accumulators

Accumulators made of Hastelloy material with 1L capacity was used to store the oil and surfactant and equilibrate at the reservoir temperature before injecting into the core holder. This special material is used for any prevention against corrosive fluids used during the process. Water is injected from the pump into the bottom of the accumulator, where the floating piston containing an o-ring displaces the injection fluid out of the accumulator and into the core holder through an inline filter of 0.5 μm.

Syringe Pumps

The Teledyne™ ISCO 500D syringe pumps were used during the core flood experiments for the purpose of maintaining overburden pressure at high temperatures,

injecting the crude oil and aqueous phase into the core holder. The pump is controlled with a controller (200 ml/min max flow rate, $\pm$ 0.001 ml/min precision) capable of constant flow or constant pressure operation.

Core Holder

A steel core holder made of Hastelloy manufactured by Phoenix Instruments was used to transport the cores. The cores were loaded into a 1.5" diameter core holder. The core holder was mounted vertically, and fluids were injected from the top for gaseous phase and from the bottom for the aqueous phase. Tap water was used as an overburden fluid to compress and seal the Viton rubber sleeve in which the core was placed. The average total pressure drop across the core was measured using a pressure transducer connected to the inlet and outlet of the core holder. In few experiments, a core holder with tapped rubber sleeve was used that facilitated sectional pressure drop measurements along the core in the direction of flow of fluids, as shown in **Figure 3.13**. Pressure around the sleeve must be maintained over 700 psi (higher at times depending on the reservoir pressure) to compress the sleeve and provide a good seal between the sleeve and core. It is important to ensure that the core holder is leak proof after testing for longer duration at a stable reservoir temperature.

Figure 3.13. Coreholder used for coreflood experiments at various reservoir temperatures

Pressure Transducer System

Differential pressure transducers (Rosemount) were used to record fluid pressure drops across the core during the core flood experiments. Multiple transducers were used for sectional pressure drop and absolute pressure measurements, as shown in **Figure 3.14**. These transducers measure the deflection of an internal membrane that has a finite physical pressure tolerance. Within this tolerant limit, the current response of the transducer can be set to an arbitrary sensitivity for optimal measurement. The transducer records the pressure drop as a voltage, sends the voltage to a Data Acquisition Card connected to DATAQ, which records the voltages in tabular form in LabView. Pressure transducers are calibrated with a specialized air pressure machine (General Electric, Druck PACE6000) which generates a linear regression of voltage to pressure. This calibration curve is then used to

convert the recorded voltages in the transducer to an estimated pressure drop across the core during the experiments.

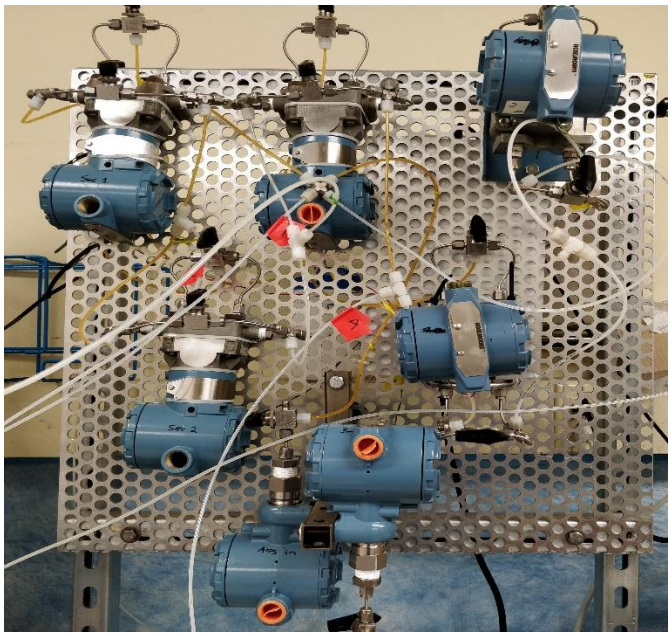

Figure 3.14. Pressure transducer system to record sectional pressure drops using Labview software

Backpressure Regulator (BPR)

Back pressure is used in some floods to improve communication between the transducer and the core, to prevent vaporization of fluids at high temperature and more importantly to maintain the reservoir working pressure for gas injection experiments. For low pressure experiments, a mechanical back pressure regulator (Swagelok) was installed on the effluent line. For high pressure experiments, a pneumatic backpressure regulator (Equilibar) was installed on the effluent line. In this case, backpressure regulator was set to 500-600 psi (to represent the reservoir pressure conditions). Flow is only transmitted through the BPR once the pressure inside the BPR rises above the value set at the head.

The pneumatic BPRs are available with different pressure rating diaphragms that can withstand variable pressure ranges depending on the need of the experiments. Note, for gas injection experiments it is critical to use zero flow BPRs to ensure that no fluid flows below the set pressure at the pneumatic valve of the BPR.

Gas Cylinders

Methane gas of ultra-high purity (greater than 99.9%) from Praxair was used for gas injection into the core for gas injection experiments. Nitrogen gas of high purity from Praxair was used for maintaining the head pressure on the BPR using a mechanical regulator with gauge and used for bulk foam experiments. Carbon dioxide gas of ultra-high purity was used during the vacuum-CO_2 alternating step before fluid saturation of the core.

Sand pack

A 6-inch long sand pack, from Autoclave, was made using carbonate sand packed into a 0.6-inch metal tube. Surfactant solution and methane gas were co-injected into the top of the sand pack to form pre-generated foam before entering the core holder.

Glass Columns

For experiments performed under high temperature and high salinity conditions, accumulators faced challenges of rust formation and degradation of the chemicals stored inside the containers at reservoir temperature. Hence, for low pressure experiments, an alternative solution to accumulators was use of glass columns (obtained from Kimble Chase) with additional metal frames to account for thermal expansion of the end pieces and prevent any fluid leakage at high temperatures. The glass columns were modified with

the metal frames to meet our experimental requirements and can withstand a maximum of 50-60 psig depending on the volume of the column, as shown in **Figure 3.15**. Instead of piston displacement, mineral oil (from the syringe pumps) was used to displace the chemical solutions inside the columns from the top since mineral oil was lighter than aqueous phase and was insoluble with water.

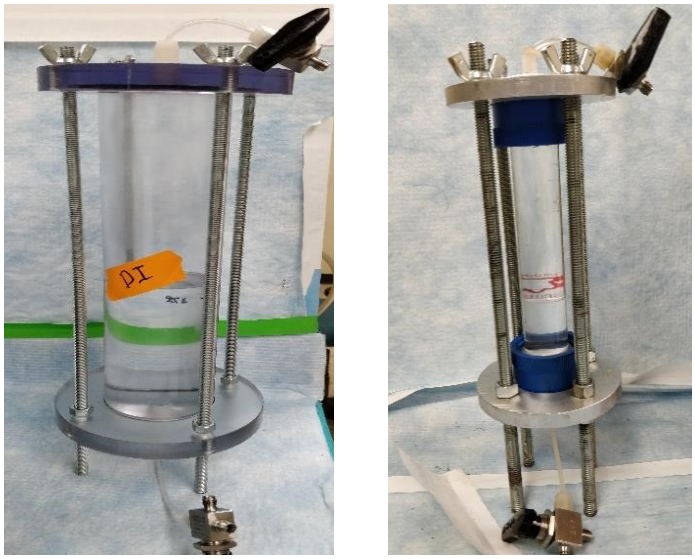

Figure 3.15. Glass columns used to inject chemical solutions during low pressure core floods

Fractional Collector

Effluent fluids were collected in regular interval using an automatic fractional collector that can collect samples in equal intervals of any desired volume when experiments are performed at a constant fluid rate. This equipment facilitates in investigating the complete fluid analysis after a core flood experiment is performed in context to oil cut, chemical breakthrough, water cut, effluent salinity, pH and viscosity profile during injection of viscous solutions for mobility control experiments. The

fractional collector is equipped to handle 15 mL graduated centrifuge plastic tubes for collection of effluent samples.

Mass Flow Controller

This device is used to accurately control the gas injection for foam injection experiments at high temperature and high-pressure conditions. Bronkhorst EL-FLOW Select series mass flow meter was used for the gas injection experiments in the laboratory, as shown in **Figure 3.16**. This instrument can measure very small flow rates in the order of 0.014 – 7 ml/min at standard conditions with pressure rating between vacuum and 400 bar. This device is equipped with digital pc-board, offering high accuracy, excellent temperature stability and fast response times. It also contains a RS-232 output that can be connected to a computer to operate the device using the software. The mass flow controller is capable of handling various gas types with the possibility of 8 different calibration curves in-built in the device.

The FLOWTUNE software is used to select the fluids for use and the working pressure and temperature conditions. This is the first step to ensure the right fluid type is selected for appropriate calibration and sensitivity of the device. The calibrated fluids for the device can be selected from a drop down based on the requirement. The FLOWDDE software is used to establish the connection of the device to the computer through RS 232 adapter. This step is critical for proper communication between the software and the mass flow controller. THE FLOWPLOT software is a visual interface with the capability of adjustment to the gas injection rate for the experiments. Based on the setpoint value of the valve opening the gas flow rate can be adjusted at the normal conditions. The PVT software

should be used to calculate the ratio of density to compensate for the desired flow rate at the reservoir conditions. This software also provides a real time monitoring of the actual flow rate based on pressure fluctuations and the target flow rate.

Figure 3.16. Mass Flow Controller EL-FLOW Select from Bronkhorst

3.3.3 Core flood Set-Up

The different types of equipment discussed in section 3.3.2 were assembled together to complete a core flood set-up. In this study, several experiments were performed at low and high reservoir working pressure. Separate core flood setups were used for these experiments. For low pressure experiments, a simplified set-up was used, as shown in **Figure 3.17**, which did not include any gas injection experiments. On the other hand, for high pressure gas injection experiments, a more elaborate set-up was used, as shown in **Figure 3.18**. The core holder, accumulators containing the crude oil and brine were placed

inside a convection oven set at reservoir temperature. The glass columns containing the chemical slugs were also placed inside the oven to equilibrate at the reservoir temperature. The low pressure BPR on the effluent line and the fractional collector to collect the effluent samples at regular intervals was placed outside the oven. For gas injection experiments, flow rate of the methane gas was controlled through a Bronkhorst mass flow controller at the room temperature. The Bronkhorst advanced flow software accounted for the thermal expansion of the gas at the reservoir temperature to estimate the accurate gas flow rate at the reservoir temperature. The methane gas was passed through 20 feet of metal tubing, allowing the gas to heat to reservoir temperature before entering the core. The surfactant was stored in an accumulator in the oven and was injected into the sand pack or directly into the core depending on the design of the experiments. The effluent fluid and methane gas are collected outside the oven. The system pressure was maintained using BPR outside the oven on the effluent line of the core holder. A visual cell was used at the sand pack outlet and before the core inlet to verify foam generation before injection into the core.

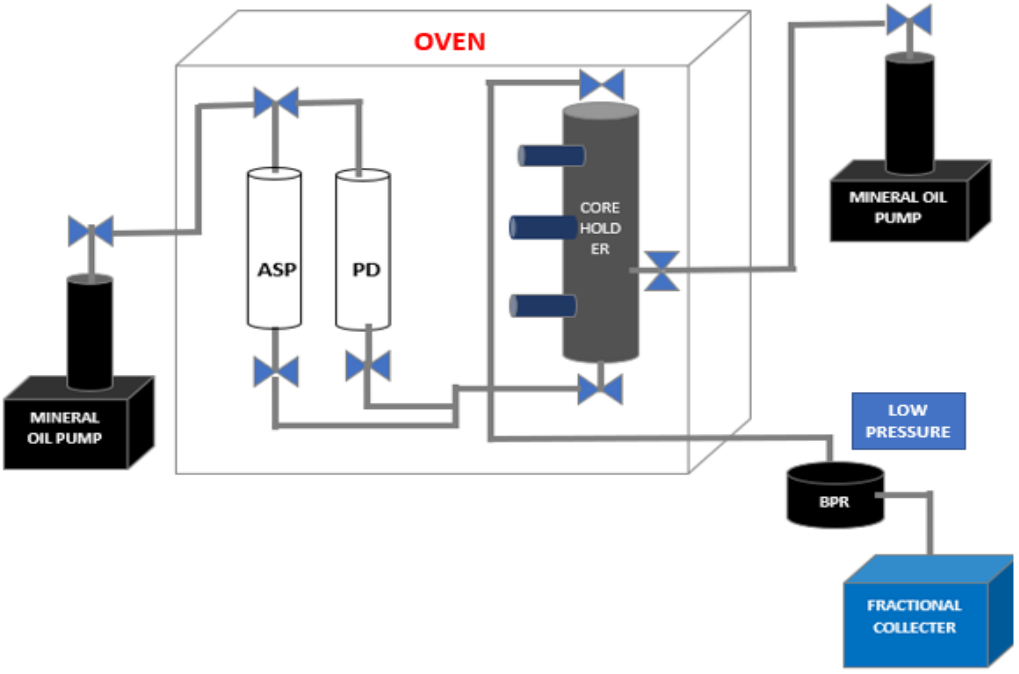

Figure 3.17. Low Pressure Core flood setup for ASP/SP corefloods

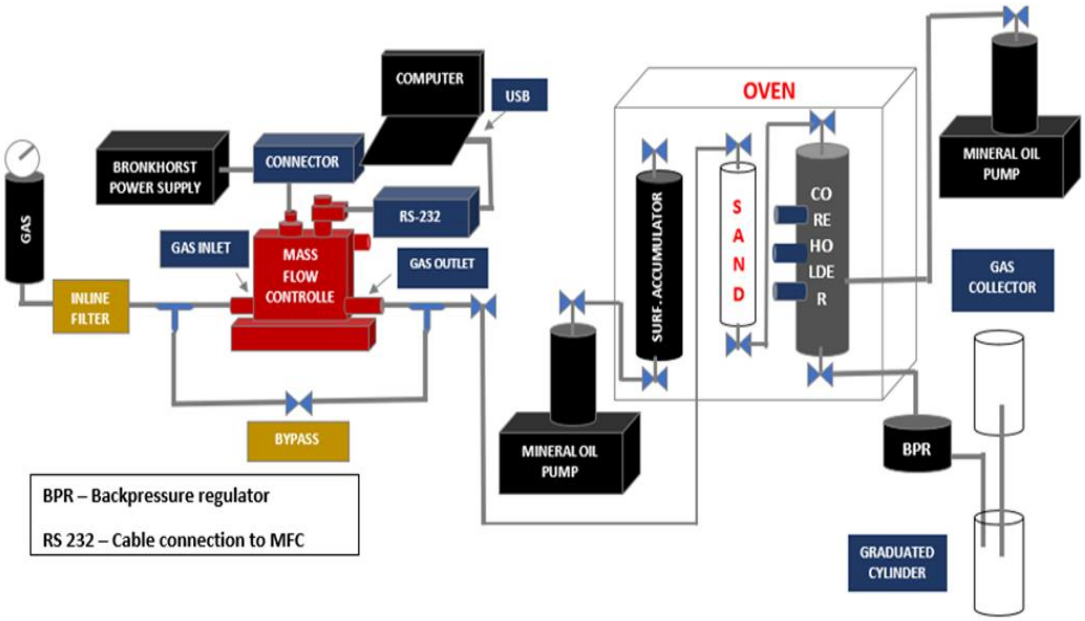

Figure 3.18. High Pressure Core flood setup for gas injection experiments

3.3.4 Core Sample Measurements

Air Porosity

One of the techniques to estimate the pore volume of the porous media is through air porosity measurements. Note, this experiment is performed with compressible fluids and requires moderate pressure and longer time to reach steady state. During this process, one of the ISCO pumps is filled with air from the air supply line, compressed to higher pressure and connected to the core holder containing the core. A digital pressure gauge and a valve were placed in between the pump and the core holder to isolate them into two different systems. One system consisted of the core holder containing the core and isolated from the atmosphere with closed valves and the other system consisted of the pump with compressed air inside. After initial recordings of the pump volume and pressure reading in the pressure gauge, the valve connecting the pump and core holder was opened. New pressure was recorded after reaching equilibrium with the two systems combined together. Then, an additional volume of air was injected into the core, the new gauge pressure and the new pump volume was recorded. Using Boyle's Law, the volume of the void space can be calculated as follows:

$$(P_1V_1 + P_2V_2)_i = (P_1V_1 + P_2V_2)_f \quad (3.13)$$

Brine Saturation by Vacuum

After air porosity was measured, the core was then vacuum saturated with injection brine. At first, core was connected to a vacuum pump. Alternating injection of CO_2 at 50 psi and vacuuming were performed for couple of times to displace any air trapped inside

the porous medium. Finally, the core was vacuumed for few hours to ensure all trapped gas was removed. After the core was vacuumed, brine was injected into the core at a constant pressure of 350 psi. Pore volume was estimated by change in pump volume during this saturation process after excluding the dead volume of the core holder.

Pore Volume Calculations

The estimation of the pore volume of the core from air porosity measurements and brine saturation was confirmed using a tracer test. During this step, a brine of higher salinity than the injection brine was injected into the core for 2-3 PVs at a constant flow rate. The effluent was collected in 5 mL samples at regular intervals, and the salinity was measured using a refractometer, shown in **Figure 3.19**. The measured brine salinities were normalized and plotted with respect to the injected volume. For carbonate cores which are mostly heterogeneous, the pore volume was estimated from the area enclosed above the normalized salinity graph, after excluding the dead volume. This estimated value from the effluent salinity profile is compared to the calculated values from the brine saturation process.

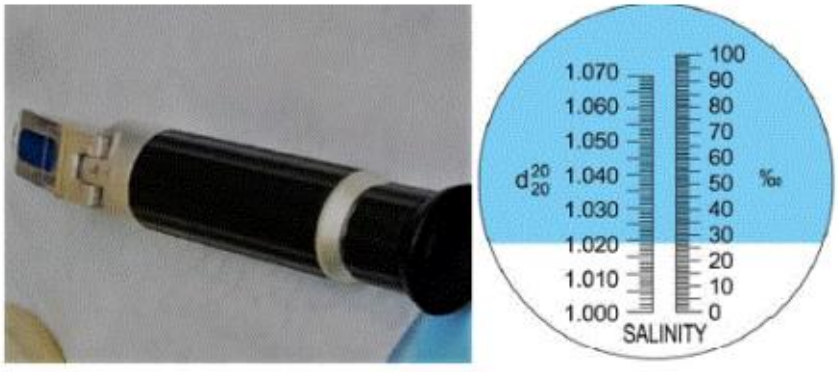

Figure 3.19. Refractometer and readings for salinity measurements

Brine Permeability

The injection brine was injected into the core at variable rates. The steady state pressure was recorded for each flow rate at room temperature condition. The average brine permeability was calculated using Darcy's Law and from the slope of a plot of pressure versus rate.

$$q = \frac{-kA\Delta P}{\mu L} \tag{3.14}$$

where q is the flow rate of the brine, A is the cross-sectional area of the core, ΔP is the pressure drop across the core, μ is the viscosity of the brine, and L is the length of the core. Additionally, in some experiments, some sectional pressure drops and permeability were also measured.

Initial Oil Saturation

Before this step was performed, the core holder containing the core was heated up to the reservoir temperature and equilibrated. Once overburden pressure was stabilized, crude oil from the accumulator was injected into the core, after passing through an inline filter of 0.5 microns, at constant pressure of 400 psi displacing the brine that was previously in the core. Oil was injected until no more water was produced. The oil saturation was estimated using the equation below,

$$S_{oi} = \frac{V_{water\ produced}}{V_P} \tag{3.15}$$

where S_{oi} is the initial oil saturation, $V_{water\ produced}$ is the volume of water that is displaced by the oil and V_P is the pore volume of the core.

Aging

After the core was saturated with oil, it was placed in a sealed glass container, capable of withstanding high temperature, and filled with crude oil. The container was placed in an oven at 80^{o}C for 3-4 weeks, to ensure that the core changed from water wet to oil wet.

Effective Oil Permeability

After aging, the carbonate cores were placed into the core holder and the effective oil permeability was measured at the reservoir temperature. At first, fresh crude oil was injected to flush out the aged oil. Then, oil was injected at variable flow rates and the steady state pressure drop across the core was recorded for each rate at reservoir temperature. The effective average oil permeability was calculated using Darcy's law with respect to oil (at connate water saturation) using the equation below,

$$q_o = \frac{-k_o A \Delta P}{\mu_o L} \tag{3.16}$$

where k_o is the effective oil permeability, q_o is the flow rate of the oil, A is the cross-sectional area of the core, ΔP is the pressure drop across the core, L is the length of the core, and μ_o is the viscosity of the oil at reservoir temperature.

Thus, oil relative permeability was estimated from the ratio of the measured oil permeability and the absolute brine permeability measured before aging the carbonate cores.

$$kro = \frac{k_{oil}}{k_{brine}} \tag{3.17}$$

3.3.5 Core flood Injection Procedures

Several types of core floods were performed in this study. The first set of core floods performed were in the absence of oil i.e., dynamic adsorption, polymer injectivity and foam flow experiments. These core floods were designed to investigate the performance of the chemicals used in the processes in terms of surfactant loss to carbonate rock surface and mobility control mechanism. The second type of core floods performed were oil displacement experiments i.e., foam injection, alkali-surfactant-polymer (ASP) and surfactant-polymer (SP) experiments to investigate the performance of these chemical formulations on improving oil recovery in carbonate rocks.

3.3.5.1 Dynamic Adsorption Experiment

Dynamic adsorption experiment was performed in outcrop limestone cores of diameter 1.5 inches and length 12 inches at the reservoir temperature. After brine saturation of the cores, the surfactant formulation was injected at 1 ft/D for about 2-3 PVs and the steady-state pressure drop across the rock was monitored. This step was followed with another 2-3 PVs injection of reservoir brine to measure desorption of surfactants and the final surfactant retention on the carbonate rock surfaces. During each of these steps, effluent fluid was collected at every 0.1 PV and samples were analyzed in the HPLC to measure the effluent surfactant concentration. The adsorption of the surfactant (q) was expressed as mg/g and calculated using the following equation,

$$q = \frac{m_{solution} * (C_o - C)}{m_{carbonate}} X\ 10^{-3} \qquad (3.18)$$

where q is the adsorption (mg/g), Co is the initial surfactant concentration (ppm), C is the final surfactant concentration (ppm), $m_{solution}$ is the mass of the surfactant solution (g), and $m_{carbonate}$ is the mass of the dry limestone outcrop core (g). Alternatively, the surfactant adsorption was also calculated from the delay in surfactant production profile to the tracer test profile performed during the brine saturation process of the carbonate core. The normalized concentration of surfactants in the effluent samples and the normalized tracer test are compared in a single plot and the area enclosed between these two graphs provides an estimation of adsorbed surfactant volume and mass. Hence, surfactant adsorption can be calculated from the loss in surfactant volume.

3.3.5.2 Polymer Injectivity Experiment

On comparison of the information obtained from MICP and DLS methods, the polymer sample after optimum shear degradation was prepared in target brine with the desired polymer concentration. This solution was then filtered using the aggressive filtration technique to ensure good filterability before injection in porous media. The final filtered solution was then degassed for couple of hours to ensure negligible oxygen to prevent any oxidative degradation during the coreflood experiments. The outcrop limestone cores were vacuum saturated with 2% KCl at first followed with a tracer test using injection brine at a higher salinity. The pore volume and heterogeneity of the porous medium were estimated from the tracer test. Polymer solutions were then injected at 1 ft/D for 3-4 PVs until steady state pressure drops were obtained at the reservoir temperatures. Effluent samples were collected at regular intervals to estimate the polymer breakthrough and viscosities for any possible degradation loss during the experiment. The resistance

factor (RF) and permeability reduction (Rk) were estimated at the injected velocity and measured shear viscosity using a viscometer. At the end of the polymer injection, an exhaustive waterflood of about 5-6 PVs was performed to estimate the residual resistance factor (RRF).

For polymer injectivity experiments at high temperatures, a thermal protection package consisting of 1000 ppm of sodium hydrosulfite and 500 ppm diethyl thiourea was added to the polymer solution during the degassing process. The oxidation reduction potential (ORP) of the treated polymer solution was measured using Oaktron Waterproof ORPTestr@10 (**Figure 3.20**) before injection to ensure the reduced state of the solution i.e., ORP below -400R mV. This step is essential to prevent thermal degradation of polymer inside the porous medium due to presence of any iron.

Figure 3.20. Oaktron Waterproof ORKTestr@10 for ORP measurements

3.3.5.3 Foam Flow Experiments

Foam flow experiments, in the absence of crude oil, were performed with the surfactant formulations screened from bulk stability tests. This step was performed to

investigate the foam strength of the surfactant formulation in a porous media and the mobility reduction ability due to generation of foam. First, the core was vacuum saturated with injection brine and brine permeability was measured. Then, about 8-10 PVs of brine and methane gas at 80% quality were co-injected at 4 ft/day into the core until the pressure drop across the core was stabilized. In some cases, this step was considered as the base case for estimation of mobility reduction. Finally, methane and surfactant solution at 80% quality were co-injected from the top into a high permeability sand pack to pre-generate foam and the effluent from the bottom of the sand pack was injected into the core. Additionally, a view cell was inserted between the sand pack and core inlet to visually observe the stable foam generated in the sand pack. This pre-generated foam was injected at 4 ft/day into the core from the top of the core holder for about 10 PVs until the total pressure drop across the core was stabilized (assuming surfactant adsorption had reached equilibrium). The pressure drop across the core was recorded with a pressure transducer system at small increments of time. Mobility reduction factor (MRF) is defined as the ratio of the steady-state pressure drop in presence of foam to the steady-state pressure drop in the base case (brine and gas at the same quality without any surfactant), i.e.,

$$\boldsymbol{MRF} = \frac{\Delta P_{surf+gas}}{\Delta P_{brine+gas}} \quad . \tag{3.19}$$

Alternatively, a surfactant pre-flush of 2 PVs was injected into the core after saturating with injection brine and pressure drops were recorded. Then, about 10 PVs of methane and surfactant solution at 80% foam quality (volumetric gas injection percentage) were co-injected into a sand pack to pre-generate foam and the effluent from the sand pack

was injected into the top of the core. Mobility reduction factor (MRF), in this case, is defined as the ratio of the steady-state pressure drop in the presence of foam to the pressure drop during surfactant solution injection, i.e.,

$$\text{MRF} = \frac{\Delta P_{surf+gas}}{\Delta P_{surfactant}} \quad . \tag{3.20}$$

Additional experiments were performed at the reservoir temperature to estimate the transition foam quality and effect of foam injection velocity on foam rheology in carbonate rocks. First, a set of experiments were performed by varying foam quality at a fixed injection velocity, and then more experiments were performed varying foam injection velocity at the transition foam quality. Note, multiple experiments were performed with and without cleaning of core at the end of each step to investigate the effect of hysteresis on the performance of foam in porous media. For cleaning of the core, at the end of each step several PVs of methanol and injection brine mixture was injected till no foam was produced followed with several PVs of injection brine. Then, brine permeability was measured to ensure no significant change in permeability between each step of foam injection. Apparent foam viscosities (μ_{af}) generated at steady state in these foam flow experiments were calculated based on the expression (assuming absolute permeability of the porous medium remains constant),

$$\mu_{af} = -\frac{\mathbf{k}\,.\,\nabla \mathbf{P}}{\mathbf{u_T}} = -\frac{\mathbf{k}\,.\,\nabla \mathbf{P}}{\mathbf{u_W} + \mathbf{u_G}} \tag{3.21}$$

where ∇P is the pressure gradient at the steady state condition and u_T is the total injection foam velocity.

3.3.5.4 Oil Displacement Experiments

After the core had been characterized, saturated with oil and aged for 1 month, oil recovery experiments were performed to investigate the efficacy of the EOR technology developed for the reservoir. In this study, oil displacement experiments included foam injection using methane as a gas, alkali-surfactant-polymer (ASP) injection and surfactant-alkali (SP) injection in carbonate cores under different reservoir conditions. For foam injection experiments, at first, a gas injection was performed to determine secondary recovery and represent the mature carbonate reservoirs that have been gas flooded for years. The gas injection continued until no more oil was produced and pressure drops were monitored. Effluent samples were collected to calculate cumulative oil recovery and estimate the in-situ oil saturation as a function of pore volumes of fluids injected. Then, alternating slugs of surfactant solution and gas were injected to study the effect of in-situ foam generation inside the porous medium and mobility control. The total amount of surfactant solution injected in these processes were kept constant to compare the effect of slug size variations. Experiments were performed with variable slug sizes of alternating injection to investigate their performance on incremental oil recovery. Pressure drops across the core were monitored for each of these processes. Finally, more gas was injected until no additional oil was produced. Additional experiments were also performed to study the effect of combination of alternating surfactant-gas injection along with co-injection of pre-generated foam into an oil-wet carbonate core on oil recovery. In these experiments, gas injection was followed with one big slug of surfactant solution followed with additional gas injection till no oil was produced. Finally, co-injection of surfactant and gas was

performed at a fixed foam quality until no oil was produced. These experiments were designed to have more chemical injection during the core floods and investigate the economic limits of incremental oil produced for incremental chemical injected. Few experiments were also performed in a similar way replacing the first gas injection with a water flood process to have a comparative study between the processes.

For ASP/SP injection processes, the oil saturated cores were water flooded initially till it reached the residual oil saturation. Then, a small slug of low IFT chemical formulation was injected in combination with high viscosity polymer solution for favorable mobility control; followed with similar viscosity polymer solution till no oil was produced. The effluent samples were collected, and the oil cut, residual oil saturations, effluent salinity, pH and viscosity were measured. In addition, effluent samples were also prepared for surfactant adsorption measurement and effluent ion analysis. The cumulative oil production and oil cute were determined using the following equations.

$$N_p = \frac{\sum V_{oil} + V_{oil,c}}{S_{oi} * V_p} \tag{3.22}$$

$$f_o = \frac{V_{oil}}{V_{oil} + V_{water}} \tag{3.23}$$

$$Sor_{w/g} = S_{oi} - \frac{V_{oil}}{V_P}\ , \qquad Sor_c = Sor_{w/g} - \frac{V_{oil,c}}{V_P} \tag{3.24}$$

where N_p is cumulative oil produced, V_{oil} is effluent oil volume during secondary process, V_p is pore volume, Soi is initial oil saturation, f_o is oil cut, V_{oil} is effluent oil volume, and V_{water} is effluent water volume, $Sor_{w/g}$ is residual oil saturation to secondary process,

Sor_c is residual oil saturation to chemical injection, $V_{oil,c}$ is the effluent oil volume during chemical injection process.

3.3.5.5 Effluent Sample Analysis

Effluent Salinity

The salinity of the effluent samples from the fractional collector was measured using the portable refractometer. The contribution of the chemicals injected besides any salts added were calibrated to get accurate measurements of the true salinity. This analysis provides useful insight on the chemical transport and efficiency of the chemical injection process.

Effluent Ion Analysis

The ionic composition of the effluent samples was analyzed using the Dionex ICS 3000 Ion Chromatography system. This equipment can analyze several anions and cations in a variable range of concentrations. At first, standard solutions are prepared for known concentration of the desired cations and anions that would be investigated during the study and analyzed in the equipment to get an accurate calibration curve. The effluent samples are then diluted to the target concentration range and analyzed. The measured areas from the signal of each sample is converted into corresponding concentration for each ion for the calibration curve. This analysis is helpful in understanding the geochemical reactions during the chemical injection process.

Effluent Viscosity

The viscosity of the effluent samples is measured during ASP/SP processes using

the AR-G2 rheometer at the reservoir temperature. This analysis is important to investigate the successful transport of the polymer solution through carbonate rocks and also any indication of channeling or polymer degradation during the experiment due to rock mineralogy and presence of oxygen.

Effluent pH

Measurement of pH of the effluent samples are essential in a chemical injection process to study the successful propagation of alkali during the core flood or any possible consumption due to rock mineralogy. The pH of the samples was measured using the Thermo Scientific Orion 3 STAR Benchtop pH meter.

Surfactant Adsorption/Retention

The adsorption/retention of anionic surfactants was measured using a High-Performance Liquid Chromatograph (HPLC). A Dionex Ultimate™ 3000 HPLC was used to measure the adsorption of anionic surfactants in dynamic adsorption study. HPLC measures retention time of each compound present in a sample and calculates the area under the graph for each surfactant type. The measured areas can be converted into corresponding surfactant concentrations from the calibration curve obtained with standard concentrations of surfactant. This analysis is helpful in estimating the surfactant loss due to adsorption on carbonate rock surfaces, better design of chemical injection processes and any evidence of chromatographic separation of chemicals inside the porous medium.

Chapter 4[1]: Use of Surfactant Alternating Gas Injection (SAG) in Gas-Flooded Carbonate Rocks

Chapters 2 and 3 discussed the motivation and methodology of foam application as a mobility control mechanism in heterogeneous carbonate reservoirs. This chapter focuses in developing an effective foam technology in combination with wettability alteration and low interfacial tension (IFT) for application in oil-wet carbonate reservoirs. Many low permeability carbonate reservoirs are gasflooded but leave behind a large amount of residual oil. Surfactant solutions can be injected with gas to improve recovery. Surfactants and gas have the potential to form foam that can improve both oil displacement efficiency and sweep efficiency in oil reservoirs. However, in many carbonate reservoirs, foams need to overcome two adverse conditions: oil-wettability and low permeability. However, crude oils have a detrimental effect on the foam stability which can pose a severe challenge for oil-wet carbonate reservoirs where a thin film of oil on the surface of the rock can destabilize the foam in the porous medium. Hence, wettability alteration is a promising mechanism to alter the oil-wet rock surface to water-wet or intermediate-wet that can improve the in-situ foam stability. Thus, a better mobility control and higher sweep efficiency can be achieved in combination of foaming and wettability alteration.

The goal of this work is to systematically investigate the effect of wettability alteration and foaming for tertiary oil recovery in oil-wet low permeability carbonate cores at the reservoir temperature (60 ^{o}C). Two types of anionic surfactant formulations were

[1] This chapter is based on: (Ghosh and Mohanty, 2019a). Dr. Mohanty supervised the project.

studied: alkyl propoxy sulfate (APS), which exhibited low IFT, wettability alteration, and coarse foaming; and alpha-olefin sulfonate (AOS), which showed no wettability alteration, but good foaming. Low permeability rocks tend to have high capillary entry pressure at small pore throats, hence low IFT surfactant formulations help in lowering the entry barrier for the injected fluids and diverting the fluids to bypassed regions in secondary processes. Phase behavior experiments were performed to determine the optimal salinity for low oil-water IFT for a given reservoir condition. Contact angle and imbibition experiments were performed on initially oil-wet media to identify surfactants for successful wettability alteration. Co-injection of gas and surfactant solutions were performed in low permeability carbonate cores (Texas Cream limestone and reservoir cores) and at low achievable field rates to obtain mobility reduction factors in the absence of oil. Dynamic adsorption experiments were performed in Texas Cream limestone cores to estimate the surfactant adsorption. Gas floods and surfactant alternating gas (SAG) floods were performed in oil saturated carbonate cores using low-IFT surfactant formulations to estimate the effect on incremental oil recovery in gas-flooded reservoirs. The novelty of this work is in improving oil recovery in a gas-flooded oil-wet carbonate reservoir in contrast to most of the past work where foam was used after waterfloods.

4.1 MATERIALS

Table 4.1 lists the surfactants used in this study and their properties. Anionic surfactants Alfoterra S23-7S-90 (received from Sasol) and AS-40 alpha olefin sulfonate (AOS_{C14-16}) (obtained from Stepan) were used in this study. Preliminary tests like phase behavior, bulk foam experiments and foam flow experiments (with no crude oil) in the

porous media were used to screen the surfactants for further use in the study. Alfoterra is known to give ultra-low oil-water IFT. AS-40 is known to be a good foamer.

Table 4.1: Surfactants used in the present study

Name	**Structure**	**Active**	**Molecular Weight**	**Type**
S23-7S-90	C12-14 alkyl propoxy (7) sulfate	89%	691 gm/mol	Anionic
AS-40	Alpha olefin sulfonate	38.86%	444 gm/mol	Anionic

Table 4.2 lists the properties of the limestone cores (C1 – C6) used in this study. Texas Cream limestone rocks and reservoir limestone cores were used for all the experiments. Each core was about 1.5 inch in diameter. The length of the cores varied from 7.8 inches in reservoir composite core to 11.5 inches in outcrop cores. Permeabilities varied from 1.7 to 25.6 mD.

Table 4.2: List of the properties of different carbonate cores

Cores	**TX Cream Limestone (C1)**	**TX Cream Limestone (C2)**	**TX Cream Limestone (C3)**	**TX Cream Limestone (C4)**	**Reservoir Limestone (C5)**	**Reservoir Limestone (C6)**
Length (cm)	29.5	29.7	28.9	29.0	19.7	19.7
Diameter (cm)	3.76	3.76	3.74	3.76	3.76	3.76
Porosity, %	26	28	28	32	16	16
Pore Volume, ml	86	91.4	91.5	104.9	35.5	35.5
Oil Permeability @ Soi, mD	12	25.6	17.1	7.7	2.3	1.7
Initial oil saturation, Soi	0.76	0.72	0.62	0.67	0.76	0.78

Formation and injection brines used in these experiments are shown in **Table 4.3**. The reservoir crude oil had a viscosity of 11.8 cp at 60 ^{o}C, a density of 0.89 g/cm^3, and an acid number of 0.49 mg of KOH/gm of oil. The pH of the surfactant formulations was measured using pHTestr 20 (Oakton Instruments) which has the precision of $\pm$ 0.01. The pH electrode was calibrated with standard pH buffer solutions of pH 4.7 and 10. Sodium chloride, calcium chloride, sodium sulfate, magnesium chloride, and methane (research grade, Matheson) were used as received. Ethylenediaminetetraacetic sodium salt (EDTA-Na_4) was used as received from Sigma Aldrich and solution prepared in DI water.

Table 4.3: Formation and injection brine used in the study

Composition	**Formation Brine**	**Injection Brine**
Na^+	2.940 gm/L	3.636 gm/L
Ca^{2+}	0.256 gm/L	0.740 gm/L
Mg^{2+}	0.049 gm/L	0.186 gm/L
Cl^-	4.859 gm/L	7.294 gm/L
SO_4^{2-}	0.365 gm/L	0.221 gm/L
Total Salinity	8,469 ppm	12,077 ppm

The purpose of oil displacement experiments was to study the synergistic effects of wettability-alteration, low IFT and foaming in oil-wet carbonate cores performed at the reservoir temperature and pressure. These experiments were performed in reservoir limestone cores and Texas Cream limestone cores. **Table 4.4** tabulates the list of experiments, initial wettability-state of the rocks, surfactant formulation and their properties, and the objective of the experiments. The viscosities of surfactant solutions are reported at 25 ^oC and a shear rate of 10 sec^{-1}. The total concentration of surfactant in each formulation was kept constant at 0.5 wt%.

Table 4.4: Surfactant formulations used in oil displacement experiments

Core flood#	**Core, Initial Wettability**	**Surfactant formulation**	**Objective of the Experiments**	**Viscosity, cp (60 °C)**	**pH**
1	C1, Oil-wet	0.5 wt% AS-40 + 1.5 wt% EDTA + 2 wt% Na_2CO3 + Inj. Brine	Single slug of 0.5 PV (S2)	1.2	11.7
2	C2, Oil-wet	0.5 wt% AS-40 + 1.5 wt% EDTA + 2 wt% Na_2CO3 + Inj. Brine	Alternating slugs of 0.1 PV (S2) each for 5 cycles	1.2	11.7
3	C3, Oil-wet	0.5 wt% S23-7S-90 + 1.5 wt% EDTA + 2 wt% Na_2CO3 + Inj. Brine	Single slug of 0.5 PV (S1)	1.0	11.4
4	C4, Oil-wet	0.5 wt% S23-7S-90 + 1.5 wt% EDTA + 2 wt% Na_2CO3 + Inj. Brine	Alternating slugs of 0.1 PV (S1) each for 5 cycles	1.0	11.4
5	C5, Oil-wet	0.5 wt% S23-7S-90 + 1.5 wt% EDTA + 2 wt% Na_2CO3 + Inj. Brine	Alternating slugs of 0.1 PV (S1) each for 4 cycles	1.0	11.4
6	C6, Oil-wet	0.5 wt% S23-7S-90 + 1.5 wt% EDTA + 2 wt% Na_2CO3 + Inj. Brine	Alternating slugs of 0.05 PV (S1) each for 8 cycles, Alternating slugs of 0.1 PV (S1) each for 6 cycles	1.0	11.4

For all the oil displacement experiments tabulated in **Table 4.4**, the following injection scheme was followed. First, methane gas was injected at 0.5 ft/D until oil recovery stopped. Second, alternating slugs of surfactant solution and methane gas were injected at 0.5 ft/D with 1:1 slug size ratio. The slug size was varied between the experiments, as

outlined later in **Table 4.7**. Third, this alternating slug cycle was followed with additional injection of methane gas at the same rate until no incremental oil was produced. The injection scheme was developed to represent gas flooded reservoirs. Oil recovery, residual oil saturation and pressure drops were monitored during the experiments.

4.2 RESULTS AND DISCUSSIONS

4.2.1 Phase Behavior Experiments and IFT Measurement

The anionic surfactant solutions and crude oil were mixed in equal volumes (WOR 1:1) in glass pipettes and equilibrated at the reservoir temperature, 60 ^{o}C. The salinity of the brine was varied by changing the concentration of added Na_2CO_3. The surfactant concentration was kept constant at 0.5 wt% in all these experiments. Chelating agent EDTA (1.5 wt%) was added to each tube to prevent any precipitation of the alkali with divalent ions in brine. For ultra-low IFT surfactant formulations with Windsor Type III, after equilibration of the phase behavior samples at the reservoir conditions, Chun Huh's correlation was used to estimate the IFT value from the solubilization ratio at optimal salinity.

Some surfactant formulations did not generate Windsor Type III microemulsions. The pendant drop method was used to measure the IFT between oil and aqueous-phase for these solutions using a Rame-hart goniometer equilibrated at the reservoir temperature.

Figure 4.1 & **4.2** shows the phase behavior tubes (with Type III region) and solubilization ratio plot for surfactant formulation S1 respectively. The optimal salinity was found to be at 2 wt% Na_2CO_3 and Huh's correlation estimated an IFT of 0.0006 dynes/cm with a solubilization of 22. Phase behavior experiment was also performed with

formulation S2 but type III regions were not seen. Hence, IFT was measured using the goniometer and the measured value was reported to be 0.38 dynes/cm at the reservoir temperature.

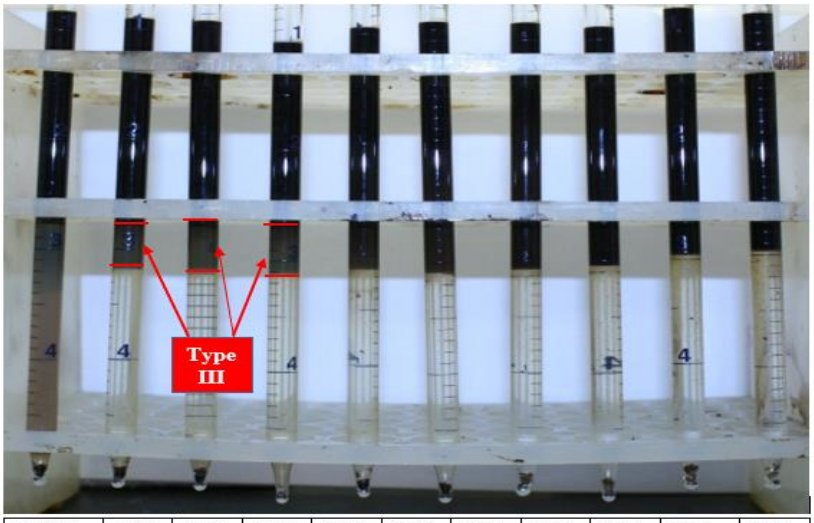

Figure 4.1. Phase behavior experiment with formulation S1 in crude oil at WOR 1

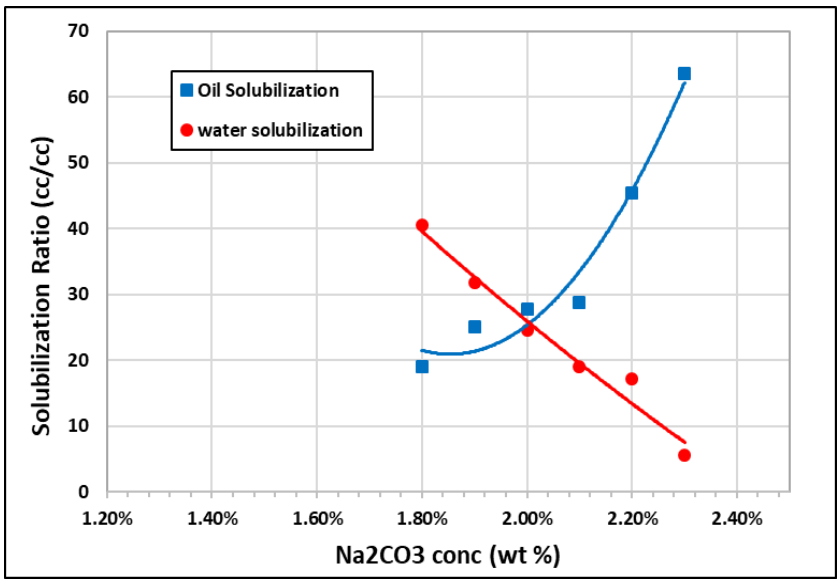

Figure 4.2. Solubilization plot for phase behavior experiment with formulation S1 in crude oil

4.2.2 Contact Angle Experiments

Qualitative contact angle experiments were performed on aged oil-wet calcite plates at the reservoir temperature (60 ^{o}C) as described under the methodology section in Chapter 3. In addition, image analysis software was used to measure the contact angles of the small oil droplets on the calcite rock surface to quantitatively estimate the degree of wettability alteration during these experiments.

Static imbibition experiments were also performed on oil-wet carbonate core plugs in optical cells to investigate the wettability altering capability of the surfactant formulations. The oil saturated core plugs (after aging in oil) were placed in the formation brine for 1-2 days at 60 ^{o}C. Then, the formation brine was replaced with the surfactant formulation and the oil production was monitored over time.

Figure 4.3a shows oil droplets on aged oil-wet calcite plates immersed in the injection brine. **Figure 4.3b** & **4.3c** shows the oil droplets on calcite plates in two anionic surfactant formulations after 24 hours. The results clearly show that the surfactant formulation S1 was successful in altering the wettability of the plate from oil-wet to intermediate-wet, whereas formulation S2 was unsuccessful. The contact angle measured was 162^{o} before treatment and changed to about 102^{o} in surfactant solution at the end of 24 hours. **Figure 4.4** shows a quantitative analysis of a single oil drop, using S1 formulation, over 4 days. The wettability changed from oil-wet to intermediate-wet and finally to water-wet conditions.

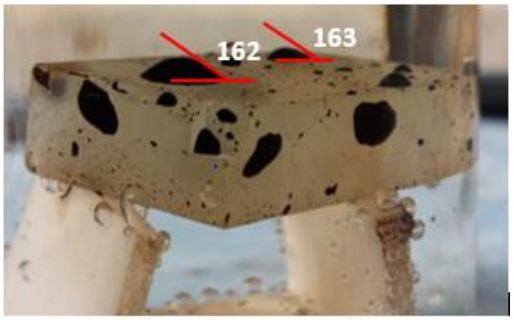

(a)

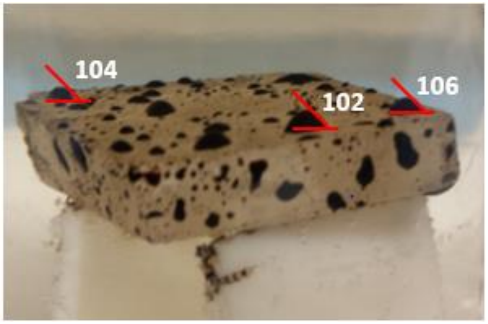

(b)

(c)

Figure 4.3. Oil droplets on the calcite plate: (a) injection brine at t=24 hours; (b) formulation S1 at t=24 hours; (c) formulation S2 at t=24 hours

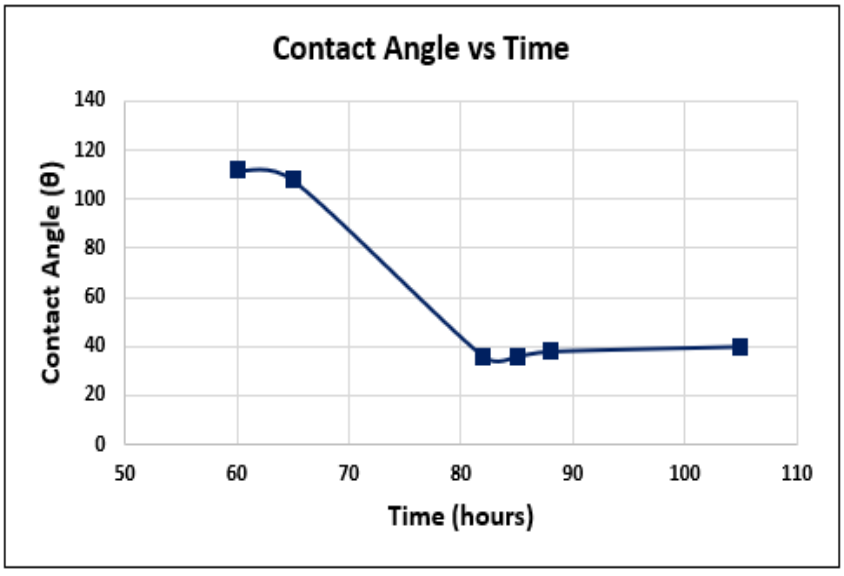

Figure 4.4. Contact angle measurement with time using surfactant formulation S1

4.2.3 Spontaneous Imbibition Experiment

The imbibition experiment was performed to investigate the ability of the surfactant formulation to alter wettability/achieve low IFT at the core scale. This experiment was performed on a reservoir core plug, aged with crude oil for 3-4 weeks. The surfactant formulation S1 was used for this experiment. The core was first immersed in the injection brine with little oil production. Then it was immersed in the surfactant solution at the optimal salinity with 2 wt% Na_2CO_3 and 1.5 wt% EDTA. The imbibition cell with the core after 2 weeks is shown in **Figure 4.5 (a)** and **(b)**. Oil droplets can be seen on the top surface of the core. A significant amount of oil had collected in the neck of the imbibition cell and the surfactant brine solution appeared dark, probably due to the oil dispersion in the surfactant solution. An emulsion breaker, emulsotron was used to break the oil in water emulsion at the end of the experiment. This oil was counted in the final oil recovery due to imbibition which was calculated to be 49.6% OOIP. **Figure 4.6** shows the cumulative oil recovery during this experiment with time. EDTA played an important role in the wettability alteration of the rock and imbibition of brine. Figure 4.5 (c) shows the imbibition experiment with formulation S2, which is non-wettability altering and the oil recovery was about 8%. This experiment showed that the surfactant formulation, S1 recovers oil by imbibition due to both wettability alteration and ultra-low IFT, whereas, S2 only recovers a minimal amount due to moderate lowering of IFT at the reservoir conditions.

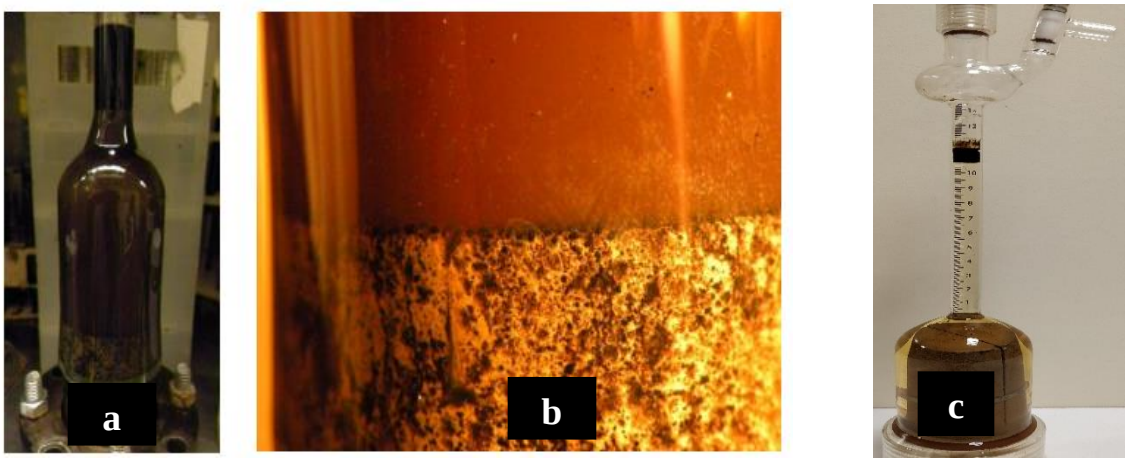

Figure 4.5. (a) Oil recovery by surfactant formulation S1 in the imbibition cell after 10 days (b) the close-up picture of the core (c) oil recovery by formulation S2 in the imbibition cell after 8 days

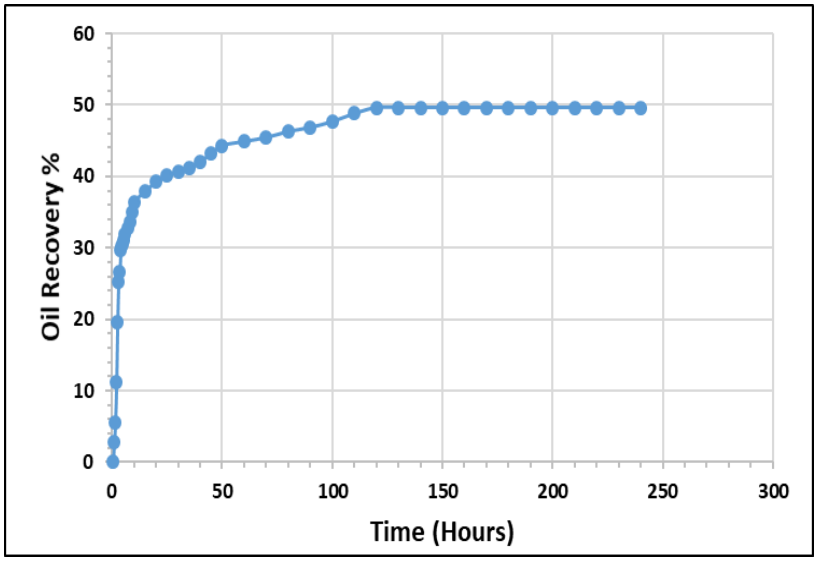

Figure 4.6. Cumulative oil recovery rate during spontaneous imbibition with formulation S1

4.2.4 Static Foam Tests

The bulk foam experiment setup for lower temperatures with the graduated cylinder (described in Chapter 3) was used for this study. During these tests, 30 ml of surfactant

solution was used for experiments without crude oil and about 5-10 vol% of crude oil for experiments with crude oil to investigate the negative effect on foam stability. Half-lives were recorded, and each experiment was repeated multiple times to account for variance in the measurements. The results for the optimum surfactant formulations S1 & S2 are described in **Table 4.5**. Average half-lives for S1 and S2 formulations were found to be 3 minutes and 80 minutes, respectively, in absence of crude oil. AOS_{C14-16} is a good foaming agent and generates stronger foam than the low IFT surfactant S23-7S-90. The table shows the negative impact of crude oil on foam stability for both S1 and S2 surfactant formulations.

Table 4.5: Static Foam Test Results

Formulation label	**Surfactant formulation**	**Viscosity, cp (60 ºC)**	**Half-life, minutes (no crude oil)**	**Half-life, minutes (with crude oil)**
S1	0.5 wt% S23-7S-90 + 1.5 wt% EDTA + 2 wt% Na_2CO3 + Inj. Brine	0.8	3.25 $\pm$ 0.25	1.3 $\pm$ 0.05
S2	0.5 wt% AOS_{C14-16} + 1.5 wt% EDTA + 2 wt% Na_2CO3 + Inj. Brine	1.2	79 $\pm$ 7	5.7 $\pm$ 1

4.2.5 Co-Injection Experiments

Gas-surfactant solution co-injection experiments were performed in Texas Cream limestone cores (with permeability between 10 - 15 mD) to investigate the ability of foam to reduce mobility in low permeability cores. The total surfactant concentration in these

experiments was kept constant at 0.5 wt%. The experiments were performed in the absence of crude oil. The brine saturated cores were equilibrated at 60 ^{o}C with a backpressure of 500 psi. A base case coreflood was also performed where co-injection of brine (no surfactant) and methane gas with 80% quality was injected at 4 ft/D immediately after brine saturation. The mobility reduction factor, calculated as a ratio of steady state pressure drop during surfactant (brine) and gas co-injection to the pressure drop during only surfactant (brine) injection, was estimated for each experiment. The results for effective mobility reduction obtained with the two surfactant formulations in low permeability cores are listed in **Table 4.6.** The mobility reduction factor varied from 4.2 to 5.7, but there was a significant increase from the base case with no surfactant solution in the aqueous phase (simultaneous water and gas injection at a WAG ratio of 1:4. This shows that presence of surfactants helps to stabilize some lamellae, reduce gas mobility and help to divert fluids. Formulation S2 had the higher half-life in the bulk stability test (without oil) and the higher mobility reduction factor in the porous medium as suggested by Jones et al. (2016). **Table 4.6** shows that in low permeability carbonate cores, only coarse foam was generated with low mobility reduction factors in presence of good foaming agents which agrees with the literature reported on foam flow in tight formations (Chabert et al., 2012).

Table 4.6: Pressure drop in foam 80% quality flow experiments without oil (60 ^{o}C)

Surfactant Formulation	**Core Permeability (mD)**	**Pressure Drop (psi) (Surfactant)**	**Pressure Drop (psi) (Surf. brine + CH_4)**	**MRF**	**Apparent Viscosity (cP)**
S1: 0.5 wt% S23-7S-90 + 1.5 wt% EDTA + 2 wt% Na_2CO3 + Inj. Brine	15.4	6.35	26.87	4.2	2.1
S2: 0.5 wt% AOS_{C14-16} + 1.5 wt% EDTA + 2 wt% Na_2CO3 + Inj. Brine	10.8	7.6	43.24	5.7	3.42
Injection Brine (no surfactant)	13.8	6.9	9.3	1.4	0.67

4.2.5.1 Foam Quality Scan Experiments

Additional experiments were performed to study the effect of foam quality (at a fixed total flow rate) on the foam strength for formulation S2 in a Texas Cream limestone of brine permeability 11.8 mD. For these experiments, the total flow rate was again kept constant at 4 ft/D at 60 ^{o}C with a backpressure of 500 psi. For each foam quality experiment, a surfactant pre-flush was injected at 2 ft/D. Then, co-injection of surfactant solution and gas were performed at the desired foam quality for about 8-10 PVs. After achieving steady state, a solution containing methanol and brine (1:1 vol ratio) were injected for several PVs to break the foam (to restore the original permeability of the porous medium with injection brine and reduce the hysteresis effect in the experiment). **Figure 4.7** shows the pressure history of the foam quality experiments after an initial surfactant

pre-flush for each quality scan. **Figure 4.8** shows the results for the mobility reduction factors generated (from values extracted at 10 PV injection) at each foam quality and the corresponding apparent foam viscosity in low permeability carbonate cores. The MRF stays under 10 for all the cases except for 70% foam quality where it is 21.3. Hence, the transition foam quality (at which the foam regime transitions from low-quality to high-quality) for this surfactant formulation at the given reservoir condition was estimated to be 70%.

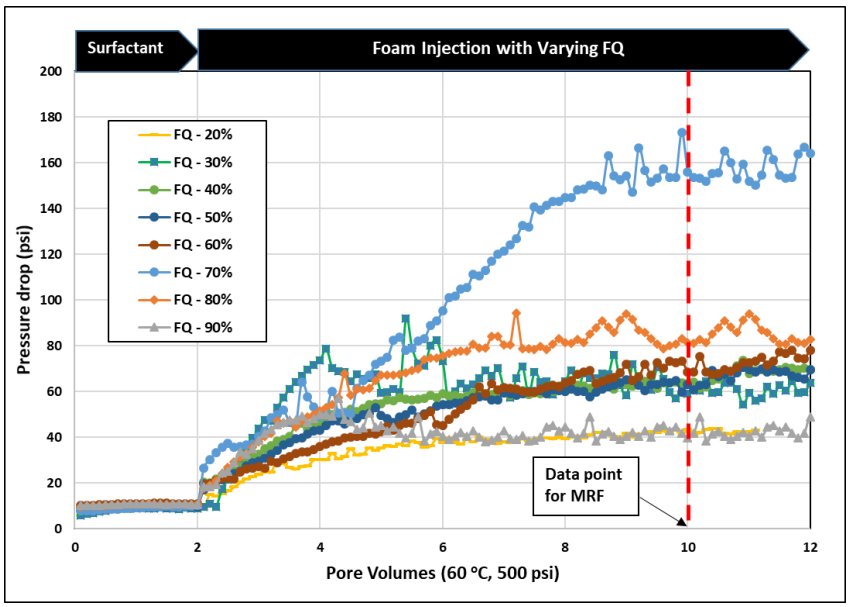

Figure 4.7. Pressure history for the foam quality scan experiments performed with surfactant formulation S2 in Texas Cream limestone

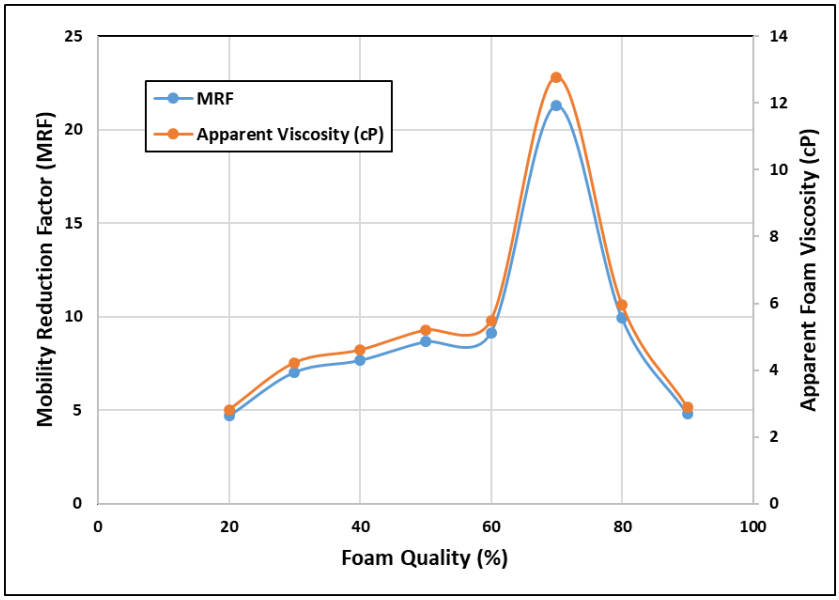

Figure 4.8. MRF and Apparent Viscosity for the foam experiments performed with formulation S2 in Texas Cream limestone at 10 PV of foam injection (60 ^{o}C, 500 psi)

4.2.5.2 Foam Injection Velocity Scan Experiments

The purpose of these experiments was to investigate the effect of foam injection velocity on foam rheology and foam generation in low permeability carbonate cores in absence of crude oil. The foam quality was fixed at the transition foam quality calculated from the previous set of experiments (i.e. 70% foam quality); was performed at 60 ^{o}C with a backpressure of 500 psi. Literature studies in the past have reported foam characterization at high injection velocities in bead packs and high permeability sandstones, but very few are available on foam generation in low permeability rocks. An attempt was made here to understand the foam rheology in tight formations and how foam strength is dependent on foam injection velocity. These experiments were performed in a Texas Cream limestone of brine permeability 13.2 mD. A surfactant pre-flush was performed, followed by co-

injection of surfactant solution and gas (methane) at varying injection velocities for about 8 PV of total foam injection at the transition foam quality. Two different sets of experiments were performed to emphasize the importance of hysteresis in foam flow in porous media. In the non-hysteresis method, after each rate experiment, the core was first thoroughly flushed with multiple PVs of injection brine followed with injection of methanol and brine (1:1 volume ratio) for about 8-10 PV until no surfactant was produced. Finally, the core was flushed with injection brine for another 10 PV to remove any trapped gas (by increasing the system pressure and compressing the gas to negligible volume), and brine permeability was measured to restore the core to its initial state. In the hysteresis method, the rates were increased consecutively without cleaning the core.

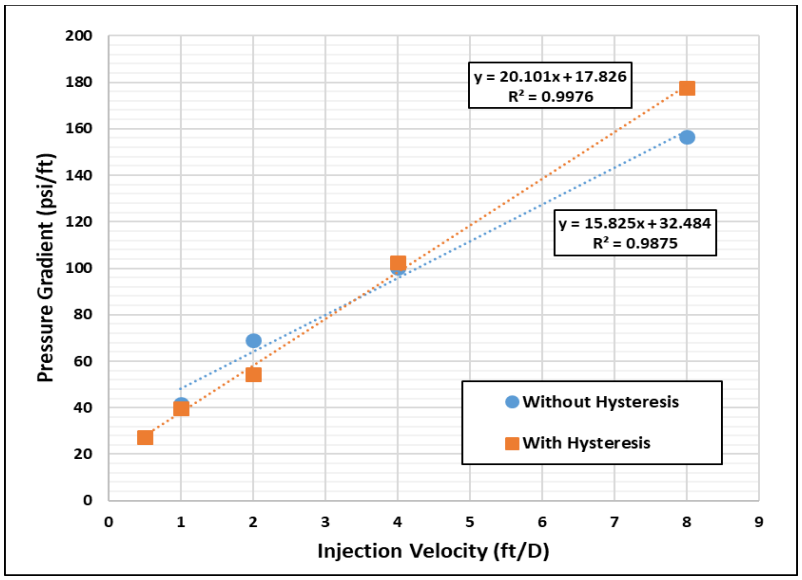

Figure 4.9. Effect of foam injection velocity with and without hysteresis at 70% foam quality with S2 (in absence of crude oil)

Figure 4.9 shows the results for the pressure gradients generated at the transition foam quality with a variation of injection velocity with and without hysteresis effect in low

permeability carbonate cores. The pressure gradient increases almost linearly with the injection velocity indicating that the foam strength does not increase with the injection velocity at a fixed foam quality. The experiments performed with and without hysteresis effect did not show any significant difference. The critical velocity to create foam generation, if any, is higher than 8 ft/D. The results also emphasize the fact that it is unrealistic to to generate strong foam in such low permeability reservoirs. Hence, experiments should be performed at realistic field achievable rates to understand foam rheology in the weak foam regime in such challenging reservoirs.

4.2.6 Dynamic Adsorption Experiments

Adsorption experiments were performed in low permeability carbonate rocks to estimate the loss of surfactant in the porous medium. Alkali was used to increase the pH of the surfactant solution and change the zeta potential of the rock surface from positive to negative, and hence, reduce the adsorption of these surfactants. A strong chelating agent EDTA was also used in the solution to prevent precipitation of the divalent ions in presence of alkali but showed traces of calcite dissolution in carbonate rocks (Ghosh et al., 2019). Dynamic adsorption experiments were performed in brine saturated Texas Cream limestone cores at 60 ^{o}C. This step was followed by a tracer test with a higher salinity brine of 40,000 ppm. The effluent salinity was measured using a refractometer. Then, we injected 2-3 PV of reservoir injection brine to restore the core to its initial state of brine saturation. The injection rate for the dynamic adsorption experiment was kept constant at 1 ft/D. 2 PV of the surfactant formulation S1 was injected into the limestone core and effluent samples were collected at every 0.1 PV. Similar adsorption experiment was also performed in Texas

Cream limestone with surfactant formulation S2. **Figure 4.10** shows the effluent concentrations for the surfactant formulations S1 and S2 and the corresponding tracer concentrations for tests 1 and 2, respectively. The delay in the concentration profile compared to the tracer test signifies the adsorption on the rock surface. The adsorption numbers estimated for S1 and S2 were 0.11 mg/gm of rock and 0.04 mg/gm of rock, respectively.

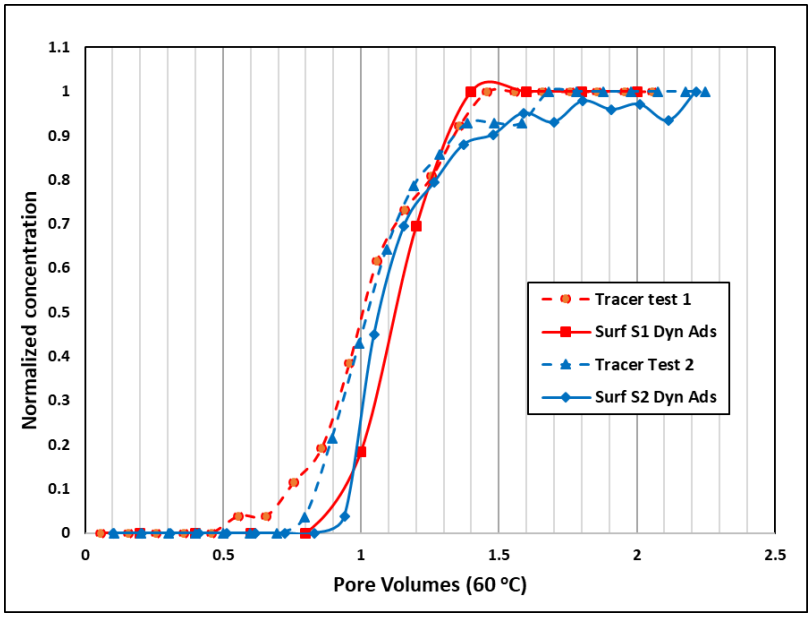

Figure 4.10. Effluent tracer and surfactant concentrations for formulations S1 & S2

4.2.7 Oil Displacement Experiments

Coreflood experiments were performed with surfactant formulations S1 and S2. The wettability-state of the cores and the surfactant formulations used for each experiment is reported previously in **Table 4.4**. A dead, reservoir crude oil of viscosity 11.8 cp (at 60 ^{o}C) was used in these experiments. The summary of the injection scheme followed in each of the experiments is provided in **Table 4.7** and the objective of the experiments are

illustrated in **Table 4.4** earlier. The slug size ratio for each of the gas and the surfactant solution was kept constant in every oil displacement experiment. All injection rates during each of the coreflood experiments were fixed at 0.5 ft/D.

Table 4.7: Summary of the injection schemes followed in oil displacement experiments

Core flooding	**1st gas slug**	**2nd alternating surfactant – gas slug**	**3rd gas slug**	**4th alternating surfactant-gas slug**	**5th gas slug**	**Injection rate (ft/D)**
1	2.5 PV	0.5 PV total of formulation S2 with 1 big slug	1.5 PV			0.5
2	2.0 PV	0.5 PV total of formulation S2 with 5 cycles 0.1 PV slug each of surfactant and gas alternating	1.5 PV			0.5
3	3.5 PV	0.5 PV total of formulation S1 with 1 big slug	2.5 PV			0.5
4	3.4 PV	0.5 PV total of formulation S1 with 5 cycles 0.1 PV slug each of surfactant and gas alternating	2 PV			0.5
5	2 PV	0.4 PV total of formulation S1 with 4 cycles 0.1 PV slug each of surfactant and gas alternating	2 PV			0.5
6	1.5 PV	0.4 PV total of formulation S1 with 8 cycles 0.05 PV slug each of surfactant and gas alternating	1.2 PV	0.6 PV total of formulation S1 with 6 cycles 0.1 PV slug each of surfactant and gas alternating	1 PV	0.5

The first coreflood was performed to investigate the performance of a foaming surfactant that does not alter wettability or achieve ultra-low IFT (formulation S2). **Figure**

4.11 shows the cumulative oil recovery, residual oil saturation (primary y-axis) and pressure drop (secondary y-axis) across the core. In Coreflood 1, a Texas Cream limestone core with an initial oil saturation of 76% (and an average oil permeability of 12 mD) was flooded with 2.5 PV of methane gas until no additional oil was produced. The oil recovery during this gas injection step was 12.2% OOIP. The average pressure drops during this stage varied between 1 and 3 psi. Then a single slug of 0.5 PV of surfactant formulation S2 was injected into the core and an additional oil recovery of 22.2% OOIP (25.3% ROIP after gasflood) was achieved during this step. The average pressure drops during this step increased from 2 psi to about 12 psi due to generation of in-situ foam. Finally, another 2 PV of methane gas was injected and the incremental oil recovery during this step was 8.4% OOIP (9.5% ROIP). The low-pressure drops indicate propagation of coarse foam (if any) through the porous medium. The cumulative oil recovery for this experiment was found to be 42.8% OOIP with an increase in oil production of about 30.6% OOIP (34.9% ROIP after gasflood) due to injection of a foaming surfactant, and the final residual oil saturation was 43.4%. The foam is very weak or almost non-existent in this low permeability rock in the presence of oil. The flow is predominantly governed by two phase flow of gas and surfactant water with some lamellae stabilized by surfactants, improving microscopic fluid diversion and oil recovery.

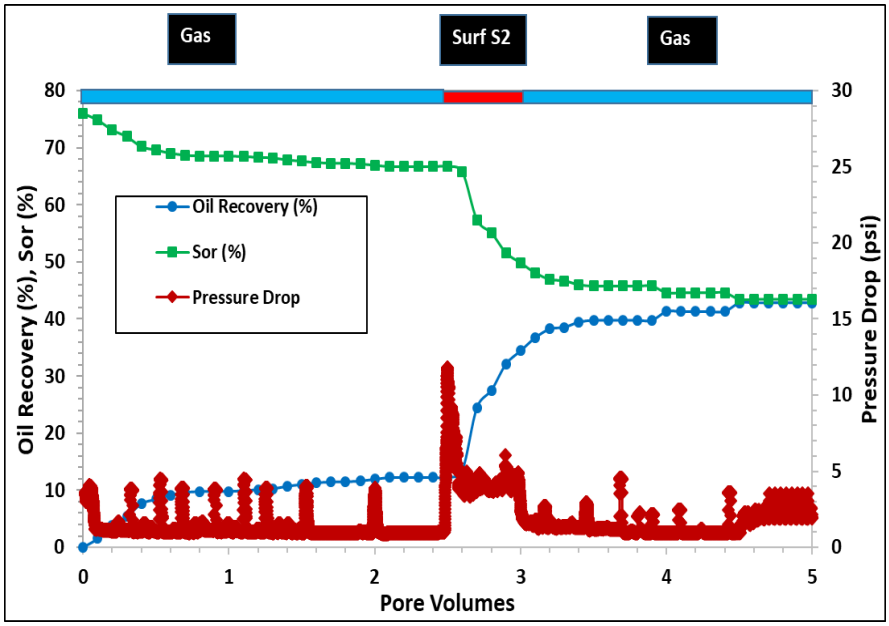

Figure 4.11. Experimental results for cumulative oil recovery & residual oil saturation (left axis), & average pressure drops (right axis) in coreflood 1

Coreflood 2 was performed to investigate the effect of smaller slug size during alternating surfactant-gas injection on the oil recovery process with the foaming (non-ultra-low IFT) formulation S2. A Texas Cream limestone core with an initial oil saturation of 72% (and an average oil permeability of 25.6 mD) was flooded with 2.0 PV of methane gas until no additional oil was produced. The oil recovery during this gas injection step was 15.6% OOIP. The pressure drops during this stage varied between 1 and 2 psi. Then alternating slugs (of 0.1 PV each) of surfactant formulation S2 and gas were injected with a total surfactant injection of 0.5 PV. Hence, 5 cycles of surfactant-alternating-gas were injected, which resulted in an incremental recovery of 25.4% OOIP (30.1% ROIP after gasflood). The average pressure drops during this step increased from 2 psi to about 10 psi due to generation of in-situ foam. Finally, another 1.5 PV of methane gas was injected and

the incremental oil recovery during this step was 3% OOIP (3.6% ROIP after gasflood). **Figure 4.12** shows the cumulative oil recovery, residual oil saturation (primary y-axis) and pressure drop (secondary y-axis) across the core. The fluctuating low-pressure drops indicate propagation of coarse foam (or just two-phase flow with rapid lamellae coalescence) through the porous medium. The ultimate cumulative oil recovery for this experiment was found to be 44% OOIP with an increase in oil production of about 28.4% OOIP (33.7% ROIP after gasflood) due to injection of a foaming surfactant only, and final residual oil saturation at the end of the experiment was reduced to 40.3%. The comparison of corefloods 1 and 2 showed that the slug size did not make a significant difference for oil recovery for the oil-wet porous medium. The residual saturation was high (about 40%) in both these experiments. The results from these corefloods show that smaller slug sizes of a foaming and non-wettability altering surfactant formulation S2 were not beneficial for improvement in incremental oil production.

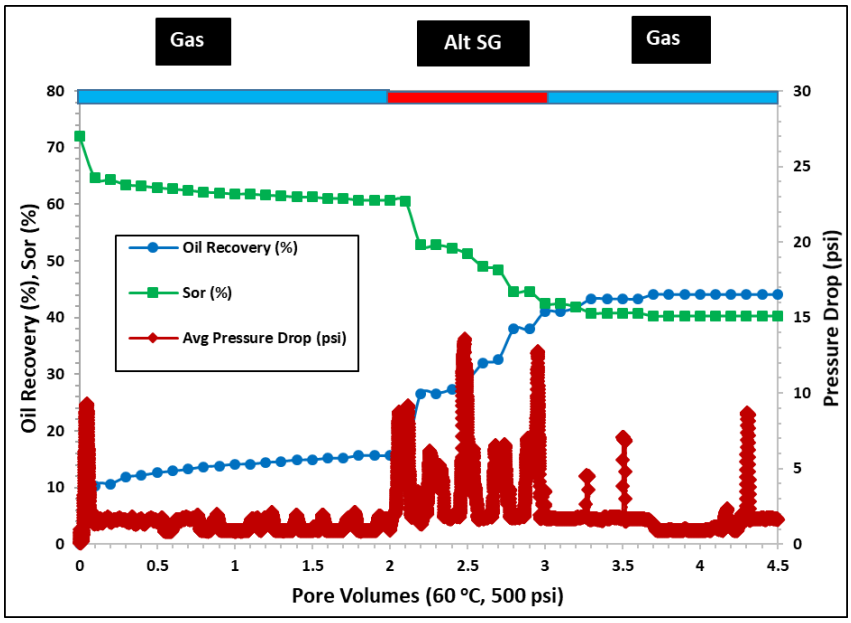

Figure 4.12. Experimental results for cumulative oil recovery & residual oil saturation (left axis), & average pressure drops (right axis) in coreflood 2

The next set of core floods were designed to investigate the performance of ultra-low IFT surfactant formulation (S1) in combination with wettability alteration and foaming abilities. In Coreflood 3, Texas Cream limestone with an initial oil saturation of 61.7% (and an average oil permeability of 17.1 mD) was flooded with 3.5 PV of methane gas. The oil recovery during this gas injection step was 36% OOIP. The pressure drops during this stage varied between 1.5 and 2 psi. Then a single slug of 0.5 PV of surfactant formulation S1 was injected into the core and an additional oil recovery of 26% OOIP (46.4% ROIP after gasflood) was achieved during this step. The average pressure drops during this step increased from 2 psi to about 18 psi due to in-situ foam generation. Finally, another 2.5 PV of methane gas was injected and the incremental oil recovery during this step was 5% OOIP (8.7% ROIP after gasflood). **Figure 4.13** shows the cumulative oil

recovery, residual oil saturation (primary y-axis) and pressure drop (secondary y-axis) across the core. The ultimate cumulative oil recovery for this experiment was found to be 67% OOIP with an increase in oil production of about 31% OOIP (55.1% ROIP after gasflood) due to injection of wettability altering surfactant with low IFT and foaming ability. The final residual oil saturation at the end of the experiment was 17%. Coreflood 3 is similar to Coreflood 1, except for the surfactant formulation. The remaining oil saturation is much smaller for surfactant formulation S1 than that for S2. This experiment clearly showed that for the oil-wet porous medium, wettability alteration and ultra-low IFT are the key mechanisms for improvement in oil recovery and not just foaming. The significant oil mobilization due to wettability alteration and microemulsion generation was absent in coreflood 1 which led to the lower oil recovery compared to the coreflood 3.

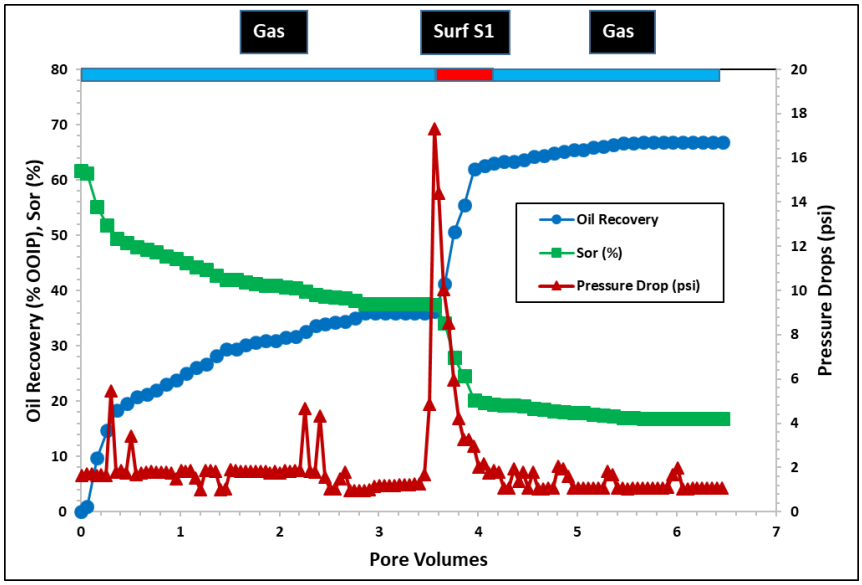

Figure 4.13. Experimental results for cumulative oil recovery & residual oil saturation (left axis), & average pressure drops (right axis) in coreflood 3

Coreflood 4 was designed to investigate the performance of smaller slug sizes during alternating injection process on incremental oil production for the wettability altering surfactant. A Texas Cream limestone with an initial oil saturation of 67% (and an average oil permeability of 7.74 mD) was flooded with 3.4 PV of methane gas. The oil recovery during this gas injection step was 41.5% OOIP. The pressure drops during this stage varied between 1.5 and 2 psi. Then alternating slugs of 0.1 PV each of surfactant formulation S1 and gas were injected with a total surfactant injection of 0.5 PV. Hence, 5 cycles of surfactant-alternating-gas were injected, which resulted in incremental recovery of 33% OOIP (56.5% ROIP after gasflood). The average pressure drops increased from 2 psi in the gas injection to about 20 psi in this alternating stage. Finally, another 2 PV of methane gas was injected and the incremental oil recovery during this step was 2% OOIP (3.4% ROIP after gasflood). **Figure 4.14** shows the cumulative oil recovery, residual oil saturation (primary y-axis) and pressure drop (secondary y-axis) across the core. The ultimate cumulative oil recovery for this experiment was found to be 76.5% OOIP with an increase in oil production of about 35% OOIP (60% ROIP after gasflood) due to injection of wettability altering surfactant with low IFT and foaming ability, and the final oil saturation was 15.7%. This experiment suggested that injection of smaller slug sizes in alternating surfactant-gas increased the oil recovery due to higher pressure drop, better mixing of surfactant and gas in-situ resulting in better mobility control and fluid diversion from more stable foam. Coreflood 4 was similar in design to coreflood 2, but with different surfactant formulations, and the results showed significant improvement in oil recovery

with smaller slug sizes primarily due to wettability alteration which improved the lamellae stability.

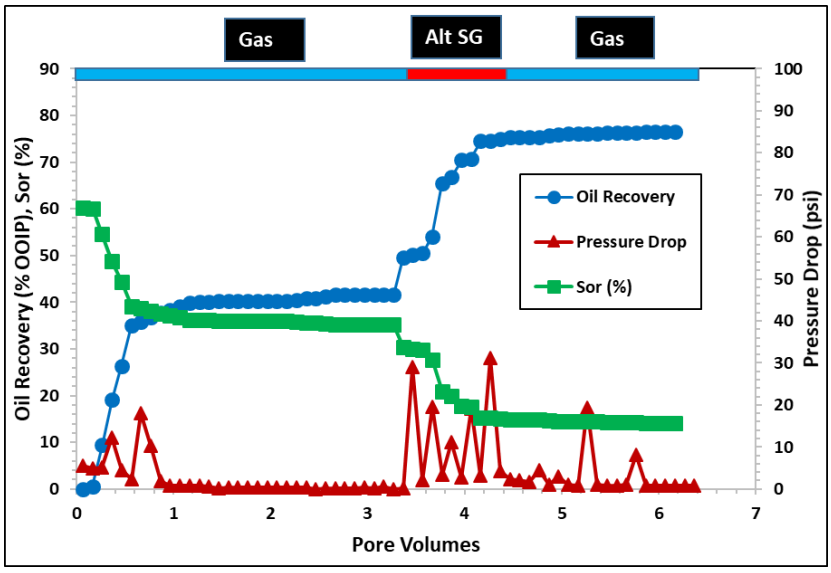

Figure 4.14. Experimental results for cumulative oil recovery & residual oil saturation (left axis), & average pressure drops (right axis) in coreflood 4

In Coreflood 5, the best performing formulation from the previous corefloods was applied in a reservoir limestone core. A reservoir core at an initial oil saturation of 76.3% (with an oil permeability of 2.3 mD) was flooded with 2.0 PV of methane gas and 12% of the OOIP was recovered during this gas injection process. The average pressure drop during this step was between 2 and 3 psi. Then alternating slugs (of 0.1 PV each) of surfactant formulation S1 and gas (methane) were injected with a total surfactant injection of 0.4 PV. 4 cycles of surfactant-alternating-gas were injected, and the incremental oil recovered was about 25% OOIP (28.2% ROIP after gasflood). There was no oil produced with the additional injection of 2 PV of methane gas after the alternating slug injections. **Figure 4.15** shows the cumulative oil recovery, residual oil saturation (primary y-axis) and

pressure drop (secondary y-axis) across the core. The significant increase in pressure drop from 3 psi to 14 psi during the alternating surfactant-gas injection step was due to in-situ generation of foam and oil mobilization through microemulsion formation. The cumulative oil recovery was 37% OOIP, oil recovery due to in-situ foam generation (over gas flood) was about 25% OOIP (28.2% ROIP after gasflood) and final oil saturation was reduced to 49%. This experiment shows that the coarse foam generated inside the porous medium was able to divert the injected fluids to the un-swept pores by reducing the mobility of the gas and increased the oil recovery. The oil recoveries were generally lower than that of outcrop cores due to lower permeability and higher heterogeneity of the reservoir core.

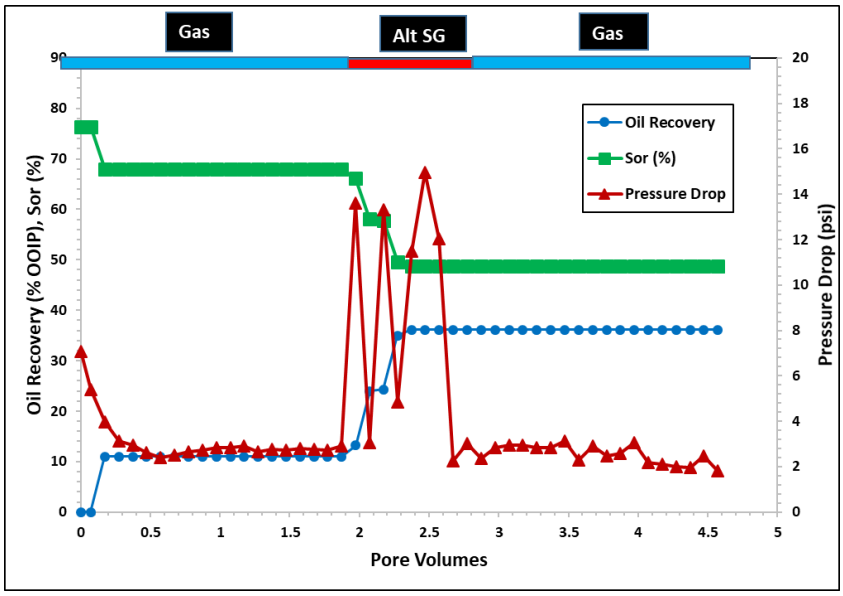

Figure 4.15. Experimental results for cumulative oil recovery, residual oil saturation (left axis), & average pressure drops (right axis) in coreflood 5

In Coreflood 6, the last coreflood scheme was repeated, but with smaller slug sizes and additional injection steps. A reservoir core with an initial oil saturation of 78.3% (with an oil permeability of 1.68 mD) was flooded with 1.5 PV of methane gas and recovered

31% of the OOIP during this first gas injection. The average pressure drops during this step varied between 8 and 10 psi. Higher oil recovery observed in this first gas injection step than in coreflood 5 (and the delayed gas breakthrough) can be attributed to a less heterogeneous core. Then alternating slugs of 0.05 PV each of surfactant formulation S1 and gas were injected with a total surfactant injection of 0.4 PV. 8 cycles of surfactant-alternating-gas were injected, and additional oil recovered was 28% OOIP (40.8% ROIP after gasflood). The average pressure drops increased from 10 psi in the gas injection step to about 65 psi in this stage. After this step, an additional injection of 1.2 PV of methane gas resulted in incremental oil recovery of 8% OOIP (12% ROIP after gasflood). To investigate the effect of more foam injection, alternating slugs of 0.1 PV each of surfactant formulation S1 and gas were injected with a total surfactant injection of 0.6 PV after the second gas injection phase. The injection of another 6 cycles of alternating slugs led to a recovery of additional 11% OOIP (15.2% ROIP after gasflood). This alternating stage realized even higher pressure drop, from 15 psi in gas injection to about 100 psi. Finally, injection of 1 PV of methane gas recovered an additional oil of 1.5% OOIP (2% ROIP after gasflood). **Figure 4.16** shows the cumulative oil recovery, residual oil saturation (primary y-axis) and pressure drop (secondary y-axis) across the core. The increase in pressure drop during the alternating surfactant gas injection phases was due to in-situ foam generation. Note, this experiment included a total surfactant injection of 1 PV split into 0.4 PV and 0.6 PV slugs with smaller slug size variation included. The experimental results also showed improvement in oil recovery due to smaller slug size of alternating surfactant and gas compared to Coreflood 5. The ultimate cumulative oil recovery was 80% OOIP; oil

recovery due to in-situ foam generation (over gas flood) was about 49% OOIP (70.1% ROIP after gasflood) and final oil saturation was reduced to 16%.

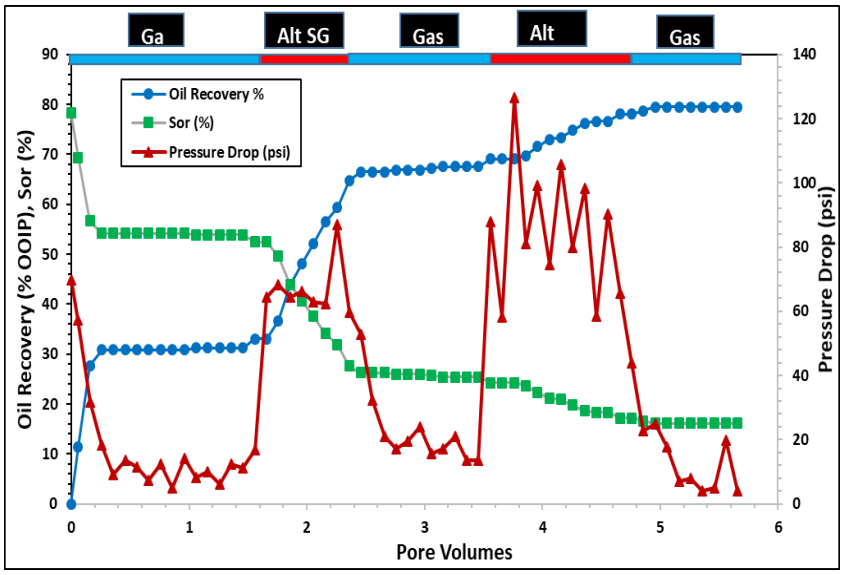

Figure 4.16. Experimental results for cumulative oil recovery, residual oil saturation (left axis), & average pressure drops (right axis) in coreflood 6

4.3. SUMMARY

Strong foam does not form in low permeability (1-50 mD) carbonates even in the absence of oil because of high limiting capillary pressure and high critical pressure gradient. Only a coarse foam forms whose behavior is very different from those in high permeability rocks. The oil displacement experiments performed in oil-wet low permeability limestone cores with surfactant formulations S1 and S2 show that ultra-low IFT with wettability alteration is beneficial in improving oil recovery after secondary gasfloods. The wettability altering surfactant makes the core water-wet which increases the stability of the foam lamellae. The lamellae are intermittently stabilized by surfactants that reduced gas mobility and diverted fluids at the pore scale to improve the oil recovery. **Table**

4.8 summarizes the results of each of the oil displacement experiments along with the objectives for each of them. Results clearly show improvement in tertiary oil recovery over secondary gasflood, with smaller slug sizes of formulation S1 from 28.2% ROIP for 0.4 PV injection to 70.1% ROIP for 1 PV injection in tight reservoir cores.

Table 4.8: Summary of the results from the oil displacement experiments (60 ^{o}C, 500 psi)

Core flooding	**Soi**	**1st gas slug**	**2nd alternating surfactant – gas slug**	**3rd gas slug**	**4th alternating surfactant-gas slug**	**5th gas slug**	**Objective of the Experiments**
1	0.76	12.2% OOIP, Sor ~0.67	25.3% ROIP, Sor ~ 0.5	34.9% ROIP, Sor ~ 0.43			Single slug of S2, 0.5 PV
2	0.72	15.6% OOIP, Sor ~ 0.61	30.1% ROIP, Sor ~ 0.42	33.7% ROIP, Sor ~ 0.40			Alternating slugs of S2, 0.1 PV each for 5 cycles
3	0.62	35.9% OOIP, Sor ~ 0.38	46.4% ROIP, Sor ~ 0.2	55.1% ROIP, Sor ~ 0.17			Single slug of S1, 0.5 PV
4	0.67	41.5% OOIP, Sor ~ 0.39	56.5% ROIP, Sor ~ 0.17	59.9% ROIP, Sor ~ 0.16			Alternating slugs of S1, 0.1 PV each for 5 cycles
5	0.76	11% OOIP, Sor ~ 0.68	28.2% ROIP, Sor ~ 0.49	28.2% ROIP, Sor ~ 0.49			Alternating slugs of S1, 0.1 PV each for 4 cycles
6	0.78	31.2% OOIP, Sor ~ 0.54	40.8% ROIP, Sor ~ 0.32	52.8% ROIP, Sor ~ 0.25	68% ROIP, Sor ~ 0.17	70.1% ROIP, Sor ~ 0.16	Alternating slugs of S1, 0.05 PV each for 8 cycles, Alternating slugs of 0.1 PV each for 6 cycles

4.4. CONCLUSIONS

Gas injection in carbonate rocks leads to poor oil recovery due to oil-wetness and heterogeneity. Foams have the potential to improve oil recovery but must overcome the challenging conditions in carbonates: oil-wettability and low permeability. This study investigates performance of 2 surfactant formulations in low permeability, oil-wet carbonate cores: one that combine wettability alteration, low IFT, and coarse foaming and the other that is only good foaming. The following conclusions are suggested from this study:

- Wettability alteration and low IFT can be achieved with anionic surfactants that also foam coarsely.
- Adsorption of the anionic surfactants studied was between 0.04 and 0.11 mg/gm of rock in presence of alkali and EDTA in tight carbonate formations.
- Imbibition experiments suggested wettability alteration with S1 (ultra-low IFT and wettability alteration surfactant), but not with S2 (foaming surfactants).
- Oil displacement experiments in oil-wet carbonate cores revealed that tertiary oil-recovery with injection of wettability-altering, low IFT surfactant can recover a significant amount of oil (about 28-70% ROIP) over the secondary gas flood.
- The foam rheology in the presence of oil suggested propagation of only coarse foam in oil-wet carbonate cores. This two-phase flow with intermittent lamellae stabilized by surfactants can divert fluid at the pore scale and improve oil recovery.

- Good foaming surfactant that does not change wettability or achieve low IFT recovered less oil compared to an ultra-low IFT and wettability altering surfactant due to unstable lamellae in oil-wet media.
- Coreflood experiments showed improvement in oil recovery with smaller slug sizes due to better mixing of surfactant and gas in-situ and better fluid diversion, and results were in agreement with the trend that ultra-low IFT and wettability altering mechanisms are key to higher oil recovery for oil-wet carbonates.

Chapter 5: Novel Application of Cationic Surfactants for Foams with Wettability Alteration in Carbonate Rocks

Chapters 4 discussed the use of anionic surfactants in surfactant-alternating-gas (SAG) processes in tertiary oil recovery processes for oil-wet low permeability carbonate formations using wettability alteration, low IFT and foaming mechanisms. The use of alkali to reduce surfactant adsorption on carbonate surfaces and generate low IFT formulations [2]requires use of a chelating agent EDTA to prevent any precipitation in presence of divalent ions. Results have shown that use of EDTA can make the chemical recovery processes very expensive and uneconomical as well as leading to formation damage for carbonate formations. Hence, an alternative solution of using cationic surfactants instead of anionic surfactants was investigated in this study. Cationic surfactants provide better compatibility with reservoir formation brine containing divalent ions due to non-alkaline formulations and lower surfactant adsorption on carbonate formations.

The objective of this chapter is to explore the synergy of wettability alteration and foaming abilities for application in oil-wet carbonate reservoirs to develop a successful foam technology at the reservoir temperature (60 ^{o}C). Several types of cationic surfactants were investigated with different degrees of wettability altering capability. Non-ionic surfactants were investigated in blend with cationic surfactants to increase the foaming abilities of the surfactant formulations. Addition of zwitterionic surfactant like lauryl betaine (LB) was also explored to study the effect on foaming properties of the surfactant

[2] This chapter is based on: (Ghosh and Mohanty, 2018). Dr. Mohanty supervised the project.

blends. Contact angle and imbibition experiments were performed on initially oil-wet media to identify surfactants for successful wettability alteration. Static foam stability tests were conducted to evaluate their foaming performance in bulk; foam flow experiments (without crude oil) were performed in porous media to estimate the foam strength. Finally, oil displacement experiments were performed to investigate the efficiency of optimum surfactant formulations in oil recovery process after a secondary process. Two different injection strategies were studied in this work: surfactant slug followed by gas injection and co-injection of surfactant with gas at a constant foam quality. Several blends of cationic, non-ionic and zwitterionic surfactants were used in the experiments.

5.1 MATERIALS

Table 5.1 lists the surfactants used in this study and their properties. Cationic surfactants, DTAB (from Sigma Aldrich), Ethoquad C/25 (from Akzonobel), and BTC (from Stepan), were chosen as they are good wettability altering agents. Non-ionic surfactant Tergitol NP (from Dow Chemical) was used as a moderate foaming agent. An in-house produced cationic Gemini surfactant GC 580 was used as it showed good wettability altering and foaming properties. Literature studies have reported use of zwitterionic surfactants like betaines as foam boosters (Basheva et al., 2000). In this scope of work, zwitterionic surfactant Lauryl Betaine (from Rhodia) was used. Anionic surfactant Bioterge AS-40 (from Stepan) was used as a good foaming agent for comparative study.

Table 5.1: Surfactants used in the present study

Name	**Structure**	**Active Content**	**Molecular Weight**	**Type**
DTAB	Dodecyltrimethylammonium bromide	>= 98%	308.34 g/mol	Cationic
BTC	Alkyl dimethyl benzyl ammonium chloride	80%	not available	Cationic
GC 580	Gemini Cationic	100%	580 gm/mol	Cationic
Tergitol NP	Alkyl Ethoxylate	100%	642 gm/mol	Non-ionic
LB	Lauryl Betaine	29%	271.4 gm/mol	Zwitterionic
Ethoquad C/25	Cocoalkylmethyl[polyoxyethylene (15)] ammonium chloride	95%	911 gm/mol	Cationic
Bioterge AS-40	$C_{14\text{-}16}$ Alpha Olefin Sulfonate	38.86%	Not available	Anionic

Table 5.2 lists the properties of the limestone cores (C1 – C6) used in this study. Texas Cream limestone rocks were used for all the experiments. Each core was about 1 ft long and 1.5 inch in diameter. Oil permeabilities (@ Soi) varied from 9.2 to 22 mD.

Table 5.2: List of the carbonate core properties used for gas flooded reservoirs

Cores	**TX Cream Limestone (CG1)**	**TX Cream Limestone (CG2)**	**TX Cream Limestone (CG3)**	**TX Cream Limestone (CG4)**	**TX Cream Limestone (CG5)**	**TX Cream Limestone (CG6)**
Length (cm)	29	29	29.8	29.5	29.6	29.5
Diameter (cm)	3.76	3.76	3.74	3.76	3.76	3.76
Porosity, %	26.25	27.65	25.4	29	30.4	26
Pore Volume, ml	84.5	89	83.3	95.2	100	86
Oil Permeability @ Soi, mD	12	9.2	13.5	12.9	22	15
Initial oil saturation, Soi	0.76	0.75	0.62	0.73	0.64	0.76

Formation and injection brine used in these experiments are tabulated in **Table 5.3**. Crude oil was obtained from a reservoir and had a viscosity of 12.6 cP at 60 ^{o}C, density of 0.89 g/cm^3, and acid number equal to 0.49 mg of potassium hydroxide/gm of oil. The viscosity was measured using an AR G2 rheometer. The pH of the various surfactant formulations was measured using pHTestr 20 (Oakton Instruments) which has the precision of $\pm$ 0.01. The pH electrode was calibrated with standard pH buffer solutions of pH 4, 7, and 10. Sodium chloride, calcium chloride, sodium sulfate, magnesium chloride, and methane (research grade, Matheson) were used as received.

Table 5.3: Formation and injection brine used in the study

Composition	**Formation Brine**	**Injection Brine**
Na^+	2.940 gm/L	3.636 gm/L
Ca^{2+}	0.256 gm/L	0.740 gm/L
Mg^{2+}	0.049 gm/L	0.186 gm/L
Cl^-	4.859 gm/L	7.294 gm/L
SO_4^{2-}	0.365 gm/L	0.221 gm/L
Total Salinity	8,469 ppm	12,077 ppm

The purpose of this study was to investigate surfactants blends with cationic/non-ionic / zwitterionic surfactants that would provide good wettability alteration and foaming properties. **Table 5.4** tabulates the list of surfactant blends used for the experiments, initial wettability-state of the rock, and properties of the surfactant formulations. The viscosities of surfactant solutions are reported at 60 ^oC and a shear rate of 10 sec^{-1}. The total concentration of surfactant in each formulation was kept at about 0.4 - 0.5 wt%.

Table 5.4: Surfactant formulations used in oil displacement experiments

Core Flood #	**Initial Wettability**	**Surfactant formulation**	**Formulation Label**	**Viscosity, cp (60 °C)**	**pH**	**IFT dyne/cm**
G1	Water-wet	0.5 wt% LB + Inj. Brine	S1	0.7	8.0	2.3
G2	Oil-wet	0.5 wt% LB + Inj. Brine	S1	0.7	8.0	2.3
G3	Oil-wet	0.2 wt% DTAB + 0.2 wt% NP-10 + Inj. Brine	S2	0.6	7.2	3.9
G4	Oi-wet	0.2 wt% GC 580 + 0.2 wt% Ethoquad C/25 + Inj. Brine	S3	0.75	7.0	0.7
G5	Oil-wet	0.3 wt% GC 580 + 0.1 wt% LB + Inj. Brine	S4	0.7	7.5	1.4
G6	Oil-wet	0.5% $C_{14\text{-}16}$ AOS + 2% Na_2CO_3 + 1.5% EDTA + Inj. Brine	S5	1.2	11.7	0.38

5.2. RESULTS AND DISCUSSIONS

5.2.1 Interfacial Surface Tension (IFT) Measurements

The interfacial tensions between the oil and the surfactant solutions were about 1 dyne/cm, not ultra-low. Hence, the pendant drop method was used to measure the IFT between oil and aqueous-phase using a Rame-hart goniometer. The surfactant formulations

and oil were mixed and allowed to equilibrate at 60 ^{o}C and used for the IFT measurement. The measured IFT values are reported in **Table 5.4**.

5.2.2 Contact Angle Experiments

Contact angle experiments were performed using aged oil-wet mineral calcite plates in optical cells at the reservoir temperature (60 ^{o}C). The procedure followed has been outlined in the methodology section in Chapter 3. Image analysis software was also used to measure the contact angles of the small oil droplets on the calcite rock surface to quantitatively estimate the degree of wettability alteration during these experiments.

Studies in literature have reported use of cationic surfactants as successful wettability altering agents (Austad and Milter, 1997). **Figure 5.1a** shows oil droplets on calcite plates immersed in the injection brine at the reservoir temperature of 60 ^{o}C. **Figure 5.1b** shows the oil droplets on calcite plates in two cationic surfactants; the shape of oil drops indicates wettability alteration. Blend of cationic and non-ionic surfactants have also shown promising application in wettability alteration of oil-wet calcite chips (Sharma and Mohanty, 2013). Oil droplets were observed on plates immersed in surfactant formulations S1-S5 (in **Table 5.4**) were observed for at least 24 hours. **Figure 5.2** shows the oil droplets on the calcite plates after t = 24 hours in the surfactant solutions. It is evident that the surfactant formulations with cationic and nonionic/zwitterionic surfactants changed the wettability of the plate from oil-wet to intermediate-wet. The contact angle was about 150^{o} before treatment and changed to about 60^{o}-90^{o} after treatment with surfactant solutions. On the other hand, anionic surfactant in formulation S5 was unable to change the wettability from oil-wet to water-wet.

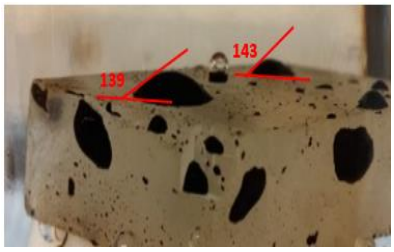

(a)

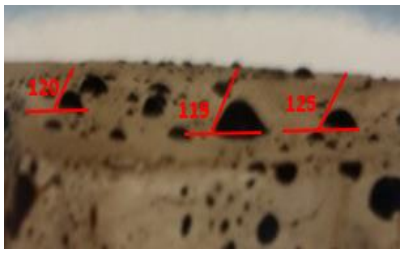

(b)

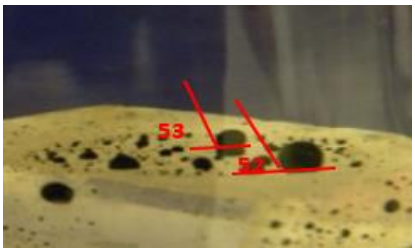

(c)

Figure 5.1. Oil droplets on the calcite plate: (a) injection brine at t=24 hours; (b) 0.4 wt% DTAB at t=24 hours; (c) 0.4 wt% BTC at t=24 hours

S1

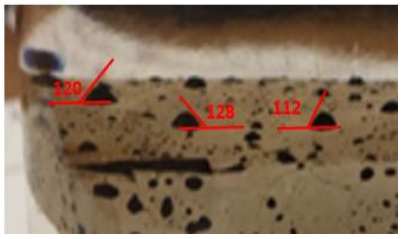

S2

S3

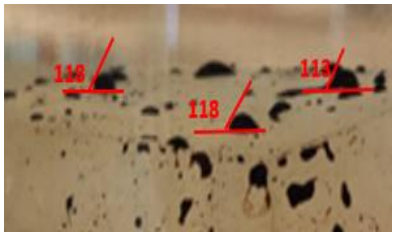

S4

S5

Figure 5.2. Oil droplets on calcite plate: at t=24 hours for the surfactant formulations S1, S2, S3, S4 and S5 from Table 5.4

5.2.3 Spontaneous Imbibition Experiment

The wettability altering ability of a surfactant solution is further quantified by this static imbibition experiment. This imbibition experiment was conducted on Texas Cream limestone plug, aged with crude oil for 3-4 weeks. The surfactant formulations S2 and S3 were used for this experiment. **Figure 5.3** shows the oil recovered from the hard brine surfactant formulation in the imbibition cell after 4 months. **Figure 5.3(a)** represents the initial oil-wet condition after equilibration with injection brine for A (surfactant formulation S2) and B (surfactant formulation S3). **Figure 5.3(b)** shows the final state of the core plugs after 4 months. The significant oil production for both formulations S2 and S3 shows that the surfactants were successful in wettability alteration and improved oil recovery through spontaneous imbibition. The oil droplets shown on the core plug face for formulation S2 also shows the clear change in contact angle to more water-wet state. Due to high IFT generated with cationic surfactants, the rate of oil production was significantly slower, hence, monitored for a longer period.

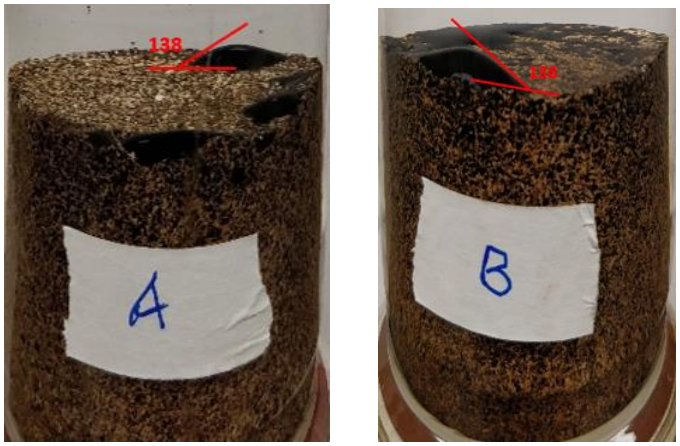

(a)

(b)

Figure 5.3. Spontaneous imbibition experiment performed with formulations S2 (label A) and S3 (label B)

5.2.4 Static Foam Tests

Static foam tests are the most common stability technique to measure the foaming ability of surfactant formulations (Vikingstad et al., 2005; Singh and Mohanty, 2015b). These experiments were performed to compare the foaming ability of various surfactant formulations used in oil-displacement experiments. These experiments were performed at 60 ^{o}C (reservoir temperature in the present study). The bulk foam experiment setup for

lower temperatures with the graduated cylinder (described in Chapter 3) was used for this study. During these tests, 30 ml of surfactant solution was used for experiments without crude oil and about 5-10 vol% of crude oil for experiments with crude oil to investigate the negative effect on foam stability. Half-lives were recorded, and each experiment was repeated multiple times to account for variance in the measurements.

Single cationic surfactants like DTAB and BTC 8358 showed weak foaming (not shown here). Anionic surfactant $C_{14\text{-}16}$ AOS was used as a good foaming agent for reference. Foaming of mixed surfactant formulations S1-S5 are shown in **Table 5.5**. Average half-lives for S1 and S2 formulations were found to be 3 minutes, 2 minutes, respectively, whereas for S3, S4 and S5 formulations the half-lives were found to be 29 minutes, 180 minutes, and 79 minutes, respectively, in absence of crude oil. GC 580 showed strong foaming on addition of a zwitterionic foam booster. Note that different proportions of surfactant blends were investigated for optimal performance based on foaming properties and tolerance to crude oil, and the best combinations have been reported. **Table 5.5** also shows the effect of crude oil on foam stability, when crude oil is vigorously mixed with the foam. It reduces foam half-life significantly.

Table 5.5: Static Foam Tests Results

Formulation label	**Surfactant formulation**	**Viscosity, cp (60 ^{o}C)**	**Half-life, minutes (no crude oil)**	**Half-life, minutes (with crude oil)**
S1	0.5 wt% LB + Inj. Brine	0.53	3 $\pm$ 0.5	2.5 $\pm$ 0.25
S2	0.2 wt% DTAB + 0.2 wt% NP-10 + Inj. Brine	0.6	2 $\pm$ 0.25	1.5 $\pm$ 0.1
S3	0.2 wt% GC 580 + 0.2 wt% Ethoquad C/25 + Inj. Brine	0.7	29 $\pm$ 2	10 $\pm$ 0.5
S4	0.3 wt% GC 580 + 0.1 wt% LB + Inj. Brine	0.7	180 $\pm$ 20	7.0 $\pm$ 0.5
S5	0.5 wt% C_{14-16} AOS + 1.5 wt% EDTA + 2 wt% Na_2CO3 + Inj. Brine	1.2	79 $\pm$ 7	5.7 $\pm$ 1

5.2.5 Foam Flow Experiments

Foam flow experiments without oil were conducted in Texas Cream limestone cores (varying between 15 - 20 mD) to investigate the strength of foams in low permeability cores. The total surfactant concentration was kept at 0.4 wt%. These experiments were conducted in the absence of oil and therefore in water-wet cores. The total flow rate in these experiments was maintained at 4 ft/D. These experiments were performed at 60 ^{o}C with a backpressure of 500 psi. Before each run, enough time (>12 hrs) was allowed to achieve isothermal conditions in the system. First, a base case was performed in which brine and gas were co-injected at 80% quality. The average pressure drop after 10 PVs of injection was recorded. Then, co-injection of surfactant formulation and gas were performed at foam quality of 80% and the average steady-state pressure drop after 10 PVs

of injection was recorded. The mobility reduction factor (calculated as a ratio of steady state pressure drop during surfactant and gas co-injection to the base case) was estimated for each experiment. **Table 5.6** summarizes the effective mobility reduction obtained with different surfactant formulations in low permeability cores. The mobility reduction factor varied from 1.5 to 5. Formulation S4 had the highest half-life in the bulk stability test and formulation S5 had the highest mobility reduction factor in absence of crude oil. In high permeability cores, typical mobility reduction factors are about 10-30 (Fuseni et al., 2017). Note the study performed in this reference was performed at a higher temperature. Hence the MRF values reported would be slightly higher at our reservoir conditions. **Table 5.6** shows that weak foam was generated in low permeability carbonate cores with low mobility reduction factors, as suggested by Chabert et. al. (2012).

Table 5.6: Pressure drop in foam 80% quality flow experiments without oil

Surfactant Formulation	**Type**	**Pressure Drop (psi) (Brine + CH_4)**	**Pressure Drop (psi) (Surf. brine + CH_4)**	**MRF**
S2: 0.2 wt% DTAB + 0.2 wt% NP-10	Cationic + Non-ionic	8.35	12.44	1.5
S4: 0.3 wt% GC 580 + 0.1 wt% LB	Cationic + Zwitterionic	3.7	14.14	3.8
S5: 0.5 wt% C_{14-16} AOS + 1.5 wt% EDTA + 2 wt% Na_2CO3	Anionic	8.84	43.93	5.0

5.2.6 Adsorption Experiments

Static adsorption experiments were performed in crushed Texas Cream limestone, filtered through 200 mesh, at the reservoir temperature. The ratio of the amount of crushed

limestone rock to the amount of surfactant solution was kept constant at 1:2 (weight ratio). The vials were shaken at regular intervals for 3 days and equilibrated at the reservoir temperature. The anionic surfactants were analyzed in HPLC, while the cationic surfactants were analyzed using a method proposed by Wang and Langley (1977). These experiments performed at the reservoir temperature showed promising results for cationic surfactants compared to anionic surfactants for carbonate rocks. The cationic surfactants showed significantly lower adsorption because of the positively charged carbonate rock surface (compared to the anionic surfactants in absence of alkali). **Table 5.7** provides a summary of the adsorption obtained with $C_{14\text{-}16}$ AOS (anionic foaming agent) and cationic surfactant GC 580.

Table 5.7: Comparative study of Static Adsorption in Texas Cream Limestone

Surfactant Concentration (wt%)	**GC 580 (mg/grock)**	**$C_{14\text{-}16}$ AOS (mg/grock)**
0.1	0.007	0.14
0.5	0.009	0.19
1.0	0.01	0.26

5.2.7 Oil Displacement Experiments

The properties of the cores used for these experiments are listed in **Table 5.2**. The cores were oil saturated at the reservoir temperature and aged at 80 ^{o}C for 3-4 weeks to ensure its oil-wetness. The aged cores before being used for core flood experiments were investigated for oil-wetness. **Figure 5.4** shows the core when a water droplet is placed on the core before and after aging. The droplet imbibes into the core in the former case indicating initial water-wetness, but does not imbibe after aging, confirming oil-wetness.

Figure 5.4. Texas Cream limestone core before (left) and after aging (right)

The oil recovery experiments were designed two different ways. A set of experiments were performed with initial gas flood as the secondary recovery process followed by chemical injection with surfactant solution and gas. A separate set of experiments were also investigated with water flood as the secondary recovery process followed by chemical injection with surfactant solution and gas.

For all the oil displacement experiments in **Table 5.4**, the following injection scheme was followed. First, a methane gas flood was conducted at 0.5 ft/day until oil recovery stopped. Second, a slug of surfactant formulation of 0.5 PV was injected into the core. Third, this slug was followed with an injection of methane gas until no additional oil was produced. Finally, surfactant solution and methane gas were co-injected at 1 ft/D with a foam quality 70-80% from the top until no additional oil was recovered. These floods are aimed at reservoirs that are gas flooded. Oil recovery and pressure drops were monitored at every step.

In order to understand the importance of wettability alteration along with foaming for incremental oil recovery in oil-wet carbonate rocks, we first performed an experiment in a water-wet core (no aging with the oil). Coreflood G1 was performed on the water-wet core CG1 (**Table 5.2**) as the base case with a moderate strength foaming surfactant formulation S1. The initial oil saturation was 76%. **Figure 5.5** shows the injection sequence, cumulative oil recovery, residual oil saturation (primary y-axis) and overall pressure drop (secondary y-axis) across the core. Methane gas was injected at 0.5 ft/D for about 2.5 PVs until no additional oil was produced. The gas flood recovery was 11% OOIP (original oil in place) and oil saturation was reduced to 67.7%. The pressure drop during the gas flood was between 1.5 psi and 2 psi. The oil recovery is low in this flood because of viscous instability associated with gas flood and capillary end effect. Then, the core was flooded with a slug of 0.5 PV of surfactant formulation S1 at the same rate resulting in an additional oil recovery of 37% OOIP. The pressure drops during this step varied between 3 psi and 8 psi. This recovery is high because the core is water-wet; water goes into smaller pores and displaces oil while the previous gas flood displaced oil from mostly larger pores. Then, this surfactant slug injection was followed with methane gas for about 2 PVs until no oil was produced. This step produced an additional oil of 4.5% OOIP with pressure drop between 2 and 3 psi. The injection of gas into some of the surfactant saturated pores can form foam which contributed to the incremental oil recovery. Finally, methane gas and surfactant formulation S1 were co-injected for about 3 PV at 1 ft/D with 70% foam quality which produced an incremental oil of approximately 8% OOIP. The pressure drop during this stage varied between 10 psi and 18 psi. The higher pressure drops in the last stage

suggest that initially in the presence of crude oil a weak foam propagated through the core, and eventually foam stability increased with decreasing oil saturation in the experiment. The ultimate cumulative oil recovery was 60.7% OOIP, oil recovery due to surfactant and foam (over gas flood) was about 41.5% OOIP and final oil saturation was reduced to 29.8%.

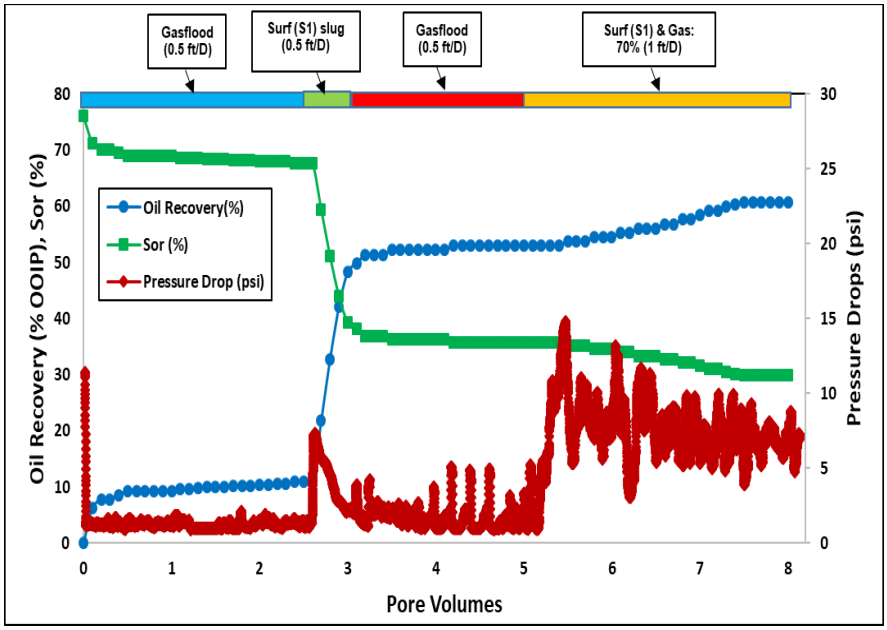

Figure 5.5. Pressure drop profile (right axis) and cumulative oil recovery & oil saturation (left axis) for coreflood G1

Coreflood G2 was performed in the oil-wet core CG2 (**Table 5.2**) with the same surfactant formulation S1 as in Core Flood 1. This surfactant does not change wettability. The initial oil saturation was 75.3%. **Figure 5.6** shows the injection sequence, cumulative oil recovery, residual oil saturation (primary y-axis) and overall pressure drop (secondary y-axis) across the core. Methane gas was injected at 0.5 ft/D for about 3 PVs until no oil was produced. The gas flood recovery was 8.2% OOIP (original oil in place) and oil

saturation was reduced to 69.1%. The pressure drop during the gas flood was between 1 psi and 1.5 psi. Again, the oil recovery due to gas flood is low because of unstable gas flood and capillary end effect. Then, the core was flooded with a slug of 0.5 PV of surfactant formulation S1 at the same rate resulting in an additional oil recovery of 22.4% OOIP. The pressure drops during this step varied from 6 psi to 10 psi. The oil recovery in this step is lower than that in Core Flood 1 because this core is oil-wet. The surfactant solution recovers oil due to a stable front contributed by surfactant itself and in-situ foam generation through mixing of methane and surfactant solution in porous medium but does not recover oil from smaller pores because of oil-wetness of the rock with respect to water. Then, the surfactant slug injection was followed with methane gas for about 1.5 PVs until no oil was produced. This step produced an additional oil of 3% OOIP with pressure drop between 1.5 and 2 psi. Foaming was the only mechanism but contributed a small incremental recovery. Finally, methane gas and surfactant formulation S1 were co-injected for about 3 PVs at 1 ft/D with 70% foam quality which produced an incremental oil of approximately 21% OOIP. The pressure drops during this stage varied between 8 psi and 14 psi. The higher pressure drops in the last stage suggest that in the presence of crude oil only a weak foam propagated through the core, and foam stability increased with decreasing oil saturation in the experiment. The ultimate cumulative oil recovery was 54.5% OOIP, oil recovery due to in-situ foam generation (over gas flood) was about 25.4% OOIP and final oil saturation was reduced to 34.4%. This core flood showed lower recovery due to injection of surfactant S1 and gas (compared to Core Flood 1) primarily due to the oil-wetness of the rock. Hence, wettability of the rock plays an important role in

foam stability in porous media and wettability alteration is crucial to stabilize foam and enhance oil recovery.

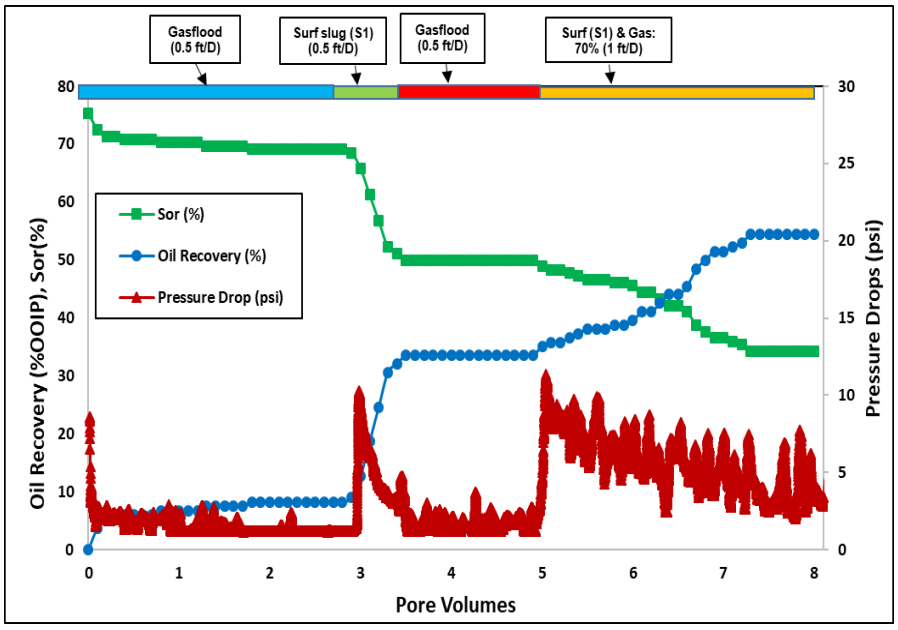

Figure 5.6. Pressure drop profile (right axis) and cumulative oil recovery & oil saturation (left axis) for coreflood G2

Coreflood G3 was conducted in the oil-wet core CG3 with a wettability altering and moderate foaming surfactant formulation S2; its properties are listed in **Table 5.2**. The oil permeability of this core was higher (13.5 mD) and the initial oil saturation was lower (62%) than the last two cores. **Figure 5.7** shows cumulative oil recovery, residual oil saturation (primary y-axis) and overall pressure drop (secondary y-axis) across the core. Methane gas was injected at 0.5 ft/D for about 5 PVs until no additional oil was produced. The gas flood recovery was 24.2% OOIP and oil saturation was reduced to 47.3%. The pressure drop during the gas flood was between 2.5 psi and 3 psi. Then, the core was flooded with a slug of 0.5 PV of surfactant formulation S2 at the same rate resulting in an

additional oil recovery of 28.3% OOIP. The oil recovery due to surfactant increased (compared to Core Flood 2) because of the wettability alteration ability of surfactant formulation, S2. The pressure drops during this step varied from 6.3 psi to 15.5 psi. This slug injection was followed with methane gas for about 2 PVs until no oil was produced. This step produced an additional oil of 4% OOIP with pressure drop between 2.5 to 3 psi. Finally, methane gas and surfactant formulation S2 were co-injected for about 1 PV at 0.5 ft/D with 80% foam quality which produced approximately 6.5% OOIP. The pressure drops during this stage varied between 2.5 psi and 4.2 psi. The low pressure drops suggest that in the presence of crude oil only weak foam propagated through the core. The ultimate cumulative oil recovery was 62% OOIP, oil recovery due to in-situ foam generation (over gas flood) was about 32.3% OOIP and final oil saturation was reduced to 23.6% (which was lower than 34.4% for Core Flood 2). This coreflood shows that a combination of wettability and weak foaming can enhance oil recovery if the reservoir is first developed with a secondary gas injection. It is important to note that the pressure drop fluctuations are not observed in this experiment due to lower sampling data frequency compared to the results in other core floods.

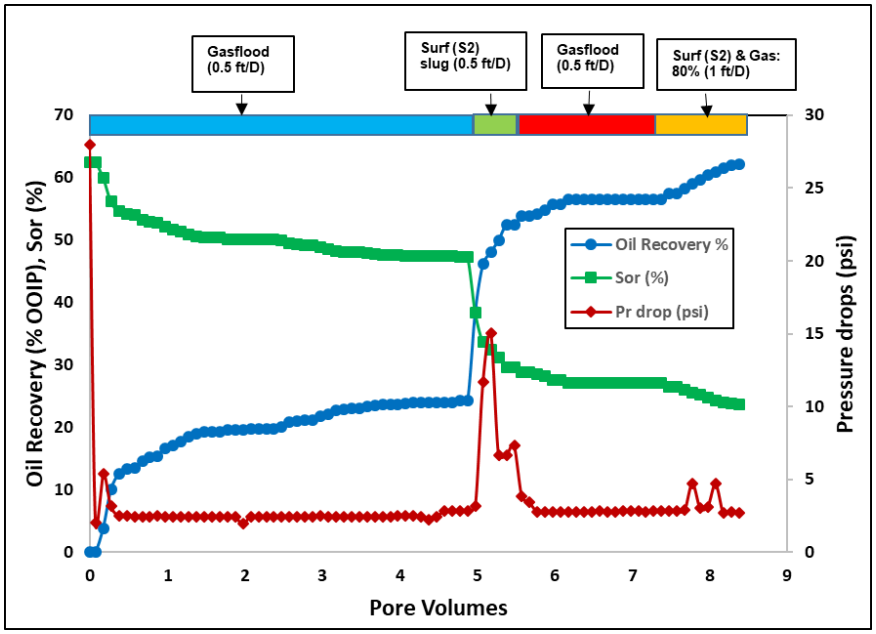

Figure 5.7. Pressure drop profile (right axis) and cumulative oil recovery & oil saturation (left axis) for coreflood G3

Based on the results from core floods 2 and 3, we performed coreflood G4 on an oil-wet core (CG4) **Table 5.2** to demonstrate the combined effect of wettability alteration and good foaming properties (surfactant formulation S3). The initial oil saturation was 63%. **Figure 5.8** shows the injection procedure, cumulative oil recovery and residual oil saturation (primary y-axis) and overall pressure drop (secondary y-axis) across the core. Methane gas was injected at 0.5 ft/D and continued for about 2.3 PVs until no additional oil was produced. The gas flood recovery was 25% OOIP (similar to that in Core Flood 3) and oil saturation was reduced to 47.3%. The pressure drop during the gas flood was between 1.5 psi and 2 psi. Then, the core was flooded with a slug of 0.5 PV of surfactant formulation S3 at the same rate resulting in additional oil recovery of 9% OOIP. The pressure drops during this step varied from 3.5 psi to 5 psi. Then, this slug injection was

followed with methane gas for about 1.5 PVs until no oil was produced. This step produced an additional oil of 2% OOIP with pressure drop between 1.5 and 2 psi. Wettability alteration and foaming were the suggested mechanisms that would contribute to the incremental oil recovery, but due to lack of aqueous stability of the surfactant solution at 25 ºC, lower recovery and pressure drop were reported in the experiment. The phase separation of the aqueous surfactant solution at this temperature resulted in injection of fluid at inconsistent mixing ratio, thus affecting the recovery and pressure drop negatively. In the last step, the surfactant solution was preheated to 60 ºC and methane gas and surfactant formulation S3 were co-injected for about 4 PVs at 1 ft/D with 70% foam quality which produced an incremental oil of approximately 43% OOIP. The pressure drops during this stage varied between 12 psi and 30 psi. The significant increase in recovery in the last stage of the experiment was primarily due to resolved issue of aqueous stability (no phase separation by pre-heating the surfactant solution at the reservoir temperature) and generation of stronger foam along with wettability alteration. The ultimate cumulative oil recovery was 78.5% OOIP, oil recovery due to in-situ/pre-generated foam was about 52% OOIP and final residual oil saturation was reduced to 13.6%. This experiment proves the significance of the combined strategy of wettability alteration with foaming as a novel method to increase oil production in oil-wet carbonate rocks after gas floods.

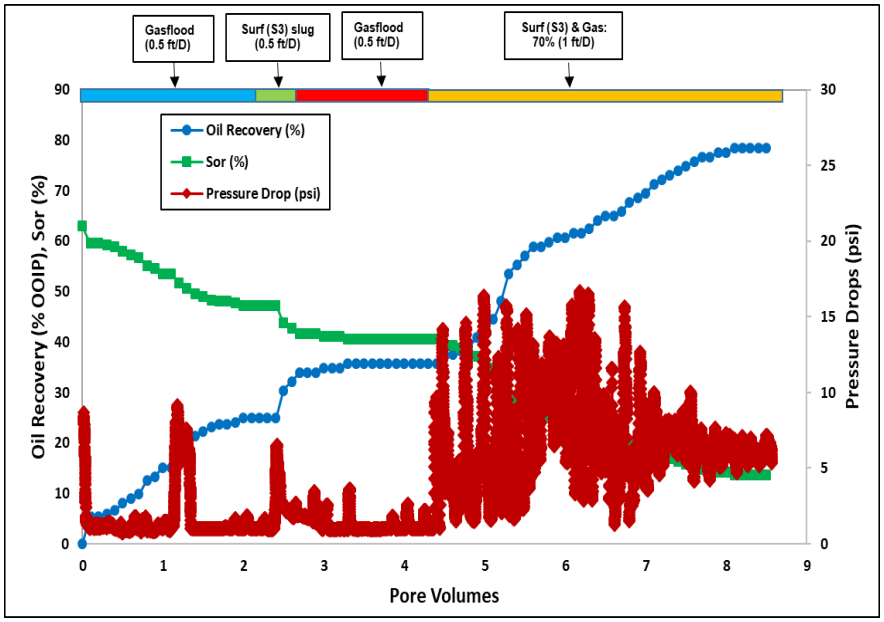

Figure 5.8. Pressure drop profile (right axis) and cumulative oil recovery & oil saturation (left axis) for coreflood G4

Coreflood G5 was conducted in the oil-wet core CG5 with another wettability altering and good foaming surfactant formulation S4; its properties are listed in **Table 5.2**. The oil permeability of this core was higher (22 mD) and the initial oil saturation was 64%. **Figure 5.9** shows cumulative oil recovery, residual oil saturation (primary y-axis) and overall pressure drop (secondary y-axis) across the core. Methane gas was injected at 0.5 ft/D for about 2 PVs until no additional oil was produced. The gas flood recovery was 22% OOIP and oil saturation was reduced to 50%. The pressure drop during the gas flood was between 0.9 psi and 1.5 psi. Then, the core was flooded with a slug of 0.5 PV of surfactant formulation S4 at the same rate resulting in an additional oil recovery of 15.5% OOIP. The oil recovery due to surfactant increased because of the wettability alteration ability of surfactant formulation, S4. The pressure drops during this step varied from 5 psi to 15 psi.

Then, this slug injection was followed with methane gas for about 1.5 PVs until no oil was produced. This step produced an additional oil of 6% OOIP with pressure drop between 2 and 3 psi. Finally, methane gas and surfactant formulation S4 were co-injected for about 3 PV at 1 ft/D with 70% foam quality which produced approximately 27% OOIP. The pressure drops during this stage varied between 7 psi and 16 psi. The significant pressure drops suggest that in the presence of crude oil moderate foam propagated through the core. The ultimate cumulative oil recovery was 70.3% OOIP, oil recovery due to in-situ foam generation (over gas flood) was about 48% OOIP and final oil saturation was reduced to 19%. This coreflood shows that a combination of wettability and good foaming can enhance oil recovery if the reservoir is developed with secondary gas injection.

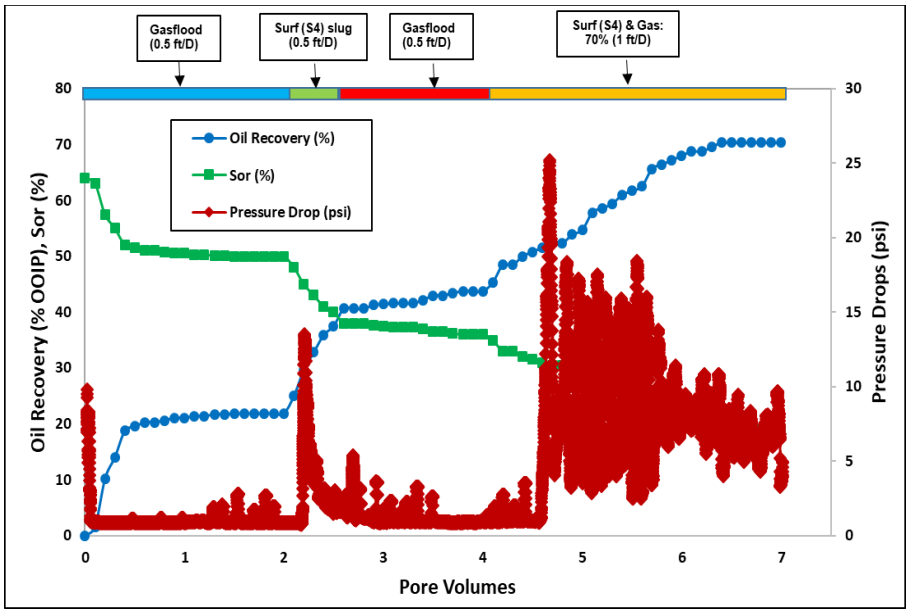

Figure 5.9. Pressure drop profile (right axis) and cumulative oil recovery & oil saturation (left axis) for coreflood G5

Coreflood G6 was conducted in the oil-wet core CG6 with a good foaming and non-wettability altering surfactant formulation S5; its properties are listed in **Table 5.2**. The oil

permeability of this core was 15 mD and the initial oil saturation was 76%. **Figure 5.10** shows cumulative oil recovery, residual oil saturation (primary y-axis) and overall pressure drop (secondary y-axis) across the core. Methane gas was injected at 0.5 ft/D for about 2.5 PV until no additional oil was produced. The gas flood recovery was 12.2% OOIP and oil saturation was reduced to 66.7%. The pressure drop during the gas flood was between 1 psi and 3 psi. Then, the core was flooded with a 0.5 PV slug of surfactant formulation S5 at the same rate resulting in an additional oil recovery of 22.2% OOIP. The oil recovery increased due to surfactant because of the lower interfacial tension (IFT) and the foaming ability of the surfactant formulation, S5. The pressure drop during this step varied from 4 psi to 11 psi. Then, this slug injection was followed with methane gas for about 1.5 PV until no oil was produced. This step produced an additional oil of 8.4% OOIP with pressure drop between 1 and 2.5 psi. Finally, methane gas and surfactant formulation S5 were co-injected for about 3 PVs at 1 ft/D with 70% foam quality which produced approximately 26% OOIP. The pressure drops during this stage varied between 2 psi and 13 psi. The larger fluctuations in pressure drops during the last phase suggest that in the presence of crude oil and no wettability alteration foam stability is poor inside the porous medium. The ultimate cumulative oil recovery was 68.8% OOIP, oil recovery due to in-situ foam generation (over gas flood) was about 56.6% OOIP and final oil saturation was 24%. This core flood shows that only good foaming with no wettability alteration is not sufficient to have maximum oil recovery if the reservoir is developed with secondary gas injection. Note that the oil recovery reported due to surfactant injection in this experiment is higher due to the additional effect of IFT reduction by use of anionic surfactant.

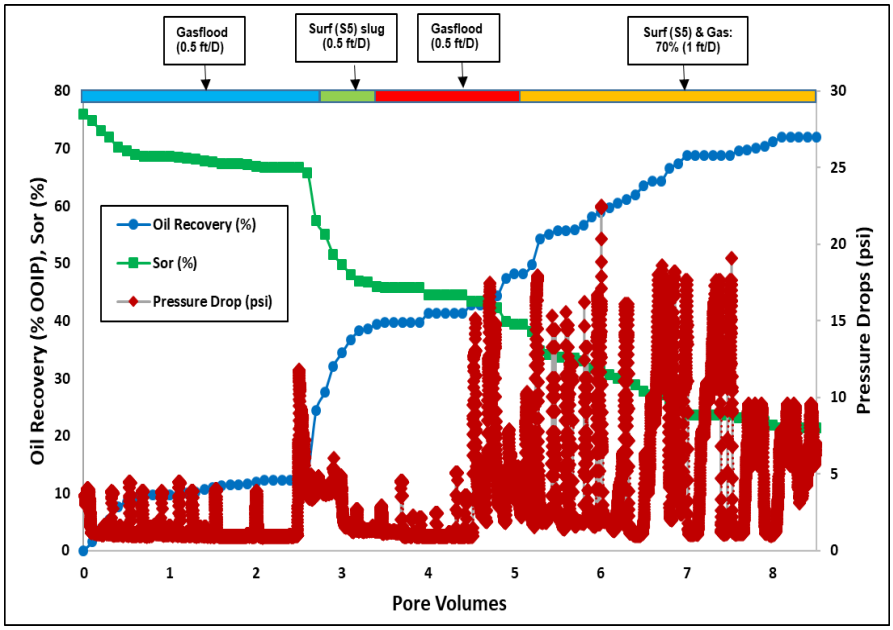

Figure 5.10. Pressure drop profile (right axis) and cumulative oil recovery & oil saturation (left axis) for coreflood G6

The above core floods were designed for an alternating injection of gas and surfactant solution followed by a co-injection of surfactant and gas at a fixed quality. Results in each of the core floods showed that the initial slug of surfactant solution with wettability altering capability helps in changing the rock from oil-wet to water-wet and helps in stabilizing the foam in porous medium at reduced oil saturations. Co-injection of surfactant solution and gas immediately after the first gas injection process would have possibly provided similar recovery results but with increased amounts of fluid injection. With reduced amount of aqueous surfactant solution in the co-injection, the wettability alteration is a slower process and hence longer time is required for foam stabilization in the porous medium. Additional experiments need to be performed to investigate this injection scheme for a comparative study.

For the recovery experiments listed in **Table 5.8**, the following injection scheme was followed. First, a water flood was conducted at 1 ft/day until oil recovery stopped followed with water flood at 5 ft/D. This step was performed to account for any oil recovery due to the end effect for an oil-wet core. Then, surfactant solution and methane gas were co-injected at 1 ft/D with a foam quality 80% from the top until no additional oil was recovered. In few experiments, an additional step of a new surfactant solution and methane gas were co-injected at 1 ft/D with a foam quality 80% from the top till no additional oil was recovered. These floods are designed for reservoirs that have been water flooded. Oil recovery and pressure drops were monitored at every step.

Table 5.8: List of the carbonate core properties used for water flooded reservoirs

Cores	**Estaillades Limestone (CW1)**	**Estaillades Limestone (CW2)**	**TX Cream Limestone (CW3)**
Length (cm)	29.7	27.6	29.5
Diameter (cm)	3.77	3.78	3.76
Porosity, %	24.7	26.0	29.1
Pore Volume, ml	82	80.5	95.2
Oil Permeability @ Soi, mD	35.5	7.4	13.5
Initial oil saturation, Soi	0.89	0.78	0.735

Table 5.9 tabulates the list of surfactant blends used for the experiments, initial wettability-state of the rock, and properties of the surfactant formulations. The viscosities

of surfactant solutions are reported at 60 ºC and a shear rate of 10 sec^{-1}. The total concentration of surfactant in each formulation was kept at about 0.4 - 0.8 wt%.

Table 5.9: Surfactant formulations used in oil displacement experiments

Core Flood #	**Initial Wettability**	**Surfactant formulation**	**Formulation Label**	**Viscosity, cp (60 ºC)**	**pH**	**IFT dyne/cm**
W1	Oil-wet	0.2 wt% BTC + 0.2 wt% NP-10 + Inj. Brine	S6	0.7	7.0	2.3
W1	Oil-wet	0.4 wt% DTAB + 0.4 wt% NP-10 + Inj. Brine	S6*	0.7	7.2	2.3
W2	Oil-wet	0.4 wt% GC 580 + Inj. Brine	S7	0.76	8.0	0.8
W3	Oil-wet	0.4 wt% GC 580 + Inj. Brine	S7	0.76	8.0	0.8
W3	Oil-wet	0.3 wt% GC 580 + 0.1 wt% LB + Inj. Brine	S8	0.75	7.7	1.9

Coreflood W1 was performed in oil-wet core CW1 with a good wettability altering and weak foaming surfactant solution S6 and S6*; its properties are listed in **Table 5.8** The oil permeability of this core was 35.5 mD and the initial oil saturation was 89%. **Figure 5.11** shows cumulative oil recovery, residual oil saturation (primary y-axis) and overall pressure drop (secondary y-axis) across the core. Water was injected at 1 ft/D for about 2 PVs until no additional oil was produced followed with additional injection of water at 5 ft/D for another 1 PV. This step was performed to reach true residual oil in oil-wet cores at

the end of water injection, accounting for end-effects in the core. The total water flood recovery was 27.4% OOIP and oil saturation was reduced to 64.6%. The pressure drops during the water flood were between 7.5 psi and 13.5 psi. Then, co-injection of injection brine and methane gas at 1 ft/D with 80% quality for about 3.5 PVs until no oil was produced. This step was considered as a base case for these oil displacement experiments where the aqueous solution did not contain any wettability altering surfactant solution. The additional oil recovery during this step was about 30% OOIP and the residual oil saturation was 38.1%. The average pressure drops varied between 5 psi and 10 psi. Note, this high incremental oil production during the base case step is unusual and possibly might be an experimental artifact or irregular fluid transport in the porous medium. After the base step, co-injection of surfactant formulation S6 with methane gas was performed at 1 ft/D with 80% foam quality for about 6.5 PVs until no oil was produced. This step resulted in an additional oil recovery of 18% OOIP and the residual oil saturation was 31%. The increase in oil recovery was primarily due to the wettability altering capability of the surfactant formulation. The average pressure drops during this step varied between 8 psi to 15 psi. Finally, an additional co-injection step with surfactant formulation S6* and methane at 1 ft/D with 80% foam quality was performed to investigate the effect of higher surfactant concentration and additional amount of wettability altering surfactant solution. The injection was continued for about 7 PV of foam injection which resulted in an additional oil recovery of 19% and the oil saturation was reduced to 14%. The pressure drops during this stage varied between 4 psi and 8 psi. The fluctuations in pressure drops during significant amount of foam injection suggest that in the presence of crude oil this

formulation generated weak foam inside the porous medium. The ultimate cumulative oil recovery was 84.1% OOIP, oil recovery due to foam injection (over water flood and base case) was about 27% OOIP and final oil saturation was 14.1%. This core flood showed evidence of good wettability alteration but poor foaming; hence not enough to have maximum oil recovery if the reservoir is developed with secondary water injection. Note that the oil recovery reported due to surfactant injection in this experiment is higher due to the additional volume of surfactant solution injected.

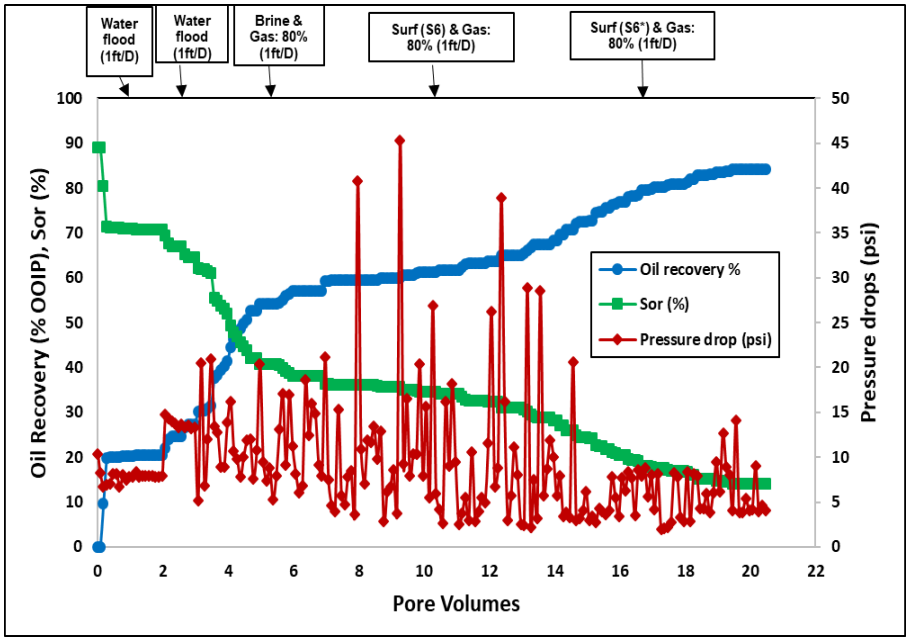

Figure 5.11. Pressure drop profile (right axis) and cumulative oil recovery & oil saturation (left axis) for coreflood W1

Coreflood W2 was performed in oil-wet core CW2 with a moderate wettability altering and moderate foaming surfactant solution S7; its properties are listed in **Table 5.8.** The oil permeability of this core was 7.4 mD and the initial oil saturation was 78%. **Figure 5.12** shows cumulative oil recovery, residual oil saturation (primary y-axis) and overall

pressure drop (secondary y-axis) across the core. Water was injected at 1 ft/D for about 2.6 PVs until no additional oil was produced followed with additional injection of water at 5 ft/D for another 1 PV. This step was performed to reach true residual oil in oil-wet cores at the end of water injection, accounting for end-effects in the core. The total water flood recovery was 63.6% OOIP and oil saturation was reduced to 28.4%. The pressure drops during the water flood were between 16 psi and 75 psi. Then, base case with co-injection of injection brine and methane gas at 1 ft/D with 80% quality for about 2 PVs until no oil was produced. The additional oil recovery during this step was about 5.4% OOIP and the residual oil saturation was 24.1%. The average pressure drops varied between 6 psi and 20 psi. After the base step, co-injection of surfactant formulation S7 with methane gas was performed at 1 ft/D with 80% foam quality for about 6 PVs until no oil was produced. This step resulted in an additional oil recovery of 9% OOIP and the residual oil saturation was 17%. The poor oil recovery can be contributed to the weak foaming and moderate wettability altering capability of the surfactant formulation. The average pressure drops during this step varied between 9 psi to 25 psi. The large fluctuations in pressure drops during significant amount of foam injection suggest that in the presence of crude oil this formulation generated weak foam inside the porous medium. The ultimate cumulative oil recovery was 78.1% OOIP, oil recovery due to foam injection (over water flood and base case) was about 9% OOIP and final oil saturation was 17%. This core flood emphasized the importance of strong good wettability alteration in combination with good foaming ability to maximize oil recovery during tertiary processes for reservoirs with secondary water injection.

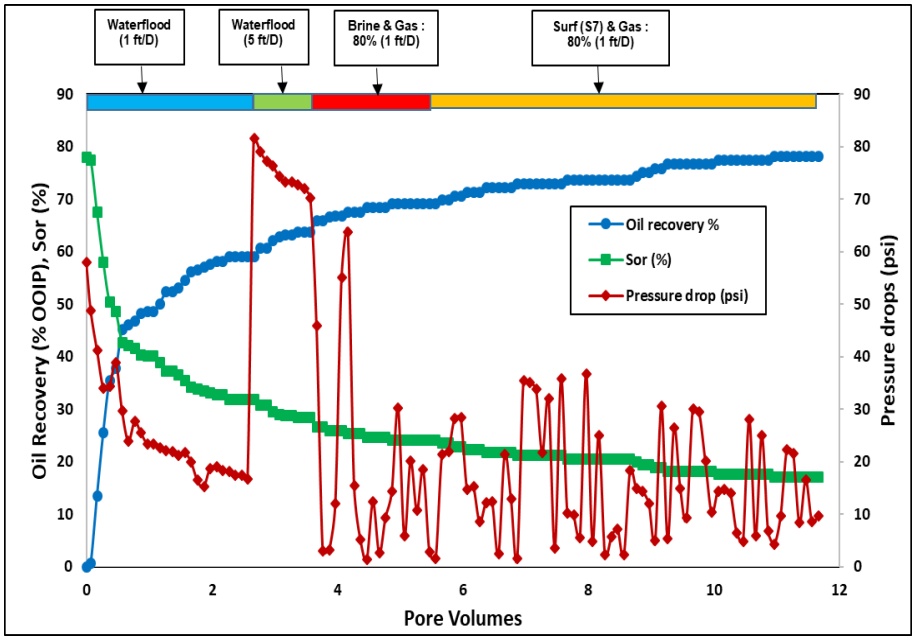

Figure 5.12. Pressure drop profile (right axis) and cumulative oil recovery & oil saturation (left axis) for coreflood W2

An additional core flood W3 was performed in oil-wet core CW3 with a moderate wettability altering and good foaming surfactant solution S7 and S8; its properties are listed in **Table 5.8** The oil permeability of this core was 13.5 mD and the initial oil saturation was 73.5%. **Figure 5.13** shows cumulative oil recovery, residual oil saturation (primary y-axis) and overall pressure drop (secondary y-axis) across the core. Water was injected at 1 ft/D for about 2.1 PVs until no additional oil was produced followed with additional injection of water at 5 ft/D for another 1 PV. This step was performed to reach true residual oil in oil-wet cores at the end of water injection, accounting for end-effects in the core. The total water flood recovery was 54.6% OOIP and oil saturation was reduced to 33.4%. The pressure drops during the water flood were between 7.5 psi and 35 psi. Then, base case with co-injection of injection brine and methane gas at 1 ft/D with 80% quality for about 2

PVs until no oil was produced. The additional oil recovery during this step was about 5.3% OOIP and the residual oil saturation was 29.5%. The average pressure drops varied between 2.7 psi and 10 psi. After the base step, co-injection of surfactant formulation S7 with methane gas was performed at 1 ft/D with 80% foam quality for about 4.5 PVs until no oil was produced. This step resulted in an additional oil recovery of 6% OOIP and the residual oil saturation was 25.3%. Finally, an additional step of co-injection of surfactant formulation S8 and methane were performed at 1 ft/D with 80% foam quality for about 2 PV. The average pressure drops during the foam injection steps varied between 2 psi and 20 psi. The poor oil recovery can be contributed to the weak foaming and moderate wettability altering capability of the surfactant formulation S7 and S8. The large fluctuations in pressure drops signify rapid foam collapse during foam injection steps which suggest that in the presence of crude oil this formulation generated weak foam inside the porous medium. The ultimate cumulative oil recovery was 69.9% OOIP, oil recovery due to foam injection (over water flood and base case) was about 10% OOIP and final oil saturation was 22.1%. This core flood emphasized the importance of strong good wettability alteration in combination with good foaming ability to maximize oil recovery during tertiary processes for reservoirs with secondary water injection.

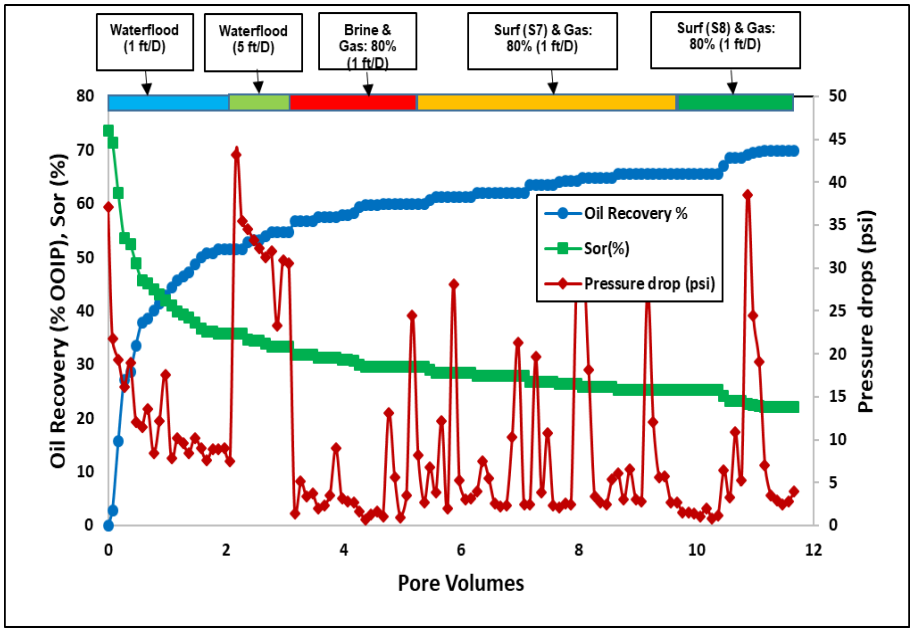

Figure 5.13. Pressure drop profile (right axis) and cumulative oil recovery & oil saturation (left axis) for coreflood W3

5.2.8 Post Core Flood Analysis

After the completion of Core Flood G5, we visually inspected the outside of the core. Some of the key findings are as follows. First, the oil saturation increased from the top to the bottom, as shown in **Figure 5.14(a)**. This is primarily due to better sweep efficiency at the top of the core (point of injection of the foam) and due to gravity drainage. Second, we observed visual evidence of fluid channeling. **Figure 5.14(b)** shows evidence of fluid channeling through the edges of the core and the water drop test proved that areas swept by the wettability altering surfactant solution were water-wet, whereas the un-swept areas were still intermediate to oil-wet. **Figure 5.14(c)** also confirms that the injection side of the core was altered from oil-wet to water-wet at the end of the experiment.

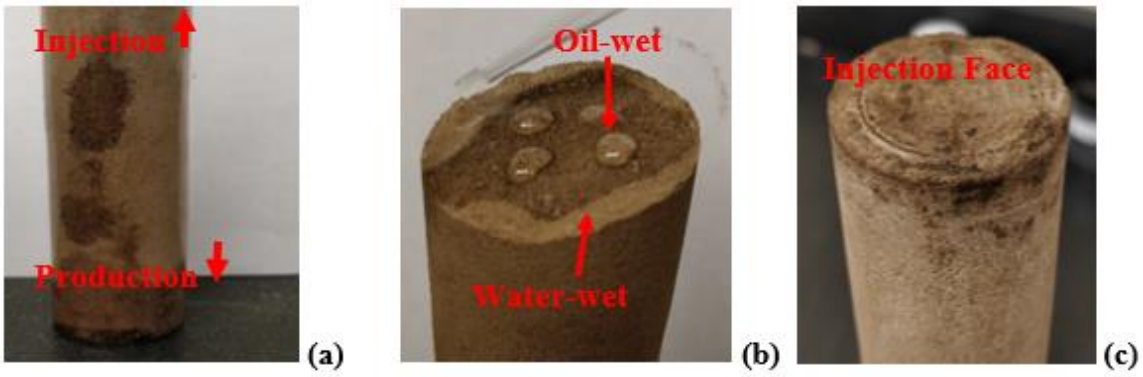

Figure 5.14. Post Experiment Analysis for Core Flood G5 – (a) fluid redistribution, (b) fluid channeling, (c) injection face

5.3 SUMMARY AND RECOVERY FACTORS

To summarize the results from the oil displacement experiments (with secondary gas injection) shown above and understand the efficiency of the processes, we have defined tertiary recovery factors (TRF) to quantify the normalized reduction in residual oil saturation due to only surfactant injection (TRF1) and surfactant-gas co-injection processes (TRF2). Tertiary recovery factor (TRF1) is calculated based on the normalized change in residual oil saturation at the end of slug injection of surfactant solution with wettability alteration, and tertiary recovery factor (TRF2) is calculated as the total normalized change in residual oil saturation at the end of surfactant and gas co-injection, after the initial gas injection process. They are defined as follows:

$$\text{TRF1} = \frac{(Sorg - Sors)}{Sorg}; \qquad \text{TRF2} = \frac{(Sors - Sorc)}{Sors}. \tag{5.1}$$

where S_{org} = residual oil saturation to initial gas injection, S_{ors} = residual oil saturation to surfactant slug and second gas slug, and S_{orc} = residual oil saturation after following surfactant and gas co-injection.

Table 5.10 summarizes the results of all the oil displacement experiments with residual oil saturations at different stages of the process and the corresponding TRF values. The results showed that core flood G3 has the highest TRF1 with good wettability alteration and moderate foaming; it proved to be the most successful in reduction of residual oil saturation in oil-wet cores by only the surfactant slug injection. Note that core flood G1 has higher TRF1 than core flood G3, but that experiment was performed in a water-wet core (base case); hence not included in the comparison. On the other hand, core floods G4 and G5, with good foaming and good wettability alteration, were the most successful in total reduction of residual oil saturation (highest TRF2) at the end of the co-injection process. In addition, the results of core flood G6 agreed where TRF1 was low due to no wettability altering capability of the surfactant formulation and the TRF2 value was high due to low IFT and good foaming ability. These results also emphasize the fact TRF1 is governed mostly on the wettability altering ability of the surfactant solution, whereas TRF2 is governed mostly by the foaming ability of the surfactant solution. The TRF values calculated agreed with our proposed strategy of synergistic effect of wettability alteration with foaming for increasing oil production.

Table 5.10: Summary of Oil Displacement Experiments with Secondary Gas Injection

Core flood #	**S_{oi}**	**S_{org}**	**S_{ors}**	**S_{orc}**	**TRF1**	**TRF2**
G1	0.76	0.68	0.36	0.3	0.46	0.17
G2	0.75	0.69	0.5	0.34	0.28	0.32
G3	0.62	0.47	0.27	0.24	**0.43**	0.11
G4	0.73	0.47	0.39	0.14	0.17	**0.64**
G5	0.64	0.5	0.36	0.19	0.28	**0.47**
G6	0.76	0.67	0.5	0.24	0.25	**0.52**

To summarize the results from the oil displacement experiments (with secondary water injection) shown above and understand the efficiency of the processes, we have defined tertiary recovery factors (TRF) to quantify the normalized reduction in residual oil saturation due to brine (no surfactant) and gas co-injection (TRF3) and surfactant-gas co-injection processes (TRF4). Tertiary recovery factor (TRF3) is calculated based on the normalized change in residual oil saturation at the end of brine and gas co-injection process (base case), and tertiary recovery factor (TRF4) is calculated as the total normalized change in residual oil saturation at the end of surfactant and gas co-injection, which followed the base case. They are defined as follows:

$$\text{TRF3} = \frac{(Sorw - Sor\ g/w)}{Sorw}; \qquad \text{TRF4} = \frac{(Sor\ g/w - Sorc)}{Sor\ g/w}. \tag{5.2}$$

where S_{orw} = residual oil saturation to initial water injection, $S_{or\ g/w}$ = residual oil saturation to brine and gas co-injection (base case), and S_{orc} = residual oil saturation after following surfactant and gas co-injection.

Table 5.11 summarizes the results of all the oil displacement experiments with residual oil saturations at different stages of the process and the corresponding TRF values. The results showed that core flood W1 has the highest TRF3 whereas core floods W2 and W3 had comparable TRF3 values. The possible explanation in the difference of the performance can be due to some abnormal water flood results obtained in core flood 1 which resulted in higher S_{orw} and possibly not true residual oil saturation. Also, the TRF3 values were directly proportional to the permeability of the porous medium for a similar pore size distribution. On comparing the results for TRF4 values, core flood W1 had the highest value compared to core floods W2 and W3 due to injection of higher amount of wettability altering and foaming surfactant solution along with gas. These results also emphasize the fact TRF3 is governed mostly on the lowering of the relative permeability of the fluid flow in presence of gas and water (no surfactant), whereas TRF4 is governed mostly by the wettability altering and foaming ability of the surfactant solution.

Table 5.11: Summary of Oil Displacement Experiments with Secondary Water Injection

Core flood #	**S_{oi}**	**S_{orw}**	**$S_{or\ g/w}$**	**S_{orc}**	**TRF3**	**TRF4**
W1	0.89	0.64	0.38	0.14	**0.41**	**0.63**
W2	0.78	0.28	0.24	0.17	0.14	0.29
W3	0.74	0.33	0.29	0.22	0.12	0.24

5.4. CONCLUSIONS

Secondary gas and water flooding in carbonate rocks is often poor due to oil-wetness and heterogeneity. Surfactant solutions and foams have the potential to improve oil

recovery but must overcome two adverse conditions in carbonates: oil-wettability and low permeability. This study evaluates several surfactant solutions and foam formulations that combine wettability alteration and foaming in low permeability oil-wet carbonate cores. The following conclusions can be drawn from this study:

- Cationic surfactants DTAB and BTC altered the wettability of the oil-wet calcite plate to water-wet but were ineffective in forming foam. The addition of a non-ionic surfactant Tergitol NP helped in the foaming ability of these formulations.

- Mixtures of in-house developed Gemini cationic surfactant GC 580 and zwitterionic surfactants were able to alter the wettability from oil-wet to water-wet and formed strong bulk foam.

- The results obtained from bulk foam tests without and with crude oil were a good indicator of the performance of the surfactant formulations in porous media in absence of crude oil and presence of crude oil, respectively. Higher half-life led to higher MRF and higher oil recovery.

- The foam generated in low permeability water-wet carbonate cores (without oil) is weak with low mobility reduction factors, of the order of 3 (compared to 20 for high permeability cores).

- Oil displacement experiments in oil-wet carbonate cores revealed that injection of wettability-altering surfactant can recover a significant amount of oil (about 20-

30% OOIP) over the secondary gas flood and about 10-20% OOIP over the secondary water flood.

- Foams with wettability altering surfactants can also recover additional oil. The foam rheology in the presence of oil suggests propagation of only weak/moderate foam in oil-wet carbonate cores.
- Post core flood analysis showed visual evidence of successful wettability alteration and fluid channeling effects due to weak foam generated in the porous media.
- Wettability alteration in synergy with foaming improves oil recovery significantly and is crucial to make foam stable in oil-wet porous media.
- Coreflood experiments performed with gas injection as secondary process performed superior to the experiments with water injection as secondary process due to lower residual oil saturation to the water injection processes.

Chapter 6: Laboratory Treatment of Synthetic Polymers for Injection in Low Permeability Carbonate Reservoirs

Chapters 4 and 5 discussed the use of anionic and cationic surfactants in foam EOR processes for tertiary oil recovery in oil-wet low permeability carbonate formations using wettability alteration, low IFT and foaming mechanisms. The negative effects of oil-wetness, heterogeneity and low permeability in carbonates on foam EOR performance were emphasized in the previous chapters. The significantly higher pressure drops required for foam generation and mobilization seemed unfeasible for field scale applications and the uncertainties in the foam behavior in challenging rock systems introduced a significant challenge in upscaling the laboratory 1-D experiments to field scale. The performances predicted from laboratory experiments could be seriously misleading for real field projects. Hence, a more robust and established mobility control agent like polymer was investigated for improvement of the performances of chemical EOR processes in oil-wet low permeability carbonate reservoirs.

The objective of this chapter is to understand the mechanisms of polymer shear degradation using a laboratory blender at high speed shearing and its effect on modification on molecular weight distribution along with viscosity loss. As a scope of this work polymers of different chemistry and molecular weight have been studied to develop a better model for prediction of viscosity loss and optimum shear degradation time for successful injection in low permeability carbonate rocks. Each of the shear degradation experiments have been performed at the polymer stock conditions prepared in different salinity brines.

The influence of physical-chemistry parameters such as viscosity, temperature, solvent quality, and polymer concentration was not in the scope of the work, even though these parameters play a significant role in polymer rheology measurements. Diluted polymer concentrations from shear degraded stocks were used for aggressive filtration tests through small filter papers and dynamic light scattering method was used to estimate the modified size distribution. Series of polymer injectivity experiments were performed in outcrop limestone cores of low permeability after comparison of the polymer size distribution from DLS with pore throat size distribution obtained from MICP measurements.

6.1 MATERIALS

Table 6.1 lists the polymers used in this study and their properties. All the polymers samples in powder form were obtained from SNF Floerger, France and BASF, USA. Properties of the samples as provided by the suppliers are summarized in the Table 6.1.

Table 6.1: Polymers used in the present study

Polymer Name	**MW (10^6 g/mol)**	**AMPS Content**
FP 3130s	3 - 5	-
FP 3230s	4 - 6	-
FP 3330s	8 - 10	-
Aspiro P 4211	8 – 10	-
AN 125 MPM	4 - 6	++
AN 125 SH	10 - 12	++
AN 125 VHM	13 - 15	++
Aspiro P5421 X	6 - 8	++
AN 132	4 - 6	+++
AN 132 SH	10 - 12	+++
SAV 55	5 - 7	++++
SAV 10	4 - 6	+++++
SAV 10 XV	10 - 12	+++++

Table 6.2 lists the properties of the limestone cores (C1 & C2) used in this study. Texas Cream limestone and Edwards Yellow limestone rocks were used for the experiments. Each core was about 1 ft long and 1.5 inch in diameter.

Table 6.2: List of the properties of different carbonate cores

Cores	**TX Cream Limestone (C1)**	**Edwards Yellow Limestone (C2)**
Length (cm)	29.5	30.1
Diameter (cm)	3.76	3.76
Porosity, %	26.8	27.65
Pore Volume, ml	84.5	90.5
Brine Permeability	15.6	12.6

The brine compositions used as part of this study are tabulated in **Table 6.3**. All the experiments were performed at ambient temperatures except the polymer injectivity tests in porous media. Synthetic formation brine and synthetic sea- water were used as part of this study. The viscosity was measured using an AR-G2 rheometer.

Table 6.3: Synthetic formation and sea water brine compositions

Composition	**Synthetic Formation Brine (ppm)**	**Synthetic Sea Water (ppm)**
Na^+	10,550	14,305
Ca^{2+}	354.4	564
Mg^{2+}	591.6	1,576
SO_4^{2-}	3645	3,816
Cl^-	16,000	24,814
Total Salinity	31,121	45,075

6.2. RESULTS AND DISCUSSIONS

6.2.1 Polymer Rheology Measurements

Polymer stock solutions with 1 wt% were prepared in DI or synthetic sea water based on the chemistry of the polymers. The final hydrated polymers after overhead mixing were used for shear degradation studies in laboratory blender at 18,000 rpm. The shearing speed was kept constant throughout the study with varying shearing time to change the total energy dissipated to the polymer solution. Conventional HPAM polymers were prepared in DI and shear degradation performed in DI as well. **Figure 6.1** shows the result of the measured viscosity at 0.1 s^{-1} (all measurements taken at 25 ^{o}C) with varying shearing time for each HPAM polymers. Each polymer sample was normalized for its molecular weight to superimpose the graphs and find a correlation to predict the viscosity at any given shearing time in a similar brine salinity. The results show a good agreement with the different polymer types. Note FP 3330s was used as the reference polymer and the measurements of the other polymers were corrected for the final correlation.

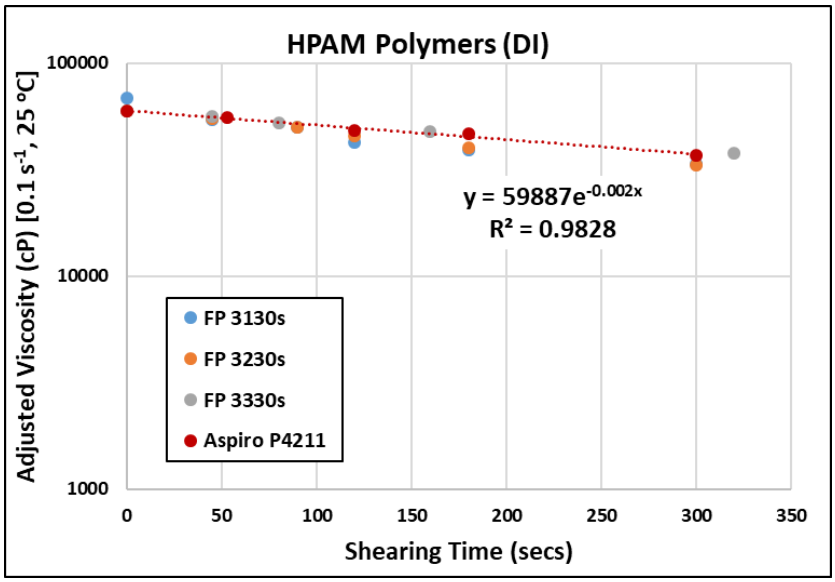

Figure 6.1. Viscosity measurement for HPAM polymers (1 wt%) in DI with varying shearing time in a laboratory blender

The general correlation to predict the shear degraded viscosity using a laboratory blender at 18,000 rpm at any shearing time for any HPAM polymers is given below:

$$\eta\ (cP) = (M_w/M_{w,\ ref}) * SF * 59887 * \exp(-0.002t) \quad (6.1)$$

where η is measured at 0.1 s^{-1} and 25 ^oC using a viscometer, t is the shearing time in the blender in seconds, $M_{w,\ ref}$ is the molecular weight of FP 3330s polymer, M_w is molecular weight of any HPAM polymer, and SF is the scale factor for each polymer. Viscosity estimations for any other HPAM polymer can be obtained using a scale factor based on their molecular weight ratios as suggested below in **Table 6.4**.

Table 6.4: Scale Factors for Viscosity Estimations of HPAM polymers

Polymer Type	**Molecular Weight (10^6 gm/mole)**	**Scale Factor (SF)**
FP 3130s	3	0.16
FP 3230s	4	0.78
FP 3330s	8	1
Aspiro P4211	8	1

Similar shear degradation viscosity measurements were performed with the polymer stock solutions for sulfonated PAMS in DI water. **Figure 6.2** shows the result of the measured viscosity at 0.1 s^{-1} with varying shearing time for each sulfonated PAM polymers. The results show a good agreement with the different polymer types after correction with their respective molecular weights. Note, in this case AN132 SH was used as the reference polymer and the measurements of the other polymers were corrected for the final correlation.

The general correlation to predict the shear degraded viscosity using a laboratory blender at 18,000 rpm at any shearing time for any sulfonated PAM polymers is given below:

$$\eta\ (cP) = (M_w/M_{w,\ ref}) * SF * 66089 * \exp(-0.004t) \qquad (6.2)$$

where η is measured at 0.1 s^{-1} and 25 ^oC using a viscometer, t is the shearing time in the blender in secs, $M_{w,\ ref}$ is the molecular weight of AN125 SH polymer and M_w is molecular weight of any HPAM polymer. The results also showed higher sensitivity to shear degradation for sulfonated PAMs compared to HPAM polymers, which suggests lower

shearing time necessary for necessary modification of polymer size distribution. On the contrary, on comparing the viscosity measurements of AN132 SH and AN125 SH in DI, the increased amount of sulfonation did not seem to affect the shear degradation of polymer and both showed similar behavior in rheological properties. Viscosity estimations for any other sulfonated PAM polymers can be obtained using a scale factor based on their molecular weight ratios and sulfonation content as suggested below in **Table 6.5**.

Table 6.5: Scale Factors for Viscosity Estimations of Sulfonated PAM polymers

Polymer Type	**Molecular Weight (10^6 gm/mole)**	**Scale Factor (SF)**
AN125 SH	8	1
AN132	4	1.4
AN132 SH	8	0.9

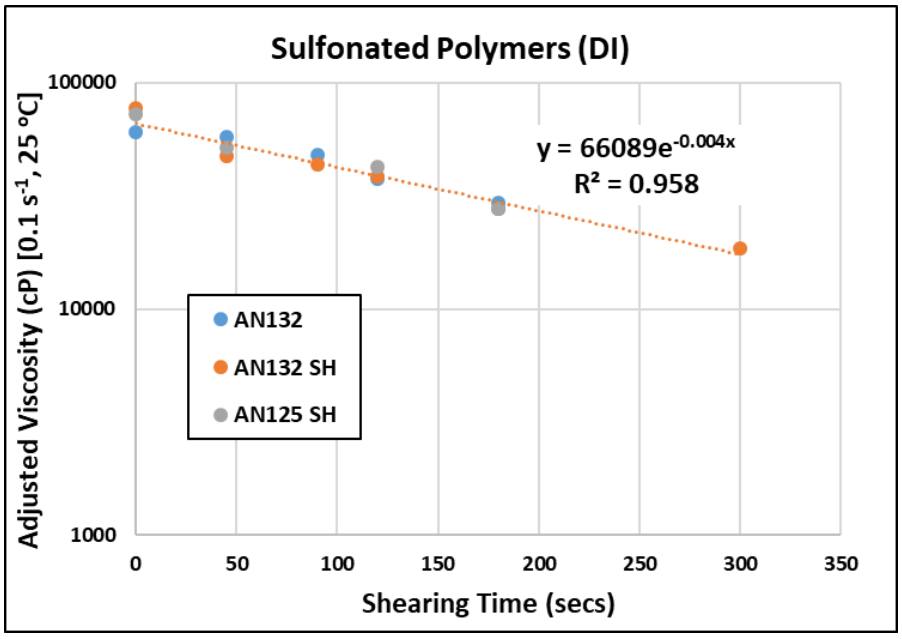

Figure 6.2. Viscosity measurement for sulfonated PAM polymers (1 wt%) in DI with varying shearing time in a laboratory blender

The shear degradation studies were also performed in synthetic sea water to investigate the effect of higher salinity and more importantly presence of divalent ions on the rate of degradation of high molecular weight polymer chains. Sulfonated PAMs and SAV polymers were used as part of this study. **Figure 6.3** shows the result of the measured viscosity at 0.1 s^{-1} with varying shearing time for each sulfonated PAM polymers. The results show a good agreement with the different polymer types after correction with their respective molecular weights. Note, in this case SAV 10 XV (highest MW) was used as the reference polymer and the measurements of the other polymers were corrected for the final correlation.

The general correlation to predict the shear degraded viscosity using a laboratory blender at 18,000 rpm at any shearing time for any sulfonated PAM polymers in synthetic sea water is given below:

$$\eta\ (cP) = (M_w/M_{w,\,ref}) * SF * 1043.7 * \exp(-0.015t) \qquad (6.3)$$

where η is measured at 0.1 s^{-1} and 25 ^oC using a viscometer, t is the shearing time in the blender in secs, $M_{w,\,ref}$ is the molecular weight of SAV 10 XV polymer and M_w is molecular weight of any sulfonated PAM or SAV polymers. The results also showed higher sensitivity to shear degradation for sulfonated PAMs compared to HPAM polymers, which suggests lower shearing time necessary for necessary modification of polymer size distribution. Viscosity estimations for any other polymer can be obtained using a scale factor based on their molecular weight ratios as suggested below in **Table 6.6**.

Table 6.6: Scale Factors for Viscosity Estimations of SAV/ Sulfonated PAM polymers

Polymer Type	**Molecular Weight (10^6 gm/mole)**	**Scale Factor (SF)**
AN125 MPM	4	1.0
AN125 SH	8	2.5
Aspiro P5421X	6	1.6
SAV 10	4	0.8
SAV 10 XV	16	1
SAV 55	5	1.5

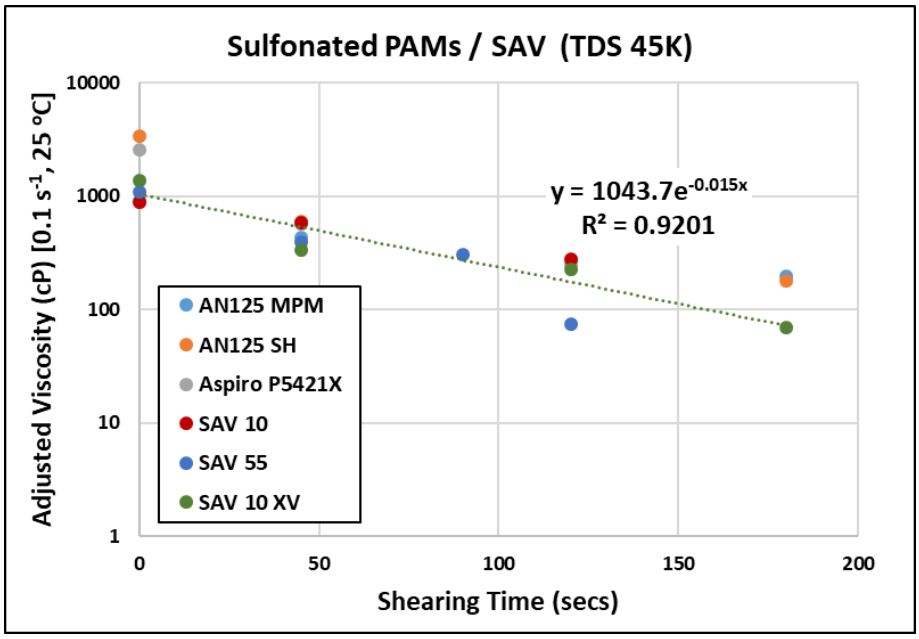

Figure 6.3. Viscosity measurement for sulfonated PAM and SAV polymers (1 wt%) in synthetic sea water with varying shearing time in a laboratory blender

The above results suggested increased shear degradation in presence of higher salinity brine (containing higher number of divalent ions) and significant viscosity loss. For a similar polymer chemistry, the viscosity retained was a function of the molecular

weight of the polymer samples. Higher molecular weight leads to higher viscosity retained at varying shearing time. On comparing the results of AN125 MPM and SAV 10 in synthetic sea water, it suggests higher sensitivity of shear degradation for higher sulfonated polymers (SAV 10) as observed earlier in the studies with DI water.

6.2.1.1 Effect of Brine Salinity on Shear Degradation

This additional experiment was performed to investigate the effect of brine salinity on a similar polymer sample and estimate the degradation rate and viscosity loss. The primary goal of any EOR polymer application is conservation of polymer viscosity at the injected polymer concentrations to make it economical. **Figure 6.4** shows the result of the measured viscosity at 0.1 s^{-1} with varying shearing time for AN125 SH polymer in DI and synthetic sea water.

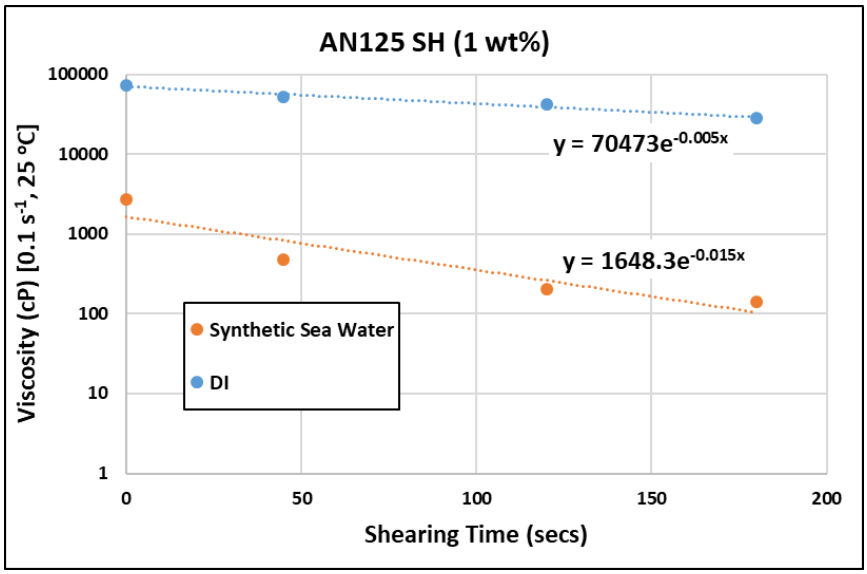

Figure 6.4. Viscosity measurement for AN125 SH (1 wt%) in synthetic sea water and DI with varying shearing time in a laboratory blender

The above results show the significant contribution of brine salinity (divalent ions) and stock viscosity on the shear degradation rate for these polymers. The effect of stock viscosity can be isolated from the salinity effect with the normalization of the viscosities measured at 0.1 s^{-1} for solutions in synthetic sea water and DI. We can deduce the following correlation to estimate the contribution of salinity on the degraded viscosity estimations after the normalization:

$$\eta\ (cP) = 1.6^* \exp(-0.01t) \qquad (6.4)$$

where η is measured at 0.1 s^{-1} and 25 ^oC using a viscometer, t is the shearing time in the blender in secs. This suggests that accounting for the accurate salinity (and hardness) in brines is crucial for estimations of degraded viscosity during mechanical degradation processes. Note, an error analysis was also performed for each of these polymer samples to estimate the difference between the predicted and measured viscosities during shear degradation. The predictions for polymer in DI were less than 10% mostly whereas higher error margin was observed for predictions in synthetic sea water.

In order to understand the underlying mechanism of presence of ions on shear degradation process, an additional experiment was performed with AN125 SH polymer sample with solutions prepared in DI and synthetic sea water for equal viscosity. Hence, measurements were compared for 0.17 wt% AN125 SH prepared in DI and 1 wt% AN125 SH prepared in synthetic sea water. **Figure 6.5** shows the result of the measured viscosity at 0.1 s^{-1} with varying shearing time for equal viscosity solutions of AN125 SH polymer in DI and synthetic sea water. Interestingly, the viscosity degradations were found to be higher in synthetic sea water than DI only after shearing time of 100 secs.

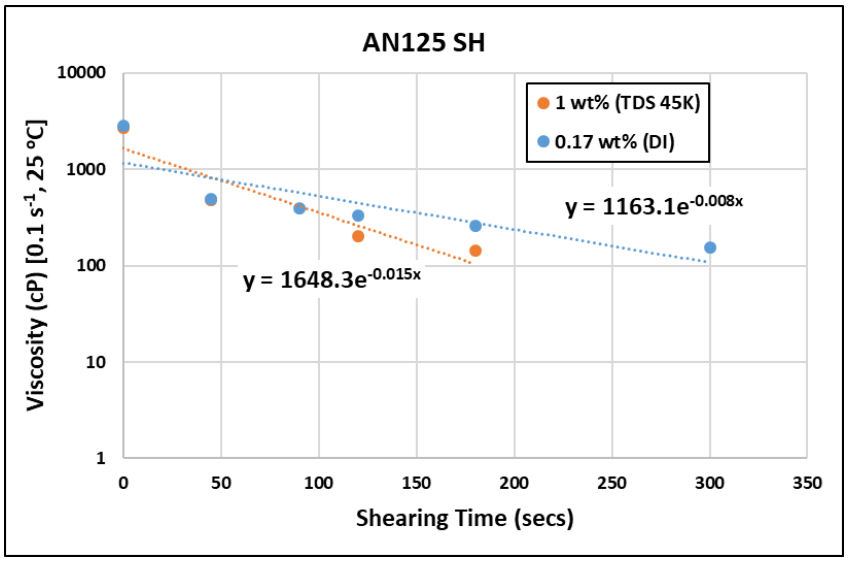

Figure 6.5. Viscosity measurement for AN125 SH in synthetic sea water and DI with varying shearing time in a laboratory blender

We can deduce the following correlation to estimate the contribution of salinity on the degraded viscosity estimations for an equal viscosity solution:

$$\eta\ (cP) = 1.4^{*} \exp(-0.007t) \qquad (6.5)$$

On comparing equations 6.4 and 6.5, we can conclude that even after normalization with stock viscosity it is not possible to completely decouple the effect of polymer solution viscosity and brine salinity and should be considered for viscosity predictions in future during shear degradation process.

6.2.2 Kinetics of Mechanical Degradation

Typical results of degradation experiments at 25 ^{o}C with a laboratory blender are presented above. For all these experiments, identical volumes of polymer solutions at 1 wt% were sheared at constant rotational speed in the blender. As seen from the results, the viscosity decreases exponentially as a function of shearing time. When expressed in terms

of degradation, the degradation asymptotically reaches a steady state depending on the rotational speed. During these experiments, constant strain rate shear degradation occurs and usually there is a critical MW_c beyond which no further degradation is observed. The molecular weight of the polymers undergoes continuous change before the steady state is obtained. Based on the viscosity measurements of the shear degraded polymers from a viscometer at very low shear rates, intrinsic viscosity calculations were performed to estimate the modified MW of the polymers after mechanical degradation. The following expression was used to estimate the intrinsic viscosity of these polymer samples (Jouenne et al., 2019):

$$\eta_{spe} = c[\eta] + 0.56*(c[\eta])^{2.17} + 0.0026*(c[\eta])^{4.72} \quad (6.6)$$

where η_{spe} is calculated from the low shear viscosity measurements using a viscometer and solvent viscosity at 25 ^{o}C. The intrinsic viscosity is estimated from a trial and error fit to the above correlation that closely matches the calculated specific viscosity. Finally, the MW is estimated from the Mark Houwink correlation:

$$[\eta] = K M^{a} \quad \text{(Mark Houwink equation)} \quad (6.7)$$

where $[\eta]$ is in L/g, M is in megaDalton (10^6 g/mol), a = 0.737 and K varies between 1.65 for polymers in DI and 0.28 for polymers in synthetic sea water. The shear thinning index (n) can also be estimated from the following equations (suggested by Jouenne et al. (2019)) to understand the effect of degradation mechanism on shear thinning behavior and elasticity of the polymers in different brine salinities.

$$n = 1 - (0.796 - 0.687*\exp(-0.059*c[\eta]) \quad (6.8)$$

where η_s is the solvent viscosity, M is the modified MW of the polymers and T is the temperature of measurement (25 ^oC).

Once the MW and intrinsic viscosity measurements were estimated, Flory Fox equation was used to estimate the radius of gyration of the polymer samples at the modified molecular weight after mechanical degradation,

$$[\eta] = \phi_0 * \frac{R_g^3}{M} \quad \text{(Flory Fox equation)} \qquad (6.9)$$

where ϕ_0 is a constant (3.69*E^24 mol^{-1}) based on the distribution of segments within the coil. **Tables 6.7-6.9** provides the summary of the intrinsic viscosity measurements, modified MW, shear thinning index (n), radius of gyration (Rg) and hydrodynamic radius (Rh) for each polymer in both DI and synthetic sea water. Note, that the MWs estimated in DI as part of this study was found to be lower than the MW ranges provided by the supplier and could be an artifact of the model used to estimate the intrinsic viscosity. On the other hand, the MW estimations in synthetic sea water were in good agreement with the values reported by the supplier.

Table 6.7: Summary of Intrinsic Viscosity, MW, n, Rg and Rh Estimations for HPAM Polymers

Polymer Type	**Brine Salinity**	**Shearing Time (secs)**	**Intrinsic Viscosity [η] (L/g)**	**MW (10^6 g/mol)**	**n**	**Rg (nm)**	**Rh (nm)**
FP 3130s	DI	0	2.01	4.14	0.414	131	169
		45	1.92	4.00	0.426	128	165
		90	1.88	3.95	0.430	126	163
		120	1.82	3.84	0.439	124	160
		180	1.79	3.81	0.443	123	158
		300	1.72	3.70	0.452	120	155
FP 3230s	DI	0	3.13	5.72	0.312	169	218
		45	3.06	5.62	0.317	167	216
		90	2.99	5.52	0.322	165	213
		120	2.92	5.44	0.326	163	210
		180	2.83	5.32	0.333	160	206
		300	2.70	5.13	0.344	155	201
FP 3330s	DI	0	4.09	6.96	0.265	198	255
		45	4.00	6.84	0.269	195	252
		80	3.82	6.62	0.276	190	245
		160	3.77	6.55	0.278	189	243
		320	3.57	6.29	0.288	183	236

Table 6.8: Summary of Intrinsic Viscosity, MW, n, Rg and Rh Estimations for Sulfonated PAMs

Polymer Type	**Brine Salinity**	**Shearing Time (secs)**	**Intrinsic Viscosity [η] (L/g)**	**MW (10^6 g/mol)**	**n**	**Rg (nm)**	**Rh (nm)**
Aspiro P4211	DI	0	4.09	6.95	0.266	197	255
		53	4.00	6.83	0.269	195	251
		120	3.77	6.55	0.278	188	243
		180	3.67	6.43	0.283	186	239
		300	3.57	6.30	0.287	183	236
AN125 MPM	Syn. Sea Water	0	0.90	5.07	0.607	108	139
		45	0.74	4.38	0.648	96	123
		180	0.56	3.59	0.696	82	106
AN125 SH	Syn. Sea Water	0	1.81	8.41	0.440	160	207
		45	1.19	6.19	0.545	126	162
		120	0.95	5.26	0.596	111	143
		180	0.86	4.87	0.619	104	134
AN125 SH	DI	0	4.21	7.09	0.261	201	259
		45	3.96	6.79	0.270	194	250
		120	3.70	6.46	0.281	186	240
		180	3.31	5.96	0.301	175	226
AN132	DI	0	3.70	6.46	0.282	186	240
		45	3.57	6.30	0.287	183	236
		90	3.51	6.22	0.291	181	233
		120	3.37	6.03	0.298	177	228
		180	3.18	5.79	0.309	171	220
		240	3.00	5.54	0.321	165	213

Table 6.9: Summary of Intrinsic Viscosity, MW, n, Rg and Rh Estimations for Sulfonated PAMs and ATBS Polymers

Polymer Type	**Brine Salinity**	**Shearing Time (secs)**	**Intrinsic Viscosity [η] (L/g)**	**MW (10^6 g/mol)**	**n**	**Rg (nm)**	**Rh (nm)**
AN132 SH	DI	0	4.22	7.12	0.261	201	260
		45	3.71	6.47	0.281	187	241
		90	3.62	6.37	0.285	184	238
		120	3.53	6.24	0.290	181	234
		180	3.33	5.98	0.300	175	226
		300	3.08	5.65	0.316	168	216
Aspiro P5421X	Syn. Sea Water	0	1.5	7.33	0.488	144	186
		45	1.00	5.47	0.584	114	147
		120	0.79	4.58	0.636	99	128
SAV 10	Syn. Sea Water	0	0.86	4.87	0.619	104	134
		45	0.76	4.44	0.644	97	125
		120	0.58	3.65	0.693	83	107
SAV 10 XV	Syn. Sea Water	0	1.63	7.79	0.467	151	195
		45	1.09	5.79	0.566	119	154
		120	0.98	5.36	0.590	112	145
		180	0.67	4.09	0.666	91	117
SAV 55	Syn. Sea Water	0	1.3	6.59	0.524	132	171
		45	1.01	5.51	0.582	115	148
		90	0.94	5.21	0.599	110	142
		120	0.59	3.71	0.689	84	108

The results clearly show reduction of polymer molecular weight distribution with increased mechanical degradation and the energy dissipated. Another interesting

observation was loss in shear thinning behavior of the polymers with increased shearing time and in higher salinity brine, as suggested by higher shear thinning index. The degradation of polymer viscosity was dependent on the polymer molecular weight, polymer chemistry, brine salinity, shearing time and energy dissipated. Hence, we hypothesize a normalized shearing time scale to superimpose the degradation results of each polymer types in the respective brine salinities for better understanding the degradation rheology. **Figure 6.6** shows the degradation rate in a blender treatment with normalized shearing time in both DI and synthetic sea water. The results show a good correlation in both brine salinities and higher degradation rate in higher saline brine as expected from the viscosity loss shown earlier. **Figure 6.7** shows the change in MW distribution during the mechanical degradation process with normalized shearing time. The molecular weight of any polymer sample exponentially decreased with increase in normalized shearing time as shown in **Figure 6.7** for both brine salinities. The results agree with the trend observed for degraded viscosity measurements with increasing shearing time, where higher rate of viscosity loss (or MW reduction) was observed in higher salinity brine. **Table 6.10** summarizes the shift factors used for the superposition of the degradation measurements and MW change for each polymer in their respective brine salinities.

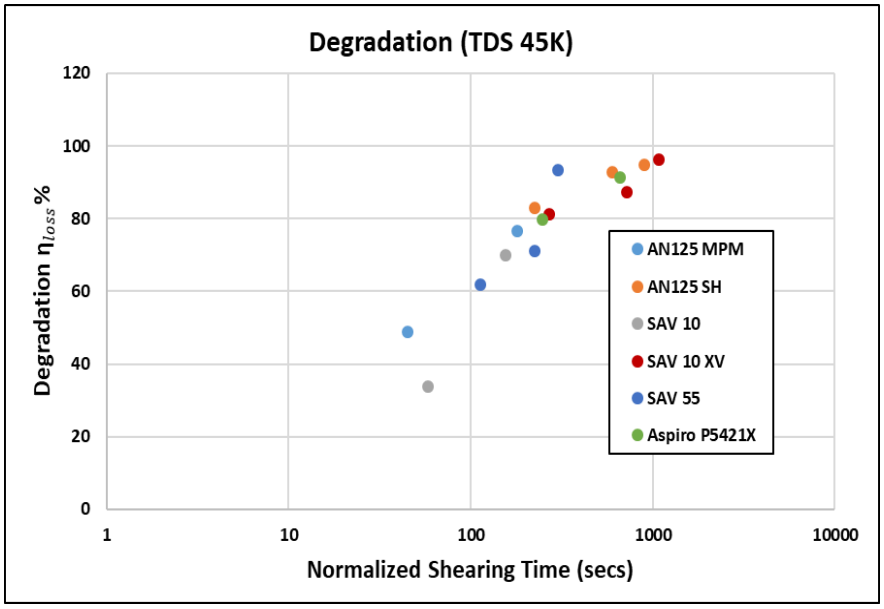

(a)

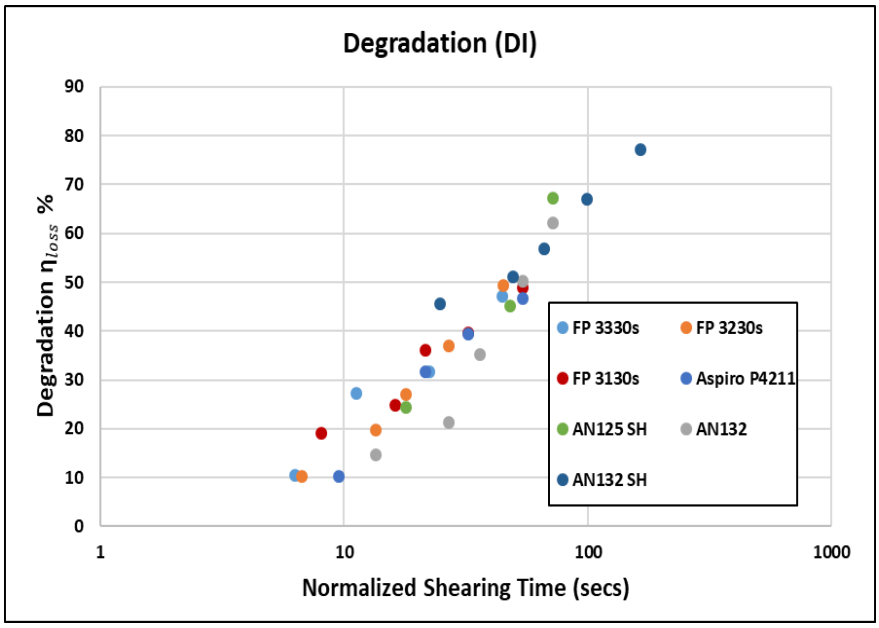

(b)

Figure 6.6. Evolution of degradation vs normalized time in (a) synthetic sea water and (b) DI (right) in a laboratory blender. The degradation measurements are taken at ultra-low shear rates

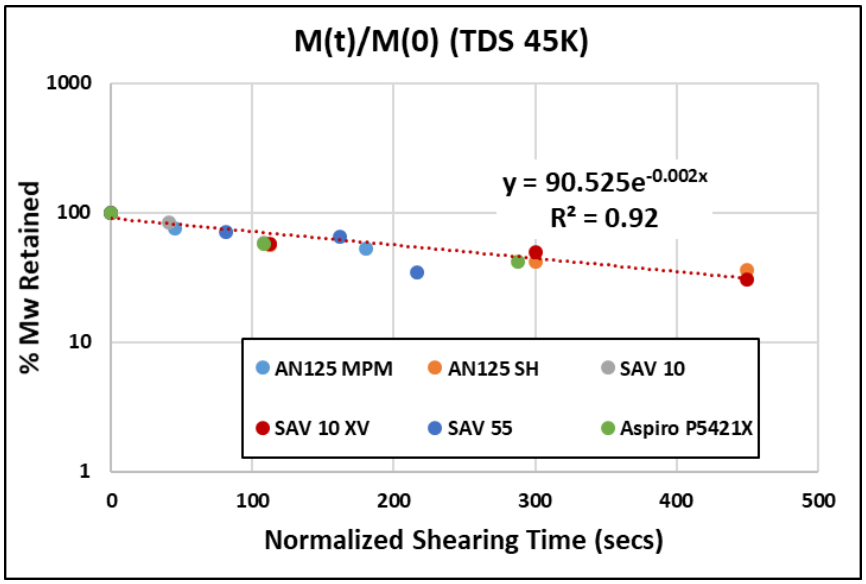

(a)

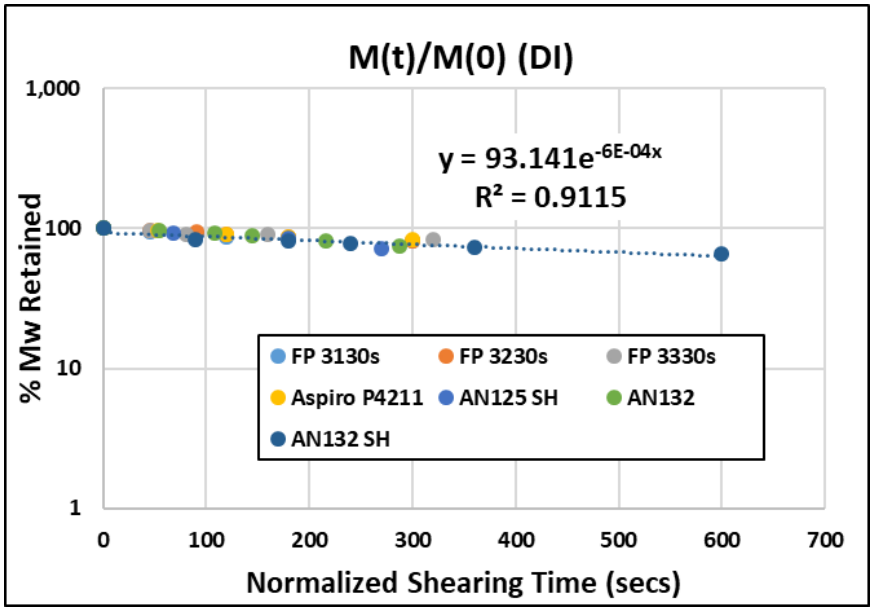

(b)

Figure 6.7. Evolution of molecular weight vs normalized time in (a) synthetic sea water and (b) DI in a laboratory blender. The degradation measurements are taken at ultra-low shear rates

Table 6.10: Shift Factors used for MW and degradation superposition graphs

Polymer Name	**Brine Salinity**	**a (Degradation)**	**b (MW change)**
FP 3130s	DI	0.18	1
FP 3230s	DI	0.15	1
FP 3330s	DI	0.14	1
Aspiro P 4211	DI	0.18	1
AN 125 MPM	Syn. Sea Water	1	1
AN 125 SH	DI	0.4	1.5
AN 125 SH	Syn. Sea Water	5	2.5
Aspiro P5421 X	Syn. Sea Water	5.5	2.4
AN 132	DI	0.3	1.2
AN 132 SH	DI	0.55	2.0
SAV 55	Syn. Sea Water	2.5	1.8
SAV 10	Syn. Sea Water	1.3	0.9
SAV 10 XV	Syn. Sea Water	6	2.5

The shift factor "a" follows a general trend based on the MW of the polymer samples as shown in **Figure 6.8**. The shift factor increases with increasing MW in synthetic sea water. Unfortunately, not a similar trend was observed in the degradation studies performed in DI. The degradation kinetics in absence of ions and the behavior of polymer coils as stretched rigid rods imparts lots of uncertainties in the process and needs more extensive studies to understand the phenomenon of shear degradation.

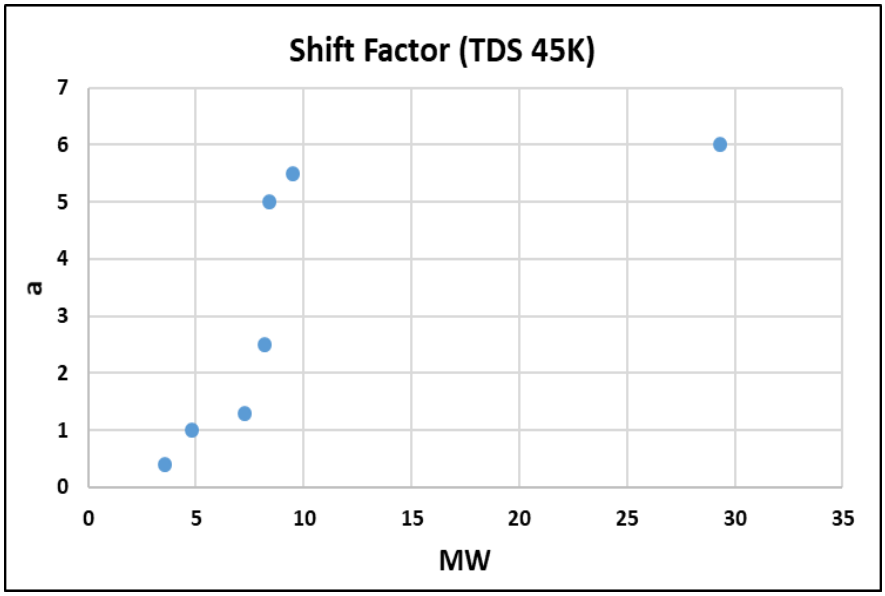

Figure 6.8. Dependence of shift factor a on molecular weight of polymer samples in synthetic sea water degradation process

The degradation results observed in synthetic sea water and DI can be combined to develop a master curve and model the predictions of the degraded viscosity. From an energy of dissipation point of view, no significant degradation was observed below a given threshold. This can be explained from the total energy dissipated to overcome the internal energy of the interactions between the polymer molecules, thus breaking the polymer backbone. **Figure 6.9** shows the superimposed plot for all the polymer samples in both synthetic sea water and DI. The black line corresponds to –

Degradation % = 0 if normalized mixing tmix < 4 secs (6.10)

Degradation % = 18.9 ln (tmix) – 26.2 for tmix > 4 secs (6.11)

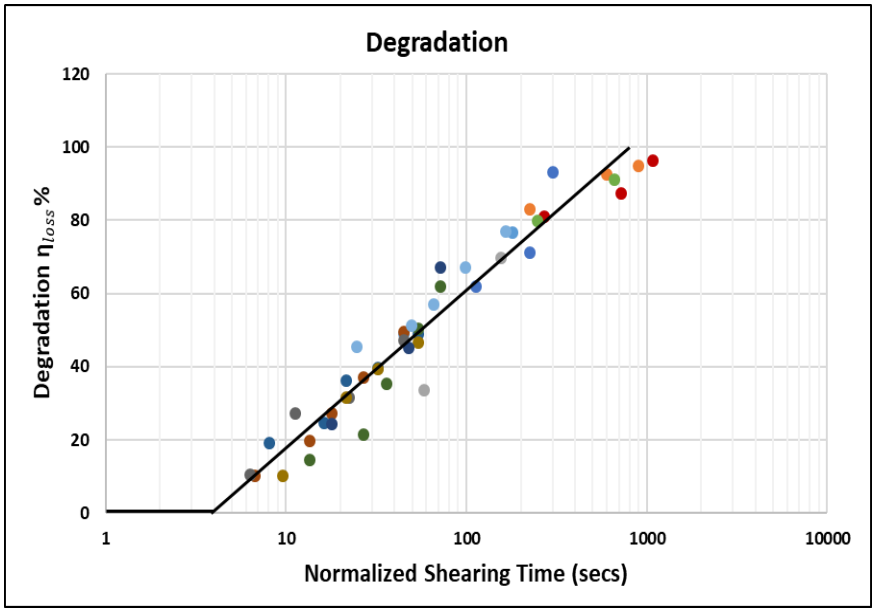

Figure 6.9. Master curve for degradation kinetics vs normalized shearing time for all polymer samples investigated in synthetic sea water and DI

6.2.3 Aggressive Filtration Process

The shear degraded solutions were then diluted to lower polymer concentrations in target brine salinities to perform filtration tests through small sized filter papers using 15 psi Argon. The solutions were filtered through 0.4, 0.2 and 0.1 microns to represent the pore throat diameters in low permeability carbonates more accurately. Small samples were taken out at each filtration step to measure any possible viscosity loss and perform size analysis to estimate the modification of molecular weight distribution. A plugging parameter β was defined to measure the resistance of flow through the filter, which is a significance of face plugging of large polymer molecules in small pore sizes. The time taken to filter a given amount of polymer solution was found to be a second-degree polynomial fit as shown in **Figure 6.10** below. Plugging parameter β was calculated as 2

times the ratio of coefficients of quadratic term and linear term. This parameter β can be directly correlated to the filterability of the polymer solution and can be used to calculate the FR_β as shown in the expression below. The details of this process have been outlined in Drivers master's thesis (2017).

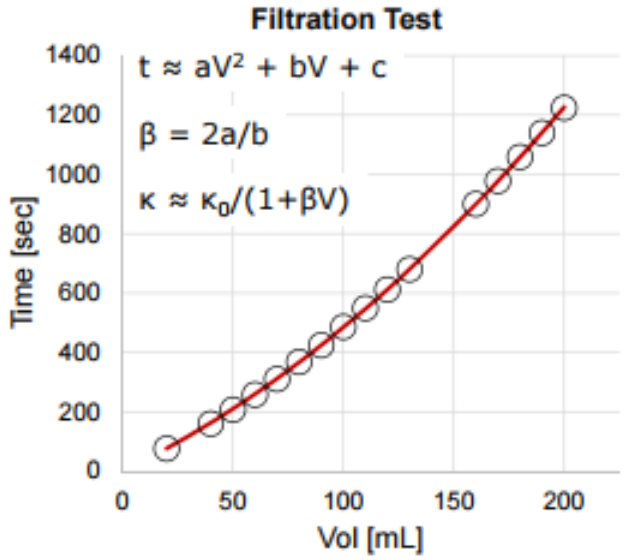

Figure 6.10. Filtration time vs filtered polymer solutions for a diluted polymer concentration in target brine salinity

$$FR_\beta = \frac{1+\beta*190\ (mL)}{1+\beta*70\ (mL)} \qquad (6.12)$$

Each of the polymer samples were investigated for polymer concentration, brine salinity and shearing time effect on the filtration properties through small sized filter papers. Some preliminary results are shown below where FP 3130s, FP 3230s and FP 3330s underwent a 3-step series filtration with 0.4, 0.2 and 0.4-microns sequentially. All these experiments were performed in synthetic formation brine of TDS 31,000 ppm at 25°C.

Figure 6.11 shows the plugging parameter β estimated for each of the polymers with no shearing, and blender shearing time of 45 secs and 180 secs.

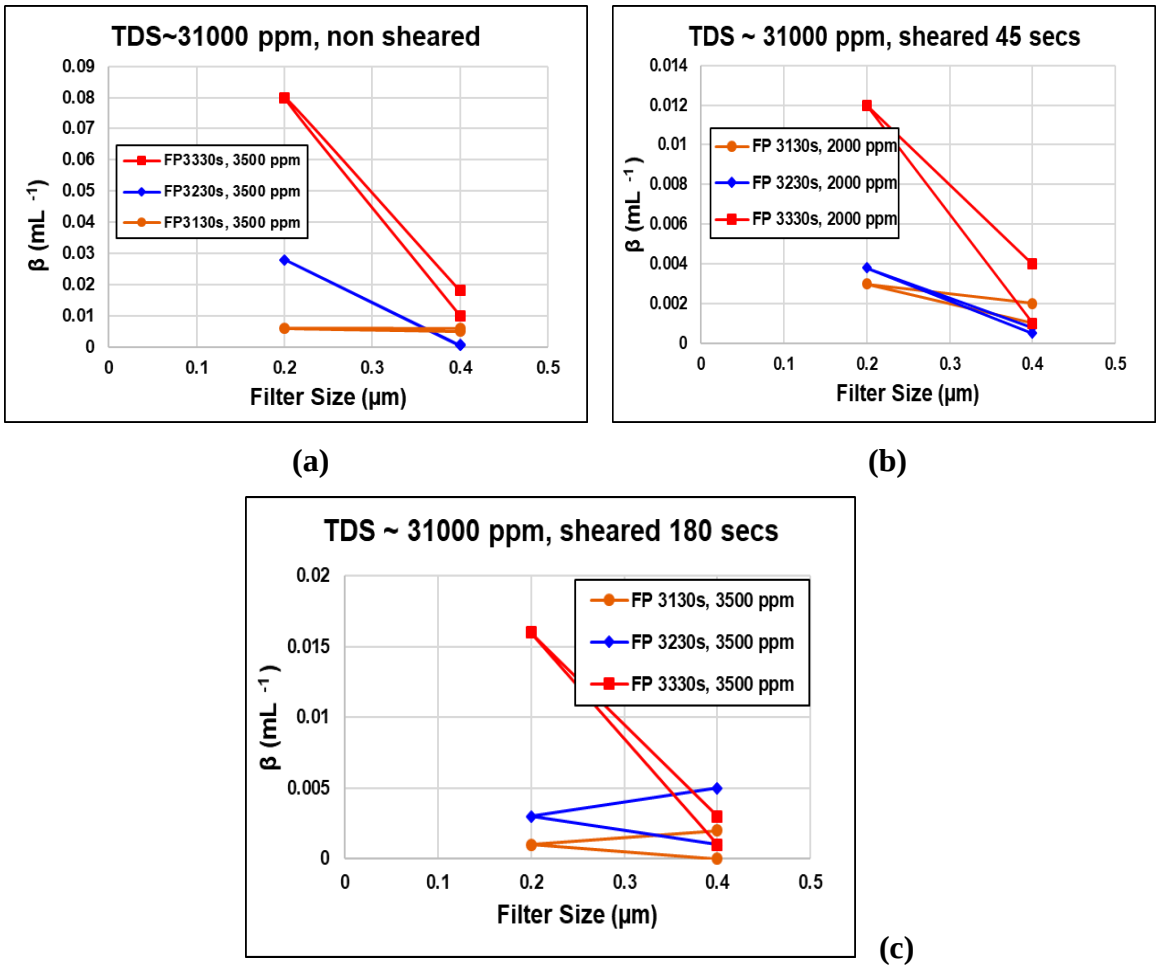

Figure 6.11. Plugging parameter β estimations during aggressive filtration tests for HPAM polymers for (a) non-degraded stock, (b) sheared stock for 45 secs, (c) sheared stock of 180 secs in synthetic formation brine

The results above clearly indicate the severe plugging behavior of the high molecular weight polymers with no shearing during filtration through 0.4 and 0.2 microns. But, significant improvement (reduction in plugging parameter β) was observed with increased shearing time as shown in **Figures 6.11 (b) and 6.11 (c)**. Also, an improvement

in filtration properties was observed during successive filtration through 0.4 microns after being filtered through 0.2 microns in between. Filtration through smaller filter papers refines the molecular weight distribution and improves the filterability through higher sized filter papers later as observed in the figures above. On comparing the results of **Figures 6.11 (b)** and **6.11 (c)**, the effect of polymer concentration was investigated for filtration through small sized filter papers and is an important factor for designing of polymer injection in coreflood experiments. Higher polymer concentration in target brine can induce interactions between the polymer chains and negatively affect the transport of these polymer solutions through small pore sizes, thus increasing the plugging parameter and reducing the filterability. The improvement in β was also found to depend on the molecular weight of the polymer samples. **Equation 6.12** can be used to convert the estimated plugging parameter β into the filtration ratio FR_β which is a widely used parameter in EOR industry for qualification of polymer injection in porous media. **Figure 6.12** shows the corresponding FR_β for each of the polymers with variation of shearing time at different filter paper sizes. The results clearly show the improvement in FR_β with increased shearing time at a given pore size. **Figure 6.12 (c)** shows that for shearing time of 180 secs the final filtration ratio FR_β at 0.4 microns for FP 3330s was found to be lower than 1.2, which was deemed necessary for successful injection in low permeability carbonate cores with brine permeability less than 20 mD.

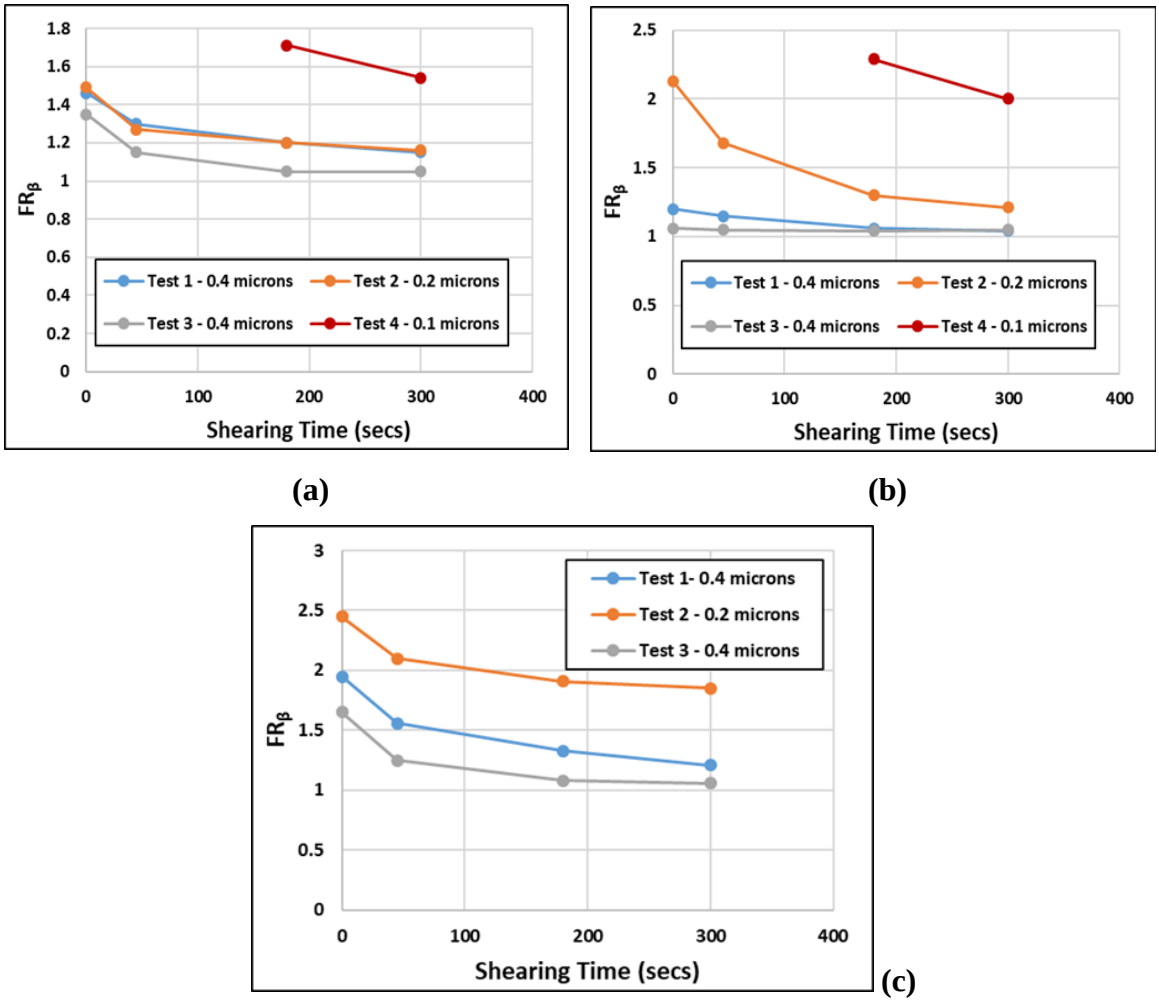

Figure 6.12. Filtration ratio vs shearing time during aggressive filtration tests for 3000 ppm of (a) FP 3130s, (b) FP 3230s and (c) FP 3330s in synthetic formation brine at different filter sizes

Additional viscosity measurements were performed at each filtration step for the above samples to observe and record any viscosity loss due to increased plugging during flow through small sized pores. **Figure 6.13** shows the viscosity measurements at 10 s^{-1} and 25 ^{o}C during filtration of FP 3130s and FP 3230s at each filtration step for shear degraded stock of 180 secs. The results show that for low molecular weight polymer FP 3130s after degradation of 180 secs the viscosity loss during filtration process even through

0.1 microns is almost negligible. On the other hand, for FP 3230s the viscosity loss at 0.2 microns was about 4% and at 0.1 microns was about 7% of the non-filtered polymer solution. A systematic evaluation of the viscosity loss at each step of the polymer pre-treatment process for injection in low permeability carbonates needs to be performed for quality control and more accurate estimation of the right dosage of polymer concentrations at the start to meet the viscosity requirements during a coreflood experiment.

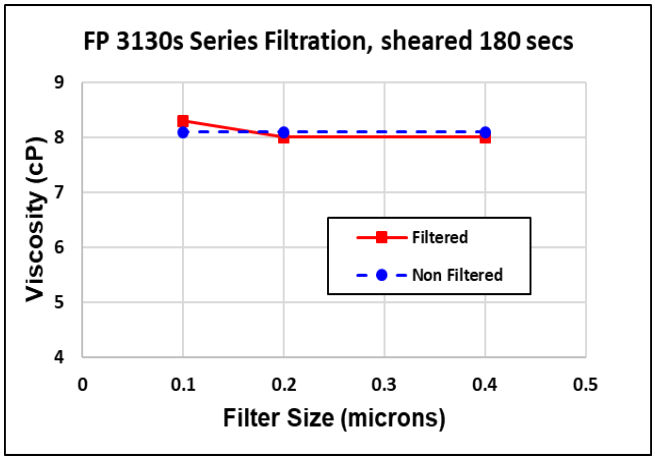

(a)

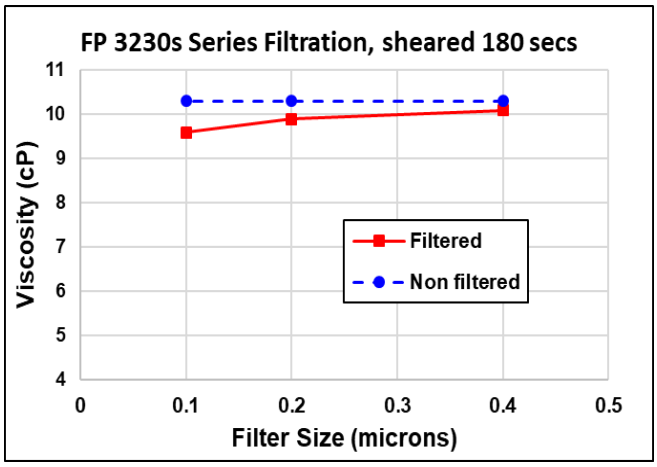

(b)

Figure 6.13. Viscosity loss vs filter size during aggressive filtration for (a) FP 3130s and (b) FP 3230s in synthetic formation brine for sheared stock of 180 secs

6.2.3.1 Critical Shearing Time for Different Filter Pore Sizes

Additional mechanical degradation and aggressive filtration tests were performed with FP 3330s to investigate the critical shearing time required to successfully transport the high MW polymers through smaller sized filter papers. **Figure 6.14 (a)** shows the performance of filtration properties with varying polymer concentration in synthetic formation brine of TDS 31,000 ppm with a shear degraded polymer stock of 300 secs. The results clearly show increase in plugging parameter (increase in FR_β) with increase in polymer concentration due to interaction of high molecular weight chains while transporting through small sized filter papers. The results also suggest higher shearing time necessary for better filtration properties through smaller filter papers. Due to the wide diversity in the pore throat distribution of low permeability carbonates, a significant fraction of the pore throats has diameters below 0.1 microns. Thus, good filterability through 0.1 microns is a necessary step to qualify the polymer solution to be injected successfully through smaller pore sizes. **Figure 6.14 (b)** shows the effect of brine salinity (after shear degradation of 300 secs) on filtration properties during the aggressive filtration treatment. The results showed that higher salinity seemed to improve the filtration through 0.4, 0.2 and 0.1 microns due to the formation of polymer coils in higher ionic environment.

All these preliminary experiments led to the development of a systematic protocol of polymer treatment process to successfully inject in low permeability formations. Based on the polymer molecular weight, polymer chemistry and brine salinity an optimum shearing time was estimated in the laboratory blender at 18,000 rpm. The shear degraded polymer stock was then diluted to desired polymer concentrations in target brine salinities

and aggressive filtration treatment was performed. The polymer solutions were filtered through 0.4, 0.2, 0.1 and 0.4 microns respectively before injecting into the porous media. The necessary condition for successful injection in carbonates with brine permeability less than 20 mD was estimated to be FR_β less than 1.2 at the final 0.4 microns filter paper.

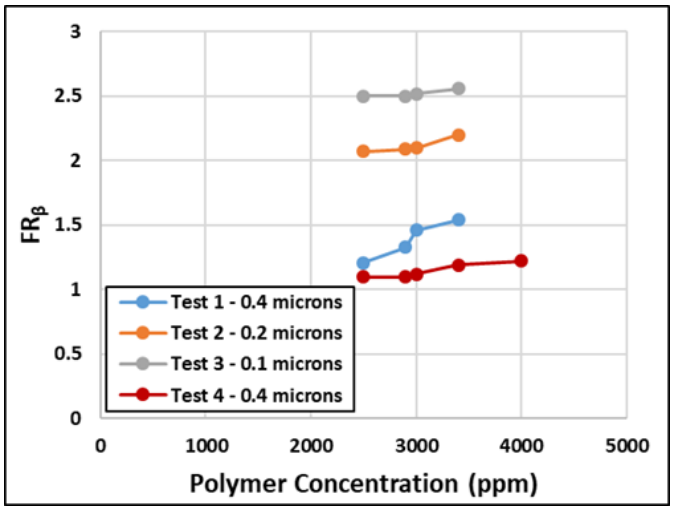

(a)

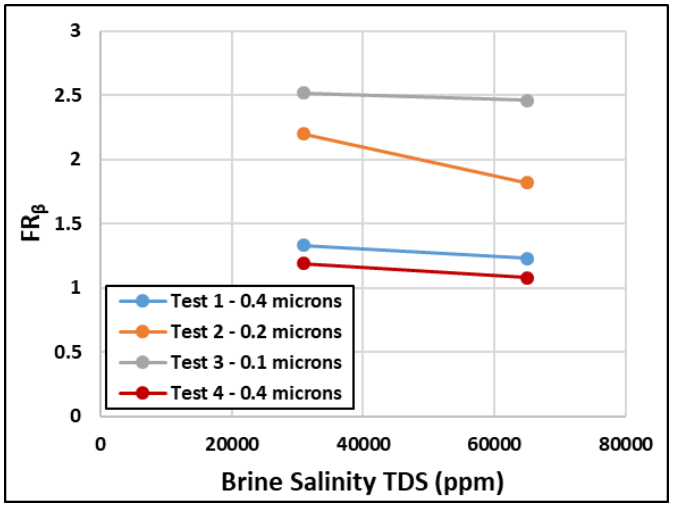

(b)

Figure 6.14. Filtration ratio vs polymer concentration for FP 3330s in TDS 31K (left) and filtration ratio vs brine salinity for 3400 ppm FP 3330s (right) of a shear degraded stock 300 secs

Similar shear degradation experiments and filtration tests were performed on sulfonated PAMs and ATBS polymers like SAV series. **Figure 6.15** shows the effect of increased shear degradation on filtration ratio FR_β in synthetic sea water for AN125 MPM polymer and the effect of increased polymer concentration on the filterability through small sized filter papers. The results showed that shearing time (represented as blend time or BT in the figures) of 120 secs was enough for this polymer for injection in low permeability carbonates since the final filtration ratio at 0.4 microns was 1. The filtration ratio after 180 secs of shearing time did not show any further improvement.

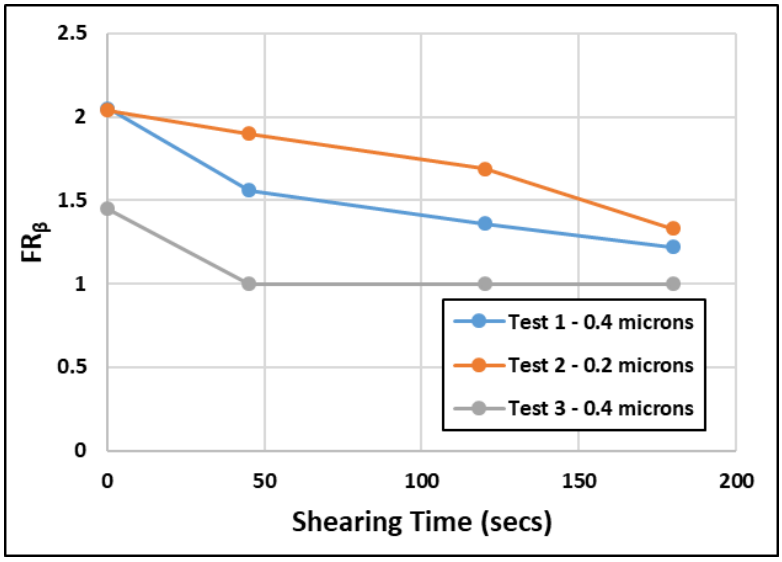

Figure 6.15. Filtration ratio vs shearing time at different filter sizes with AN125 MPM in synthetic sea water

The quality control experiment performed with AN125 SH polymer stocks prepared in DI and synthetic sea water underwent similar shear degradation studies and aggressive filtration tests. The viscosity measurements showed more aggressive degradation in a higher saline brine (high number of divalent ions) compared to DI, as

shown in **Figure 6.5**. The filtration results showed interesting filtration properties for the two different stock solutions. **Table 6.11** and **Table 6.12** summarizes the filtration test results for AN125 SH in both brine systems. On comparing the results from **Tables 6.11** and **6.12**, it clearly shows the improved filtration properties (lower plugging parameter) for the higher salinity brines due to coiled structure of the polymer samples in higher ionic brines. But, the final filtration ratios FR_β for each shear degraded sample were almost comparable and qualified for injection in low permeability carbonates. Hence, based on the outcome of these experiments and to conserve most of the viscosity during the shear degraded experiments, preparation of the polymer stock in DI generates higher viscosity at the injected polymer concentration. This approach might be beneficial to compensate on the high dosage of polymer concentrations used to meet the viscosity requirements after shear degradation.

Table 6.11: Summary of filtration tests for AN125 SH (1% stock in DI)

Polymer Type	**AN125 SH (DI)**				
Filter Size	**Beta**	**F.R.$_\beta$**	**Salinity (ppm)**	**Conc (ppm)**	**Shearing Time (secs)**
1.2	0.011	1.76			
0.8	0.0054	1.47			
0.65	0.0073	1.58	45000	3000	0
0.4	0.131	2.54			
0.2	0.0067	1.92			
0.4	0.0025	1.26	45000	2000	45
0.4	0.004	1.38			
0.2	0.0075	1.59			
0.4	1.20E-03	1.13	45000	2000	120
0.4	0.0033	1.32			
0.2	0.005	1.44			
0.1	0.367	2.65			
0.4	1.00E-03	1.12	45000	3000	180

Table 6.12: Summary of filtration tests for AN125 SH (1% stock in sea water)

Polymer Type	**AN125 SH TDS 45K**				
Filter Size	**Beta**	**F.R.$_\beta$**	**Salinity (ppm)**	**Conc (ppm)**	**ShearingTime (secs)**
1.2	0.006	1.5			
0.8	0.009	1.68			
0.65	0.014	1.94	45000	3000	0
0.4	0.002	1.21			
0.2	0.011	1.76			
0.4	0.003	1.26	45000	2000	45
0.4	0.0005	1.05			
0.2	0.003	1.3			
0.4	2.00E-03	1.2	45000	2000	120
0.4	0.001	1.07			
0.2	0.003	1.55			
0.1	0.003	2.16			
0.2	3.00E-03	1	45000	3000	180

Additional experiments were performed with ATBS polymers like SAV 10, SAV 10 XV and SAV 55 to investigate the shear degradation properties and filtration properties through small sized filter papers. Each of the polymer stocks with 1 wt% were prepared in synthetic sea water. **Figure 6.16** summarizes the results from the filtration tests for each polymer with varying shearing time in the blender. Similar trends were observed with improvement in filtration properties on increasing shearing time and small increase in FR_β was observed with increase in polymer concentration as well. An optimum shearing time of 120 secs, 180 secs, and 120 secs were estimated for SAV 10, SAV 10 XV and SAV 55 polymers respectively. The higher shearing time for SAV 10 XV was an artifact of the higher MW of the polymer compared to SAV 10. These results agree with the trend observed earlier where higher shearing time was required for higher MW polymers.

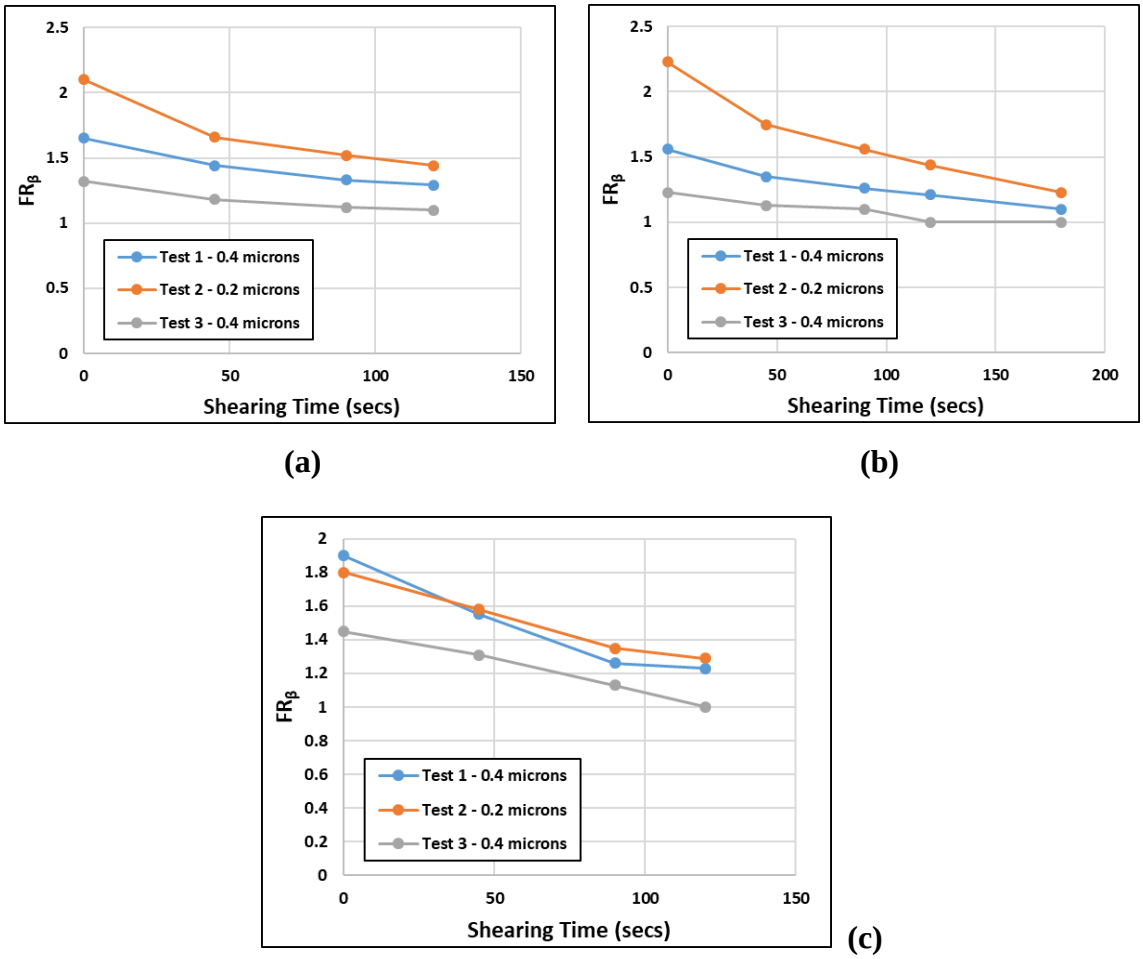

Figure 6.16. Filtration ratio vs shearing times at different filter sizes for (a) SAV 10, (b) SAV 10 XV, and (c) SAV 55 with all stocks prepared in synthetic sea water

6.2.4 Size Analysis of Polymer Solutions – Dynamic Light Scattering (DLS)

To investigate and understand the modification of polymer molecular weight distribution through mechanical degradation, polymer samples were diluted to different concentrations for analysis in DelsaNano analyzer for qualitative estimation of molecular size distribution (or changes in hydrodynamic radius Rh). This preliminary test was performed to determine the optimum concentration for size analysis measurement without any interaction between polymer molecules and aggregates being formed. **Figure 6.17 (a)**

shows the size analysis for 250 ppm, 500 ppm, 750 ppm and 1000 ppm for FP 3330s polymer prepared in synthetic formation brine of TDS 31,000 ppm and modified formation brine of TDS 20,000 ppm. The results showed general trend with 250 ppm and 500 ppm, but at 750 ppm and 1000 ppm there were interference due to possible interaction between polymer molecules and formation of aggregates. **Figure 6.17 (b)** shows the size analysis for 250 ppm, 500 ppm, 750 ppm and 1000 ppm for FP 3230s polymer prepared in synthetic formation brine of TDS 31,000 ppm with sheared and non-sheared polymer stock. Similar interactions between polymer molecules were observed at 1000 ppm. Based on this preliminary test, 500 ppm diluted samples of polymer solutions were seemed appropriate for performing size analysis experiment and henceforth, all measurements were performed at 500 ppm polymer concentration for different polymer types.

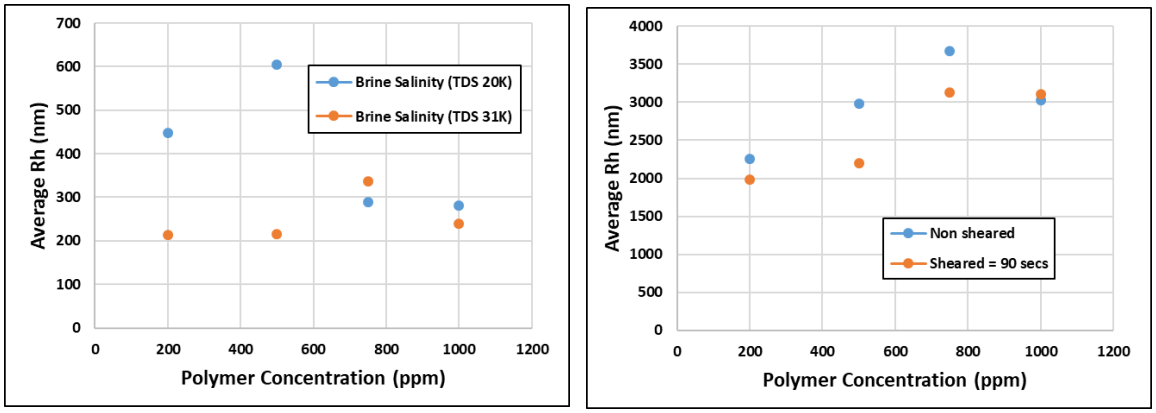

(a) **(b)**

Figure 6.17. Size analysis for FP 3330s in synthetic and modified formation brines (left) and size analysis for FP 3230s in TDS 31K for sheared and non-sheared polymer stock (right) with varying polymer concentrations

Previous results showed how the MW distribution changed with increasing mechanical degradation and the size analysis study showed results in agreement with the

behavior. **Figure 6.18** shows the modification of size distribution (or hydrodynamic radius Rh of polymer molecules) of FP 3130s, FP 3230s and FP 3330s in DI with the variation of shearing time. The results show decrease of high-molecular weight molecules (can be related to decrease in Rh) and polydispersity index with increased shearing time for all polymer samples. The magnitude of change of Rh and polydispersity index is a function of the polymer molecular weight, with higher Rh and polydispersity index for higher MW polymers.

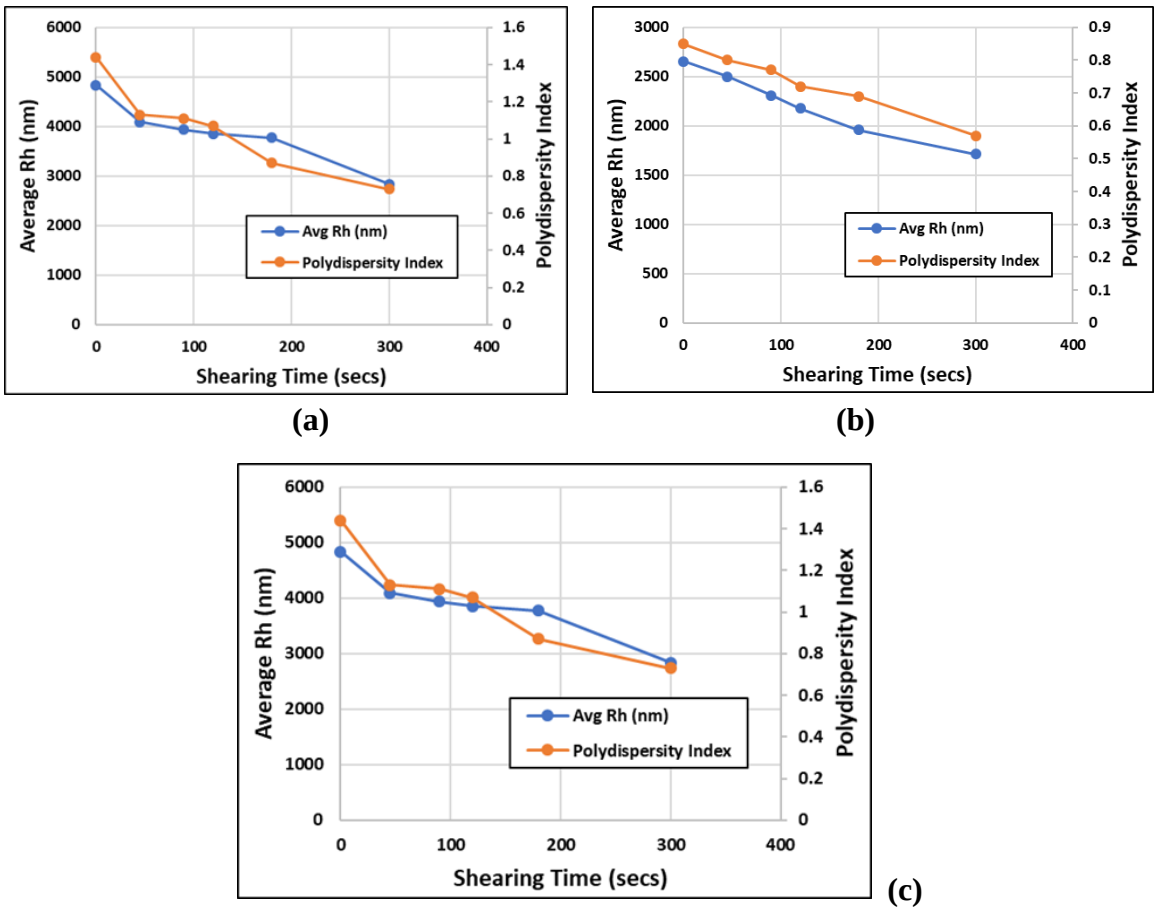

Figure 6.18. Variation of Rh and polydispersity index with varying shearing time for (a) FP 3130s, (b) FP 3230s and (c) FP 3330s in DI

6.2.4.1 Effect of Aggressive Filtration on Modification of Size Distribution

Samples were taken out at each filtration steps to observe any small modifications to the size distribution of the polymer samples after aggressive filtration process. **Figure 6.19** shows the size analysis of samples for FP 3230s in synthetic formation brine (stock degraded for 180 secs) taken at 3 step filtration– 0.4, 0.2 and 0.1 microns respectively. The results clearly show slight reduction in the high MW tail chains during aggressive filtration and slight shift towards the left. This shift in size distribution can explain the small viscosity loss observed during the filtration step, as reported earlier. The final size distribution of the polymer solution in dilute concentrations can be used to infer information regarding the transportability in low permeability carbonate cores after comparing with the pore throat distribution of the porous media.

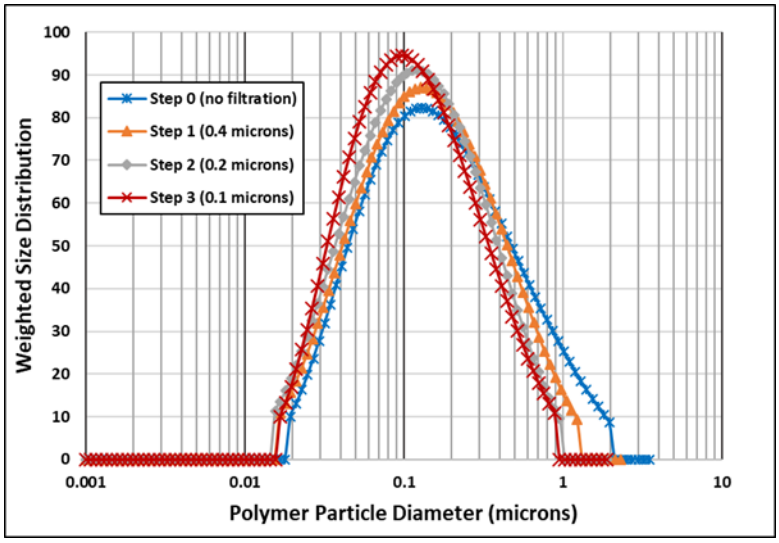

Figure 6.19. Size analysis for FP 3230s in synthetic formation brine with shear degraded stock of 180 secs during successive filtration steps

Similar size analysis was performed on the other polymer types in varying brine salinities with shear degradation performed in either DI or synthetic sea water. **Figure 6.20** shows the change in hydrodynamic radius and polydispersity index due to shear degradation of different degree for AN125 MPM, AN125 SH and Aspiro P5421X. The results showed varying degree of size modification based on polymer molecular weight, with higher MW resulting in higher reduction of the larger sized particles in the solution.

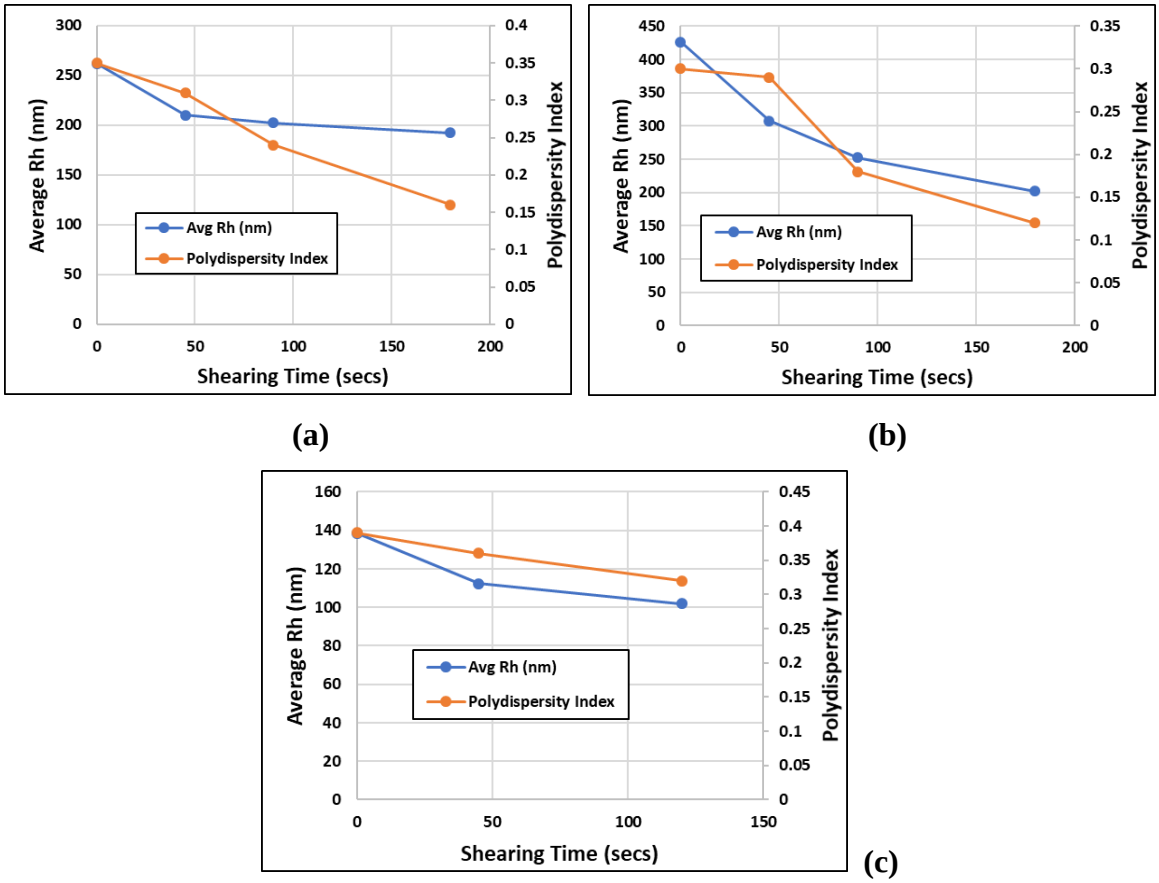

Figure 6.20. Variation of hydrodynamic radius Rh and polydispersity index with varying shearing time for (a) AN125 MPM, (b) AN125 SH, (c) Aspiro P5421X in synthetic sea water

Polymers containing different monomers like ATBS were also investigated for size distribution during the shear degradation process. These experiments were performed to study the shear sensitivity to different polymer chemistries and the consequent modification of polymer size distribution. **Figure 6.21** shows the change in hydrodynamic radius and polydispersity index with varying shearing time for SAV 10, SAV10 XV and SAV 55 polymers. The results indicate that polymer MW has more impact on the size distribution of the polymers and their modification with increasing shearing time than the chemistry of the polymers. But more experiments need to be performed to deduce some definitive conclusions.

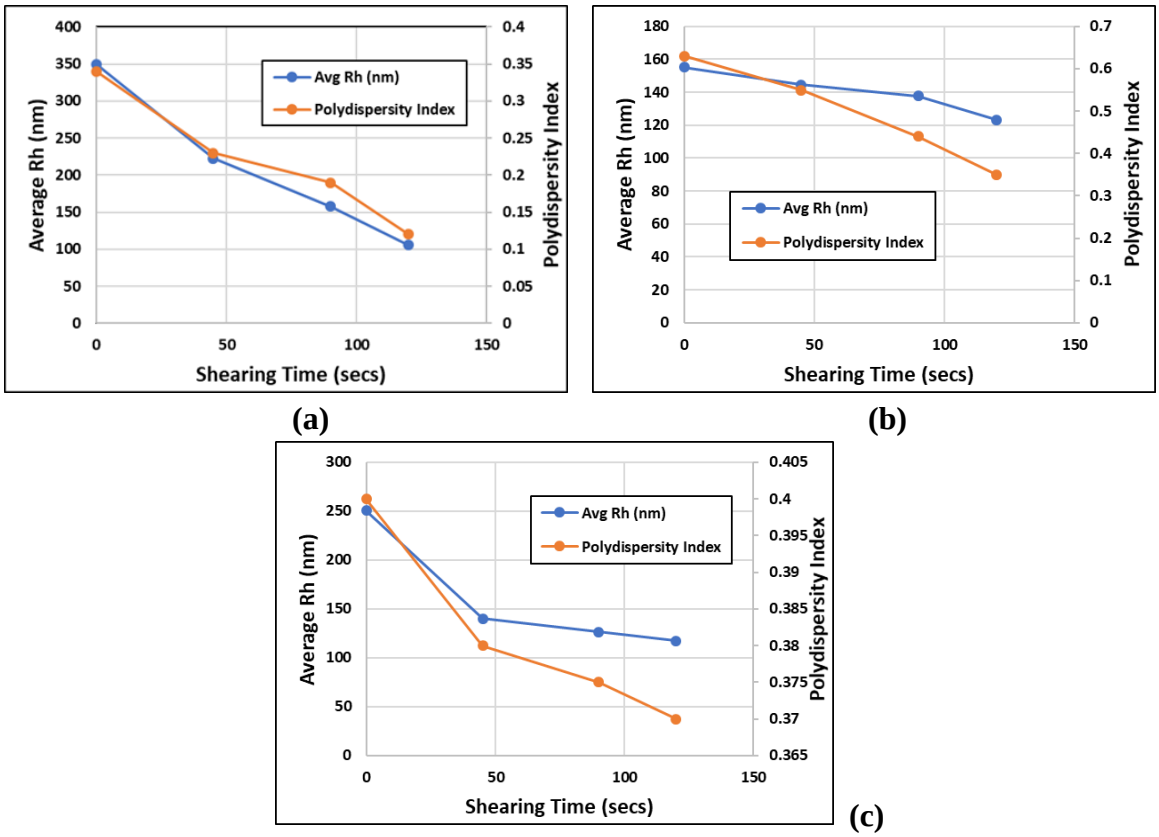

Figure 6.21. Variation of hydrodynamic radius and polydispersity with varying shearing time for (a) SAV 10, (b) SAV 55, (c) SAV 10 XV in synthetic sea water

Additional size analysis experiments were performed during the aggressive filtration tests for SAV 55 to observe the modifications during filtration through small sized filter papers. **Figure 6.22** shows the size modification for SAV 55 with 2000 ppm through 3 step filtration – 0.4 microns (Test 1), 0.2 microns (Test 2) and 0.4 microns (Test 3) filter paper for varying shearing times of 45 secs and 90 secs. The analysis performed on the final filtration step at 0.4 microns showed improvement in the molecular size distribution with the polymer tending towards less polydispersity. All the size analysis results for each of the polymers investigated showed similar trends in size distribution compared to the behavior of plugging parameter (or FR_{β}) during successive filtration tests.

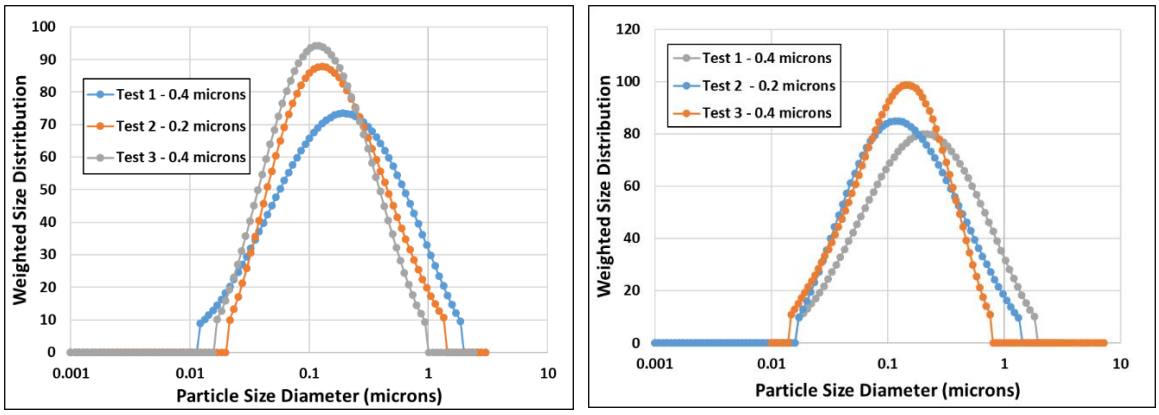

Figure 6.22. Size analysis for SAV 55 (2000 ppm) in synthetic sea water during aggressive 3 step filtration for (a) shearing time = 45 secs and (b) shearing time = 90 secs

6.2.5 Comparative Study of Rh Measurements from DLS and Intrinsic Viscosity Method

In order to understand the efficiency and usefulness of the size analysis measurements performed with DLS analysis, a comparison was performed with the

hydrodynamic radius Rh measurements from intrinsic viscosity method and DLS for a given polymer in a similar brine system. Note, that the DLS measurements were performed at diluted polymer concentration of 500 ppm whereas intrinsic viscosity measurements were performed at the polymer stock concentration of 10,000 ppm. **Figure 6.23** shows the comparison results for Rh measurements from these methods for different polymer samples with variation of shearing time. The results show good agreement of the measurements of Rh from the two methods and shows a good correlation fit to predict the change in Rh for sulfonated polymers and ATBS polymers in synthetic sea water during shear degradation studies in laboratory blender. Hence, this analysis provides evidence of the robustness of the DLS method applied at dilute concentrations to compare the polymer size distribution with pore throat distribution for a give porous media.

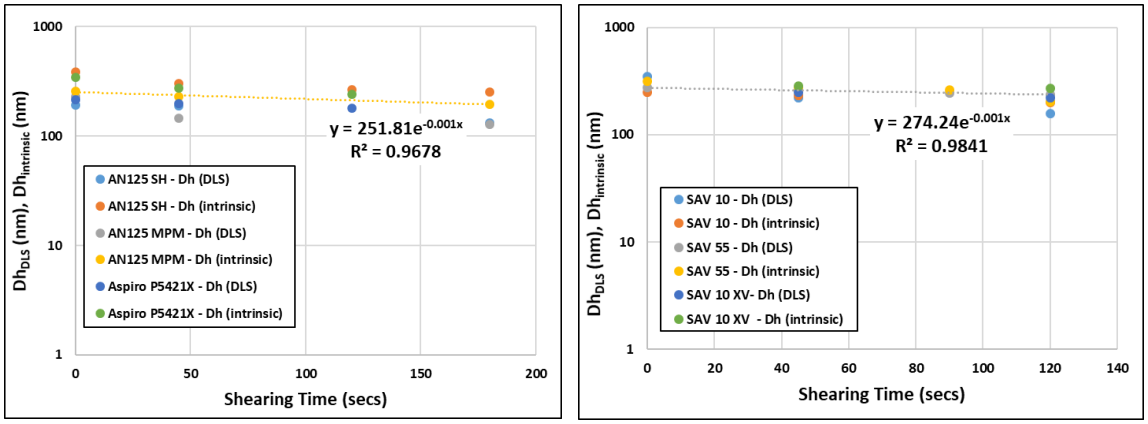

Figure 6.23. Comparative study of Rh measurements from DLS and intrinsic viscosity methods for sulfonated polymers (left) and ATBS polymers (right) in synthetic sea water

6.2.6 Pore Throat Distribution – Mercury Injection Capillary Pressure (MICP)

The key design parameter for successful injection of high molecular weight polymer solutions into low permeability carbonate reservoirs with wide pore throat

diameter distribution is to compare the final polymer size distribution after shear degradation and aggressive filtration tests with the pore throat distribution obtained from MICP tests. Hence, multiple MICP tests were performed in various outcrop limestones of low permeability (K_{brine} < 40 mD) and varying heterogeneity to understand the diversity in pore throat distribution for similar average permeability. These measurements clearly showed that using a single critical pore throat diameter obtained from the average permeability might not be an accurate measurement for qualification of polymer injection based on the ratio of polymer radius of gyration (Rg) and average pore throat diameter. It is crucial to obtain the whole pore throat distribution and compare the size distribution to investigate and understand the overlap between the two size distributions and infer useful information for successful polymer injection. Outcrop limestones like Texas Cream, Indiana limestone, Silurian Dolomite and Edwards Yellow limestone were used as part of the study. The pore throat diameter distributions obtained from MICP tests for each of these rocks are shown in **Figure 6.24**. The results clearly showed the heterogeneity of the porous media for similar average permeability rocks. Edwards Yellow limestone seemed to have more homogeneous pore structure whereas Texas Cream limestone had bimodal pore distribution and Indiana limestone (more heterogeneous than others) has trimodal pore throat distribution. Another interesting observation was the variation of the fraction of pore space below 1-micron pore throat diameter for each porous media. The results showed more than 55% of the total pore space residing below 1 micron for Texas Cream, less than 5% of the total pore space residing below 1 micron for Edwards Yellow, more than 43% of the total pore space residing below 1 micron for Indiana limestone core and less than

6% of the total pore space residing below 1 microns for Silurian Dolomite core. Hence, a polymer solution of average radius of gyration Rg between 0.1-1 microns might transport successfully through Edwards Yellow and Silurian Dolomite but might experience plugging problems in Texas Cream or Indiana limestone cores.

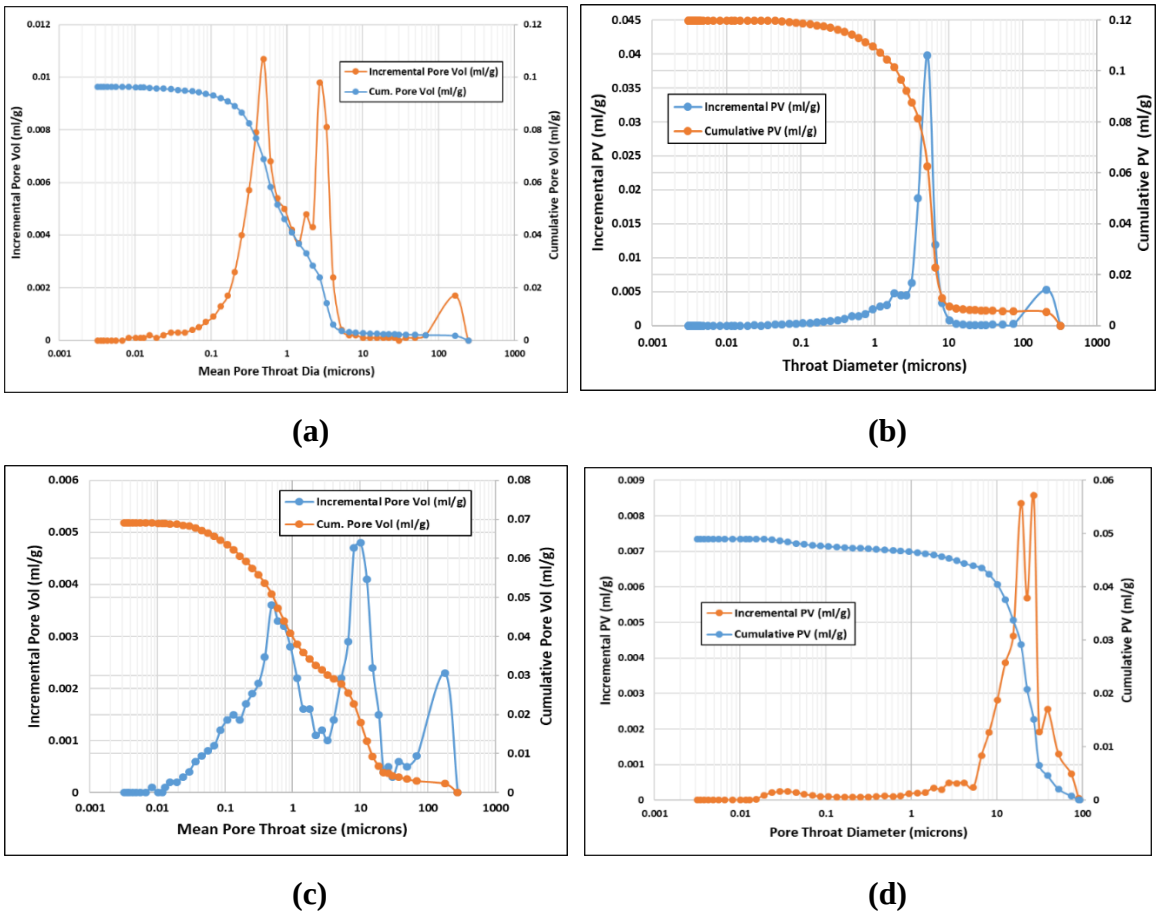

Figure 6.24. Pore throat distribution obtained from MICP tests for (a) Texas Cream limestone, (b) Edwards Yellow limestone, (c) Indiana limestone, (d) Silurian Dolomite cores of similar permeability

The Kozeny Carman equation is typically used to predict the average hydraulic radius with respect to permeability, porosity, tortuosity and shape factor of the consolidated porous media.

$$k = C_0 \tau^2 r_h^2 \varphi \quad (6.13)$$

where k is the average brine permeability, τ is the tortuosity of the porous medium, C_0 is the shape factor, r_h is the hydraulic radius and φ is the porosity of the porous media. For all estimations of r_h, we have used C_0 = 2.5 and τ = 1.414. **Table 6.13** below summarizes the results of the estimations of average hydraulic radius for different porous media under investigation. Note, very limited resource on the accurate measurements of C_0 and τ are available for complex and consolidated carbonate cores. Hence, a certain degree of uncertainties is involved in the estimations of r_h for these rock samples.

Table 6.13: Estimations of Rh from Kozeny Carman equation

Rock Type	**K brine (mD)**	**Porosity**	**Rh (microns)**
Texas Cream	15	0.268	0.106
Edwards Yellow	12.5	0.28	0.094
Indiana Limestone	22.5	0.16	0.168
Silurian Dolomite	38.5	0.15	0.227

On comparing the estimations of Rh from Kozeny Carman equation and results from MICP study, it is evident that even for similar Rh estimations the pore throat distribution of the carbonates is very different from each other. The estimations of radius of gyration for polymer samples from intrinsic viscosity measurements and the hydraulic radius for low permeability carbonates are comparable, hence based on the literature studies reported earlier where polymer radius should be atleast 6 times higher than pore throat radius none of these shear degraded polymers would be able to transport successfully

through these cores. On the other hand, Rh estimation for Edwards Yellow limestone (K_{brine} ~ 12.5 mD) was 0.09 microns whereas the pore throat distribution from MICP shows most of the pores lying between 1 – 10 microns. Our results led to the conclusion that estimations based on Kozeny Carman equation for a heterogeneous porous media like carbonates might not be the right approach and pore throat distribution from MICP studies might provide more useful information for injection of polymers in low permeability carbonate rocks.

To justify our conclusion, we compared the polymer size distribution with the pore throat distribution for different carbonate cores with similar average brine permeability. **Figure 6.25** shows the superimposition of the distributions for FP 3330s prepared in synthetic formation brine (TDS 31K) and outcrop limestone cores Texas Cream, Edwards Yellow and Indiana limestone. The results clearly show the difference in overlap between the particle size distributions with the pore throat distribution for different porous media. The diluted sample of FP 3330s (from shear degraded stock) showed majority of the particles to be less than 1 microns, but due to significant portion of the pore throats available between 0.1 -1 microns for both Texas Cream and Indiana limestone this polymer sample would experience plugging issues and unsuccessful polymer transport. On the other hand, Edwards Yellow (of similar permeability) showed very minimal overlap due to majority of the pore throats lying between 1-10 microns. Hence, from this observation our conclusions can be more definitive about the robustness of this method to compare the polymer size distribution with pore throat distribution for qualification of polymer injection in low permeability carbonate cores.

Additional coreflood experiments were also performed with Texas Cream limestone and Edwards Yellow limestone to show evidence of our hypothesis above based on the steady state pressure drop and effluent viscosities measured. A polymer solution with 2500 ppm FP 3330s prepared in synthetic formation brine was injected in Texas Cream limestone (k_{brine} ~ 15 mD) after the polymer stock was shear degraded for 300 secs. The injected viscosity at the reservoir temperature (40 ^{o}C) was about 18 cP and the effluent viscosity measured was only 1.8 cP after 2.5 PV of polymer injection. The pressure drops never reached steady state and showed evidence of face plugging and unsuccessful polymer transport. On the other hand, a similarly treated polymer solution of FP 3330s (2500 ppm) was injected in Edwards Yellow limestone (k_{brine} ~ 12.5 mD). The effluent viscosity reached to about 95% of the injected viscosity within 1.1 PV of polymer injection and no evidence of face plugging was observed. Hence, this coreflood was a success for injection of shear degraded solution of FP 3330s. **Figure 6.26** shows the pressure drops recorded during the injection of FP 3330s in Edwards Yellow limestone at the reservoir temperature (40 ^{o}C).

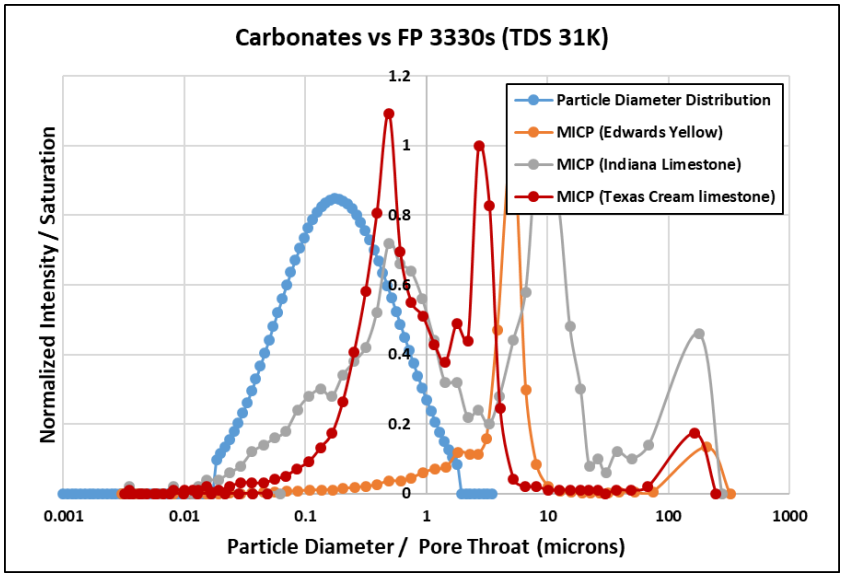

Figure 6.25. Pore throat distribution obtained from MICP tests for (a) Texas Cream limestone, (b) Edwards Yellow limestone, (c) Indiana limestone and polymer size distribution for FP 3330s in synthetic formation brine

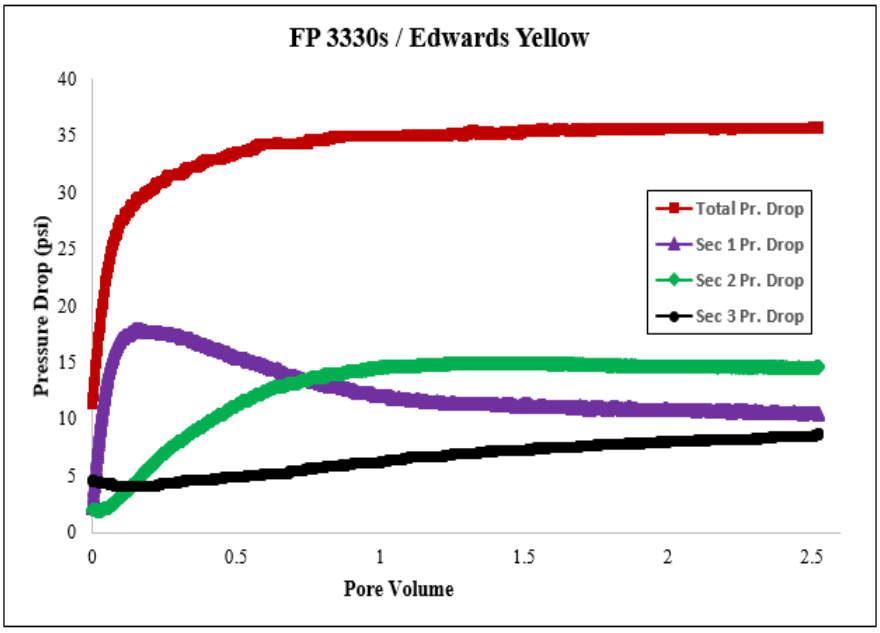

Figure 6.26. Pressure drop profile during FP 3330s injection in Edwards Yellow limestone core

The above coreflood experiments prove our hypothesis and emphasize the importance of investigating the pore throat distribution from MICP and polymer size distribution from DLS measurements in order to accurately predict the transport of polymer solutions in low permeability carbonate cores. The estimations based on the average hydraulic radius from Kozeny Carman equation can be misleading for these experiments. More extensive research needs to be performed to develop a systematic protocol for qualification of polymer injection in tight formations at laboratory scale and develop more robust methods for upscale to field scale applications.

6.3. CONCLUSIONS

In chemical EOR processes, acrylamide-based copolymers of high molecular weight are typically used to achieve maximum viscosity and reduce polymer dosages. The molecular weight, polydispersity, radius of gyration of polymers can be estimated from techniques like size exclusion chromatography or dynamic light scattering. But, injection of high molecular polymers in tight formations can severely affect injectivity due to plugging behavior. Hence, shear degradation technique was successfully used as a tool to probe the molecular weight distribution of the high molecular weight polymer molecules for successful injection in low permeability carbonate reservoirs. Aggressive filtration technique was implemented to modify the polymer size distribution further to achieve good filterability of the shear degraded polymers. This study provided insight to the following conclusions:

- Shear degradation of polymers resulted in exponential decay of low shear rate viscosity with increasing shear time in the laboratory blender for all types of polymer chemistry and varying brine salinities.
- Conventional HPAM polymers showed higher resistance to viscosity loss during shear degradation treatment compared to sulfonated PAMs in DI
- The magnitude of viscosity loss was a function of molecular weight of the polymer, polymer chemistry and brine salinity.
- Higher viscosity loss (or enhanced degradation) was observed in presence of higher brine salinity with divalent ions compared to DI for a similar polymer type.
- A master curve was established to predict the degradation for any given polymer in any given brine salinity using a shift factor which was proportional to the MW of the polymer.
- The modified MW estimated from the intrinsic viscosity of shear degraded polymers was used to calculate the hydraulic radius and shear thinning index of each polymer.
- Loss of shear thinning behavior was observed with increasing shearing time and brine salinity for each of the polymers investigated.
- Aggressive filtration tests through small sized filter papers proved to be a good technique for fine refinement of molecular weight distribution and removing larger particles for successful injection in low permeability carbonates.

- Plugging parameter β was successfully used to represent the plugging behavior of high MW polymers through small pore sizes in porous media and estimate equivalent filtration ratios for qualification of polymers to be injected.
- Higher shearing time was necessary to degrade higher MW polymers to transport through smaller sized pores with minimum loss in viscosity during filtration process.
- Quality control experiment results showed promising results of shear degradation of polymers prepared in DI compared to synthetic sea water in respect to viscosity conservation during the treatment.
- Size analysis technique using DLS was successfully implemented to observe the modification of polymer size distribution during shear degradation and reduction of polydispersity.
- A robust method of comparison of polymer size distribution from DLS with pore throat distribution from MICP was developed for qualification of polymer injection in low permeability carbonates.
- Successful coreflood experiments were performed to validate the hypothesis and the results agreed with the method developed.

Chapter 7: Novel Application of Associative Polymers as Effective Mobility Control Agent in Low Permeability Carbonates

Chapter 6 discussed the benefits of the novel polymer pretreatment and aggressive filtration techniques to modify the molecular weight distribution of high molecular weight polymers for successful injection in low permeability carbonates with wide pore size distribution. The predictive correlations developed from blender shear degradation study proved to be an effective tool in laboratory scale to predict viscosity loss for any polymer grade in different brine salinities at the ambient temperature. A robust approach of comparison between polymer size distribution from dynamic light scattering method and pore throat size distribution from mercury injection capillary pressure was established for qualification of injection of polymers in low permeability carbonate reservoirs. The results emphasized the benefits of shear degraded high molecular weight polymers compared to low molecular weight polymer, with no shear degradation, due to polydispersity of the polymer molecules. The shear degradation mechanism led to significant viscosity loss for the synthetic polymers, hence higher dosage of polymer was required to meet the viscosity requirements of an EOR process. Hence, a more robust and shear resistant polymer could be more beneficial for use in low permeability reservoirs which can compensate significant viscosity loss, lower the dosage of polymer used, thus making the process more economical.

To the best of our knowledge most of the literature studies on application of associative polymers have been focused on high permeability reservoirs. Associative

polymers have shown more shear stability compared to synthetic polymers since the viscosity is dependent on the polymer network formation and not only on the molecular weight. Shear degradation possibly breaks the weak intermolecular network but – in contrast to high molecular weight synthetic polymers – the polymer backbone remains intact (Reichenbach-Klinke et al., 2011). In this study, a systematic evaluation of different types of associative polymers (AP) with varying molecular weight and hydrophobicity content in different brine salinities and injectivity experiments in low permeability carbonate cores have been performed. Additional experiments were performed to investigate the effect of the interaction between hydrophilic surfactants and hydrophobic monomers in the polymers on its thermo-thickening effect. A similar shear degradation and aggressive filtration technique, as described in Chapter 6, was performed on associative polymers for injection in low permeability cores. In addition to basic rheological measurements, filtration ratios, shear degradation studies, a comparative study of AP to conventional HPAM polymers for sweep enhancement was also investigated.

7.1 MATERIALS

Four different associative polymers were investigated as part of this study. **Table 7.1** lists the details of each of the polymer samples used. Common salts such as sodium chloride (NaCl), sodium sulfate (Na_2SO_4), calcium chloride (as $CaCl_2.2H_2O$) and magnesium chloride (as $MgCl_2.6H_2O$) were obtained from Fischer Scientific. All the polymers were initially screened for viscosity yield in synthetic sea-water brine and synthetic formation water, typical of middle-eastern reservoirs. The composition of various brines used in associative polymer testing are shown in **Table 7.2**. The polymers were

initially mixed to a concentration of 10,000 ppm in DI water and hydrated for 24 hours with magnetic stir bar at 250 rpm. The mother solution was then further hydrated with an overhead mixer at 500 rpm for about 3 hours. The stock solution was then then diluted to desired concentrations prepared in target brines and subsequently shear viscosities were measured using a rheometer AR-G2 manufactured by TA instruments. The polymer solutions were filtered through Sterlitech polycarbonate filters of varying sizes (depending on the permeability of the porous media) to measure the filtration ratios using 15 psi of Argon at 25 ^{o}C.

Table 7.1: Description of Polymers used in this study

Polymers	**Molecular Weight (MDa)**	**Hydrophobic Content**
A	4-6	+++++
B	5-7	++++
C	10-13	+++
D	8-10	+++++

Table 7.2: Brine Compositions

Ions	**Synthetic Sea Water**	**Synthetic Formation Brine**	**Synthetic Modified Brine**
Na^{+}	14,305	44,787	32,594
Ca^{2+}	564	2,394	1,662
Mg^{2+}	1,576	89	684
Cl^{-}	24,814	73,421	53,978
SO_4^{2-}	3,816	309	1,712
TDS (ppm)	45,075	121,000	90,630

Table 7.3 lists the properties of the limestone cores used in this study. Indiana limestone and Edwards Yellow limestone rocks were used for the experiments. Each core was about 1 ft long and 1.5 inches or 2 inches in diameter. The absolute permeability of the porous media was estimated through sectional pressure drops at room temperature and reservoir temperature, 60 ^{o}C.

Table 7.3: Properties of cores used in polymer transport experiments

	Flood # C1	**Flood # C2**	**Flood # C3**	**Flood # C4**	**Flood # C5**	**Flood # C6**	**Flood # C7**
Core	Edwards Yellow limestone	Indiana limestone	Indiana limestone	Edwards Yellow limestone	Edwards Yellow limestone	Indiana limestone	Edwards Yellow limestone
Diameter (cm) x Length (cm)	3.76 x 30.4	5.03 x 28.3	5.03 x 28.1	5.1 x 30.0	5.1 x 30.1	5.05 x 30.2	3.76 x 30.4
Porosity (%)	26.8	14.6	13.42	26.8	26.5	13.5	26.8
Brine Permeability (md)	13	44	23	20	26	300	18

Table 7.4 lists the single-phase polymer injectivity experiments performed in outcrop limestone cores to understand and investigate the polymer rheology of associative polymers in different brine salinities at the reservoir temperature (60 ^{o}C). Additional experiments were also performed to study the effect of shear degradation on polymer transport properties.

Table 7.4: List of polymers injectivity experiments (60 ^{o}C)

Coreflood #	Polymer	Concentration (ppm)	Shear Degradation	Injected Shear Viscosity (cP) @ 10 s^{-1}	Brine Salinity (ppm)
C1	FP 3330s	2500	Yes, Blender Shear Time ~ 300 secs	8.5	45,075
C2	D	1000	No	2.06	45,075
C3	D	2000	No	3.2	45,075
C4	D	1000	Yes, Blender Shear Time ~ 90 secs	2.2	45,075
C5	D	5000	Yes, Blender Shear Time ~ 90 secs	6.6	45,075
C6	C	1200	No	7.1	45,075
C7	D	2500	Yes, Blender Shear Time ~ 90 secs	3.3	121,000
C8	FP 3330s	5000	Yes, Blender Shear Time ~ 360 secs	4.6	121,000

7.2 RESULTS AND DISCUSSIONS

7.2.1 Polymer Viscosity Measurements

Each of the polymers (A, B, C and D) is prepared in synthetic sea water and synthetic formation water with concentrations varying from 0.1 - 0.5 wt% for viscosity measurements at 25 ^{o}C and 60 ^{o}C. Similar samples are prepared for the conventional HPAM 3330s for comparative study. The viscosities are measured using the TA instruments AR-G2 rheometer parallel plate configuration. All the polymers tested show typical shear thinning behavior similar to conventional HPAM polymers in both synthetic

sea water and formation brine at 60 °C as shown in **Figure 7.1.** This suggests good injectivity near wellbore at increased shear rates and reversible polymer network formation at low shear rates (usually observed deep in the reservoir). The significantly high viscosities obtained at low shear rates for APs can be beneficial for propagation into the reservoir and achieve higher sweep efficiency. The results indicate that for synthetic sea water and synthetic formation brine the viscosities generated at 10 s^{-1} and 60 °C with a similar MW associative polymer (compared to HPAM 3330s) were almost 3.6 times and 3.3 times higher than the viscosity with HPAM 3330s respectively. This clearly explains the benefits of use of associative polymers in high salinity brines at this reservoir temperature.

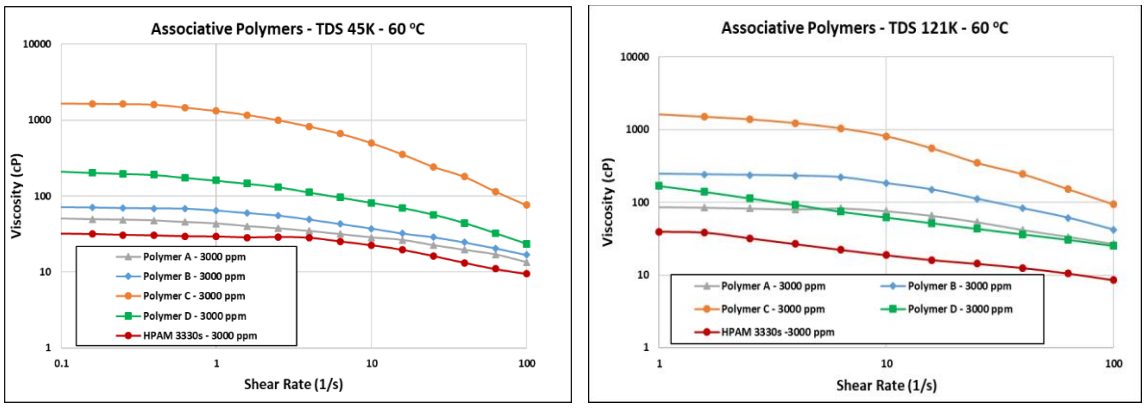

Figure 7.1. Shear viscosity measurements of associative polymers and FP 3330s in (a) synthetic sea water and (b) synthetic formation brine

Additionally, shear viscosity measurements as a function of varying polymer concentration was performed in both synthetic sea water and formation brine at both 25 °C and 60 °C. **Figures 7.2 and 7.3** show the effective viscosity ratio measurements (defined as the ratio of the polymer viscosity to the solvent viscosity at a given temperature) as a

function of concentration for polymers A, B, C and D in both brine salinities. For each of the polymers, viscosity decreases as temperature increases; however, relative polymer viscosity increases as temperature increases. Hence, a thermo-thickening effect is observed with the APs which has been suggested in several literature studies (Reichenbach-Klinke et al., 2013).

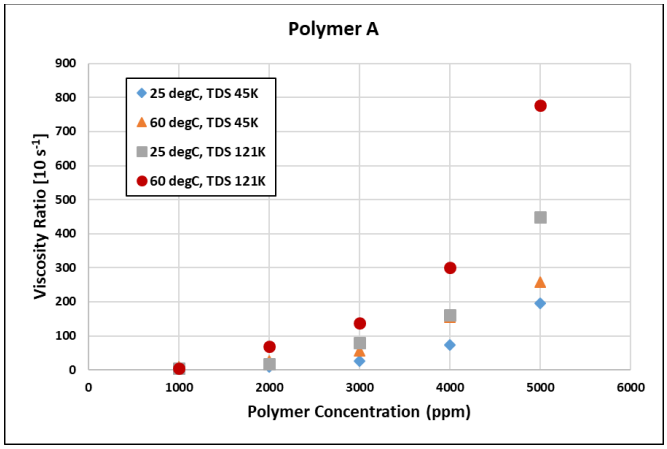

(a)

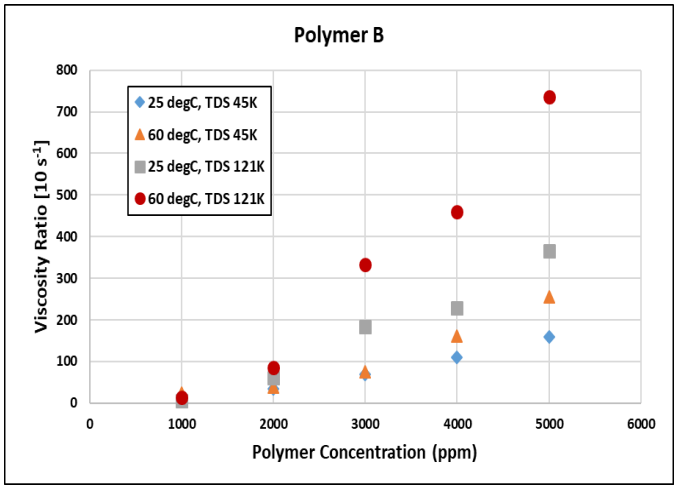

(b)

Figure 7.2. Effective viscosity ratio vs polymer concentration in sea water and formation brine for (a) polymer A and (b) polymer B at 25 ^{o}C and 60 ^{o}C

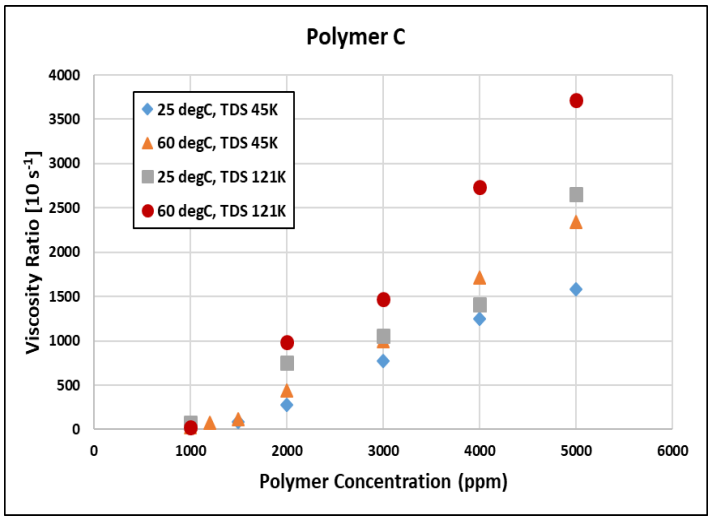

(a)

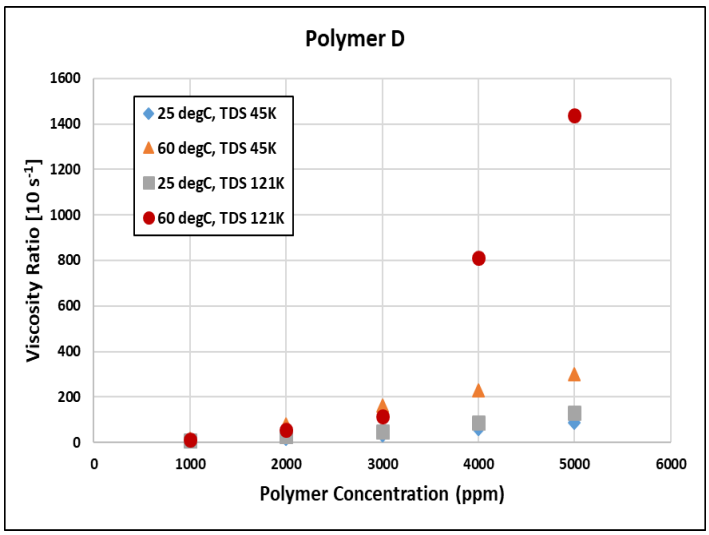

(b)

Figure 7.3. Effective viscosity ratio vs polymer concentration in sea water and formation brine for (a) polymer C and (b) polymer D at 25 ºC and 60 ºC

The results clearly show the increased viscosity at higher brine salinity and increased hydrophobic polymer network in presence of high number of divalent ions in contrast to conventional HPAM 3330s. This behavior of associative polymers shows great potential of application in high salinity carbonate reservoirs with requirement of lower polymer concentrations to achieve target viscosity. **Figure 7.4** shows the effective viscosity

ratio measurements as a function of concentration for HPAM 3330s in both brine salinities. The results show similar viscosity ratio for both salinities at 25 ^{o}C and 60 ^{o}C, hence no thermo-thickening effect. We can also conclude from the rheology measurements that each of these APs have a critical polymer concentration beyond which the hydrophobic polymer network is enhanced and results in significantly higher resistance factors during a coreflood experiment. The onset of this critical polymer concentration is dependent on the polymer molecular weight, hydrophobicity content and brine salinity – higher the MW lower the critical polymer concentration, higher the brine salinity lower the polymer concentration. The results also suggest that higher divalent ions in the brine salinity promotes the hydrophobic polymer network, thus increasing the viscosity significantly.

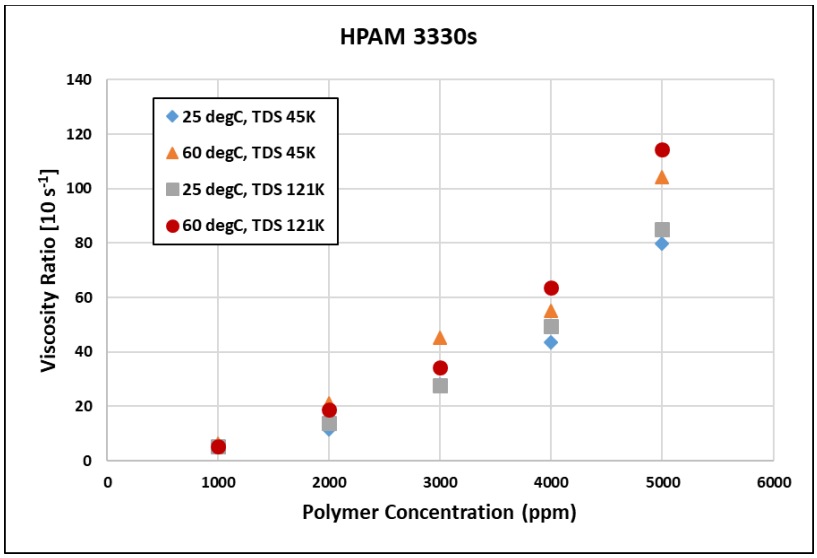

Figure 7.4. Effective viscosity ratio vs polymer concentration in sea water and formation brine for HPAM 3330s at 25 ^{o}C and 60 ^{o}C

7.2.1.1 Effect of Hydrophilic Surfactants on Polymer Rheology

Literature studies have reported possible interaction between surfactants and hydrophobic monomers in associative polymer molecules, thus losing the benefits of the hydrophobic polymer network and apparent high viscosities. The hydrophilic tails in anionic surfactants can neutralize the hydrophobic monomers in the polymer molecules reducing polymer-polymer interactions. In this study we investigated the mechanisms of interaction between surfactants and associative polymers in different brine salinities at 25 ^{o}C and 60 ^{o}C. The surfactant blend used as part of this study was C_{28}-45PO-20EO-COONa (0.5%) and C_{15-18} IOS (0.5%) with surfactant and polymer solutions prepared in synthetic sea-water and synthetic modified brine of TDS 90,630 ppm (composition detailed provided in **Table 7.2**). **Figures 7.5 and 7.6** show the effective viscosity ratio with 1 wt% total surfactant blend as a function of concentrations for polymers A, B, C and D in both brine salinities. For each of the polymers, shear viscosity measurements showed a significant reduction in presence of surfactants due to reduced hydrophobic network but still showed evidence of thermo-thickening effect (of similar magnitude) at higher temperatures and higher salinity brines. Hence, these associative polymers can prove to be useful in use of chemical flood designs as well for harsh reservoir conditions.

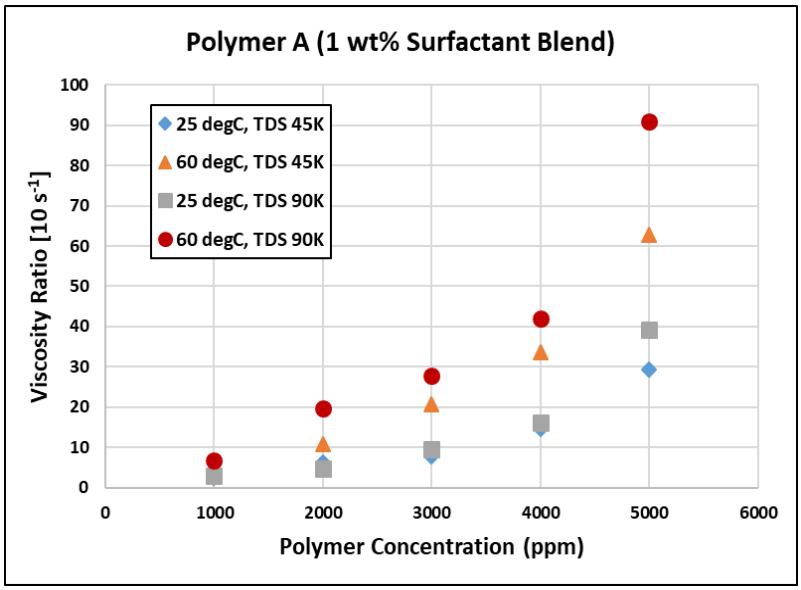

(a)

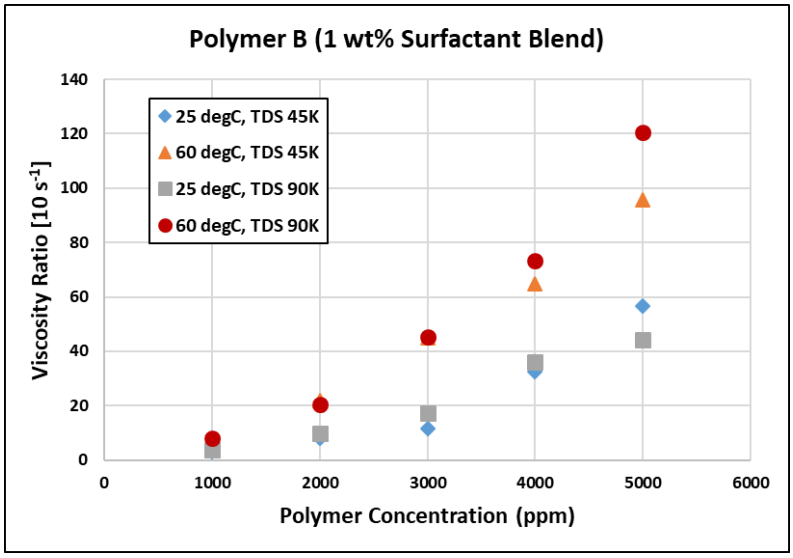

(b)

Figure 7.5. Effective viscosity ratio vs polymer concentration in sea water and synthetic brine (TDS 90K) with 1% surfactant blend for (a) polymer A and (b) polymer B at 25 ^{o}C and 60 ^{o}C

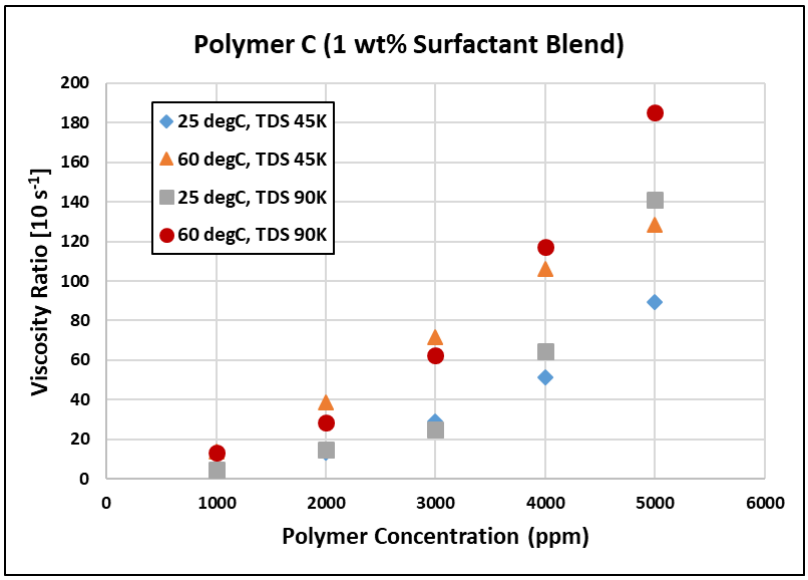

(a)

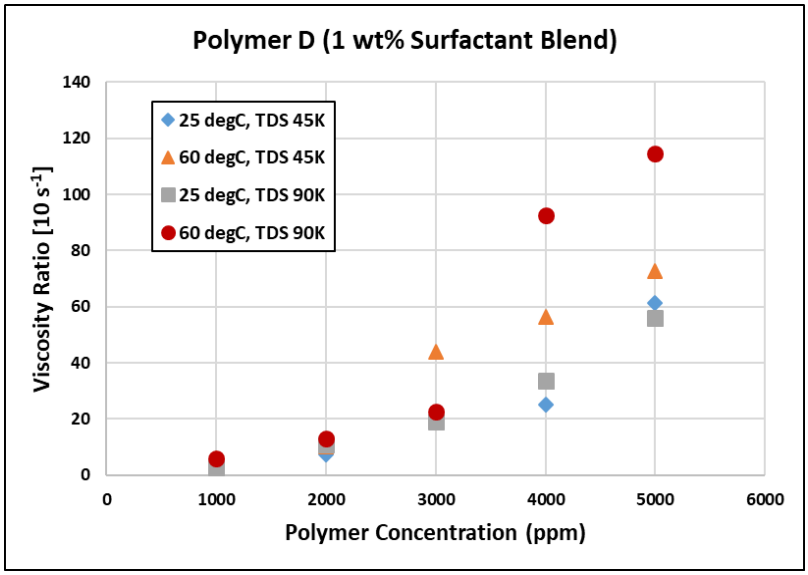

(b)

Figure 7.6. Effective viscosity ratio vs polymer concentration in sea water and synthetic brine (TDS 90K) with 1% surfactant blend for (a) polymer C and (b) polymer D at 25 ^{o}C and 60 ^{o}C

7.2.2 Shear Degradation Studies

Injected polymer solutions undergo enormous shear stress at the interface between the continuous phase in the wellbore and the matrix formation for a very short time. This

applied shear stress is dependent on the injection rate of the polymer solution and rock properties. Typically, the shear stress leads to irreversible breakage of long chain polymer backbone, which results in significant viscosity loss. Hence, a high dosage of common EOR polymers are necessary in the field to compensate for this effect (Morel et al., 2010).

Initial measurements of polymer stock (1 wt%) viscosity for associative polymers and HPAM 3330s showed that on increasing the mixing from 250 rpm to 500 rpm in an overhead mixer, for a duration of 3 hours, affected the polymer bulk viscosity. A careful observation showed small increases in polymer viscosity measured at 10 s^{-1} at varying temperatures for associative polymers whereas HPAM 3330s showed small decrease. It was also observed the magnitude of change of viscosity for APs depended on the molecular weight, hydrophobicity content and measurement temperature – higher the hydrophobicity higher the increase in viscosity and higher the temperature higher the increase in viscosity due to thermo-thickening effect. **Table 7.5** lists the change in viscosity and viscosity ratio (estimated as the ratio of viscosity @ 10 s^{-1} at two different mixing speeds) for different APs and HPAM 3330s at different temperatures based on the chemistry of the polymers. Polymers A and C showed similar change in viscosity at both temperatures even for different MW range and hydrophobicity content. Polymer B with intermediate MW and hydrophobic content showed significant increase in viscosity at increased shear mixing, whereas HPAM 3330s showed small decrease in viscosity with increased shear mixing.

Table 7.5: Shear Stability of Associative polymers

	Viscosity of stock (1 wt%) at 10 s^{-1} @ 250 RPM (cP)		**Viscosity ratio of stock (1 wt%) at 10 s^{-1} @ 500 RPM (cP)**	
Polymer Type	**25 ºC**	**60 ºC**	**25 ºC**	**60 ºC**
A	1349.7	1207.4	1.07	1.11
B	1248.3	810.0	1.30	1.66
C	3239.1	2457.7	1.08	1.12
D	1982.1	1925.9	1.15	1.35
HPAM 3330s	2057	1028.5	0.97	0.96

Additional shear degradation experiments were performed in a Waring laboratory blender to investigate the shear resistance abilities of the associative polymers compared to HPAM polymers. Each of these shear degradations were performed at 18,000 rpm with a fixed amount of mass for varying amount of times to tailor the molecular weight distribution, thus helping in successful injection in low permeability reservoirs. The shear degraded solutions were diluted to 500 ppm concentrations for size analysis using DLS method. A preliminary test was performed with polymer A, 1 wt% stock prepared in DI, to investigate the shear degradation properties for AP polymers in absence of any ions. Diluted polymer solutions with 2000 ppm were prepared in synthetic sea water to further study the filtration properties of the shear degraded polymer stocks. The results showed significantly higher resistance to shear degradation in absence of ions since the degraded polymer solution failed to transport through 0.2 microns even with 7 mins of shearing time. Hence, for the rest of the polymers shear degradation studies were performed with stock

prepared in synthetic sea water. An additional experiment was also performed with polymer A, 1 wt% stock prepared in synthetic sea water, to understand the effect of divalent ions on shear degradation mechanism**. Figure 7.7** shows the comparison between the degraded viscosity measurements for polymer A stocks prepared in DI and synthetic sea water, measured at 25 ^{o}C. The change in viscosity loss is significantly higher in synthetic sea water which signifies higher degradation rate in presence of divalent ions. The results also verify the fact that these APs are more shear resistant than conventional HPAMs in a similar brine salinity. Another important observation was the loss in shear thinning behavior for the polymer samples prepared in synthetic sea water compared to DI at lower shear rates. The summary of the results of shear degradation studies for polymers A and D is listed in **Table 7.6**.

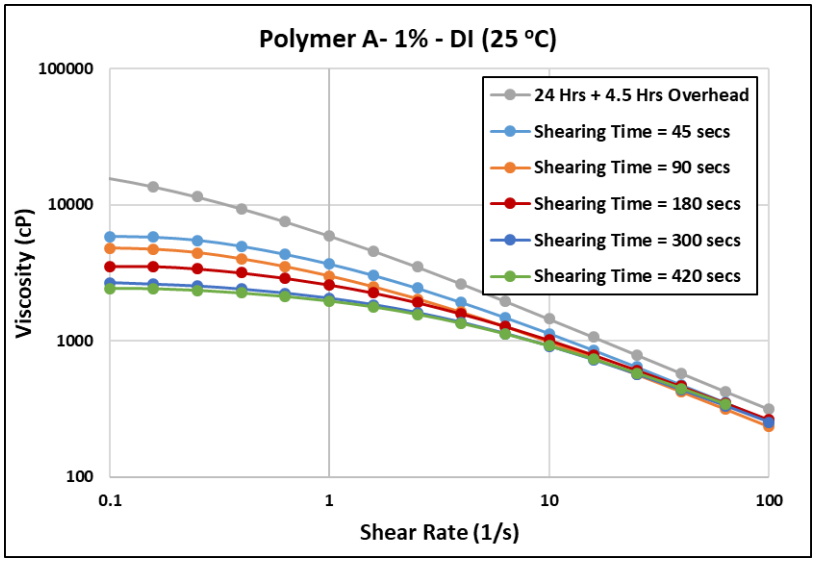

(a)

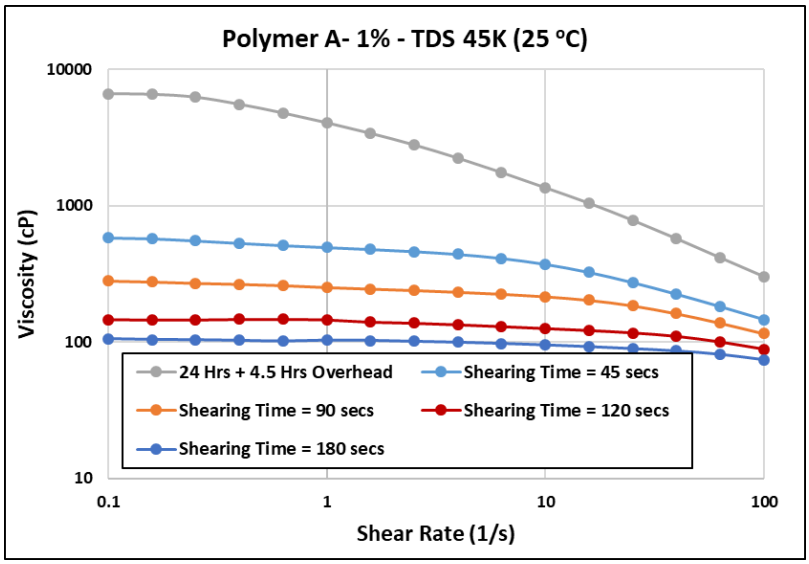

(b)

Figure 7.7. Viscosity measurements with varying shearing time in laboratory blender for polymer A with 1 wt% stock prepared in (a) DI and (b) synthetic sea water

Table 7.6: Summary of Viscosity Measurements during shear degradation studies at 25 C

Polymer Type	**Brine Salinity**	**Shearing Time (secs)**	**Percentage of Viscosity Retained (@ 0.1 s^{-1})**	**Percentage of Viscosity Loss (@ 0.1 s^{-1})**
A	DI	0	100	0
		45	85.14	14.86
		90	69.6	30.4
		180	51.42	48.6
		300	38.85	61.15
		420	35.38	62.62
A	TDS 45K	0	100	0
		45	8.79	91.2
		90	4.25	95.75
		120	2.21	97.8
		180	1.6	98.4
D	TDS 45K	0	100	0
		45	6.98	93.02
		90	6.41	93.6
		180	4.38	95.6
		300	1.8	98.2

7.2.2.1 Effect of mechanical shear degradation on polymer molecular distribution modification

Polymers A and D (1 wt% stock prepared in synthetic sea water) were investigated for shear degradation studies and their effect on molecular weight distribution modification through laboratory blenders. Samples were taken out after each shearing time for each polymer to prepare them for size analysis using DLS method at a diluted concentration of

500 ppm. **Figure 7.8** shows the polymer size distribution change for polymers A with varying amount of shearing time at 18,000 rpm in the mechanical blender for 1 wt% stock prepared in DI and synthetic sea water. Results clearly show reduction in polydispersity of particle size distribution with increasing shearing time and the effect of shear degradation in presence and absence of divalent ions for the same polymer type. The results signify that shear degradation is significantly enhanced in presence of divalent ions that leads to fast polymer chain breakage, also suggested by the summary results in **Table 7.6**. Hence, an optimization of shearing time based on brine salinity is key to developing a robust method during polymer pre-treatment for injection in low permeability carbonate reservoirs. The polymer size distribution (obtained from DLS) can then be compared with the pore throat distribution (obtained from MICP) for a given porous media to quantitatively estimate if the polymer solution would successfully transport with no face plugging, as shown in **Figure 7.10**.

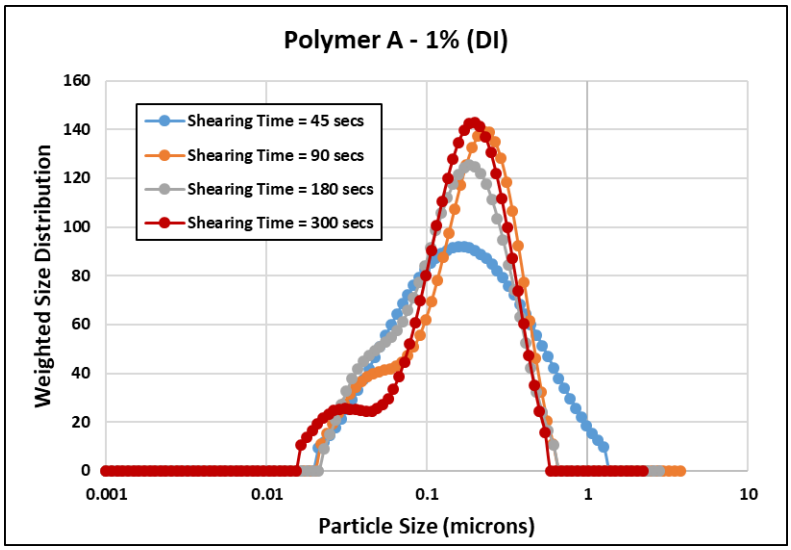

(a)

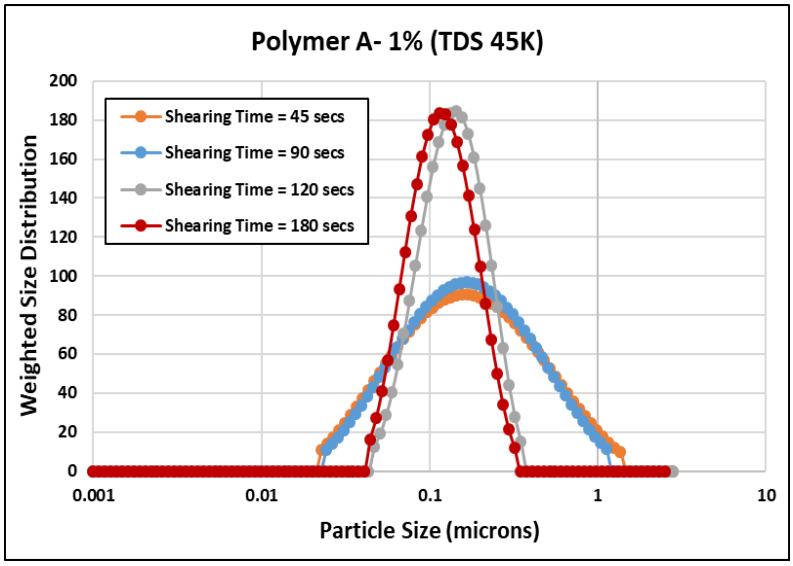

(b)

Figure 7.8. Polymer size distribution modification with shear degradation for polymer A with 1 wt% stock prepared in (a) DI and (b) synthetic sea water

Figure 7.9 shows the size distribution for polymer D (stock prepared in synthetic sea water) with varying amount of shear time. The result shows that for this polymer batch shearing time of 90 secs was found to be optimum based on the modified size distribution from DLS and pore throat diameter distribution from mercury injection capillary pressure

(MICP) test for any porous media (limestone cores), as shown in **Figure 7.10**. The key for successful injection of polymer in tight formations is minimal overlap between polymer particle diameter distribution and pore throat diameter distribution of a porous medium, as suggested from **Figure 7.10**. Hence, from the results observed even for similar permeability carbonates due to wide pore size distribution polymer D would transport successfully in Edwards Yellow but not in Indiana limestone or Texas Cream limestone (significant overlap between particle size and pore throat).

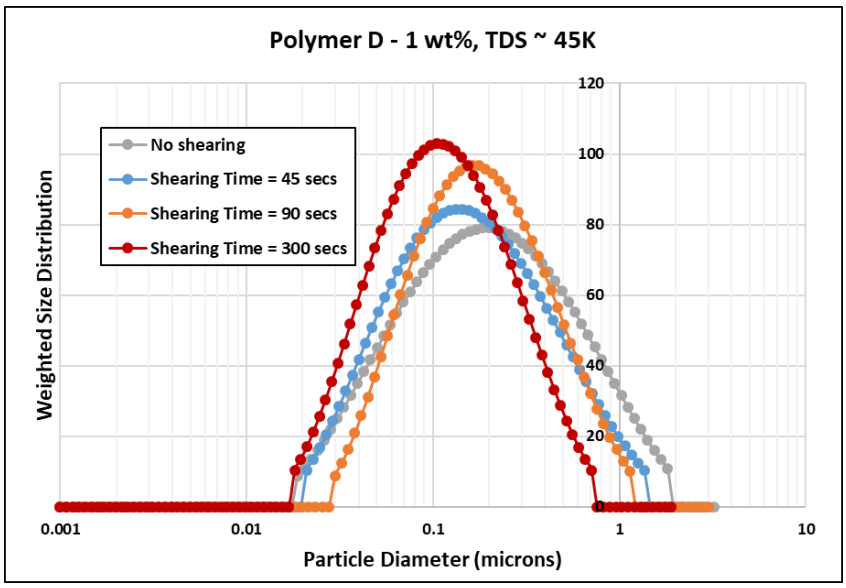

Figure 7.9. Polymer size distribution for polymer D (stock prepared in synthetic sea water) using DLS method at various blender shearing time

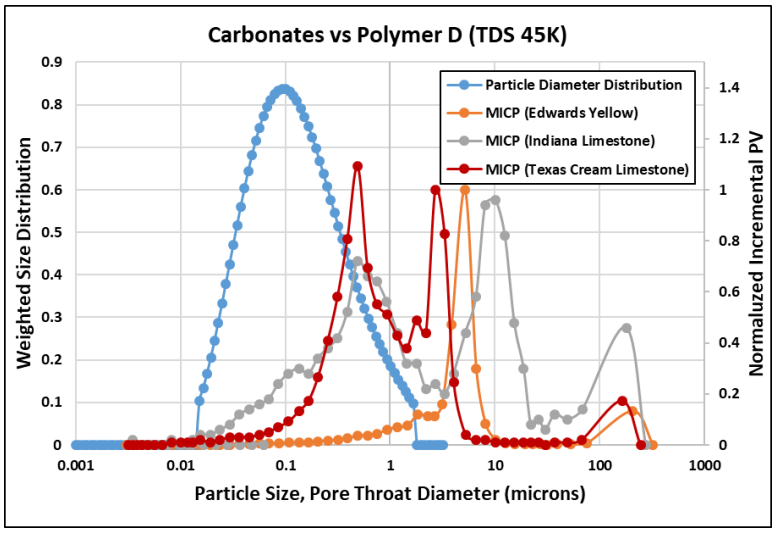

Figure 7.10. Polymer size distribution for diluted polymer D solution with 1000 ppm (@ Shearing time = 90 secs) vs pore throat diameter distribution of limestone cores (K_{brine} ~ 15 - 20 mD)

7.2.2.2 Effect of Polymer Concentration on Size Analysis

Unlike conventional HPAM polymers, the concentration of associative polymers plays an important role in the formation of hydrophobic polymer networks that affects the polymer rheology and hydrodynamic size of the polymer particles in the aqueous phase. Hence, understanding of the effect of the polymer concentration is important in the design of polymer corefloods for tight formations. **Figure 7.11** shows the effect of 3 different concentrations for polymers B, C and D during size analysis measurements in synthetic sea water. The results clearly show based on the chemistry of the polymer and number of hydrophobic monomers in each affects the size distribution of the polymer samples. Polymer C with the least amount of hydrophobicity does not show any significant effect of polymer concentration on size analysis. On the other hand, Polymer B with higher hydrophobicity shows increase of average particle size with increasing polymer

concentration. Thus, based on the type of polymer under consideration concentration needs to be appropriately chosen during size analysis and comparison with the pore throat distribution for associative polymers for robust design.

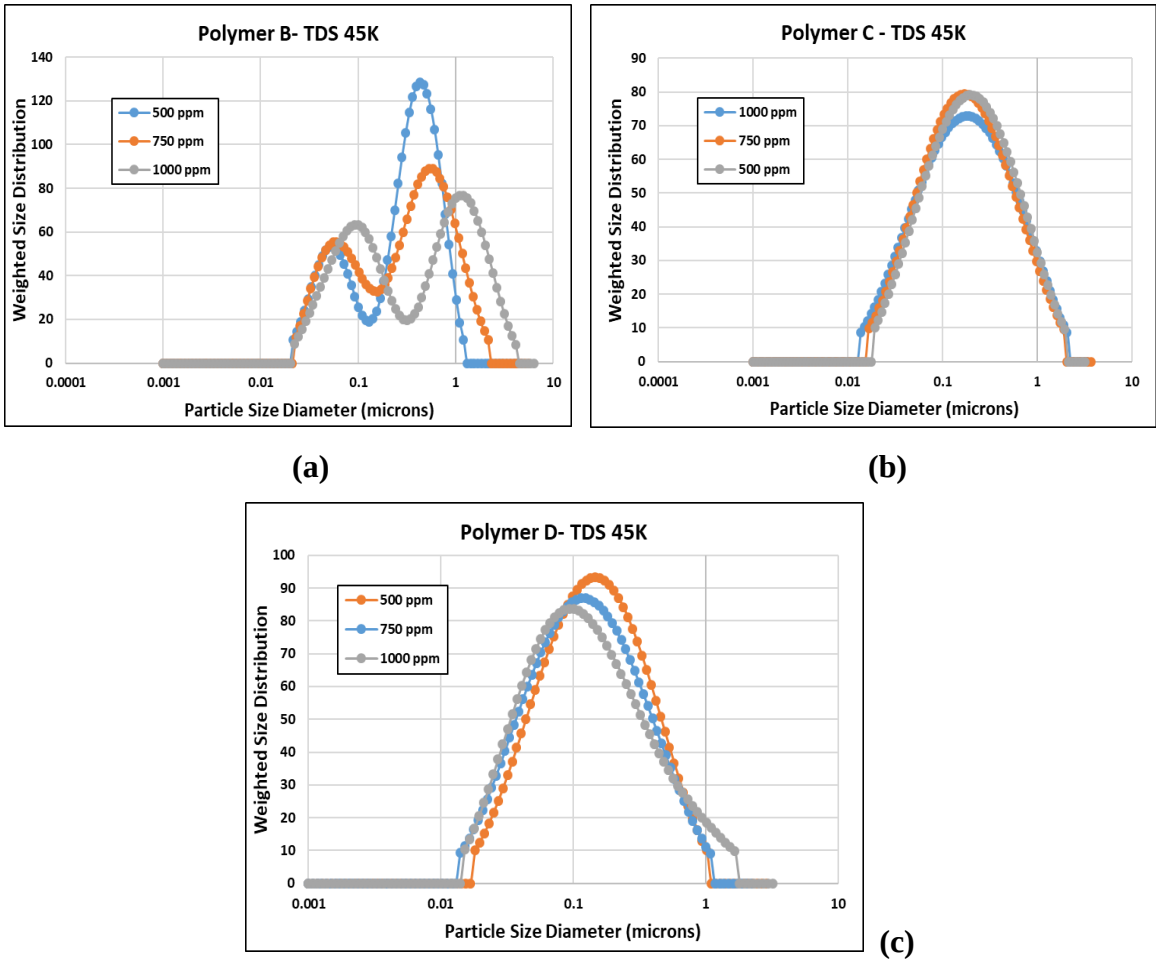

Figure 7.11. Polymer size distribution for different concentrations in synthetic sea water for (a) polymer B, (b) polymer C, (c) polymer D

7.2.3 Aggressive Filtration Treatment

The shear degraded polymer stocks are diluted to the target polymer concentrations in the injected brine salinities for injection in a porous medium. The diluted polymer solutions are then filtered through polycarbonate membrane filters to ensure successful

transport in porous media and good filterability. For injection in low permeability carbonates, filtrations were performed through 0.4, 0.2- and 0.4-microns filter papers respectively with Argon at 15 psi. Results showed that the filtration ratio (F.R.) of 1.2 (or less) at the final step (0.4 microns) was deemed necessary for successful injection in low permeability formations (less than 30 mD). **Table 7.7** summarizes the results of the plugging parameter β and F.R. for each shear degradation sample with polymer D (stock prepared in synthetic sea water) and aggressive filtration tests performed. The plugging parameter β is a significance of filter cake resistance build up during the filtration tests and is analogus to face plugging behavior in coreflood experiments. An increase in β (and in F.R.) was observed with decrease in filter size, whereas increase in shearing time reduced β during filtration through same filter size. Samples were taken out at each filtration step to measure the particle size distribution and its modification through each filtration step. **Figure 7.12** shows the particle size distribution for polymer D (stock prepared in synthetic sea water) with 2000 ppm in synthetic sea water at each filtration steps after shearing time of 90 secs. Few interesting observations were made during this experiment. The particle size distribution first shifted lower after 0.4-micron filtration, then apparently shifted to higher size after filtration through 0.2 microns which can be a result of forced association between hydrophobic monomers at such low filter sizes and high-pressure gradient. The final filtration step showed some hysteresis effect at 0.4 microns due to the possible modification of the polymer network in the previous step. This behavior can result in higher resistance factors generated during a coreflood experiment as the polymer solution transports through smaller pores.

Table 7.7: Aggressive Filtration Tests with Polymer D (TDS ~ 45K)

Polymer Type	**Polymer D**				
Filter Size	**Beta**	**F.R.**	**Salinity (ppm)**	**Conc (ppm)**	**Blend Time (secs)**
0.4	0.00012	1.02	45000	1000	0
1	0.0050	1.44			
0.4	0.0048	1.43	45000	2000	0
0.4	0.001	1.12			
0.2	0.0047	1.42			
0.4	0.0018	1.19	45000	2000	45
0.4	0.0008	1.09			
0.2	0.0072	1.57			
0.4	0.0006	1.06	45000	2000	90
0.4	0.0007	1.08			
0.2	0.0089	1.65	45000	2000	180
0.4	0.001	1.11			
0.2	7.70E-03	1.6	45000	2000	300
0.2	0.00066	1.55			
0.4	0.00011	1.01	45000	5000	90

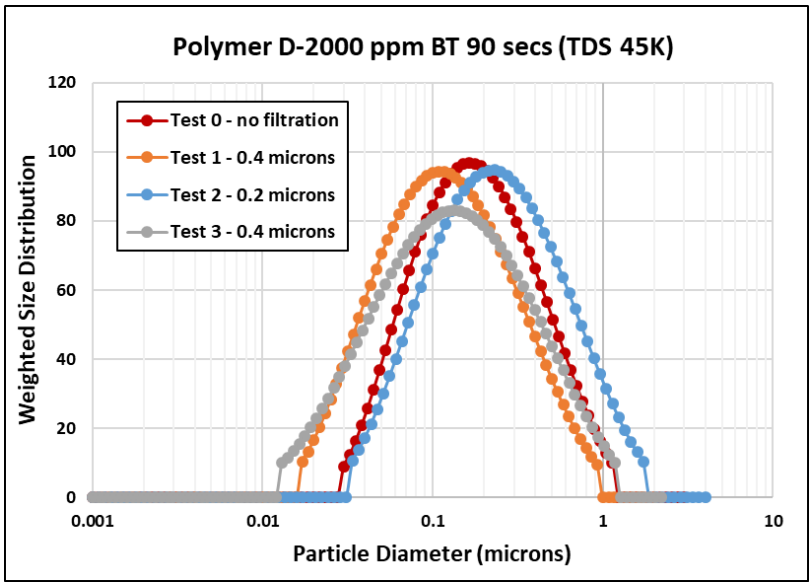

Figure 7.12. Polymer size distribution modification during aggressive filtration for polymer D (stock prepared in synthetic sea water)

7.2.4 Polymer Injectivity Experiments

A series of coreflood experiments were performed in low permeability carbonate reservoirs at a temperature of 60 ^{o}C with synthetic sea water and synthetic formation brine as injection brines. The working temperature was chosen based on the existing literature studies and the product limitations. The list of coreflood experiments have been listed in **Table 7.4**. First, a base case experiment (coreflood C1) was performed with HPAM 3330s in an outcrop Edwards Yellow limestone core which was vacuum saturated with 2% KCl at first. A tracer test was performed to estimate the heterogeneity of the porous medium and pore volume. The properties of the core are listed in **Table 7.8**. After completion of the tracer test, a polymer solution of HPAM 3330s with 2500 ppm prepared in synthetic sea water (polymer stock shear degraded for 300 secs in DI) was deoxygenated and injected into the porous medium. The polymer solution was injected for about 3 PV at 0.8 ft/D

superficial velocity and the effluent viscosities were measured. The pressure drops reached steady state around 1 PV (shown in **Figure 7.13**) and the effluent viscosity reached steady state around 1-1-1.2 PV of polymer injection. Note, the permeability during the polymer flood was estimated using the injected shear viscosity of 8.5 cP @ 10 s^{-1} at the reservoir temperature (60 ^{o}C). At the end of polymer injection, an exhaustive waterflood of 10 PV was performed to estimate the residual resistance factor (RRF) for this coreflood. The summary of the coreflood results is provided in **Table 7.9** with measurements of permeability reduction (Rk), resistance factor (RF) and RRF for this experiment.

$$\mathrm{Rk} = \frac{K_{brine}}{K_{polymer}} \tag{7.1}$$

$$\mathrm{RF} = \frac{\Delta P\ (polymer\ flood)}{\Delta P\ (brine\ flood)} \tag{7.2}$$

$$\mathrm{RRF} = \frac{\Delta P\ (brine\ flood\ after\ polymer)}{\Delta P\ (brine\ flood)} \tag{7.3}$$

Table 7.8: Core properties for coreflood C1

Core Properties		**Edwards Yellow limestone Brine Permeability**	
Diameter (cm)	3.76	**Whole Core (mD)**	13
Length (cm)	30.4	**Section 1 (mD)**	9
Mass (g)	673.7	**Section 2 (mD)**	12
Bulk Volume (mL)	338.3	**Section 3 (mD)**	10
Porosity	0.268	**Section 4 (mD)**	15
Area (cm^2)	11.13		
Pore Volume (mL)	90.5		

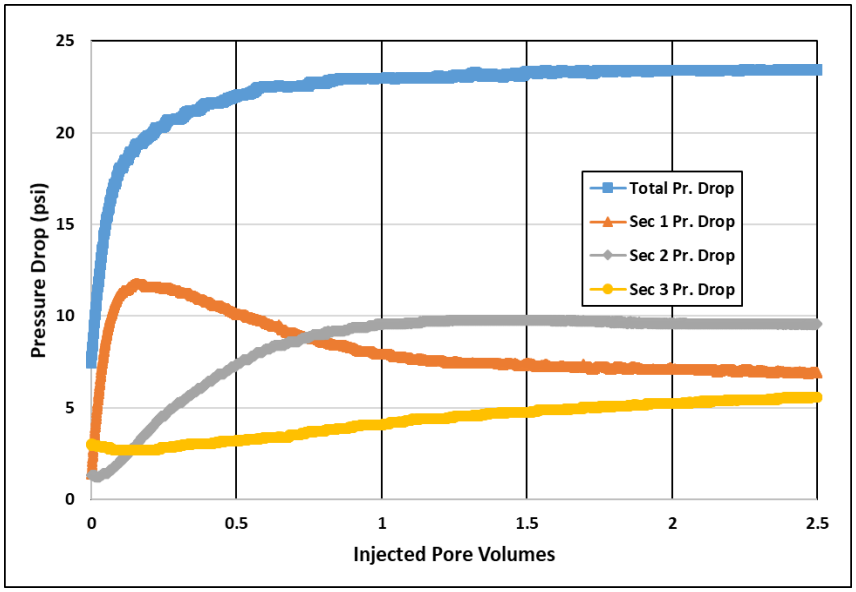

Figure 7.13. Pressure drops during injection of 2500 ppm HPAM 3330s (shear degradation of 300 secs) prepared in synthetic sea water at 60 ^{o}C.

Table 7.9: Summary of experimental results for coreflood C1

	Rk	**RF**	**RRF**
Whole Core (mD)	0.92	18.55	1.35
Section 1 (mD)	1.09	15.55	1.67
Section 2 (mD)	0.61	27.86	1.12
Section 3 (mD)	1.18	14.28	1.71

Coreflood C2 was performed in an outcrop Indiana limestone core which was vacuum saturated with 2% KCl at first. A tracer test was performed to estimate the heterogeneity of the porous medium and pore volume. The properties of the core are listed in **Table 7.10**. After completion of the tracer test, a polymer solution of polymer D with 1000 ppm prepared in synthetic sea water (no shear degradation) was deoxygenated and injected into the porous medium. The polymer solution was injected for about 6 PV at 2

ft/D superficial velocity and the effluent viscosities were measured. The pressure drops reached steady state around 2-3 PVs and the effluent viscosity reached steady state around 1.5-2 PV of polymer injection. At the end of polymer injection, an exhaustive waterflood of 10 PV was performed to estimate the residual resistance factor (RRF) for this coreflood. The summary of the coreflood results is provided in **Table 7.11** with measurements of permeability reduction (Rk), resistance factor (RF) and RRF for this experiment. The polymer adsorption estimated during this coreflood was about 84.2 µg/gm of rock at the reservoir temperature (60 ^{o}C).

Table 7.10: Core properties for coreflood C2

Core Properties		**Indiana Limestone Brine Permeability**	
Diameter (cm)	5.03	**Whole Core (mD)**	44
Length (cm)	28.3	**Section 1 (mD)**	32
Mass (g)	1307	**Section 2 (mD)**	53
Bulk Volume (mL)	562.2	**Section 3 (mD)**	44
Porosity	0.146	**Section 4 (mD)**	50
Area (cm^2)	19.86		
Pore Volume (mL)	82.3		

Table 7.11: Summary of experimental results for coreflood C2

	Rk	**RF**	**RRF**
Whole Core (mD)	1.9	8.0	3.1
Section 1 (mD)	0.9	3.7	3.5
Section 2 (mD)	1.9	7.8	2.8
Section 3 (mD)	2.5	10.2	3.34
Section 4 (mD)	2.4	10.2	3.05

The results clearly show that the resistance factors are at least 2 times higher than the permeability reduction for each of the core sections. This provides an evidence for propagation of 2 polymer fronts through the porous medium. The first polymer front corresponds to the polymer viscosity and the second polymer front resulting from polymer retention and permeability reduction. The apparent viscosity of the polymer solutions is estimated to be higher than the rheological viscosity measured in a rheometer. Another important factor for successful implementation of polymer flooding is low RRF which signifies low polymer retention. In this coreflood C2, a high RRF resulted even after injection of 10 PV of brine after polymer injection. Hence, a better understanding of the mechanisms of associative polymer re-dissolution in the brine is required.

Coreflood C3 was performed in an outcrop Indiana limestone core which was vacuum saturated with 2% KCl at first. A tracer test was performed to estimate the heterogeneity of the porous medium and pore volume. The properties of the core are listed in **Table 7.12**. After completion of the tracer test, a polymer solution of polymer D with 2000 ppm prepared in synthetic sea water (no shear degradation) was deoxygenated and injected into the porous medium. The polymer solution was injected for about 6 PV at 1 ft/D superficial velocity and the effluent viscosities were measured. The pressure drops never reached true steady state but showed momentary steady state around 4 PV of polymer injection. The effluent samples showed loss in viscosity due to face plugging and filtering of polymer molecules during the transport experiment. Note, the permeability during the polymer flood was estimated using the injected shear viscosity of 3.2 cP @ 10 s^{-1} at the reservoir temperature (60 ^{o}C). The summary of the coreflood results is provided in **Table**

7.13 with measurements of permeability reduction (Rk) and resistance factor (RF) after 4 PV of polymer injection. The resistance factors for section 3 and 4 might not be true estimations since it did not reach steady state.

Table 7.12: Core properties for coreflood C3

Core Properties		**Indiana Limestone Brine Permeability**	
Diameter (cm)	5.03	**Whole Core (mD)**	23
Length (cm)	28.3	**Section 1 (mD)**	19
Mass (g)	1307	**Section 2 (mD)**	20
Bulk Volume (mL)	562.2	**Section 3 (mD)**	27
Porosity	0.134	**Section 4 (mD)**	28
Area (cm^2)	19.86		
Pore Volume (mL)	75.5		

Table 7.13: Summary of experimental results for coreflood C3

	Rk	**RF**
Whole Core (mD)	12.1	44.18
Section 1 (mD)	26.9	113.57
Section 2 (mD)	6.7	24.39
Section 3 (mD)	13.6	23.33
Section 4 (mD)	5.8	20.95

The significantly higher Rk and RF values for section 1 and whole core provides evidence of face plugging at the inlet of the core. **Figure 7.14** shows the pressure drops during the injection of the polymer solution. As observed the pressure drop seemed to reach a temporary steady state around 4 PV of polymer injection and with more injection the face

plugging became more aggressive leading to significant pressure build-up. Hence, the conclusion from this experiment was that it might be very difficult to successfully transport the polymer solutions (with no prior shear degradation) even at low concentrations through such low permeability carbonate formations.

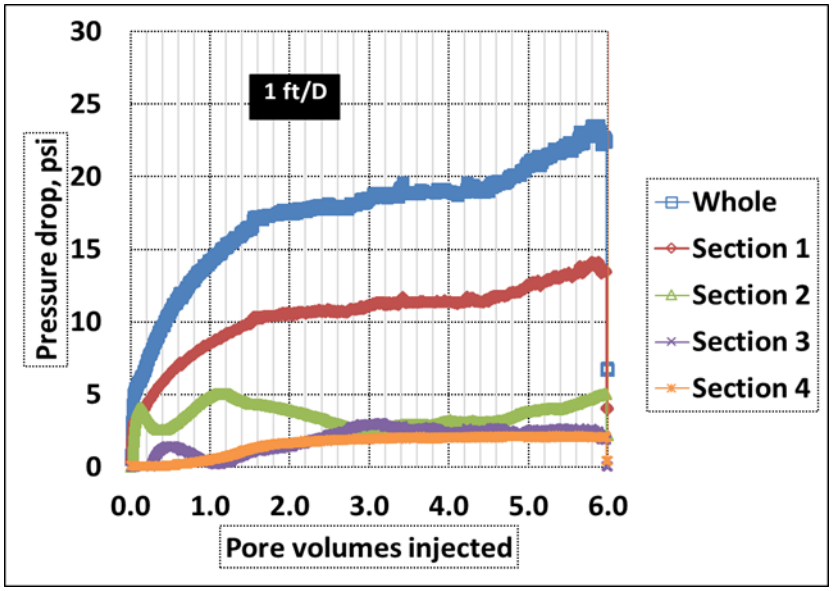

Figure 7.14. Pressure drops during injection of 2000 ppm polymer D (no shear degradation) prepared in synthetic sea water at 60 ^{o}C.

Based on the first two coreflood performances, it was found to be necessary to shear degrade the polymer stock solutions to successfully inject in low permeability carbonate rocks. Coreflood C4 was performed in an outcrop Edwards Yellow limestone core which was vacuum saturated with 2% KCl at first. A tracer test was performed to estimate the heterogeneity of the porous medium and pore volume. The properties of the core are listed in **Table 7.14**. After completion of the tracer test, a polymer solution of polymer D with 1000 ppm prepared in synthetic sea water (stock shear degraded for 90 secs in synthetic sea water) was deoxygenated and injected into the porous medium. The polymer solution

was injected for about 3 PV at 1 ft/D superficial velocity and then increased to 2 ft/D for another 3 PV of injection. The pressure drops reached semi steady state between 2-3 PV of polymer injection. Note, the permeability during the polymer flood was estimated using the injected shear viscosity of 2.2 cP @ 10 s^{-1} at the reservoir temperature (60 ^{o}C). At the end of polymer injection, an exhaustive waterflood of 10 PV was performed to estimate the residual resistance factor (RRF) for this coreflood. The summary of the coreflood results is provided in **Table 7.15** with measurements of permeability reduction (Rk), resistance factor (RF) and RRF for this experiment. The polymer adsorption during this experiment was estimated to be 137.65 µg/gm of rock.

Table 7.14: Core properties for coreflood C4

Core Properties		**Edwards Yellow Limestone Brine Permeability**	
Diameter (cm)	5.05	**Whole Core (mD)**	19
Length (cm)	30.0	**Section 1 (mD)**	9
Mass (g)	1235	**Section 2 (mD)**	21
Bulk Volume (mL)	614.14	**Section 3 (mD)**	28
Porosity	0.268	**Section 4 (mD)**	43
Area (cm^2)	20.47		
Pore Volume (mL)	164.4		

Table 7.15: Summary of experimental results for coreflood C4

	Rk	**RF**	**RRF**
Whole Core (mD)	4.0	8.0	2.34
Section 1 (mD)	2.8	5.5	1.66
Section 2 (mD)	4.7	9.4	2.69
Section 3 (mD)	6.5	13.1	3.73
Section 4 (mD)	4.2	8.5	2.34

The results of coreflood C4 clearly showed reduction in apparent viscosity generated by polymer D in the porous medium based on the ratio of RF/Rk values. On comparing the results of coreflood C4 with coreflood C2 we observed a reduction in RRF during waterflood with shear degraded polymer solutions, which can be promising for applications in low permeability formations. **Figure 7.15** shows the pressure drop profile during injection of shear degraded polymer D and the results summarized in **Table 7.15** are estimated at the end of the polymer injection experiment.

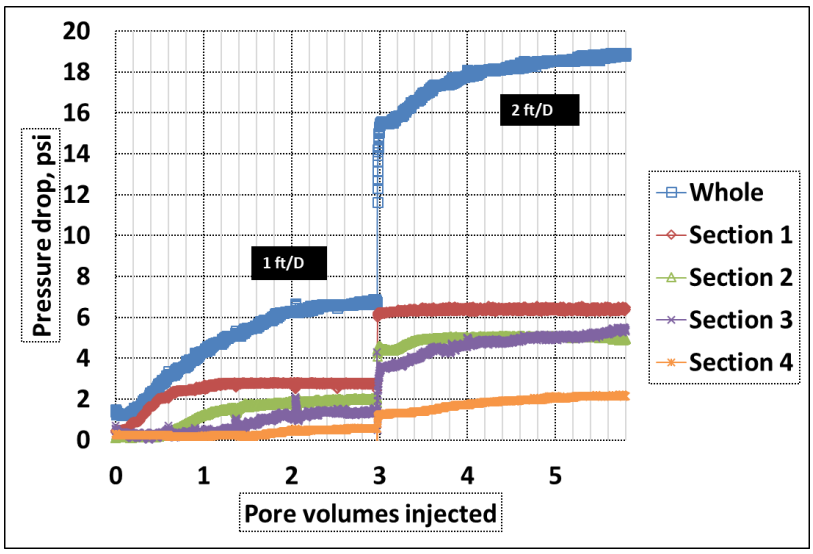

Figure 7.15. Pressure drops during injection of 1000 ppm polymer D (shear degraded for 90 secs) prepared in synthetic sea water at 60 ^{o}C.

Next coreflood was designed to investigate the upper limit of polymer concentration that could be injected in low permeability carbonate formations. Coreflood C5 was performed in an outcrop Edwards Yellow limestone core which was vacuum saturated with 2% KCl at first. A tracer test was performed to estimate the heterogeneity of the porous medium and pore volume. The properties of the core are listed in **Table 7.16**.

After completion of the tracer test, a polymer solution of polymer D with 5000 ppm prepared in synthetic sea water (stock shear degraded for 90 secs in synthetic sea water) was deoxygenated and injected into the porous medium. The polymer solution was injected for about 5 PV at 1 ft/D superficial velocity and then increased to 1.5 ft/D for another 3 PV of injection. The pressure drops reached semi steady state between 5-6 PV of polymer injection whereas the effluent viscosity measurements showed steady state around 2 PV of polymer injection. Note, the permeability during the polymer flood was estimated using the injected shear viscosity of 6.6 cP @ 10 s^{-1} at the reservoir temperature (60 ^{o}C). At the end of polymer injection, an exhaustive modified waterflood (mixture of glycerol + synthetic sea water) of 5 PV was performed to estimate the residual resistance factor (RRF) for this coreflood. This approach was taken to provide a favorable mobility ratio during the waterflood process depending on the high apparent viscosities generated during the polymer injection experiment. The summary of the coreflood results is provided in **Table 7.17** with measurements of permeability reduction (Rk), resistance factor (RF) and RRF for this experiment. The polymer adsorption during this experiment was estimated to be 446.6 µg/gm of rock, which is significantly higher than the previous corefloods. The significant loss of polymer at such higher polymer concentration in low permeability can be one of the possible reasons of high RFs and RRFs generated during the coreflood.

Table 7.16: Core properties for coreflood C5

Core Properties		Edwards Yellow Limestone Brine Permeability	
Diameter (cm)	5.1	**Whole Core (mD)**	26
Length (cm)	30.1	**Section 1 (mD)**	28
Mass (g)	1231.5	**Section 2 (mD)**	29
Bulk Volume (mL)	617.42	**Section 3 (mD)**	25
Porosity	0.265	**Section 4 (mD)**	24
Area (cm^2)	20.51		
Pore Volume (mL)	163.6		

Table 7.17: Summary of experimental results for coreflood C5

	Rk	RF	RRF (glycerol + SW)
Whole Core (mD)	5.9	77.5	9.01
Section 1 (mD)	4.7	61.9	3.66
Section 2 (mD)	5.7	75.9	8.47
Section 3 (mD)	7.2	93.5	11.81
Section 4 (mD)	5.4	70.4	10.59

The polymer viscosity measurements were normalized to the injected viscosity. **Figure 7.16** shows the result of effluent viscosity measurements for first 4 PV of polymer injection. It is evident that the measured viscosity of the effluent samples increased by more than 2 times at the steady state. A possible explanation for this behavior could be attributed to the thermo-thickening effect and enhanced hydrophobic polymer network that led to modification of the polymer structure after transport through low permeability carbonate formations. The summarized results in **Table 7.17** also shows significantly higher RF

measurements (6 times higher than Rk) and higher RRF with glycerol and sea water mix. This coreflood also provided evidence of 2 polymer fronts – first viscosity front that reached steady state around 2 PV and second front due to polymer retention and permeability reduction with pressure drop reaching state around 5-6 PV. The results showed great potential of application of associative polymers with high concentrations but at the expense of significantly higher polymer retention in the porous medium. This was identified as one of the key challenges in the design of an experiment for injection of associative polymers in low permeability carbonates.

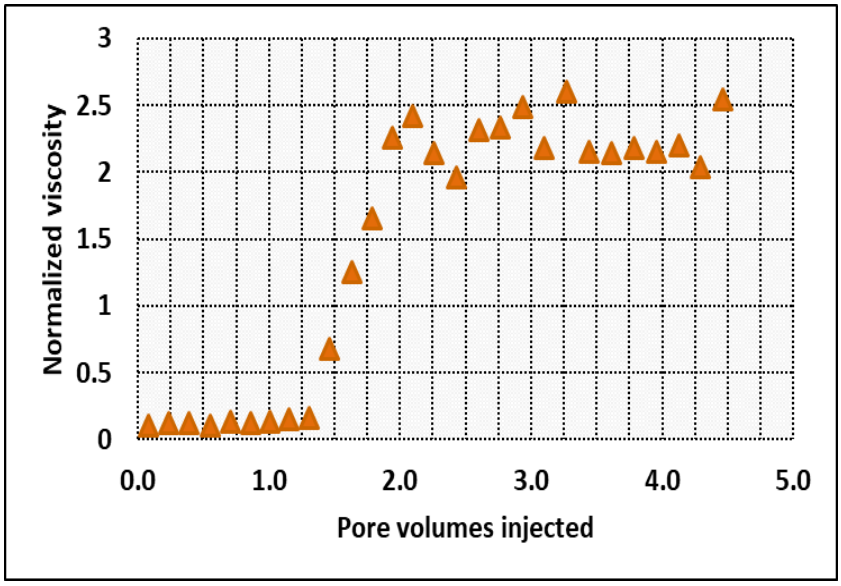

Figure 7.16. Normalized effluent viscosity measuements during coreflood C5 at 60 ^{o}C

An additional coreflood was performed to study the transport property of polymer C (highest MW) in a high permeability carbonate core. Coreflood C6 was performed in an outcrop Indiana limestone core which was vacuum saturated with 2% KCl at first. A tracer test was performed to estimate the heterogeneity of the porous medium and pore volume.

The properties of the core are listed in **Table 7.18**. After completion of the tracer test, a polymer solution of polymer C with 1200 ppm prepared in synthetic sea water (no shear degradation) was deoxygenated and injected into the porous medium. The polymer solution was injected for about 5 PV at 2 ft/D superficial velocity. The pressure drops reached semi steady state between 4.5-5 PV of polymer injection whereas the effluent viscosity measurements showed steady state around 2 PV of polymer injection. At the end of polymer injection, an exhaustive waterflood of 10 PV was performed to estimate the residual resistance factor (RRF) for this coreflood. The summary of the coreflood results is provided in **Table 7.19** with measurements of permeability reduction (Rk), resistance factor (RF) and RRF for this experiment. The high RF and RRF values obtained at lower permeability sections are consistent with the results from the previous corefloods. This coreflood also emphasized the potential of associative polymers to generate high RF values in high permeability carbonates even at low concentrations.

Table 7.18: Core properties for coreflood C6

Core Properties		**Indiana Limestone Brine Permeability**	
Diameter (cm)	5.05	**Whole Core (mD)**	303
Length (cm)	30.2	**Section 1 (mD)**	247
Mass (g)	1379.7	**Section 2 (mD)**	195
Bulk Volume (mL)	604.2	**Section 3 (mD)**	294
Porosity	0.135	**Section 4 (mD)**	597
Area (cm^2)	20.01		
Pore Volume (mL)	81.4		

Table 7.19: Summary of experimental results for coreflood C6

	Rk	RF	RRF
Whole Core (mD)	0.96	29.3	4.97
Section 1 (mD)	0.96	25.8	2.54
Section 2 (mD)	1.15	31.3	7.63
Section 3 (mD)	0.90	25.3	4.23
Section 4 (mD)	0.6	21.2	4.8

Coreflood C7 was performed to study the transport property of polymer D in high salinity formation brine in presence of enhanced polymer network in a low permeability carbonate core. Coreflood C7 was performed in an outcrop Edwards Yellow limestone core which was vacuum saturated with 2% KCl at first. A tracer test was performed to estimate the heterogeneity of the porous medium and pore volume. The properties of the core are listed in **Table 7.20**. After completion of the tracer test, a polymer solution of polymer D with 2500 ppm prepared in synthetic formation brine (shear degraded stock for 90 secs in synthetic sea water) was deoxygenated and injected into the porous medium. The polymer solution was injected for about 5 PV at 1 ft/D superficial velocity and then increased to 1.5 ft/D for additional 3 PV of polymer injection. The pressure drops reached steady state between 5-6 PV of polymer injection whereas the effluent viscosity measurements showed steady state after 2.5 PV of polymer injection. Note, the permeability during the polymer flood was estimated using the injected shear viscosity of 3.3 cP @ 10 s^{-1} at the reservoir temperature (60 ^{o}C). At the end of polymer injection, an exhaustive waterflood of 10 PV was performed to estimate the residual resistance factor (RRF) for this coreflood. The

summary of the coreflood results is provided in **Table 7.21** with measurements of permeability reduction (Rk), resistance factor (RF) and RRF for this experiment. The high RF and RRF values obtained at lower permeability sections are consistent with the results from the previous corefloods and agrees with the trend of thermo-thickening effect observed in bulk rheology measurements at higher salinities. This coreflood also emphasized the potential of associative polymers to generate high RF values in high permeability carbonates even at low concentrations, especially at high salinities. The polymer adsorption during this experiment was estimated to be 173.53 µg/gm of rock, which suggests higher polymer loss at higher salinities. **Figure 7.17** shows the pressure drops recorded during the coreflood experiment and **Figure 7.18** shows the normalized effluent viscosity plot, which also suggests thermothickening effect on effluent samples.

Table 7.20: Core properties for coreflood C7

Core Properties		**Edwards Yellow Limestone Brine Permeability**	
Diameter (cm)	3.76	**Whole Core (mD)**	18
Length (cm)	30.1	**Section 1 (mD)**	13
Mass (g)	663.0	**Section 2 (mD)**	21
Bulk Volume (mL)	334.2	**Section 3 (mD)**	22
Porosity	0.28	**Section 4 (mD)**	20
Area (cm^2)	11.1		
Pore Volume (mL)	93.1		

Table 7.21: Summary of experimental results for coreflood C7

	Rk	RF	RRF
Whole Core (mD)	5.6	33.2	3.34
Section 1 (mD)	4.9	30.06	2.79
Section 2 (mD)	6.0	33.37	2.66
Section 3 (mD)	5.8	32.69	3.08
Section 4 (mD)	6.5	36.54	4.98

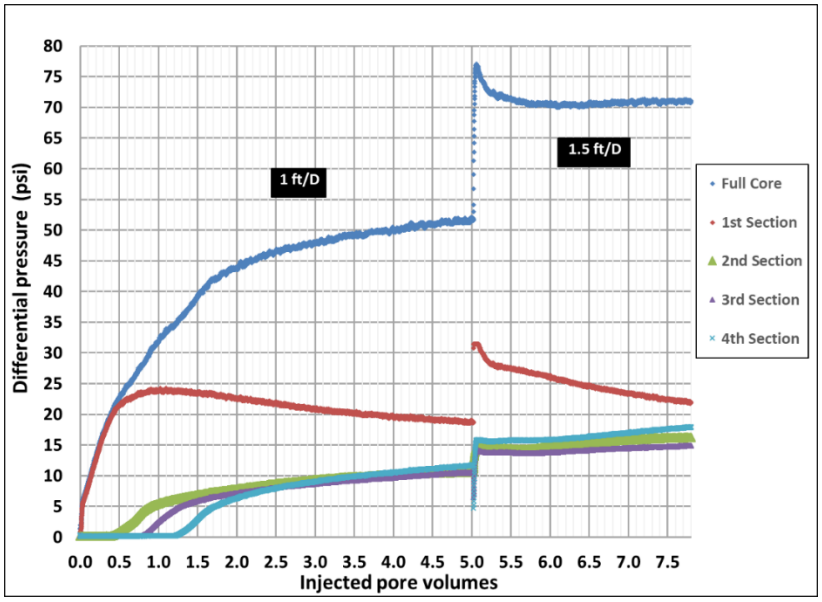

Figure 7.17. Pressure drop with polymer A (shear degraded stock of 90 secs) containing 2500 ppm in synthetic formation brine during coreflood C7 at 60 ºC

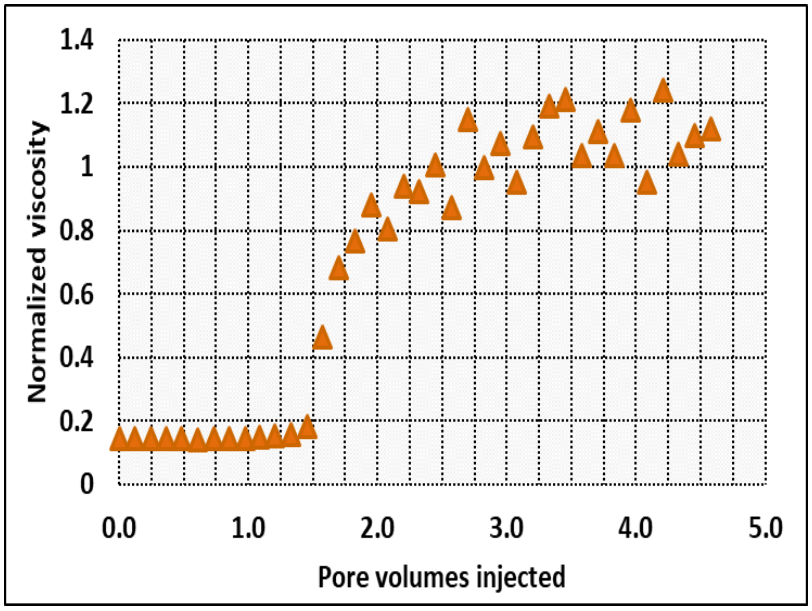

Figure 7.18. Normalized effluent viscosity measurements during coreflood C7 at 60 ^{o}C

The final coreflood C8 was performed to study the transport property of conventional HPAM polymer FP 3330s in higher salinity formation brine to compare its performance to polymer D (as described in coreflood C7) in a low permeability carbonate core. Coreflood C8 was performed in an outcrop Edwards Yellow limestone core which was vacuum saturated with 2% KCl at first. A similar tracer test was performed to estimate the heterogeneity of the porous medium and pore volume. The properties of the core are listed in **Table 7.22**. After completion of the tracer test, a polymer solution of FP 3330s with 2500 ppm prepared in synthetic formation brine (shear degraded stock for 360 secs in DI) was deoxygenated and injected into the porous medium. The polymer solution was injected for about 4 PV at 2 ft/D superficial velocity. A second batch of polymer solution of FP 3330s with 5000 ppm prepared in synthetic formation brine (shear degraded stock for 360 secs in DI) was deoxygenated and injected into the core for about 4 PV at 1 ft/D

superficial velocity. At the end of the second polymer injection, an exhaustive waterflood of 15 PVs was performed to estimate the true residual resistance factor (RRF) for this coreflood. The summary of the coreflood results is provided in **Table 7.23** with measurements of permeability reduction (Rk), resistance factor (RF) and RRF for this experiment. The high RF and RRF values obtained in low permeability carbonates with the use of FP 3330s can be explained due to non-ideal behavior in section 1, which suggests slow plugging behavior during the experiment. The polymer adsorption during this experiment was estimated to be 113.83 µg/gm of rock. **Figure 7.19** shows the pressure drops recorded during the second polymer injection experiment, which suggests slow build-up of pressure over time. The effluent viscosities reached steady state around 2-2.5 PV for first polymer injection step and in less than 1 PV for the second polymer injection, as shown in **Figure 7.20**.

Table 7.22: Core properties for coreflood C8

Core Properties		**Edwards Yellow Limestone Brine Permeability**	
Diameter (cm)	3.77	**Whole Core (mD)**	16
Length (cm)	30.8	**Section 1 (mD)**	10
Mass (g)	694.0	**Section 2 (mD)**	15
Bulk Volume (mL)	343.81	**Section 3 (mD)**	22
Porosity	0.261	**Section 4 (mD)**	17
Area (cm^2)	11.2		
Pore Volume (mL)	89.8		

Table 7.23: Summary of experimental results for coreflood C8

	Rk	RF	RRF
Whole Core (mD)	3.22	29.64	10.9
Section 1 (mD)	3.58	32.92	8.6
Section 2 (mD)	3.51	32.26	11.3
Section 3 (mD)	3.08	28.3	15.6
Section 4 (mD)	2.21	20.92	9.1

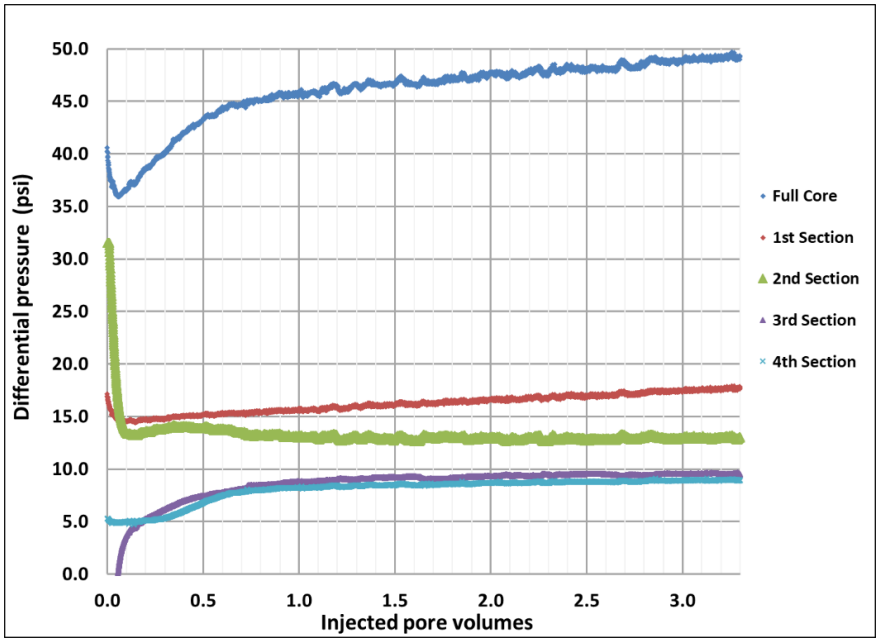

Figure 7.19. Pressure drop with polymer FP 3330s (shear degraded stock of 360 secs) containing 5000 ppm in synthetic formation brine during coreflood C8 at 60 ^{o}C

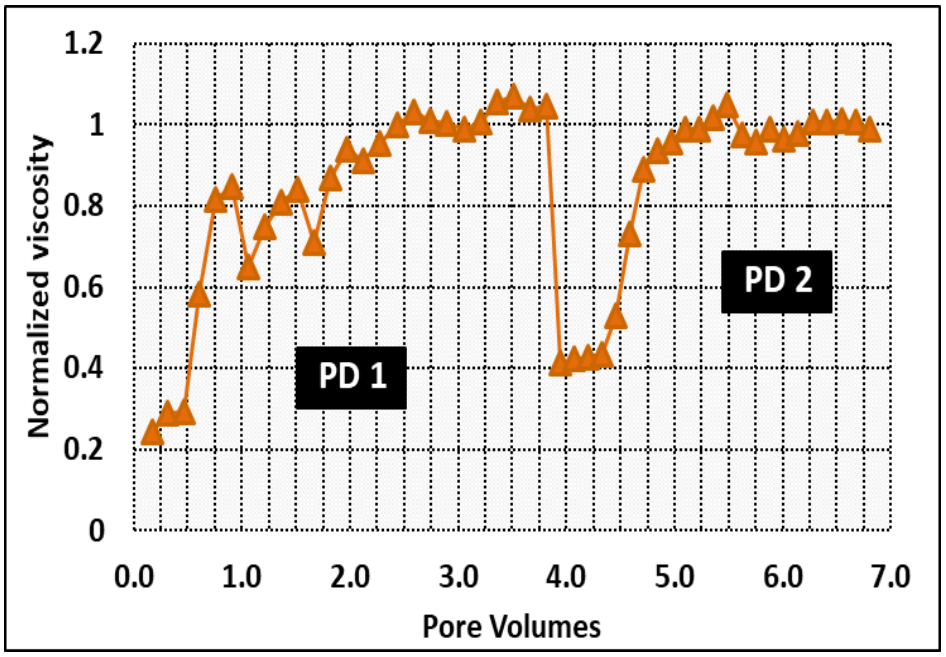

Figure 7.20. Effluent viscosity measurements for coreflood C8 with FP 3330s in synthetic formation brine at 60 ^{o}C

7.3 DISCUSSIONS

The above coreflood experiments with associative polymers showed a good potential for application in high salinity high temperature carbonate reservoirs. These polymers have shown significant increase in viscosity due to enhanced hydrophobic polymer network formation and high RFs generated during the experiments. In order to investigate the effect of polymer network on RF generated in porous media and to compare their performance with conventional HPAM 3330s, a normalized resistance factor (RF*) was established (calculated as the ratio of RF to the normalized viscosity measured from the viscometer); where normalized viscosity is defined as the ratio of the injected polymer shear viscosity to the brine viscosity at the reservoir temperature (60 ^{o}C). The results of each of the corefloods (performed at 60 ^{o}C) are summarized in **Table 7.24** below.

Associative polymers show evidence of enhanced hydrophobic association during flow through constricted pore throats in porous media which is absent in conventional HPAM 3330s. Hence, polymer rheology with HPAM 3330s is primarily viscous dominated whereas for associative polymers reversible polymer network plays an important role and can provide better conformance control at low shear shear rates. Experiment with higher salinity brine showed promising results with enhanced polymer network formation in presence of increased divalent ions, as suggested by higher RF*. This result shows higher RF* at lower polymer concentrations for higher salinity brine, compared to the results of coreflood 5. On comparing the results of corefloods C7 and C8, a clear benefit of the use of associative polymer D is established compared to conventional FP 3330s in high salinity brines at higher temperatures, where higher RF* could be developed at lower polymer concentrations.

Table 7.24: Summary of coreflood experiments (60 ^{o}C)

Coreflood #	Polymer Type	Blender Shearing Time (secs)	Rk (whole)	RF (whole)	RF* (whole)
1	HPAM 3330s	300	0.92	18.55	1.1
2	Polymer D	0	1.9	8.0	1.9
3	Polymer D	0	12.1	44.18	12.1
4	Polymer D	90	4.0	8.0	4.0
5	Polymer D	90	5.9	77.2	5.85
6	Polymer C	0	0.96	29.3	4.07
7	Polymer D	90	5.6	33.2	5.5
8	HPAM 3330s	360	3.2	29.64	3.22

7.4 CONCLUSIONS

This work illustrated the potential of associative polymers compared to conventional HPAM 3330s for application as EOR mobility control in porous media at high temperatures and high salinity reservoirs. The following conclusions can be drawn:

- Associative polymers showed thermothickening behavior at higher temperatures and stronger hydrophobic interactions in higher saline brines to generate higher bulk viscosities.
- The critical polymer concentration for enhanced network formation was found to be dependent on polymer MW, polymer concentration, associative content, salinity of the brine and temperature.
- Presence of surfactants led to a reduction of hydrophobic network but still showed evidence of thermothickening behavior in moderate to higher salinities.
- Mechanical shear degradation was successfully applied to modify the molecular weight distribution and inject in low permeability carbonate reservoirs by comparing the pore throat distribution from MICP and particle size analysis from DLS method.
- Shear degraded polymers showed significant improvement in polymer transport in low permeability cores with reduction in RRF.
- Each coreflood experiment showed evidence of 2 polymer fronts – viscosity transport and permeability reduction - due to reversible retention in presence of polymer network.

- RF* values showed a positive correlation with polymer concentration, polymer molecular weight and associative content.
- Higher RF* values were obtained at lower polymer concentrations in presence of higher salinity brine due to enhanced polymer network for associative polymers compared to conventional HPAM 3330s.
- Polymer adsorption for HPAM 3330s and associative polymers (after shear degraded stock) in low permeability carbonates were comparable and suggests higher loss of polymers in tight formations. Hence, associative polymers at lower concentrations can prove to be more beneficial to make polymer flooding more economical.

Chapter 8: Chemical Flooding in Low Permeability Carbonate Rocks

Waterflood in low permeability carbonat[3]e reservoirs (<50 mD) leaves behind a substantial amount of oil due to capillary trapping. Surfactant floods can improve oil recovery from these reservoirs by lowering the interfacial tension (IFT); however, there are several challenges such as polymer injectivity, presence of divalent ions, geochemical interactions with chemicals and rock surface, pore-scale heterogeneity, and oil-/mixed-wettability. Chapters 6 introduced the novel concept of mechanical shear degradation of high molecular weight polymer molecules in combination with aggressive filtration process to tailor design the polymer molecules for injection in low permeability reservoirs. This polymer pre-treatment process showed promising potential in successfully extending the polymer injectivity to lower permeability range in carbonate reservoirs. Chemical floods can be applied in a variety of reservoir conditions. Alkali-surfactant-polymer/surfactant-polymer (ASP/SP) floods can improve the oil recovery from carbonate reservoirs through generation of low IFT formulations. Alkali interact with organic acids in the oil to form soap in situ and reduce anionic surfactant adsorption. Surfactants along with soaps lower the interfacial tension between oil and water. Polymers provide mobility control and increase sweep efficiency.

The objective of this chapter is to address the following challenges: polymer transport in low permeability carbonate cores, surfactant interaction with formation brine during alkaline-surfactant-polymer (ASP) floods and geochemical interactions of EDTA

[3] This chapter is based on: (Ghosh, Sharma and Mohanty, 2019). Dr. Mohanty supervised the project and Dr. Sharma helped in simulation studies.

containing ASP formulations. The polymer injectivity issue was addressed through a systematic investigation of polymer pre-treatment process as described earlier in Chapter 6. Shearing of high molecular weight polymers and successive filtration treatment were performed to improve polymer size distribution. Single phase polymer transport experiments were performed in low permeability carbonate rocks, and a robust polymer treatment protocol was developed. Additional experiments were performed to perform a comparative study of the polymer hydrodynamic radius through Dynamic Light Scattering (DLS) method to the pore throat diameter distribution in the porous medium through Mercury Intrusion Capillary Pressure (MICP) method. Surfactant phase behavior and aqueous stability experiments were performed to develop ultralow IFT ASP and SP formulations with a reservoir crude oil. ASP and SP core floods were performed in oil-wet low permeability limestone rocks. The oil recovery, pressure drop, effluent ionic composition, effluent viscosity and effluent surfactant concentrations were measured. PHREEQC simulations were performed to understand geochemical reactions during ASP floods. In addition, SP core floods were performed at the reservoir temperature, 40 ^{o}C, for performance comparison to ASP core floods.

8.1 MATERIALS

Commonly available and inexpensive chemicals were used in the surfactant formulation. Alcohol propoxy sulfate surfactants (PS) were obtained from Sasol and Internal Olefin Sulfonate surfactants (IOS) were obtained from Shell Chemicals. Ethoxy Isobutanol (IBA-EO), Tristyrylphenol propoxy ethoxy carboxylate (TSPC) and Ethylhexanol Propoxy sulfate (EPS) were synthesized in our laboratory. Polymer FP

3130S, 3230S, and 3330S were obtained from SNF Floerger (Cedex, France). The molecular weights of these samples varied from 3-10 million Daltons. Common salts such as sodium chloride (NaCl), sodium sulfate (Na_2SO_4), calcium chloride (as $CaCl_2.2H_2O$) and magnesium chloride (as $MgCl_2.6H_2O$) were obtained from Fischer Scientific. Alkalis such as sodium carbonate (Na_2CO_3) and sodium hydroxide (NaOH) were also obtained from Fischer Scientific. The oil was a degassed stock tank oil from a reservoir. This oil was mixed with cyclohexane (15 vol%) to get a "surrogate oil" of 8 cP at the reservoir temperature. The viscosity was measured using an AR G2 rheometer. Reservoir and outcrop limestone cores (Texas Cream limestone and Edwards Yellow limestone) were used as porous media.

Table 8.1 lists the properties of the limestone cores (C1 – C6) used in this study. Outcrop Texas Cream limestone and Edwards limestone rocks, and reservoir limestone rock were used for the experiments. Each outcrop core was about 1 ft long and 1.5 inch in diameter, whereas the reservoir core (comprised of core plugs) was only 8.25 inches long and 1.5 inch in diameter. The absolute brine permeabilities varied from 12.6 to 22 mD. The outcrop limestone cores were oil saturated through displacement method after vacuum saturation with injection brine. The reservoir limestone core was oil saturated after injection of pre-set volume of injection brine under vacuum to obtain high initial oil saturation with the surrogate crude oil. All the saturated carbonate rocks were aged at high temperature (~80 °C) in the crude oil for about 3-4 weeks to make them oil-wet.

Table 8.1: Core properties used in polymer transport and ASP/SP core floods

Core	Texas Cream limestone (C1)	Edwards Yellow limestone (C2)	Limestone Reservoir core (C3)	Edwards Yellow limestone (C4)	Edwards Yellow limestone (C5)	Edwards Yellow limestone (C6)
Diameter(cm) x Length (cm)	3.76 x 28.7	3.76 x 30.4	3.76 x 21	3.76 x 29.6	3.78 x 30	3.77 x 30.3
Porosity (%)	27.6	26.8	17.6	25.7	26.8	24.9
Pore Volume (mL)	88.0	90.5	41.0	84.4	90.2	84.2
Brine Permeability (mD)	15	12.6	22	20.7	17.3	15.6
Initial Oil Saturation (Soi)	-	-	0.90	0.81	-	0.76

Formation brine obtained from the reservoir water analysis was used in all the experiments in this study. The composition of the brine is listed in **Table 8.2**. The pH of the various surfactant formulations was measured using pHTestr 20 (Oakton Instruments) which has the precision of $\pm$ 0.01. The pH electrode was calibrated with standard pH buffer solutions of pH 4, 7, and 10.

Table 8.2: Composition of the formation brine

Ions	Concentration (ppm)
Na^+	10,550
Ca^{2+}	354.4
Mg^{2+}	591.6
SO_4^{2-}	3645

Cl^-	16,000
Total Salinity (TDS)	31,121

Systematic experiments were performed to investigate different aspects of the challenges faced in developing a low IFT surfactant formulation for successful chemical flooding application in low permeability carbonate reservoirs. **Table 8.3** lists the sequential experiments performed in this study to address each of the challenges described earlier.

Table 8.3: List of experiments and simulations

Surfactant Phase Behaviors	
A1	Ultralow IFT ASP surfactant formulation containing PS and IOS surfactants
A2	Ultralow IFT ASP surfactant formulations containing TSPC, IOS and EPS surfactants
A3	Ultralow IFT SP surfactant formulations containing TSPC, IOS and EPS surfactants
Polymer Treatment and Transport	
C1	Polymer injection in a low permeability Texas Cream limestone
C2	Polymer injection in a low permeability Edwards Yellow limestone core
ASP Core floods	
C3	Oil recovery ASP core flood in a low permeability core using surfactant formulation A1
C4	Oil recovery ASP core flood in a low permeability Edwards Yellow limestone core using formulation A2
C5	Single phase ASP core flood in a low permeability Edwards Yellow limestone core using surfactant formulation A2
C6	Oil recovery SP core flood in a low permeability Edwards Yellow limestone core using formulation A3
PHREEQC Calculations	
D1	Interaction of EDTA with limestone rocks

8.2 RESULTS AND DISCUSSIONS

8.2.1 Phase Behavior Experiments

Phase behavior experiments were performed to identify surfactant formulations which gave ultralow IFT with the "**surrogate oil**" and were aqueous stable at the optimum salinity at the reservoir temperature (40 ^{o}C). Aqueous solutions were prepared with 1 wt% total surfactant (or mixture of surfactants) mixed with injection brine and chelating agent EDTA along with co-solvent and alkali. Among several formulations examined during this study, four surfactant formulations, shown in **Table 8.4**, were found to give ultralow IFT with the oil as well as aqueous stability at the reservoir condition. 1.5 wt% of EDTA was added to chelate divalent ions in the formation brine for the first three formulations. The first surfactant formulation (A1a) contained PS and IOS surfactants along with IBA-EO co-solvent in the proportions shown in **Table 8.4**. The formulation was found to give ultralow IFT at about 35,000 ppm and aqueous stability up to 37,500 ppm. **Figure 8.1** shows the oil and water solubilization curves for this formulation. The solubilization ratio at the optimum salinity was found to be 17. Using Huh's equation, this ratio corresponds to an IFT of about 10^{-3} dynes/cm. Surfactant formulation was further optimized by lowering the concentration of IOS to 0.2 wt% (formulation A1b). **Figure 8.2** shows the phase behavior tubes obtained using surfactant formulation 1b.

Additional ultralow IFT surfactant formulations were developed using TSPC, IOS, and EPS surfactants as shown in **Table 8.4**. The formulations were found to give ultralow IFT and aqueous stability up to the optimum salinity, both with and without adding EDTA to the formulation. Formulation A2 was performed with varying Na_2CO_3 concentration

whereas formulation A3 was performed with varying NaCl concentration. **Figures 8.3** and **8.4** show the phase behavior tubes and solubilization curves for formulation 2 and **Figure 8.5 and 8.6** show the phase behavior tubes and the solubilization curves for formulation 3.

Table 8.4: Ultralow IFT surfactant formulations identified from surfactant screening studies

Set #	**Surfactant formulation**	**Ultra-low Region (TDS)**	**WOR**	**Aqueous stability (TDS)**
A1a	0.5% PS + 0.5% IOS + 0.5% IBA-EO	35,000 ppm	3	37,500 ppm
A1b	0.5% PS + 0.2% IOS + 0.5% IBA-EO	46,000 - 53,500 ppm	3	52,000 ppm
A2	0.35% TSPC + 0.35% IOS + 0.3% EPS	68,500 - 78,500 ppm	3	75,000 ppm
A3	0.35% TSPC + 0.35% IOS + 0.3% EPS	63,500 - 68,500 ppm	3	70,000 ppm

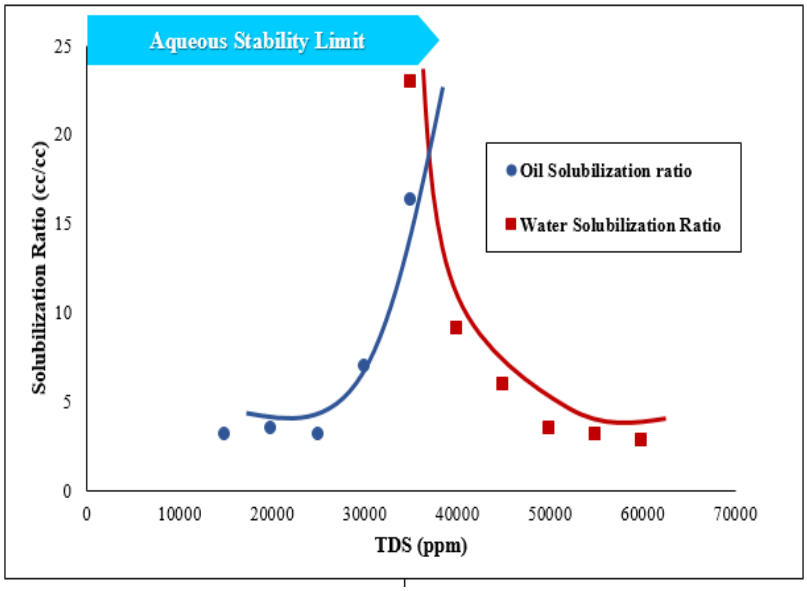

Figure 8.1. Oil and water solubilization plots obtained using surfactant formulation A1a

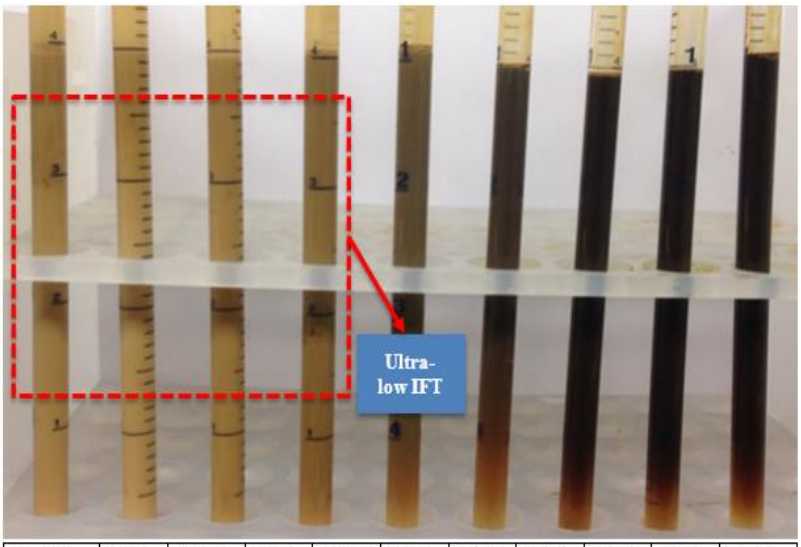

Na_2CO_3 (wt%)	1.5%	1.75%	2.0%	2.25%	2.5%	2.75%	3.0%	3.25%	3.5%	3.75%

Figure 8.2. Phase behavior tubes obtained using surfactant formulation #A1b. Ultralow IFT region can be observed between 1.5-2.25 wt% Na2CO3.

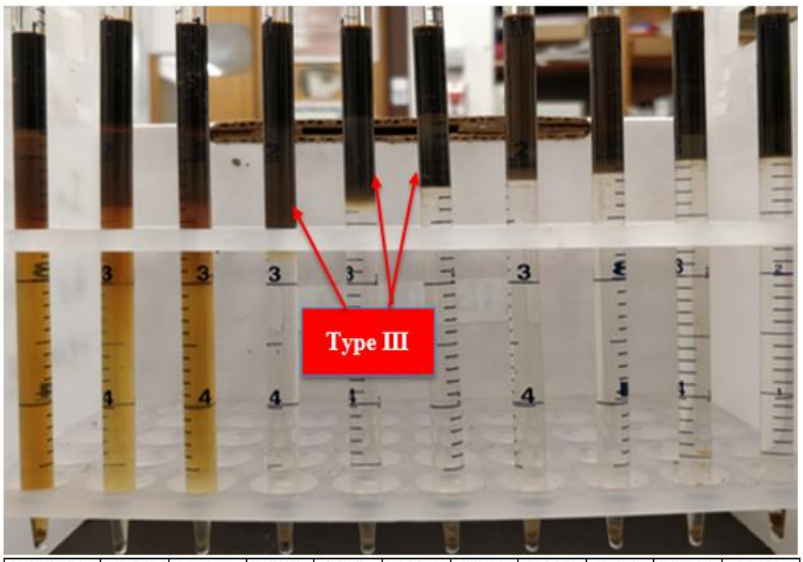

Na_2CO_3 (wt%)	2.75%	3.0%	3.25%	3.5%	3.75%	4.0%	4.25%	4.5%	4.75%	5.0%

Figure 8.3. Phase behavior tubes obtained using surfactant formulation#A2. Type III region can be observed between 3.5-4.0 wt% Na2CO3.

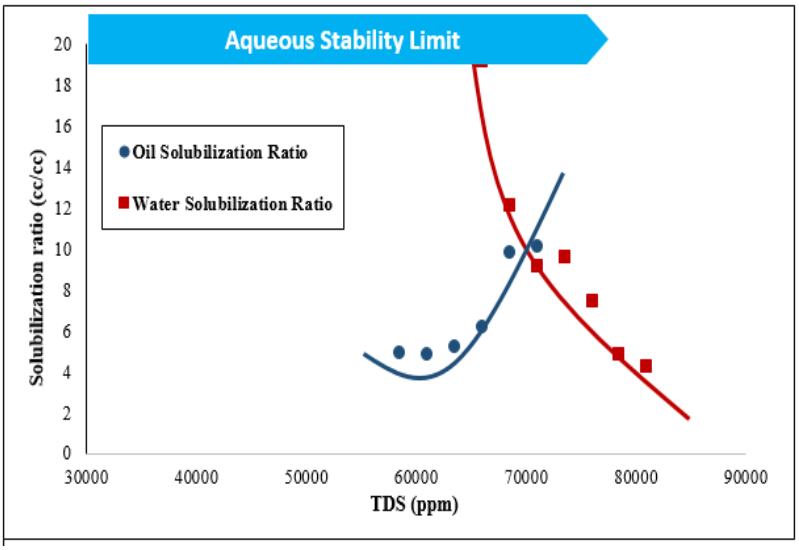

Figure 8.4. Oil and water solubilization plots obtained using surfactant formulation A2

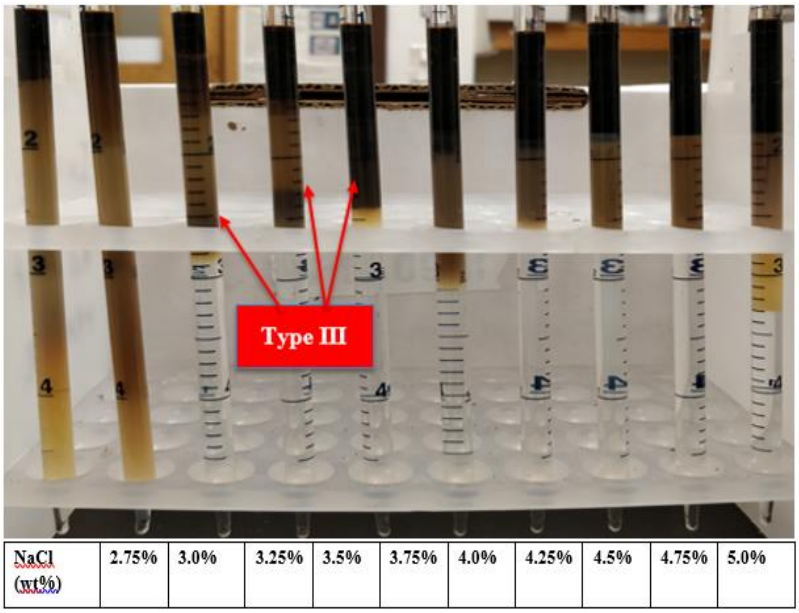

Figure 8.5. Phase behavior tubes obtained using surfactant formulation#A3. Type III region can be observed between 3.25-3.75 wt% NaCl

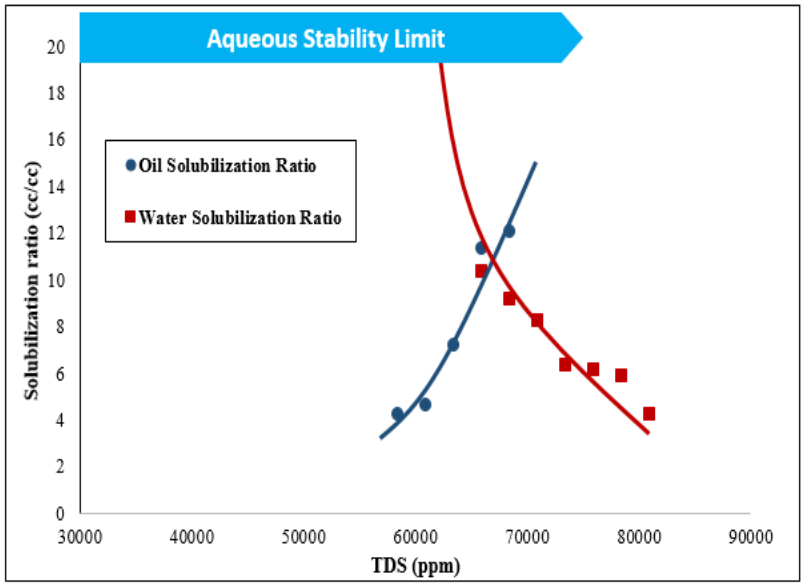

Figure 8.6. Oil and water solubilization plots obtained using surfactant formulation A3

8.2.2 Polymer Treatment and Transport

8.2.2.1 Polymer pre-treatment for injection

Due to potential transport issues of high MW polymers in low permeability rocks, a polymer pre-treatment was developed to improve their transport. 1 wt% polymer stock solutions were prepared in deionized water using an overhead mixer at 500 rpm for about 4 hours. The polymer stock solution was sheared in a commercial blender at 2000 rpm for different times, and the viscosity loss was monitored, as shown in **Figure 8.7**. The viscosity reduction is larger for the first 100 seconds of blending. A blending time of 300 seconds at 2000 rpm was chosen as the optimum blend time for subsequent experiments. Polymer solutions were prepared, from sheared polymer stock solutions, at desired salinities and filtration was performed successively through 0.4-micron, 0.2-micron, 0.1-micron, 0.2-micron, and 0.4-micron filters. **Figure 8.8** shows the effect of shearing on the

hydrodynamic diameter distribution of the polymer from dynamic light scattering. A reduction in polymer hydrodynamic diameter, and a shift towards low molecular weight is observed after the treatment. Series filtration, as described above, showed progressive improvement in the filterability of the polymer solutions. Hence, the polymer solutions were considered suitable for injection in low permeability formations (<20 mD) for final filtration ratios (F.R.) at 0.4-micron filter to be less than 1.2.

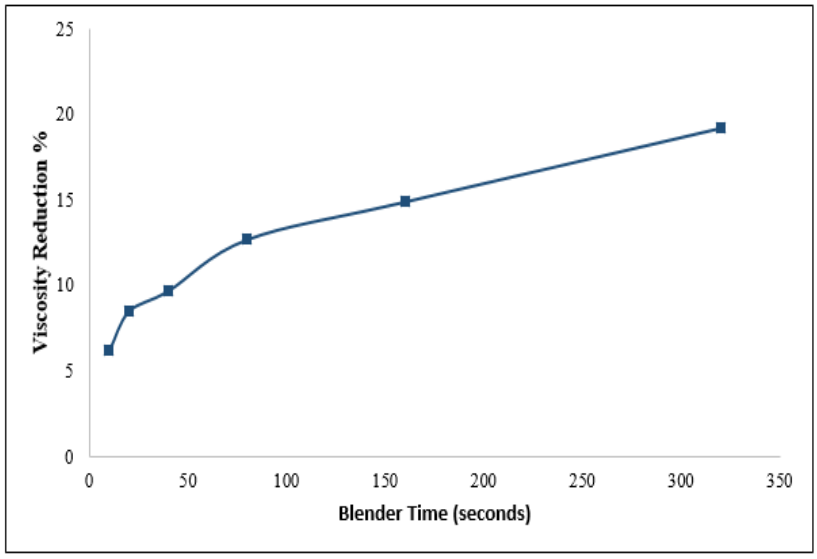

Figure 8.7. Loss in viscosity of 1 wt% Flopaam 3330S polymer, prepared in DI water, as a function of blending time. The viscosity values of blended polymer solutions were compared with the viscosity of original polymer solution at the shear rate of 10 s-1 to calculate the loss

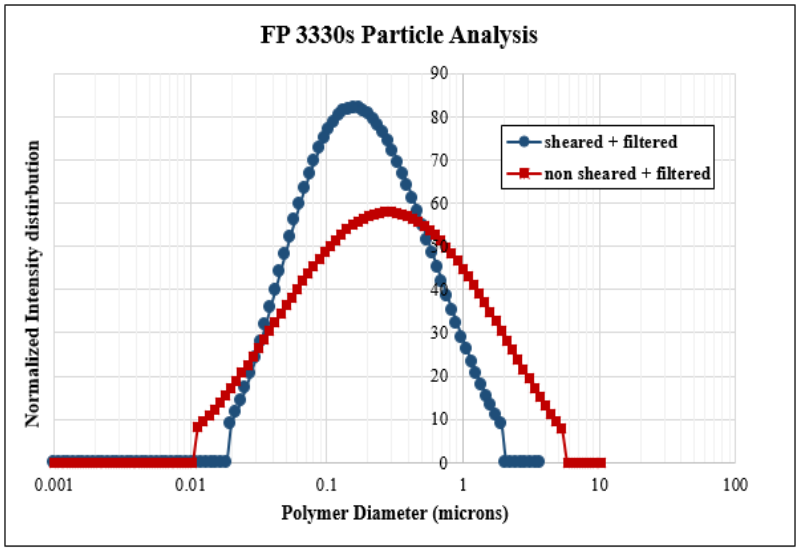

Figure 8.8. Comparison between polymer size distribution for FP3330s with and without shearing of the polymer stock solution

8.2.2.2 Polymer Injection in Texas Cream limestone

A 3500 ppm FP 3330S polymer solution was prepared in formation brine after treating the polymer stock solution using the blending/shearing and filtration treatment described above. A polymer solution was injected into a 15 mD Texas Cream limestone core (experiment C1 in **Table 8.1**) at reservoir temperature and effluent samples were collected. The viscosity of the injected solution at room temperature was 30 cP (at 10 s^{-1}). The viscosity of effluent samples collected from the core is shown in **Figure 8.9**. The effluent viscosity increased to only 1.8 cP even after about 2.5 PV injection; much less than the viscosity of the injected solution. In addition, the pressure drops across the core kept on increasing indicating polymer plugging. This polymer could not be transported through the 15 mD Texas Cream core.

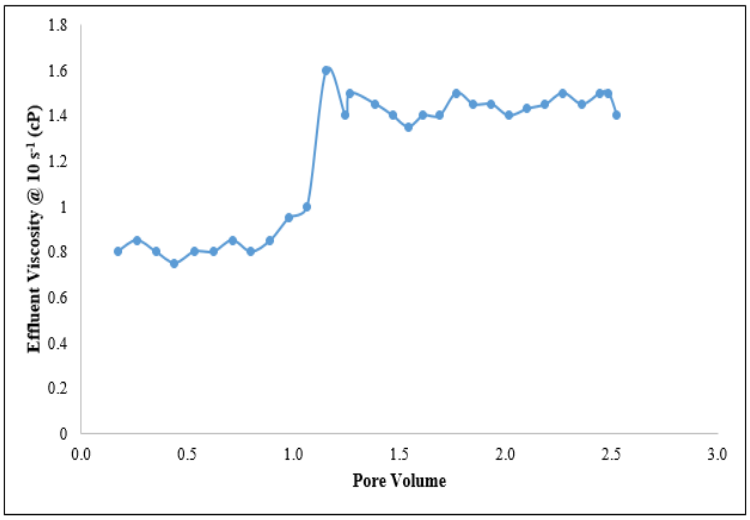

Figure 8.9. Effluent viscosity on injection the treated polymer in a Texas Cream limestone

8.2.2.3 Polymer Injection in Edwards Yellow limestone

To further understand polymer transport in low permeability rocks, another set of experiments were performed by injecting polymer solutions of varying molecular weights in an outcrop Edwards Yellow limestone (described as experiment C2 in **Table 8.1**). The properties of the core are given in **Table 8.1**. Polymer solutions were prepared in formation brine and treated using the procedure described above. **Table 8.5** lists the polymer solutions injected sequentially in this core flood at 40 ^{o}C.

Table 8.5: Injected Polymer Fluid Properties

Solution No	**Polymer Type**	**Polymer concentration (ppm)**	**PV Injected**	**Viscosity (cP at 10 s^{-1})**
1	FP 3130S	5000	1.1	14
2	FP 3230S	4000	2.8	15.8
3	FP 3330S	2500	2.2	19.1

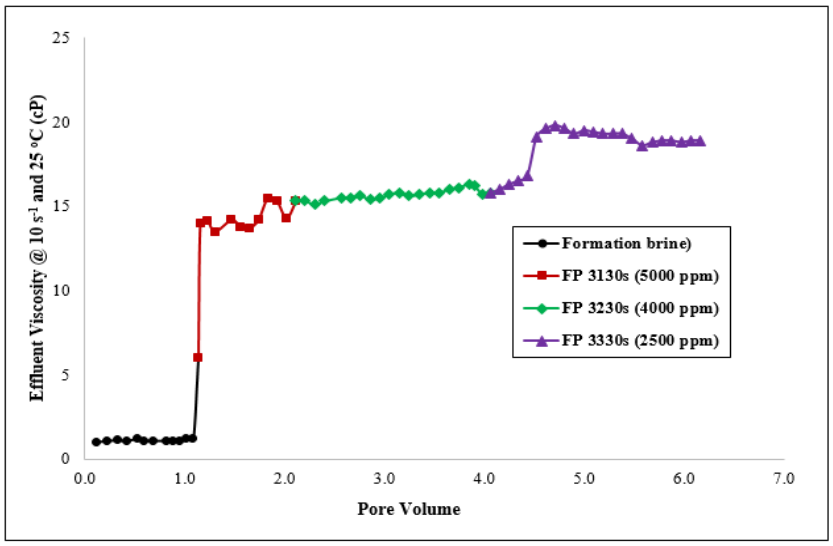

Figure 8.10. Effluent viscosity on injection treated polymer in the Edwards Yellow limestone core

The viscosities of the effluent samples collected during the core flood are shown in **Figure 8.10**. The results show that effluent viscosity reached to about 95% of the injected viscosity within about 1.1 pore volume injection, indicating that these polymers successfully transported in this core. The pressure drop data during the last polymer solution injection (FP 3330S) is shown in **Figure 8.11**. The sectional pressure drops seemed to have stabilized after about 2 PV polymer injection, indicating that plugging was not observed during this core flood.

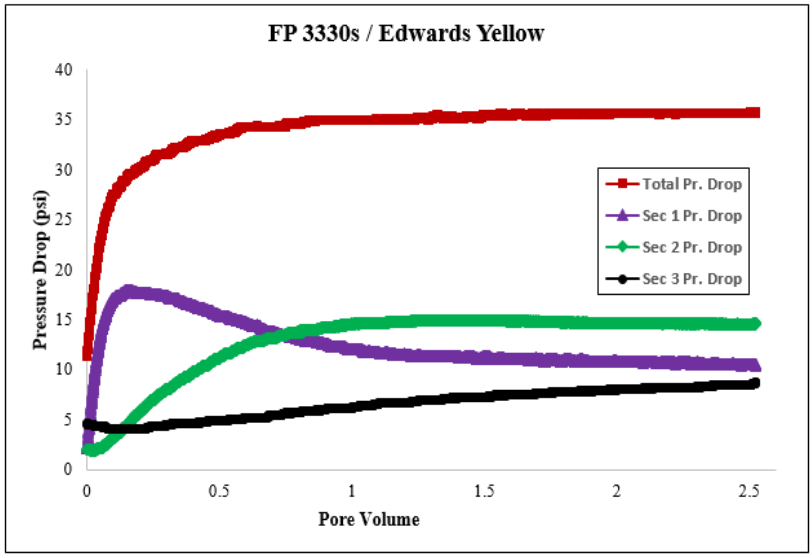

Figure 8.11. Pressure drop profile during FP 3330s injection in Edwards Yellow limestone core

Note that the two cores used for polymer injection were of similar permeabilities. However, successful polymer transport was observed in Edwards Yellow limestone core (experiment C2), but not in the Texas Cream core (experiment C1). **Table 8.6** gives the summary of the filtration ratios (F.R.) for FP 3330S obtained at each filtration step for experiments C1 and C2. A comparison between the polymer hydrodynamic diameter and pore throat diameter of Texas Cream limestone and Edwards Yellow limestone were performed to get further insight into the core flood results. The pore throat diameter distributions of these rocks were obtained through mercury injection capillary pressure (MICP) measurements. The hydrodynamic diameter of a polymer solution was obtained using dynamic light scattering. A comparison of polymer diameter distribution (injected solution) with pore throat diameters of Texas Cream limestone and Edwards Yellow limestone are shown in **Figures 8.12** and **8.13**, respectively. **Figure 8.12** shows a large

peak in pore diameters at 0.5 micron for Texas Cream limestone. A significant part of the polymer has a hydrodynamic diameter larger than these pores. This size overlap could be the reason for face plugging. A similar comparison was performed with an outcrop Edwards Yellow limestone rock of similar permeability. The pore throat size distribution (obtained from MICP) was significantly different from Texas Cream limestone rock. **Figure 8.13** below shows the comparison of the pore throat diameter distribution to polymer hydrodynamic diameter (treated injected solution). The pore throat diameter peaked at 5 microns for Edwards Yellow limestone. A significantly lower overlap was observed in this experiment, which ensured successful polymer transport of similar viscosity solution.

Table 8.6: Polymer Filtration Test Summary

Step #	**Filter size (microns)**	**Experiment C1 (Texas Cream limestone) F.R.**	**Experiment C2 (Edwards Yellow limestone) F.R.**
1	0.4	1.33	1.54
2	0.2	1.91	2.03
3	0.1	2.6	2.4
4	0.2	1.64	1.75
5	0.4	1.08	1.1

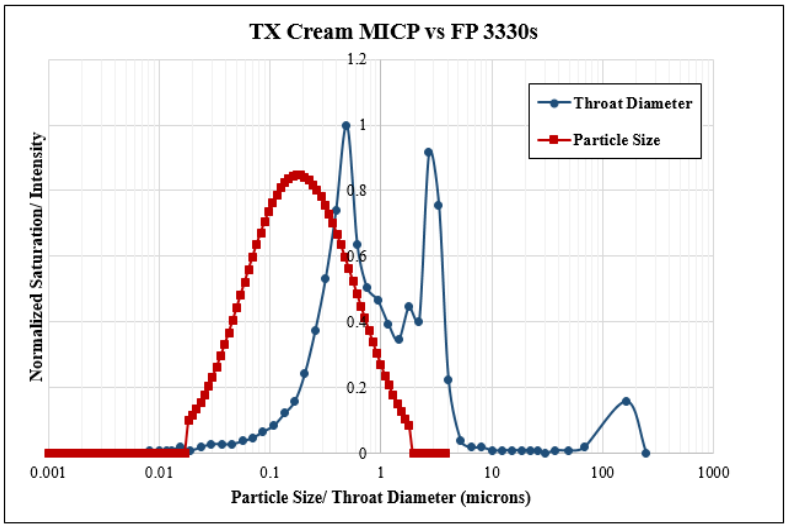

Figure 8.12. Comparison between treated polymer diameter distribution and pore throat diameter distribution of Texas Cream limestone core obtained from MICP

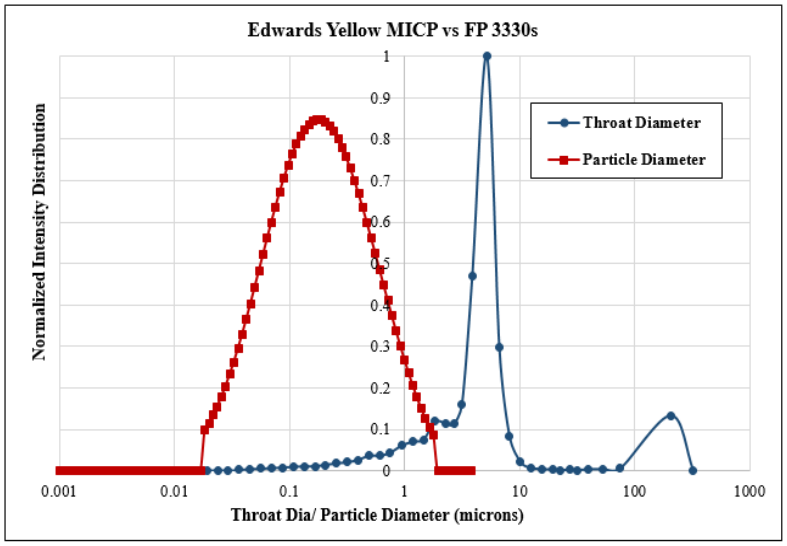

Figure 8.13. Comparison between treated polymer diameter distribution and pore throat diameter distribution of Edwards Yellow limestone core obtained from MICP

The above experiments C1 and C2 emphasize the importance of pore throat size distribution and pore network for successful polymer transport especially for low

permeability rocks of similar permeability. It is important to determine the pore size distribution of reservoir rock and choose polymers for pretreatment accordingly.

8.2.3 ASP/SP Core floods

After aging, fresh surrogate crude oil was injected in cores as aging process could result in changing the composition of the crude oil. ASP core floods were conducted in low permeability limestone cores to test the ultralow IFT surfactant formulations developed previously. Polymer treatment procedure, discussed previously, was used for preparing the ASP slugs and polymer drives in these core floods. In this study, two oil displacement ASP experiments were performed in limestone cores, one single phase ASP experiment was performed in outcrop limestone and one oil displacement SP experiment was performed in outcrop limestone core. The details of the injection scheme followed in core flood C3 is listed in **Table 8.7**.

Table 8.7: Injection sequence followed in ASP core flood C3

Fluid Injection Steps	**Pore Volumes**	**Chemical Composition**
Waterflood (1 ft/D)	1.5	Formation Brine
Waterflood (5 ft/D)	1.2	Formation Brine
High Salinity Pre-Flush (0.45 ft/D)	0.5	Formation Brine + 4% NaCl
ASP Slug (0.3 ft/D) 26.06 cP at 40 ^{o}C (10 s^{-1})	0.5	0.5% PS + 0.2% IOS + 0.5% IBA-EO + Formation Brine +2% Na_2CO_3 + 1.5% EDTA + 2600 ppm FP3330S
Polymer Drive 1 (0.35 ft/D) 17.53 cP at 40 ^{o}C (10 s^{-1})	0.5	Formation Brine +1.5% EDTA + 2800 ppm FP3330S
Polymer Drive 2 (0.3 ft/D) 30 cP at 40 ^{o}C (10 s^{-1})	2.2	Formation Brine + 3000 ppm FP3330S

In this experiment, a limestone reservoir core was aged for 3-4 weeks, after which fresh crude oil was injected through the core before the start of the experiment. The initial oil saturation for this aged reservoir core was about 0.9. Waterflood was performed at 1 ft/D for 1.5 PV after which the injection rate was increased to 5 ft/D for another 1.2 PV to remove the end effects. The total oil recovery after waterflood was 45.5% OOIP. High salinity pre-flush was then performed for about 0.5 PV at 0.45 ft/D to achieve a favorable salinity gradient during the ASP core flood. The total oil recovery due to water injection after this step was 45.7% OOIP and the residual oil saturation was 0.48.

0.5 PV of ASP slug was injected next at 0.3 ft/D followed by 1.5 PV of polymer drive 1 at 0.35 ft/D. Finally, 2.2 PV of polymer drive 2 was injected at 0.3 ft/D. **Figure 8.14** shows oil recovery, oil cut and remaining oil saturation as a function of PV injected. An oil bank was created by the ASP slug that broke through at about 0.4 PV (after chemical injection), the oil cut increased to 0.4 by 1 PV and slowly declined to zero by 2 PV. The additional oil produced due to ASP flood was 31.2% OOIP or 57% ROIP. The total oil recovery at the end of the experiment was 76.8% OOIP and the residual oil saturation was about 0.21. No surfactant was detected in the effluent samples indicating that all the injected surfactant was retained in the core. It is also possible that type I region was not encountered in the core flood since polymer slug 2 was prepared in a hard brine which might have kept the surfactants trapped in the microemulsion phase during the flood. The pressure drops associated with the polymer drive were like that associated with the ASP slug, implying stability of the chemical flood. The stable pressure drop data also confirmed that the polymer was transported through the rock with no face plugging.

The ionic composition of the core flood effluent samples was measured using ion chromatography. **Figure 8.15** shows an increase in calcium ions and a decrease in magnesium ions during the core flood possibly due to preference of EDTA for calcium over magnesium. Also, since polymer drive 2 was prepared in the formation brine (without EDTA), the effluent calcium and magnesium concentrations slowly reached the injected concentrations.

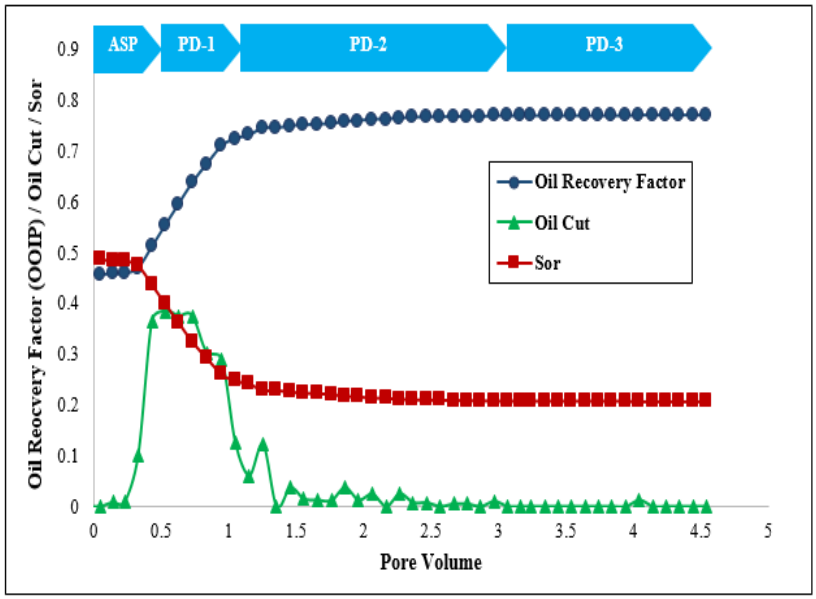

Figure 8.14. Oil recovery, oil cut, and remaining oil saturation for ASP core flood C3

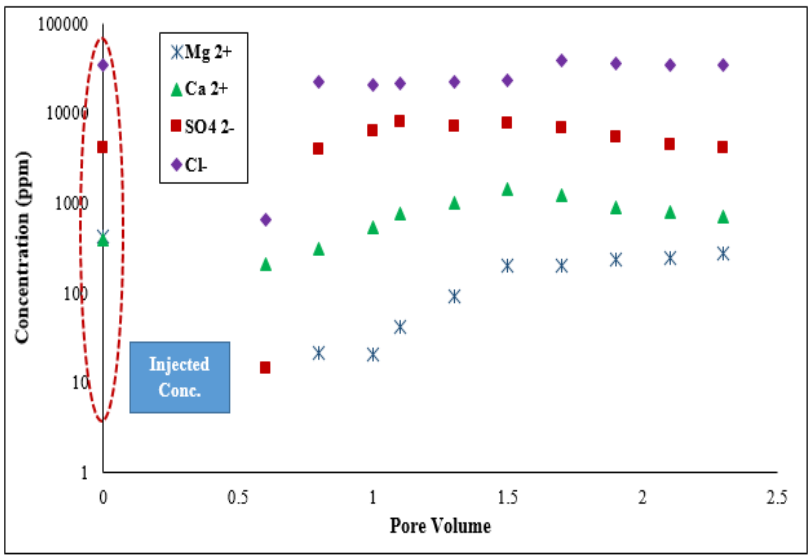

Figure 8.15. Ionic composition of the effluent samples collected from ASP core flood C3

ASP Core flood C4 was conducted using an Edwards Yellow limestone core similar to the one in which successful polymer transport was observed (experiment C2). The surfactant formulation developed in experiment A2 was used in this experiment. The injection sequence followed in this experiment is shown in **Table 8.8**. In this experiment, the core was aged for 1 week after which "surrogate oil" was injected through the core before the start of the experiment. The initial oil saturation for this aged outcrop core was 0.81. Waterflood was performed using formation brine at 1 ft/D for 2.0 PV. The total oil recovery after this stage was 59.6% OOIP. After this stage, waterflood was performed at variable rates of 0.5 ft/D and 0.8 ft/D to measure the end relative permeability of water at residual oil saturation. The final oil recovery at the end of this stage was 60.0% OOIP. The end relative permeability values were used for estimating the polymer requirement in the ASP slug and the subsequent polymer drives. High salinity pre-flush was then performed for about 1.3 PV at 0.7 ft/D to ensure a favorable mixing zone at the chemical slug front.

The total recovery due to water injection after this step was 60.3% OOIP and the residual oil saturation was about 0.32.

An ASP slug of 0.4 PV was injected at 0.3 ft/D followed by polymer drive 1 of about 0.5 PV. Polymer drive 2 was injected next for about 0.5 PV followed by polymer drive 3 injected for another pore volume. **Figure 8.16** shows oil recovery, oil cut and remaining oil saturation as a function of PV injected. An oil bank was created by the ASP slug that broke through at about 0.45 PV; the oil cut increased to 0.45 by 0.5 PV and slowly declined to zero by 1.5 PV injected. The additional oil produced due to ASP flood was about 26.6% OOIP. The total oil recovery at the end of the experiment was 86.9% OOIP and the residual oil saturation was about 0.11. The oil recovery during the chemical flood was 67% ROIP.

Table 8.8: Injection sequence followed during ASP core flood C4

Fluid Injection Steps	**Pore Volume**	**Chemical Composition**
Waterflood (1 ft/D)	2.0	Formation Brine
High Salinity Pre-Flush (0.7 ft/D)	1.3	Formation Brine + 5% NaCl
ASP Slug (0.3 ft/D) 19.48 cP at 40 ^{o}C (10 s^{-1})	0.4	Formation Brine + 0.35% TSPC + 0.35% IOS + 0.3% EPS + 3.25% Na_2CO_3 + 1.5% EDTA + 2500 ppm FP3330S
Polymer Drive 1 (0.3 ft/D) 26.76 cP at 40 ^{o}C (10 s^{-1})	0.5	Formation Brine + 1.5% EDTA + 2600 ppm FP3330S + 2.25% Na_2CO_3
Polymer Drive 2 (0.3 ft/D) 27.1 cP at 40 ^{o}C (10 s^{-1})	0.5	Formation Brine + 2600 ppm FP3330S + 1.5% EDTA + 1% Na_2CO_3
Polymer Drive 3 (0.3 ft/D) 26.96 cp at 40 ^{o}C (10 s^{-1})	1.0	Formation Brine + 2900 ppm FP3330S

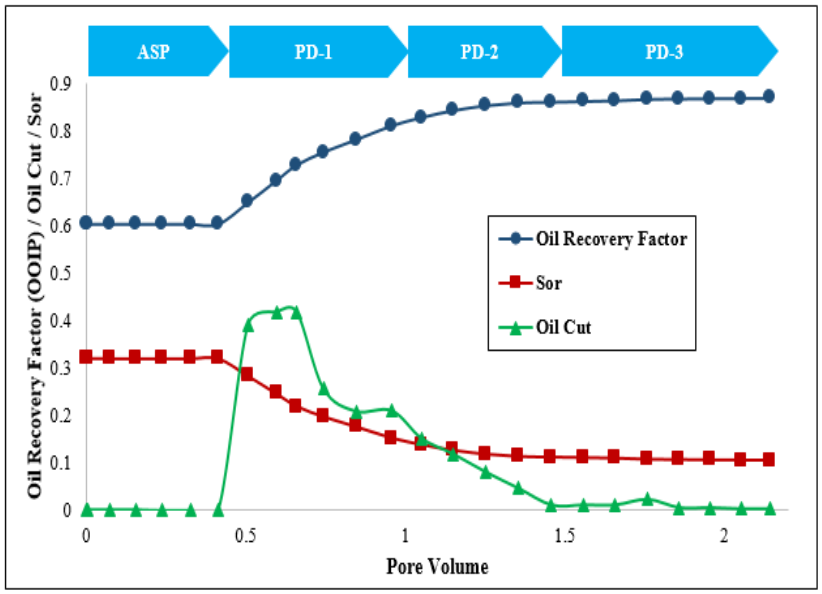

Figure 8.16. Oil recovery, oil cut and remaining oil saturation from ASP core flood C4

Based on the end relative permeability data, the viscosity required for a stable displacement during the chemical flood was about 19.29 cP. The viscosities of the injected ASP slug and the polymer drives were 19.48 cP, 26.76 cP, 27.1 cP and 26.96 cP, respectively. The first 2 polymer drives were chelated with EDTA. The third polymer drive was prepared in formation brine without EDTA. Effluent surfactant concentration was measured using HPLC, and the surfactant retention during the core flood was 0.40 mg/gm-of-rock with 21.5% of the surfactant recovered. The viscosity and pH of the effluent samples were measured using a rheometer and a pH meter, respectively (**Figures 8.17**). A pH value of about 10.2 was observed after 1 PV injection indicating a good pH propagation through the core. About 90% of the injected viscosity was observed at about 1 PV. Gradual pressure buildup was observed at the later stage of the chemical flood indicating some plugging. It appears that there was significant pore connectivity that allowed the polymer

transport to occur with some fraction of pores experiencing face plugging, thus leading to increase in pressure drop.

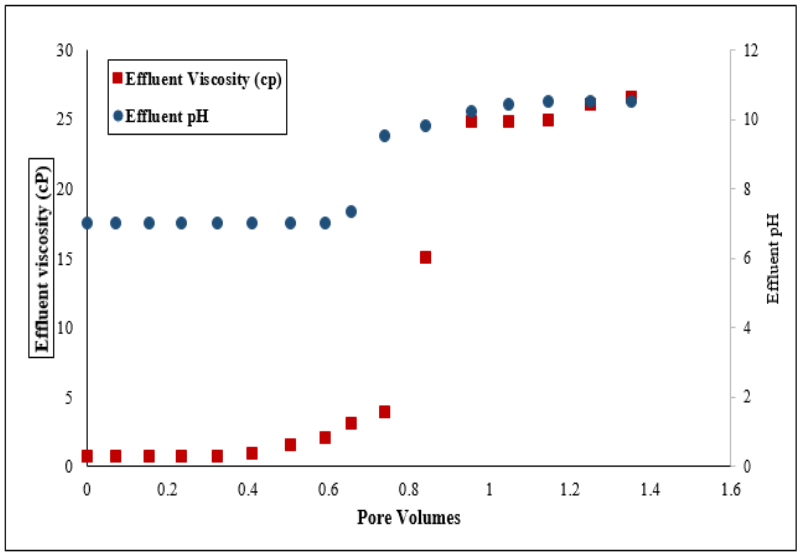

Figure 8.17. Effluent viscosity and pH from ASP core flood C4

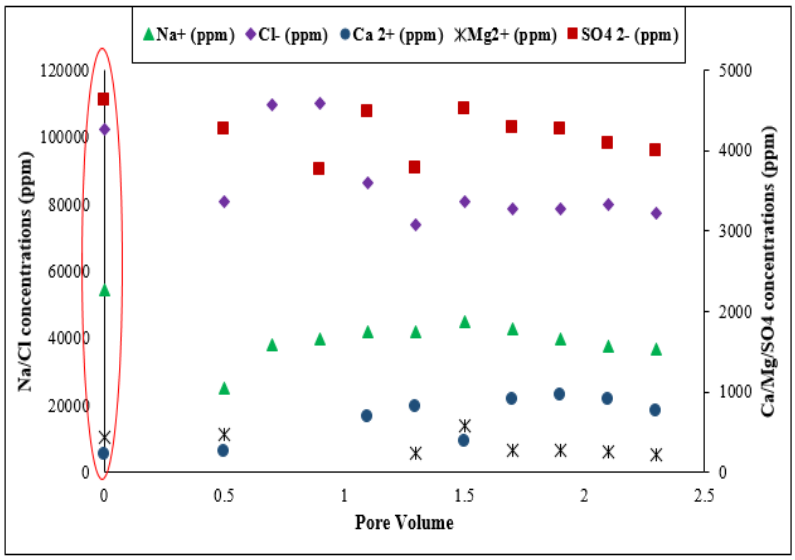

Figure 8.18. Effluent ion analysis using Ion Chromatography for ASP core flood C4

The ionic composition of the core flood effluent samples was measured using ion chromatography. **Figure 8.18** shows that an increase in calcium ions and a decrease in magnesium ions was observed during the core flood possibly due to preference of EDTA for calcium over magnesium (similar to what we observed in ASP core flood C3). Also, since polymer drive 3 was prepared in the formation brine (without ETDA), the effluent calcium and magnesium concentrations started approaching the injected concentrations.

Another ASP core flood C5 was conducted in a similar Edwards Yellow limestone core, but in the absence of any oil. This experiment was conducted to study surfactant adsorption. The injection scheme was kept the same as ASP core flood C4, and similar viscosity solutions were injected for comparative study (**Table 8.9**).

Table 8.9: Injection sequence followed during single phase ASP core flood C5

Fluid Injection Steps	**Pore Volume**	**Chemical Composition**
Waterflood (1 ft/D)	2.0	Formation Brine
High Salinity Pre-Flush (1.5 ft/D)	1.0	Formation Brine + 6% NaCl
ASP Slug (0.5 ft/D) 21 cP at 40 ^{o}C (10 s^{-1})	0.4	Formation Brine + 0.35% TSPC + 0.35% IOS + 0.3% EPS + 4% Na_2CO_3 + 1.5% EDTA + 3000 ppm FP3330S
Polymer Drive 1 (0.5 ft/D) 19.94 cP at 40 ^{o}C (10 s^{-1})	0.65	Formation Brine + 1.5% EDTA + 3400 ppm FP3330S + 2% Na_2CO_3
Polymer Drive 2 (0.5 ft/D) 26 cP at 40 ^{o}C (10 s^{-1})	0.8	Formation Brine + 3500 ppm FP3330S + 1.5% EDTA + 1% Na_2CO_3
Polymer Drive 3 (0.5 ft/D) 22.36 cP at 40 ^{o}C (10 s^{-1})	0.8	Formation Brine + 4000 ppm FP3330S

An ASP slug of 0.4 PV was injected followed with polymer drive 1 of about 0.65 PV. Polymer drive 2 was injected next for about 0.8 PV followed by polymer drive 3 injected for another 0.8 PV. The injection rate was kept constant at 0.5 ft/D for all the steps. **Figure 8.19** shows the effluent viscosity, effluent pH and effluent surfactant concentration as a function of PV injected. The polymer transport was good since more than 90% of the injected viscosity was observed at the effluent after 1 PV of injection. Effluent surfactant concentration was measured using HPLC; surfactant broke through at about 1.1 PV and peaked at 1.3 PV. The surfactant retention during the core flood was 0.4 mg/gm of rock with about 31.9% of the surfactant recovered.

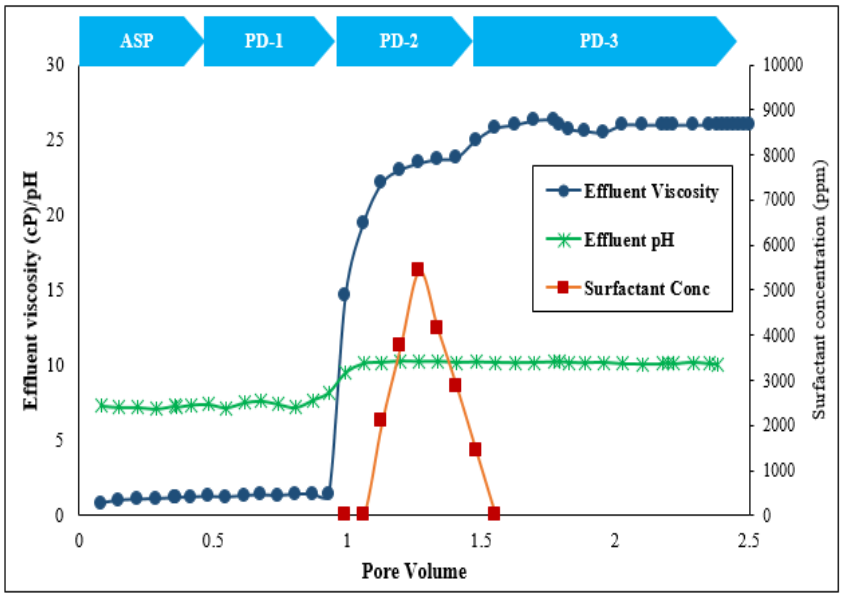

Figure 8.19. Effluent viscosity, pH and surfactant concentration from single phase ASP core flood C5

Additionally, a SP Core flood C6 was performed in Edwards Yellow limestone core similar to the one in core flood C4 as an alternative to the ASP process described earlier.

The surfactant formulation developed in experiment A3 was used in this experiment. The injection sequence followed in this experiment is shown in **Table 8.10**. In this experiment, the core was aged for 1 week after which "surrogate oil" was injected through the core before the start of the experiment. The initial oil saturation for this aged outcrop core was 0.76. Waterflood was performed using formation brine at 1 ft/D for 2.0 PV. The total oil recovery after this stage was 53% OOIP. After this stage, waterflood was performed at variable rates of 0.5 ft/D and 0.8 ft/D to measure the end relative permeability of water at residual oil saturation. The final oil recovery at the end of this stage was 54% OOIP. The end relative permeability values were used for estimating the polymer requirement in the SP slug and the subsequent polymer drives. High salinity pre-flush was then performed for about 0.75 PV at 1 ft/D to ensure a favorable mixing zone at the chemical slug front. The total recovery due to water injection after this step was 54% OOIP and the residual oil saturation was about 0.35.

An SP slug of 0.4 PV was injected at 0.2 ft/D followed by polymer drive 1 of about 0.6 PV. Finally, polymer drive 2 was injected next for about 1.5 PV. **Figure 8.20** shows oil recovery, oil cut and remaining oil saturation as a function of PV injected. A significant oil bank was created by the SP slug that broke through at about 0.45 PV; the oil cut increased to 0.50 by 0.7 PV and slowly declined to zero by 1.4 PV injected. The additional oil produced due to SP flood was about 31% OOIP. The total oil recovery at the end of the experiment was 85% OOIP and the residual oil saturation was about 0.11. The oil recovery during the chemical flood was 67% ROIP. The polymer transport was good since more than 95% of the injected viscosity was observed at the effluent after 1.1 PV of injection.

Effluent surfactant concentration was measured using HPLC; surfactant broke through at about 1.05 PV and peaked at 1.2 PV. The surfactant retention during the core flood was 0.3 mg/gm of rock with about 50.6% of the surfactant recovered.

Table 8.10: Injection sequence followed during single phase SP core flood C6

Fluid Injection Steps	**Pore Volume**	**Chemical Composition**
Waterflood (1 ft/D)	2.0	Formation Brine
High Salinity Pre-Flush (1.0 ft/D)	0.75	Formation Brine + 5% NaCl
SP Slug (0.2 ft/D) 20.7 cP at 40 ºC (10 s^{-1})	0.4	Formation Brine + 0.35% TSPC + 0.35% IOS + 0.3% EPS + 3.5% NaCl + 3500 ppm FP3330S
Polymer Drive 1 (0.2 ft/D) 21.6 cP at 40 ºC (10 s^{-1})	0.6	Formation Brine + 2.5% NaCl + 3800 ppm FP3330S
Polymer Drive 2 (0.2 ft/D) 23.8 cP at 40 ºC (10 s-1)	1.5	Formation Brine + 1.5% NaCl + 3500 ppm FP3330S

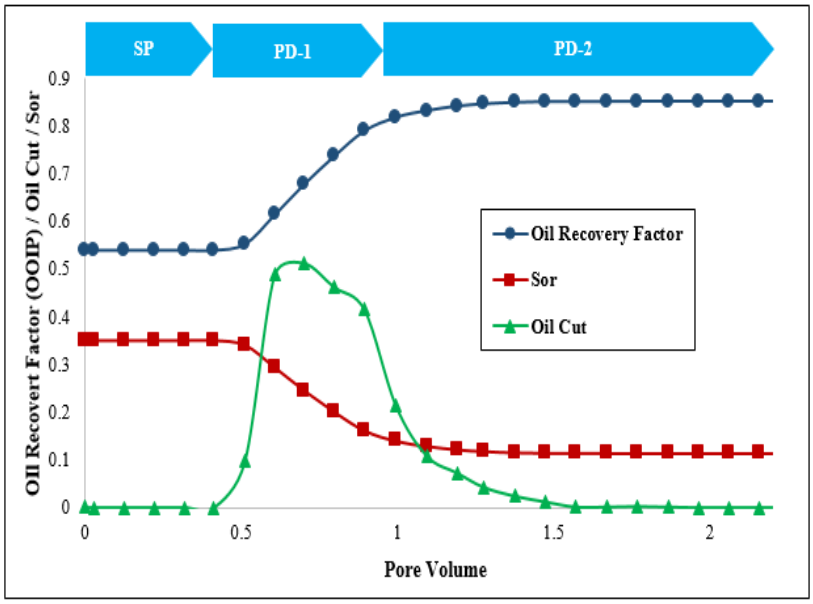

Figure 8.20. Oil recovery, oil cut and remaining oil saturation from ASP core flood C6

Note that the surfactant retention reported for a SP core flood C6 (0.3 mg/grock) was slightly lower than the surfactant retention reported for an ASP core flood C4 (0.4 mg/grock) for the same surfactant combination in a similar limestone core. The possible explanations for this difference can be attributed to 1) the wettability alteration of the limestone core to more water-wet in presence of alkali for ASP leading to increased surfactant adsorption; 2) the HPLC equipment sensitivity difference between two measurements which contributed to higher retention estimation in core flood C4. The assumption is with a reduced sensitivity of the HPLC low concentration of the surfactant was not detected in core flood C4 possibly.

8.2.4 Geochemical Interactions using PHREEQC

In ASP surfactant formulations, EDTA was added to prevent precipitation of divalent cations, from formation brine, in the presence of sodium carbonate. This formulation was used for conducting oil recovery core floods in limestone rocks. These rocks can interact with EDTA, and therefore calculations were performed in PHREEQC to investigate these interactions in detail and understand the effect of these interactions on fluid and rock properties (Parkhurst et al., 2013). Due to complex mineralogy of carbonate formations and high reactivity of these minerals even at low temperatures, an understanding of geochemical interactions of various injected chemicals with the rock is important. These interactions can alter the composition of ASP slug and polymer drives, in addition to affecting rock properties (Sharma, 2016). Due to EDTA, precipitation of divalent cations was not observed in ASP slugs and polymer drives. However, effluent ion analysis from ASP core floods showed very different calcium and magnesium

concentrations; possibly due to the interaction of EDTA with limestone rocks. A higher calcium concentration and a lower magnesium concentration (than their respective injected concentrations) can be seen in the effluent ion analysis of ASP core flood C4 shown in **Figure 8.18**. Important reactions of EDTA and limestone rock are listed in **Table 8.11**. From **Table 8.11**, it was noticed that EDTA has a higher preference to complex calcium ions compared to magnesium ions. In the ASP slug, enough EDTA was added such that both calcium and magnesium ions were complexed. However, when such a solution was injected in a limestone rock, it is possible that EDTA dissolves additional calcium ions from the rock which in-turn resulted in precipitation of complexed Mg ions in the form of dolomite.

Table 8.11: Important reactions when EDTA is injected into limestone rocks

Reaction	**log_k**
$Ca^{+2} + Edta^{-4} = CaEdta^{-2}$	12.4
$Mg^{+2} + Edta^{-4} = MgEdta^{-2}$	10.6
$CaCO_3\ (s) = Ca^{+2} + CO_3^{-2}$	-8.475
$CaMg(CO_3)_2 = Ca^{+2} + Mg^{+2} + 2CO_3^{-2}$	-17

Flow simulations were performed in PHREEQC to further confirm the potential interactions of EDTA with limestone rock discussed above. A comparison of effluent ions obtained from ASP core flood C4 and the PHREEQC simulation is shown in **Figure 8.21**. A good agreement between effluent ions obtained from ASP core flood C4 and the PHREEQC simulation can observed.

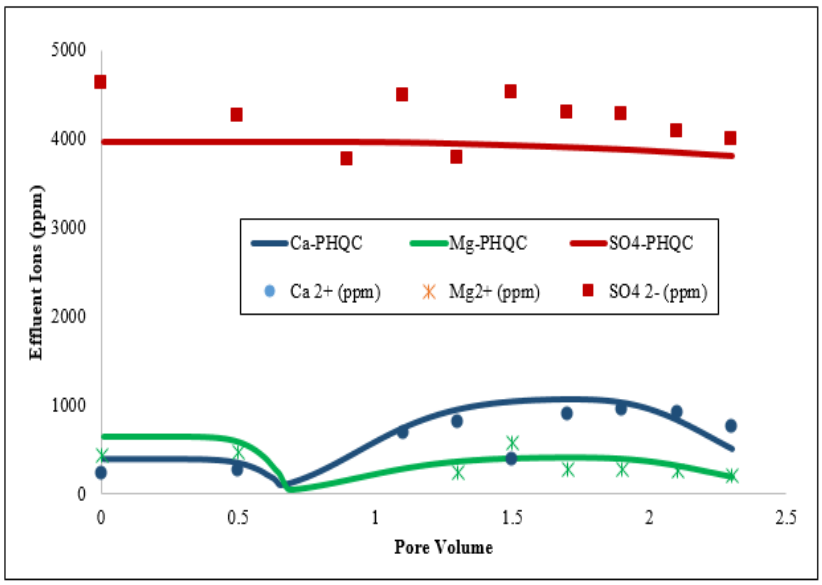

Figure 8.21. Comparison of effluent ions obtained from ASP core flood C4 and PHREEQC simulations

8.3 SUMMARY AND CONCLUSIONS

This study addresses three challenges for alkaline-surfactant-polymer processes for low permeability carbonate reservoirs: polymer injection in low permeability carbonate cores, ASP/SP formulation with the produced water (with divalent ions), and geochemical interactions of such ASP slugs in limestones. Polymer was successfully injected into low permeability carbonate cores (< 15 mD) after the pre-shearing/filtration treatment. The ultra-low IFT ASP/SP formulations developed with same blend of surfactants generated similar phase behavior results and similar incremental oil in oil recovery experiments. Addition of chelating agents like EDTA in ASP formulations in presence of divalent ions can lead to formation damage due to strong reaction of EDTA with limestone rocks, as shown in experimental results and PHREEQC simulations.

The following conclusions can be made.

- Polymer hydrodynamic radius must be much smaller than the pore throat radii for the polymers to be transported. Mercury porosimetry data should be studied before polymer selection.
- Shearing and successive filtration can be used to reduce the hydrodynamic radii of polymers. This preprocessing worked with the HPAM polymer used in this study for the Edwards Yellow limestone, but not for Texas Cream limestone.
- An ultralow IFT ASP formulation can be developed with a formation brine with a significant number of divalent ions by using a chelating agent. Also, ultralow IFT SP formulation was developed in formation brine.
- Tertiary ASP core flood increased the cumulative oil production to 77% OOIP in a field core and 87% OOIP in an outcrop core. SP core flood increased the cumulative oil recovery to 85% OOIP in an outcrop core.
- EDTA present in ASP slugs was found to react with limestone rocks and the geochemical model in PHREEQC successfully simulated the reactions.
- The surfactant retention was limited to 0.3-0.4 mg/gm of rock in the core floods. Low retention reported for SP showed promising potential for EOR applications in carbonate cores.

Chapter 9: Surfactant-Polymer (SP) Processes for High Temperature and High Salinity Carbonate R[4]eservoirs

Waterflood in oil-wet carbonate reservoirs leaves behind a substantial amount of oil due to negative capillary forces and channeling caused due to channeling in these heterogeneous porous media. Surfactant floods can improve oil recovery from these reservoirs by lowering the interfacial tension (IFT) and requires a mobility control mechanism using polymer for better sweep efficiency; however, there are several challenges such as polymer thermal stability, presence of divalent ions, surfactant-brine-polymer compatibility, pore-scale heterogeneity, and oil-/mixed-wettability. Chapters 8 showed successful implementation of the novel concept of mechanical shear degradation of high molecular weight polymer molecules in combination with aggressive filtration process to tailor design the polymer molecules for injection in low permeability reservoirs. This polymer pre-treatment process showed promising potential in successfully extending the alkali-surfactant-polymer (ASP) and surfactant-polymer (SP) processes to lower permeability range in carbonate reservoirs. Chemical floods like SP processes can be applied in a variety of reservoir conditions through implementation of ultra-low IFT, mobility control and wettability alteration.

The goal of this research was to develop a successful surfactant-polymer technology for application in high temperature and high salinity reservoirs, especially where the high salinity produced/formation brine can be reused for injection as part of the

[4] This chapter is based on: (Ghosh and Mohanty, 2019b). Dr. Mohanty supervised the project.

chemical formulation. Hence, specialty chemicals tolerant to high salinity and high temperature were investigated for the scope of this study. The objective of this chapter is to address the following challenges: surfactant interaction with formation brine containing high concentration of divalent cations and thermal stability and transport of polymers in carbonate rocks at high temperatures. Surfactant phase behavior experiments were performed to identify promising surfactant candidates which showed ultralow IFT with crude oil and aqueous stability at high temperature in high salinity and high hardness brines. A systematic study was performed to understand the effect of surfactant hydrophobe length on phase behavior, oil recovery, and surfactant retention in core flood experiments. Novel surfactants with very short hydrophobes and cosolvent-like properties were also included to further optimize the phase behavior. Surfactants of larger hydrophobe length, containing similar number of EO and PO groups, gave higher solubilization ratio (and lower IFT) and lower optimum salinity. Specialty synthetic polymers with good thermal stability and salinity tolerance (TDS > 90,000 ppm) were investigated for their transport in single-phase core floods. Results showed successful transport of polymer, without degradation in-situ, and improvement in mobility control. SP core floods were conducted using selected formulations in Indiana limestone cores. Core flood experiments showed significant increase in oil recovery over waterflood after the injection of the chemical formulation. Successful polymer transport was observed in SP core floods at high temperature.

9.1 MATERIALS

Specialty chemicals developed in-house were used in the surfactant formulations. Alcohol propoxy ethoxy carboxylate (PEC) surfactants with varying hydrocarbon lengths were synthesized in our laboratory. Internal Olefin Sulfonate surfactants (IOS) were obtained from Shell Chemicals. Sulfonated polyacrylamide AN-125 VHM was obtained from SNF Floerger (Cedex, France). The molecular weight of this sample varied from 12-16 million Daltons. Common salts such as sodium chloride (NaCl), sodium sulfate (Na_2SO_4), calcium chloride (as $CaCl_2.2H_2O$) and magnesium chloride (as $MgCl_2.6H_2O$) were obtained from Fischer Scientific. The sea-water with total dissolved solids (TDS) approximately 45,075 ppm comprised of 14,305 ppm Na^+, 564 ppm Ca^{2+}, 1,576 ppm Mg^{2+}, 24,814 ppm Cl^-, and 3,816 ppm SO_4^{2-}. The formation brine comprised of 46,450 ppm Na^+, 4,345 ppm Ca^{2+}, 162 ppm Mg^{2+}, 79,487 ppm Cl^-, and 560 ppm SO_4^{2-} with a TDS of approximately 131,000 ppm. The synthetic injection brine was prepared by mixing 45% sea water and 55% formation brine (by weight) with a TDS of approximately 92,336 ppm. The crude oil used for this study had a viscosity of 8.3 cP at the reservoir temperature, 80 ^oC. Outcrop Indiana limestone cores were used for the oil recovery and polymer injection experiments.

Phase behavior experiments were performed to identify surfactant formulations which give ultralow IFT with the crude oil and are aqueous stable beyond the optimum salinity. The experiments are listed in **Table 9.1**. Aqueous solutions were prepared with 1 wt% total surfactant (or mixtures of surfactants) mixed in various composition brines including the injection brine and the formation brine. The amounts of injection and

formation brines were varied such that a gradual increase in the salinity was obtained. For the initial set of experiments, oil and aqueous solutions were mixed in 1:3 volume ratio. The samples were equilibrated at the reservoir temperature, after continuous mixing for about 1 week, and their phase volumes were observed. The solubilization of oil and water in a microemulsion phase was calculated from the phase volumes. The optimum salinity (where equal oil and water solubilization ratios were observed in the microemulsion phase) and the corresponding IFT were estimated. The effects of cosolvent on phase behavior were examined in terms of interfacial tension, ultra-low IFT region (robustness), optimal salinity, macro-emulsion formation/properties, equilibration time, and aqueous stability. The viscosity of the phases, especially micro-emulsion and macro-emulsion phases were examined qualitatively. Aqueous solutions with and without polymer were similarly prepared and equilibrated at the reservoir temperature to obtain aqueous stability limits of surfactant formulations. Additional experiments were performed by lowering total surfactant concentration (keeping the ratio of each surfactant same) to study the effect of surfactant dilution on the performance of the formulation and robustness in the coreflood experiment. The best performing surfactant formulations were used to perform additional phase behavior experiments in presence of polymers to investigate the effect of surfactant-polymer synergy on the performance of the formulation.

Table 9.1: List of experiments

Surfactant Phase Behavior	
A1	Surfactant formulation containing C28-45PO-20EO-COO^- (0.5%) and C_{15-18} IOS (0.5%) surfactants
A2	Surfactant formulation containing C24-35PO-40EO-COO^- (0.5%), C_{19-23} IOS (0.25%) and C_{15-18} IOS (0.25%) surfactants + Phenol-5EO (0.25%)
A3	Surfactant formulation containing C28-45PO-20EO-COO^- (0.35%) and C_{15-18} IOS (0.35%) surfactants
A4	Surfactant formulation containing C28-45PO-20EO-COO^- (0.2) and C_{15-18} IOS (0.2%) surfactants
A5	Surfactant formulation containing C24-35PO-40EO-COO^- (0.35%), C_{19-23} IOS (0.175%) and C_{15-18} IOS (0.175%) surfactants + Phenol-5EO (0.175%)
A6	Surfactant formulation containing C24-35PO-40EO-COO^- (0.2%), C_{19-23} IOS (0.1%) and C_{15-18} IOS (0.1%) surfactants + Phenol-5EO (0.1%)
A1P	Surfactant formulation containing C28-45PO-20EO-COO^- (0.5%) and C_{15-18} IOS (0.5%) surfactants in presence of AN125 VHM (0.2%)
A2P	Surfactant formulation containing C24-35PO-40EO-COO^- (0.5%), C_{19-23} IOS (0.25%) and C_{15-18} IOS (0.25%) surfactants + Phenol-5EO (0.25%) in presence of AN125 VHM (0.2%)
Polymer Treatment and Transport	
B1	Polymer injection in Indiana Limestone core at the reservoir temperature
SP Corefloods	
C1	Oil recovery SP coreflood in Indiana limestone core using surfactant formulation A1
C2	Oil recovery SP coreflood in Indiana limestone core using surfactant formulation A2
C3	Oil recovery SP coreflood in an oil-wet Indiana limestone core using surfactant formulation A2

C4	Oil recovery SP coreflood in Indiana limestone core (higher Soi) using surfactant formulation A2
C5	Oil recovery SP coreflood in Indiana limestone core (higher Soi) using surfactant formulation A5
C6	Oil recovery SP coreflood in Indiana limestone core (higher Soi) using surfactant formulation A2

Formation brine, obtained from the reservoir water analysis, sea water, and synthetic injection brine were used in all the experiments in this study. The composition of the brines is listed in **Table 9.2**. The pH of the various surfactant formulations was measured using pHTestr 20 (Oakton Instruments) which has the precision of $\pm$ 0.01. The pH electrode was calibrated with standard pH buffer solutions of pH 4, 7, and 10.

Table 9.2: Composition of the synthetic sea-water, formation brine & injection brine

Ions	**Sea- Water Concentration (ppm)**	**Formation Brine Concentration (ppm)**	**Synthetic Injection Brine Concentration (ppm)**
Na^+	14,305	46,450	31,985
Ca^{2+}	564	4,345	2,643
Mg^{2+}	1,576	162	798
Cl^-	24,814	79,487	54,884
SO_4^{2-}	3,816	560	2,025
TDS	45,075	131,004	92,336

9.2. RESULTS AND DISCUSSIONS

9.2.1 Phase Behavior Experiments (Without Polymer)

Surfactant phase behavior experiments were conducted to identify formulations with ultralow IFT in absence of alkali. In the screening and optimization process, several formulations were evaluated and the most promising formulations (found to give ultralow

IFT with the oil as well as aqueous stability at the reservoir temperature) are listed in **Table 9.3**. Surfactant blends with varying number of hydrocarbon chain length, varying number of EO and PO groups with COO- hydrophilic tail in combination with sulfonates were explored during this experiment. The molecular structures of these surfactants are shown in **Figure 9.1**. The initial set of experiments showed ultr-low IFT using one large hydrophobe carboxylate surfactant in combination with C_{15-18} IOS; however, the formulations required adjustment to improve the robustness and solubilization ratio. Tolerance to the hardness (divalent ions) of the formation water/sea-water was also required, hence, higher numbers (>30) of EO were typically required on the carboxylate surfactant (as observed from the phase behavior experiments with lower surfactant concentrations). However, the formulations had to balance the hydrophilic and lipophilic components in the formulation; hence, a mixture of two IOS surfactants in combination with a more hydrophilic carboxylate was investigated. Co-solvent was also added to this optimized formulation to improve the equilibration time and reduce the viscosity of the macro-emulsions generated.

Formulation A1 comprised of C28-45PO-20EO-COONa (0.5 wt%) and C15-18 IOS (0.5 wt%) prepared in mixture of formation brine and sea-water with a significant number of divalent ions. On the other hand, formulation A2 comprised of C_{24}-35PO-40EO-COONa (0.5 wt%), C_{15-18} IOS (0.25 wt%), C_{19-23} IOS (0.25 wt%), and Phenol-5EO (0.25 wt%) prepared in mixture of formation brine and sea-water. Each of these phase behavior experiments were performed at a water-oil ratio (WOR) of 3. Additional experiments were performed for formulations A1 and A2 with lower total surfactant concentrations (keeping

the surfactant ratios constant) to investigate the effect of surfactant dilution and the surfactant/divalent ions ratio on the robustness of the formulation developed. **Table 9.3** summarizes the results of these formulations in terms of optimum solubilization ratio, optimum salinity, and aqueous stability at the reservoir temperature (80 ^{o}C). Using Huh's equation, the IFTs at optimum salinity for surfactant formulations A1 and A2 were calculated to be 0.0021 and 0.0015 dynes/cm respectively. The results of the dilution tests (formulations A3-A6) showed improvement in solubilization ratio with a more significant drop in optimal salinity for formulation A1 compared to formulation A2. It can be concluded that formulation A2 with higher EO groups in the carboxylate surfactant generated a more robust formulation in presence of high divalent ions at high temperature. **Figures 9.2-9.7** show the phase behavior tubes illustrating the Winsor Type III region and the corresponding solubilization ratio plots for formulations A1- A6. As observed in **Figure 9.2 (a)** and **Figure 9.7 (a)** the 5th tube seems to be still reaching equilibrium as an interface was observed in the microemulsion phase, which seemed more accurate in estimation of optimum solubilization ratio.

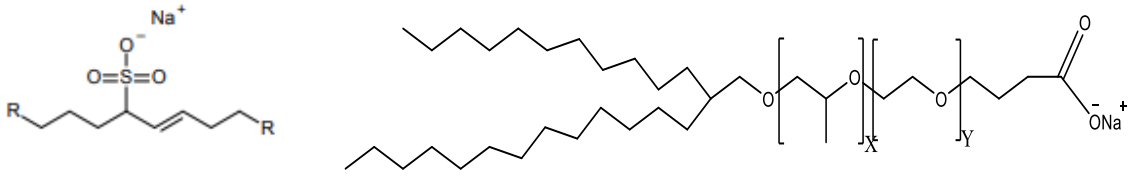

where R = C_{15-18} or C_{19-23} C_{24-28}-xPO-yEO-COONa

Figure 9.1. Structure of surfactant molecules C15-18 IOS/ C19-23 IOS (left) and C24-28-xPO-yEO-COONa (right)

Table 9.3: Phase behavior experiments at ambient pressure without polymer (80 ^{o}C)

Set #	**Surfactant formulation**	**Optimal Salinity (TDS)**	**σ* (cc/cc)**	**Aqueous stability (TDS)**
A1	0.5% C_{28}-45PO-20EO-COO^- + 0.5% C_{15-18} IOS	80,000 ppm	12	102,500 ppm
A2	0.5% C_{24}-35PO-40EO-COO^- + 0.25% C_{15-18} IOS + 0.25% C_{19-23} IOS + 0.25% Phenol-5EO	70,000 ppm	16	97,500 ppm
A3	0.35% C_{28}-45PO-20EO-COO^- + 0.35% C_{15-18} IOS	68,000 ppm	18	95,500 ppm
A4	0.2% C_{28}-45PO-20EO-COO^- + 0.2% C_{15-18} IOS	68,000 ppm	20	92,000 ppm
A5	0.35% C_{24}-35PO-40EO-COO^- + 0.175% C_{15-18} IOS + 0.175% C_{19-23} IOS + 0.175% Phenol-5EO	64,000 ppm	20	95,000 ppm
A6	0.2% C_{24}-35PO-40EO-COO^- + 0.1% C_{15-18} IOS + 0.1% C_{19-23} IOS + 0.1% Phenol-5EO	62,000 ppm	22	94,000 ppm

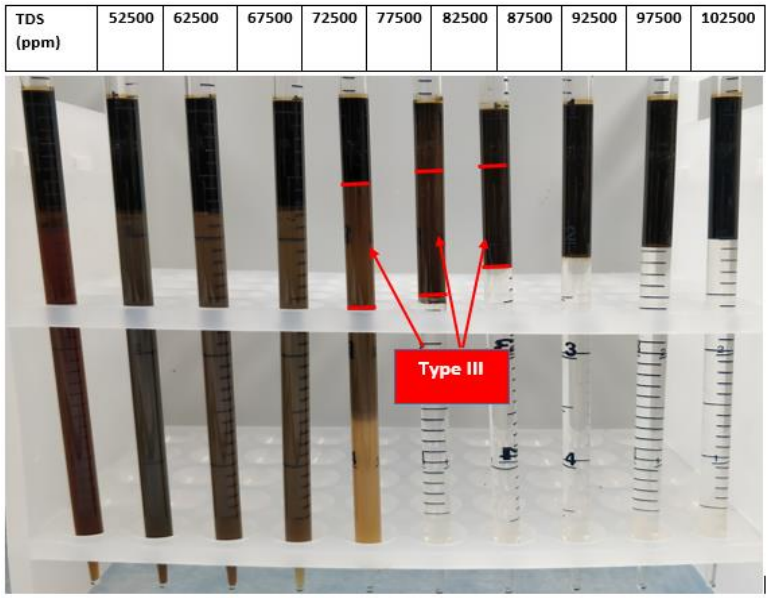

(a)

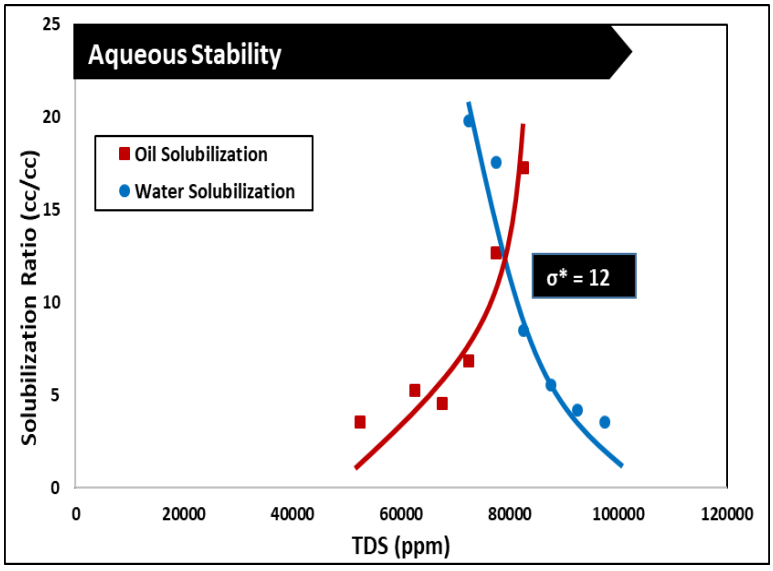

(b)

Figure 9.2. (a) Phase behavior experiment using surfactant formulation A1. Type III region between TDS 77.5K–87.5K ppm; (b) Solubilization ratio plot for surfactant formulation A1

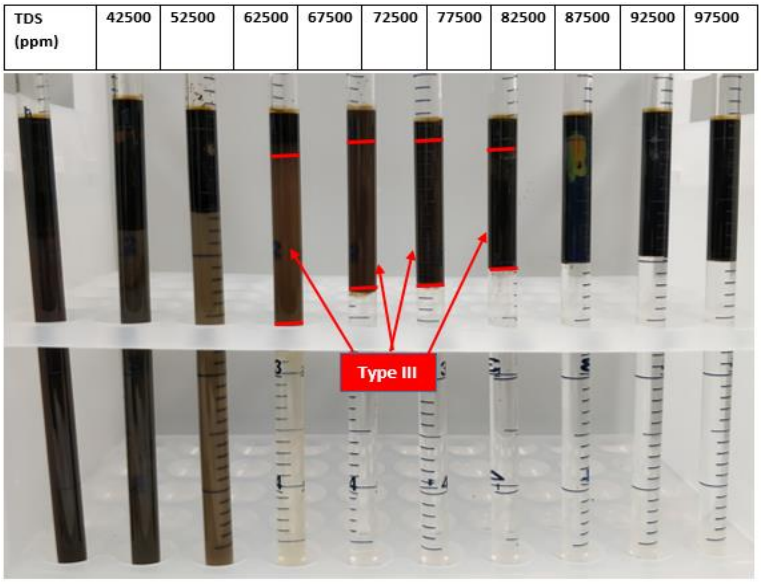

(a)

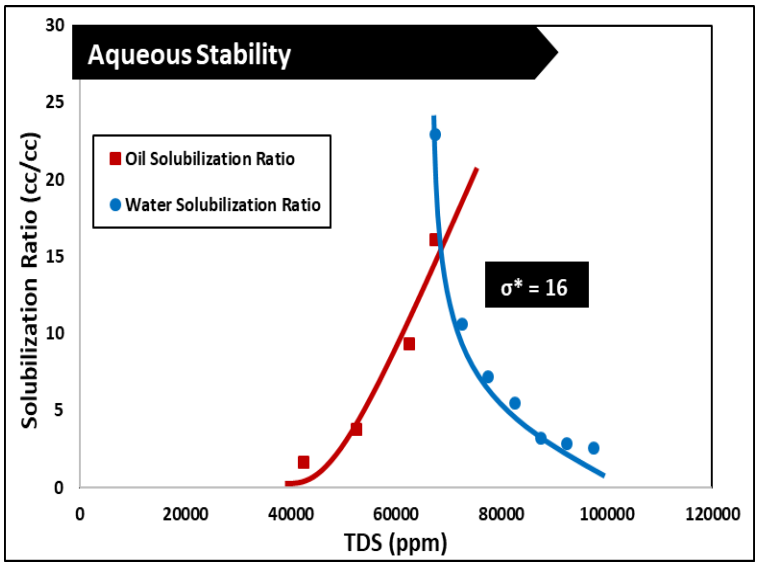

(b)

Figure 9.3. (a) Phase behavior experiment using surfactant formulation A2. Type III region between TDS 67.5K–82.5K ppm; (b) Solubilization ratio plot for surfactant formulation A2

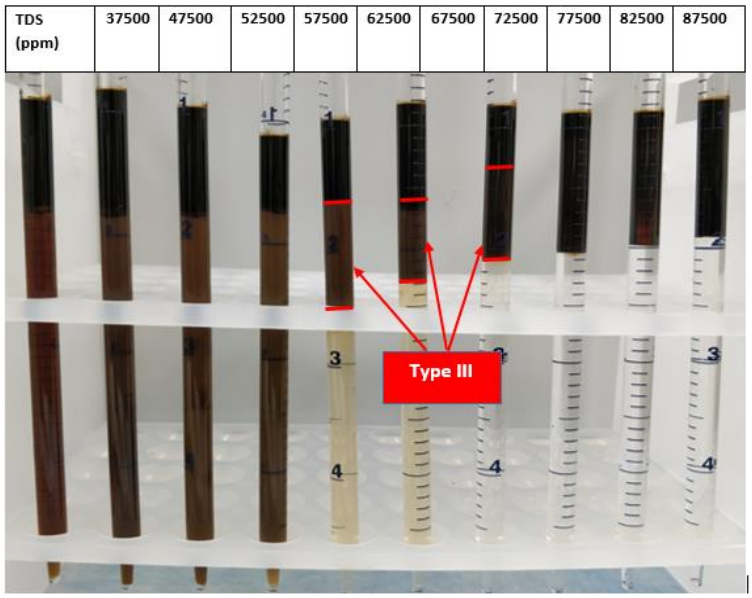

(a)

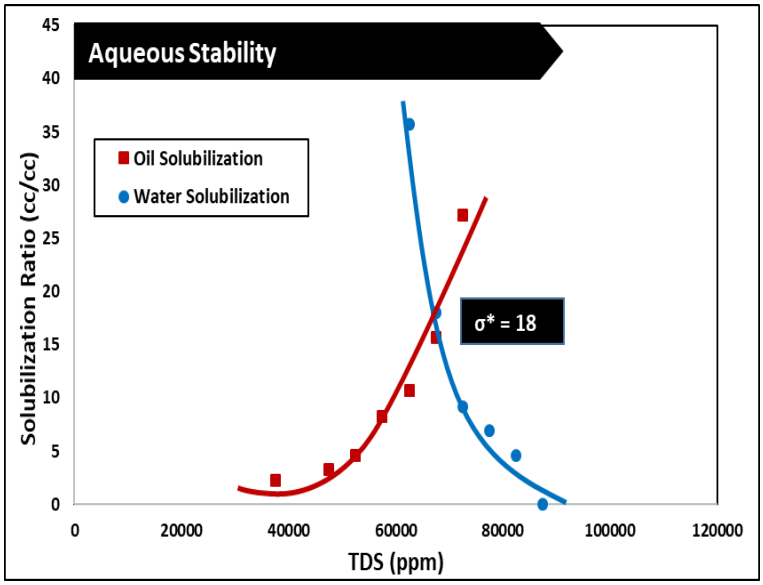

(b)

Figure 9.4. (a) Phase behavior experiment using surfactant formulation A3. Type III region between TDS 62.5K–72.5K ppm; (b) Solubilization ratio plot for surfactant formulation A3

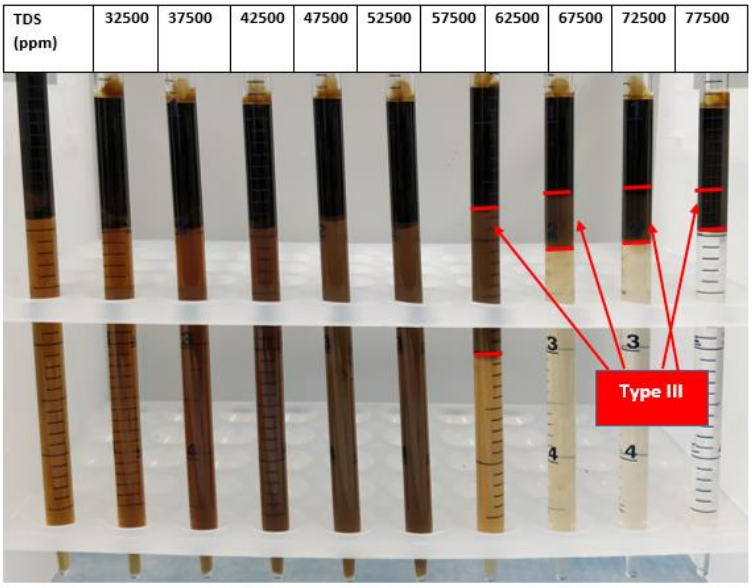

(a)

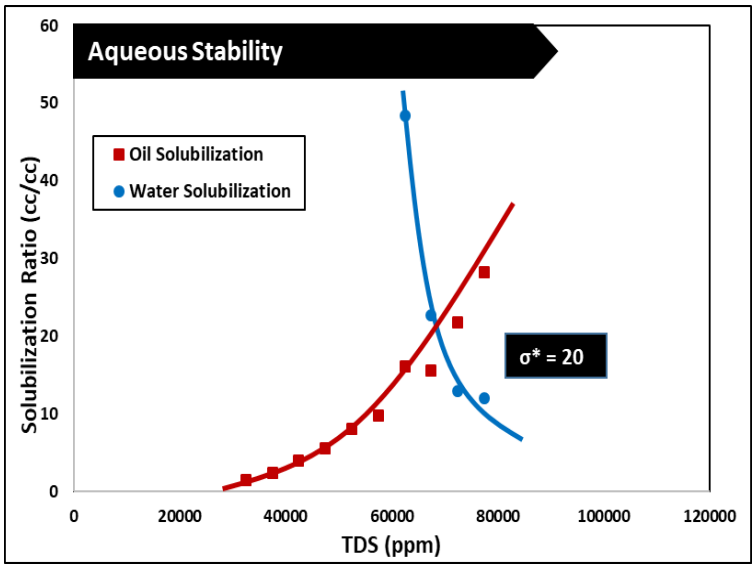

(b)

Figure 9.5. (a) Phase behavior experiment using surfactant formulation A4. Type III region between TDS 62.5K–77.5K ppm; (b) Solubilization ratio plot for surfactant formulation A4

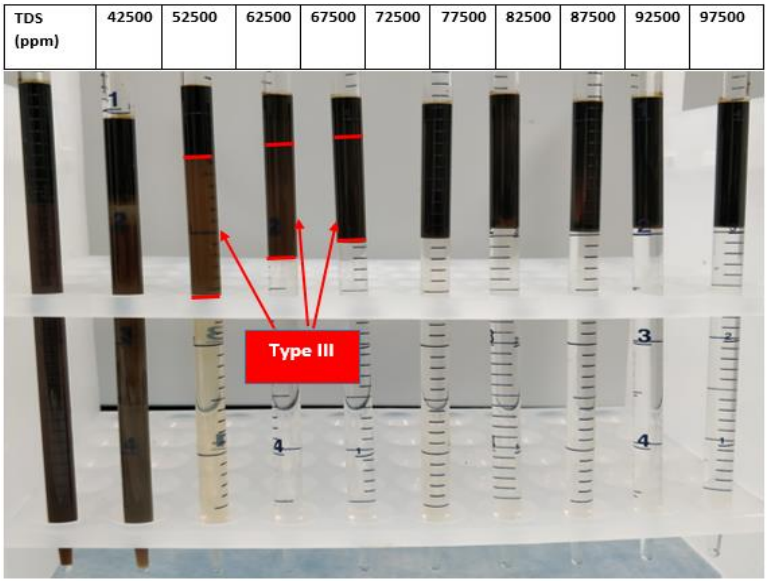

(a)

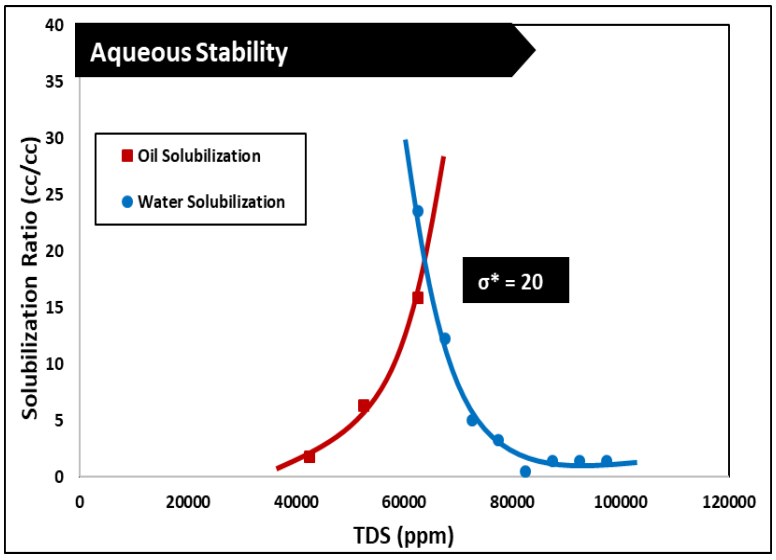

(b)

Figure 9.6. (a) Phase behavior experiment using surfactant formulation A5. Type III region between TDS 62.5K–72.5K ppm; (b) Solubilization ratio plot for surfactant formulation A5

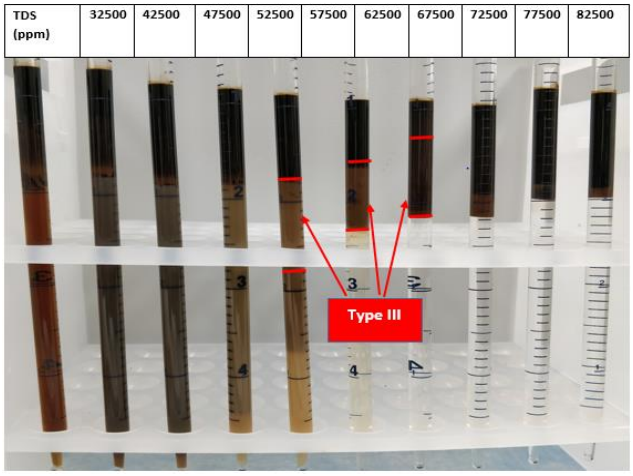

(a)

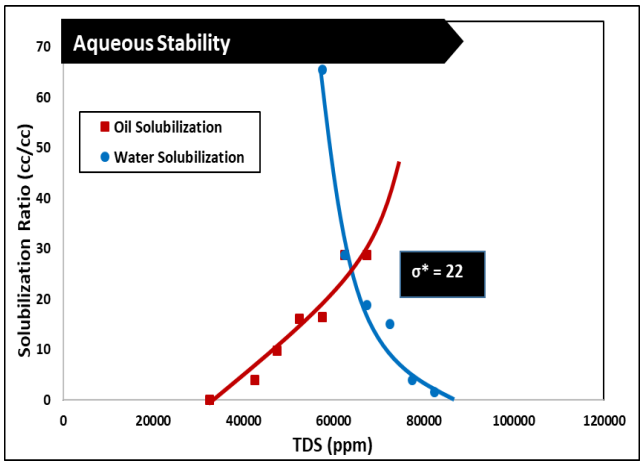

(b)

Figure 9.7. (a) Phase behavior experiment using surfactant formulation A6. Type III region between TDS 57.5K–67.5K ppm; (b) Solubilization ratio plot for surfactant formulation A6

The shift in optimum salinity with reduction of total surfactant concentration and changing surfactant to divalent ions ratio is as expected. But, the improved behavior of both the surfactant formulations at lower concentrations are not conclusive. One possible hypothesis can be due to some of the naphthenic acids present in the crude oil that might be helping in the formation of soaps and improving the performance, even though the oil is inactive and does not contribute towards TAN measurements. On the other hand, a

similar behavior was also observed with a different crude oil in a similar HTHS environment as suggested by Ghosh et al. (2018).

9.2.2 Phase Behavior Experiments (With Polymer)

Additional phase behavior experiments were performed with the most promising formulations A1 and A2 in presence of AN125 VHM polymer to investigate the effect of polymer-surfactant interaction on the phase behavior. Each of the pipettes contained 2000 ppm of AN125 VHM polymer in addition to brine, surfactants and oil. **Table 9.4** summarizes the results of the experiments in terms of optimum solubilization ratio, optimum salinity, and aqueous stability at the reservoir temperature (80 ^{o}C). The results showed a significant change in optimal salinity for formulation A1P compared to formulation A1 whereas formulation A2P showed a similar optimal salinity as formulation A2. Both formulations showed small improvements in the solubilization ratio in the presence of polymer. **Figures 9.8** and **9.9** show the phase behavior tubes illustrating the Type III region and the corresponding solubilization ratio plots for formulations A1P and A2P.

Table 9.4: Phase behavior experiments at ambient pressure with polymer (80 ^{o}C)

Set #	Surfactant formulation	Optimal Salinity (TDS)	σ* (cc/cc)	Aqueous stability (TDS)
A1P	0.5% C_{28}-45PO-20EO-COO^- + 0.5% C_{15-18} IOS + 0.2% AN125 VHM	67,000 ppm	10	97,600 ppm
A2P	0.5% C_{24}-35PO-40EO-COO^- + 0.25% C_{15-18} IOS + 0.25% C_{19-23} IOS + 0.25% Phenol-5EO + 0.2% AN125 VHM	70,000 ppm	15	92,600 ppm

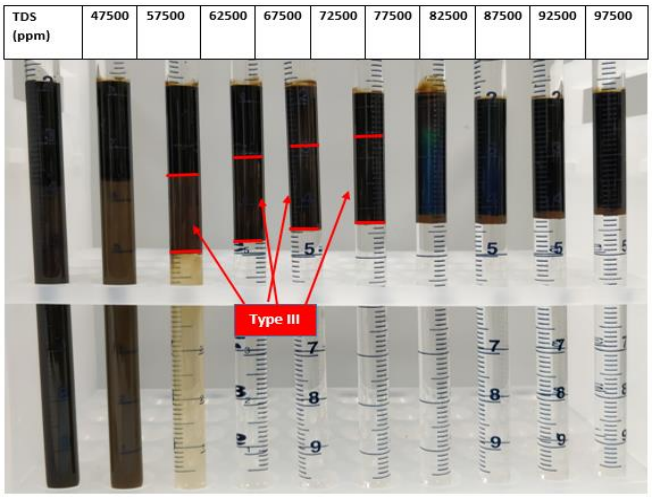

(a)

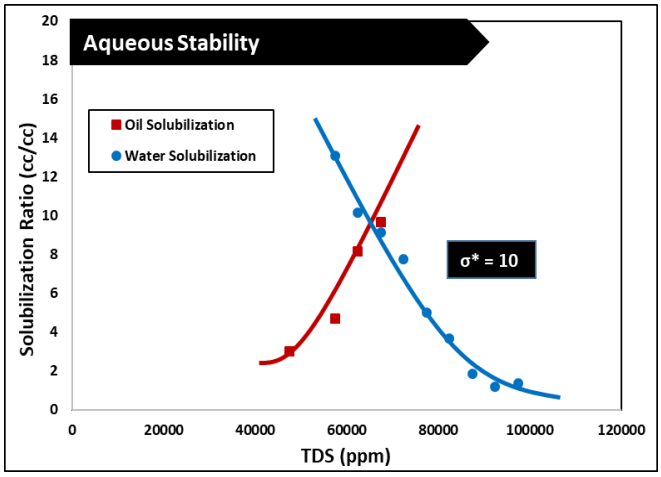

(b)

Figure 9.8. (a) Phase behavior experiment using surfactant formulation A1P. Type III region between TDS 62.5K–77.5K ppm; (b) Solubilization ratio plot for surfactant formulation A1P

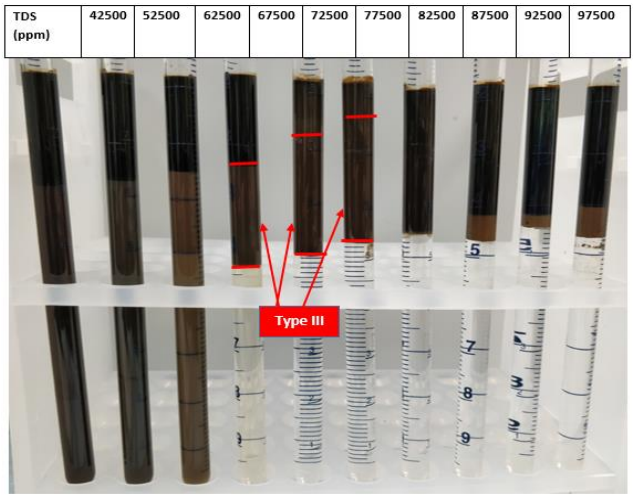

(a)

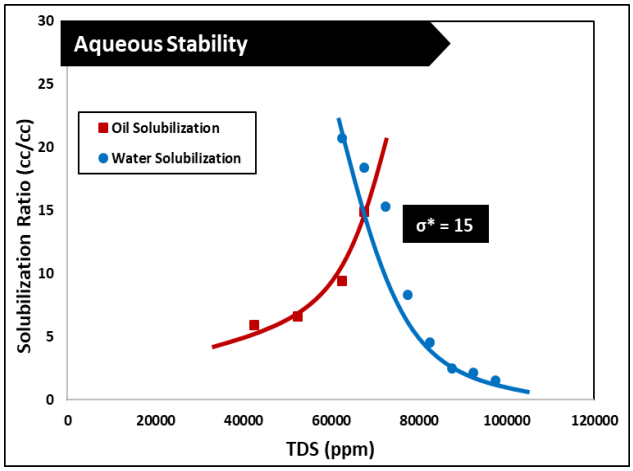

(b)

Figure 9.9. (a) Phase behavior experiment using surfactant formulation A2P. Type III region between TDS 67.5K–77.5K ppm; (b) Solubilization ratio plot for surfactant formulation A2P

9.2.3 Polymer Treatment and Injectivity Test

The polymer protection package was added to the deoxygenated polymer solution to inhibit polymer degradation inside the porous medium at high temperatures. The treated polymer solution was filtered through 1.2-micron filter and the measured filtration ratio (F.R.) was 1.2. Before the polymer solution was injected into the porous medium during

coreflood B1, a tracer test was performed to study the heterogeneity of the porous medium. The properties of the outcrop limestone are listed below in **Table 9.5**. After the tracer test, about 1-2 PV of injection brine (with 500 ppm sodium dithionite) was injected to ensure the reduced state of the core. The polymer solution, with 5000 ppm AN125 VHM in sea-water, was injected at 1 ft/D for about 2 PV and the superficial velocity was increased to 2 ft/D for another 1 PV of fluid injection. The effluent viscosities were measured to investigate the propagation of polymer and the results showed that beyond 1.7 PV of polymer injection, the effluent viscosity matched the injected viscosity. Hence, no polymer degradation was observed in this transport experiment at 80 ^{o}C. As part of this study thermal stability tests with polymer were only monitored for 1 month, but long term thermal stability tests with similar polymers under similar working conditions are available in the literature (Levit and Pope, 2008). **Figure 9.10** summarizes the results of the tracer test and the effluent viscosity for the transport study. The delay in the polymer front breakthrough signifies the polymer adsorption (and inaccessible pore volume) in the carbonate core. The residual resistance factor measured for this core was about 2.6. The measured retention in this experiment was about 76 µg/g of rock. These value is in agreement with polymer retention measurements reported with similar polymer samples in different rock types where it varies between 40-100 µg/g of rock (Broseta et al., 1995; Manichand and Seright, 2014; Zhang and Seright, 2014). The other key observation from this experiment was the improvement in the sweep efficiency due to polymer (as observed in **Figure 9.10** around 1.5 PV of fluid injection), even though the breakthrough of the polymer was early around 0.5 PV due to heterogeneity of the core. **Figure 9.11** shows the

pressure drop during the polymer flood, which verifies the successful polymer transport and the absence of plugging in the porous medium. The pressure drop recording showed some fluctuations at the beginning due to variations in the BPR pressure.

Table 9.5: Rock Properties for coreflood B1

Core Properties		**Indiana Limesteone Brine Permeability**	
Diameter (cm)	3.77	**Whole Core (mD)**	220
Length (cm)	30.1	**Section 1 (mD)**	229
Mass (g)	769.2	**Section 2 (mD)**	214
Bulk Volume (mL)	336.0	**Section 3 (mD)**	229
Porosity	0.151	**Section 4 (mD)**	218
Area (cm^2)	11.16		
Pore Volume (mL)	50.6		

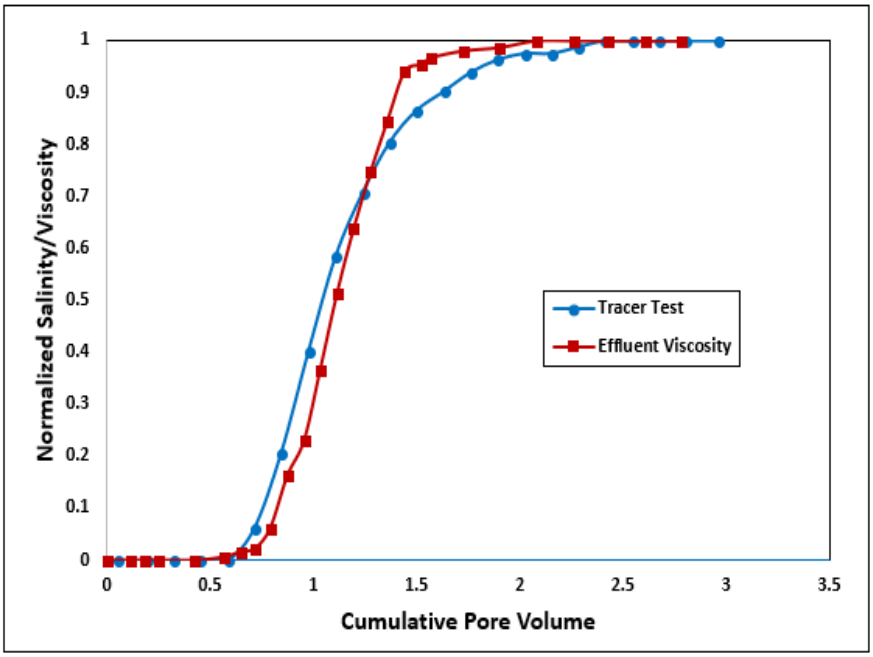

Figure 9.10. Effluent tracer and viscosity results for AN125 VHM injectivity test in Indiana limestone

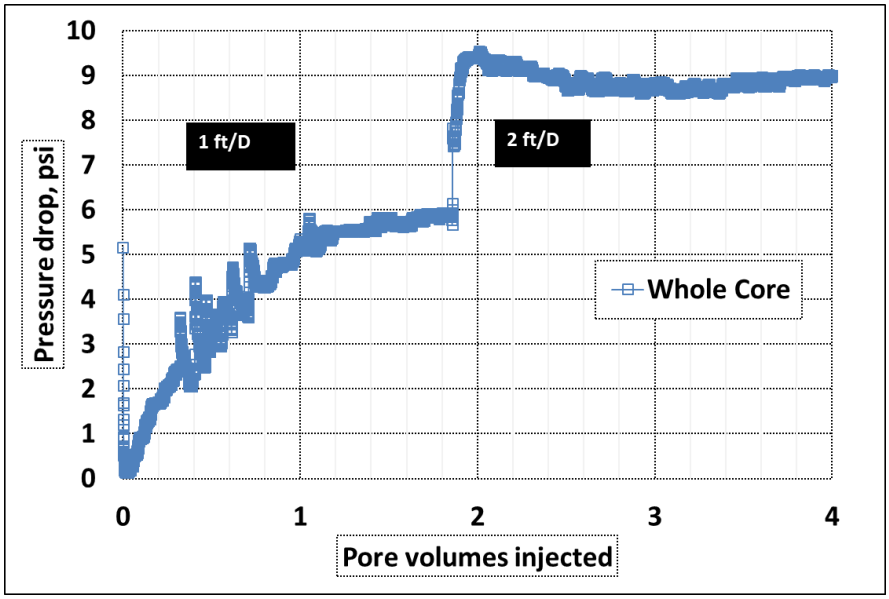

Figure 9.11. Pressure drop data for the polymer injectivity test in Indiana Limestone core at 80 ºC

9.2.4 SP Corefloods

SP corefloods were performed in Indiana limestone cores to test the promising surfactant formulations developed in this study. The polymer solution used for SP slugs and polymer drives were prepared in the way discussed previously for the injectivity test. SP coreflood C1 was conducted in a limestone core (properties listed in **Table 9.6**), which had been waterflooded previously, with **surfactant formulation A1**. The detailed injection scheme followed in this experiment is shown in **Table 9.7**. Each of the injected fluids were deoxygenated with argon and oxygen scavengers were added as well (in all the corefloods).

Table 9.6: Rock Properties for SP coreflood C1

Core Properties (Water-wet)		**Indiana Limestone Oil Permeability**	
Diameter (cm)	3.77	**Whole Core (mD)**	353
Length (cm)	30.1	**Section 1 (mD)**	530
Mass (g)	769.2	**Section 2 (mD)**	268
Bulk Volume (mL)	336.0	**Section 3 (mD)**	334
Porosity	0.146	**Section 4 (mD)**	373
Area (cm^2)	11.16		
Pore Volume (mL)	49.0		
Soi	0.56		

Table 9.7: Injection sequence followed in SP coreflood C1

Fluid Injection Steps	**Pore Volumes**	**Chemical Composition**	**TDS (ppm)**
Waterflood (2 ft/D), pH ~ 4.0	3-4	Synthetic Injection Brine	92,336 ppm
SP Slug (1 ft/D) 41 cP at 80 ^oC (10 s^{-1}), pH ~ 4.0	0.6	0.5% C_{28}-45PO-20EO-COO^- + 0.5% C_{15-18} IOS + Formation Brine + Syn. Injection Brine + 6000 ppm AN125 VHM	86,000 ppm
Polymer Drive (1 ft/D) 48 cP at 80 ^oC (10 s^{-1}), pH ~ 4.0	2.5	Sea-Water Brine + 6000 ppm AN125 VHM	43,500 ppm

The initial oil saturation was 56%. Waterflood was performed at 2 ft/D for about 4 PV until oil production ceased. The total oil recovery for waterflood was 51% OOIP and the residual oil saturation was 0.28. The injection rates were subsequently increased to measure pressure drops and estimate the water relative permeability at the waterflood residual at 80 ^oC.

The 2-component chemical formulation A1 was used for this experiment to investigate the performance in an Indiana limestone core. 0.6 PV of SP slug was injected at 1 ft/D followed by a single polymer drive of about 2.5 PV at 1 ft/D. **Figure 9.12** shows the oil recovery, the oil cut, and the remaining oil saturation as a function of PV injected. An oil bank was created by the SP slug that broke through early at about 0.3 PV (after chemical injection), an oil cut of 20% was maintained until 0.6 PV of chemical injection and a long-tapered oil production was observed until 2 PV. The additional oil produced due to SP flood was 71% ROIP. The total oil recovery at the end of the experiment was 86% OOIP and the residual oil saturation was about 0.08. The effluent viscosity measurements showed successful polymer transport during the experiment with almost 100% of the injected viscosity of SP slug recovered at 1.6 PV of fluid injection. The surfactant retention estimated during this experiment was about 0.32 mg/g of rock.

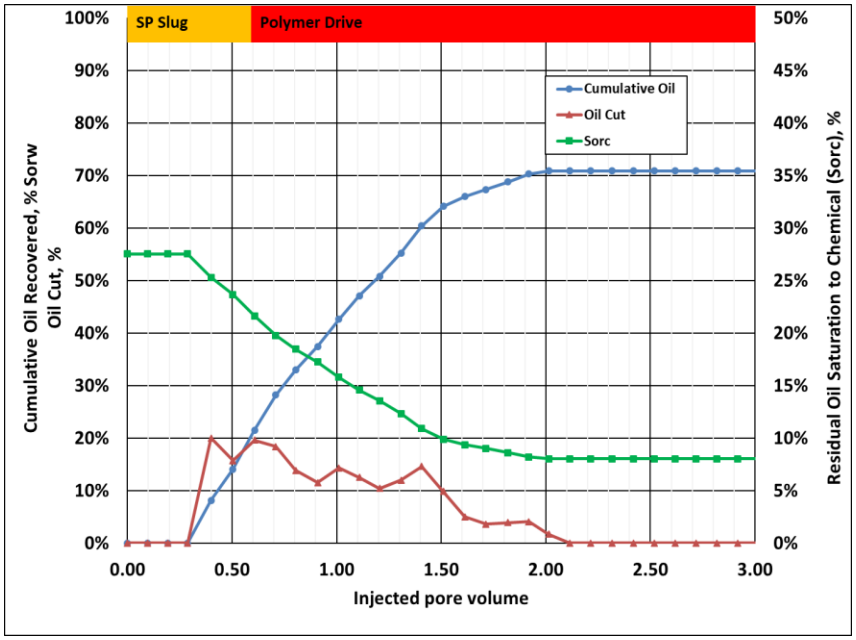

Figure 9.12. Oil recovery, oil cut, and remaining oil saturation for SP coreflood C1

The pressure drops recorded during the experiment were as expected, with a final steady state pressure gradient of 5 psi/ft at the end of the coreflood. The primary reason for a low recovery during chemical flood can be explained by inefficient salinity gradient and the lowering of the optimal salinity in presence of polymer as observed in phase behavior experiment A1P. The results of the effluent salinity and viscosity measured are shown below in **Figure 9.13**.

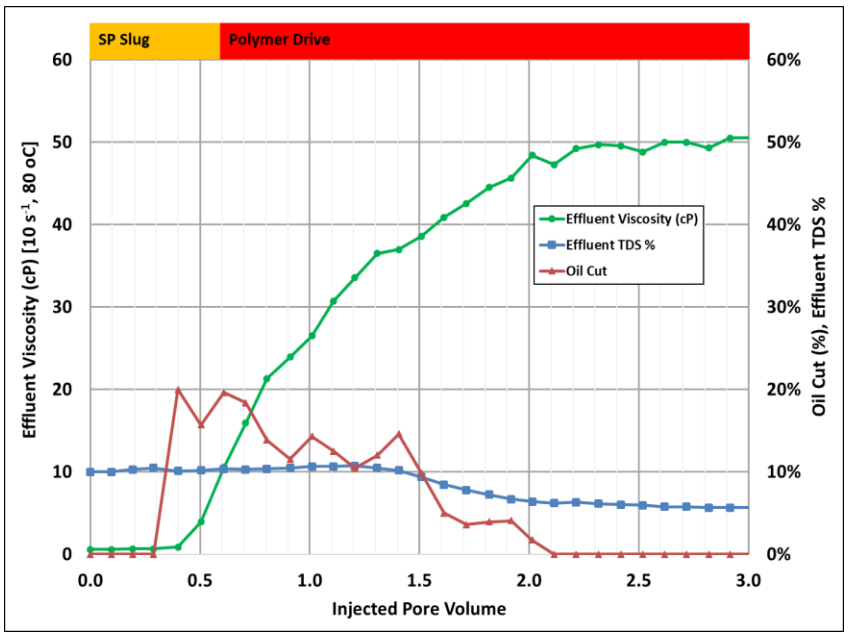

Figure 9.13. Effluent salinity, oil cut, and effluent viscosity for SP coreflood C1

Coreflood C2 was conducted in an outcrop limestone core (core properties listed in **Table 9.8**), which had been waterflooded previously, with surfactant formulation A2. The detailed injection scheme followed in this experiment is shown in **Table 9.9**.

Table 9.8: Rock Properties for SP coreflood C2

Core Properties (Water-wet)		Indiana Limesteone Oil Permeability	
Diameter (cm)	3.77	**Whole Core (mD)**	275
Length (cm)	30.1	**Section 1 (mD)**	351
Mass (g)	769.2	**Section 2 (mD)**	230
Bulk Volume (mL)	336.0	**Section 3 (mD)**	270
Porosity	0.151	**Section 4 (mD)**	279
Area (cm^2)	11.16		
Pore Volume (mL)	50.6		
Soi	0.50		

Table 9.9: Injection sequence followed in SP coreflood C2

Fluid Injection Steps	Pore Volumes	Chemical Composition	TDS (ppm)
Waterflood (2 ft/D), pH ~ 4.0	4.0	Synthetic Injection Brine	92,336 ppm
SP Slug (1 ft/D) 70 cP at 80 ^oC (10 s^{-1}), pH ~ 3.54	0.6	0.5% C_{24}-35PO-40EO-COO^- + 0.25% C_{19-23} IOS + 0.25% C_{15-18} IOS + 0.25% Phenol-5EO + Formation Brine + Syn. Injection Brine + 7500 ppm AN125 VHM	79,000 ppm
Polymer Drive (1 ft/D) 96 cP at 80 ^oC (10 s^{-1}), pH ~ 4.0	2.5	Sea-Water Brine + 0.25% Phenol-5EO + 7500 ppm AN125 VHM	30,000 ppm

The initial oil saturation was 50% in coreflood C2. Waterflood was performed at 2 ft/D for 3.5 PV, until oil production stopped. The total oil recovery after waterflood was 60% OOIP and the residual oil saturation was 0.20. The injection rates were increased for a short period to estimate the water relative permeability at the waterflood residual at 80 ^oC.

The 3-component chemical formulation A2 (along with a cosolvent) was used in this experiment to investigate the performance in Indiana limestone core. 0.6 PV of SP slug was injected at 1 ft/D followed by a single polymer drive of about 2.5 PV at 1 ft/D. As part of the optimization process a cosolvent was added to the polymer drive as well to improve the effective salinity gradient, polymer transport and reduce surfactant retention. **Figure 9.14** shows the oil recovery, the oil cut, and the remaining oil saturation as a function of PV injected. An oil bank was created by the SP slug that broke through at about 0.3 PV (after chemical injection), an oil cut of 15% was maintained until 1.3 PV of chemical injection and a long-tapered oil production was observed until 2.5 PV. The additional oil produced due to SP flood was 88% ROIP. The total oil recovery at the end of the experiment was 95.2% OOIP and the residual oil saturation was about 0.02. A similar early breakthrough of the oil bank was observed again during this coreflood even in the presence of significantly higher polymer concentration. This suggests that mobility control was not an issue in the previous coreflood, rather salinity gradient is more important for a robust coreflood design. Another observation of a long tail of oil bank also explains an inefficient salinity gradient due to slow transition into Type I emulsions during the coreflood. The effluent viscosity measurements showed successful polymer transport during the experiment with almost 100% of the injected viscosity of SP slug recovered at 1.4 PV of fluid injection. The pressure drops recorded during the experiment were as expected from the significantly high viscosity injected with final steady state pressure gradient of 9 psi/ft at the end of the coreflood. The effluent salinity and viscosity measurements along with oil cut are shown in **Figure 9.15**. The surfactant retention estimated during this experiment

was about 0.15 mg/g of rock. This coreflood results clearly show the benefits of adding cosolvent to the formulation in chemical slug and polymer drive in the performance of the coreflood.

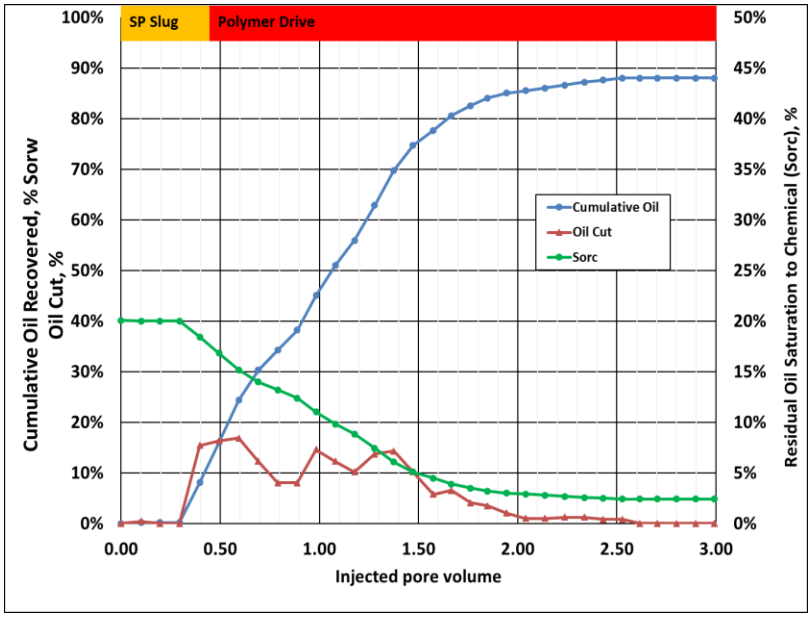

Figure 9.14. Oil recovery, oil cut, and remaining oil saturation for SP coreflood C2

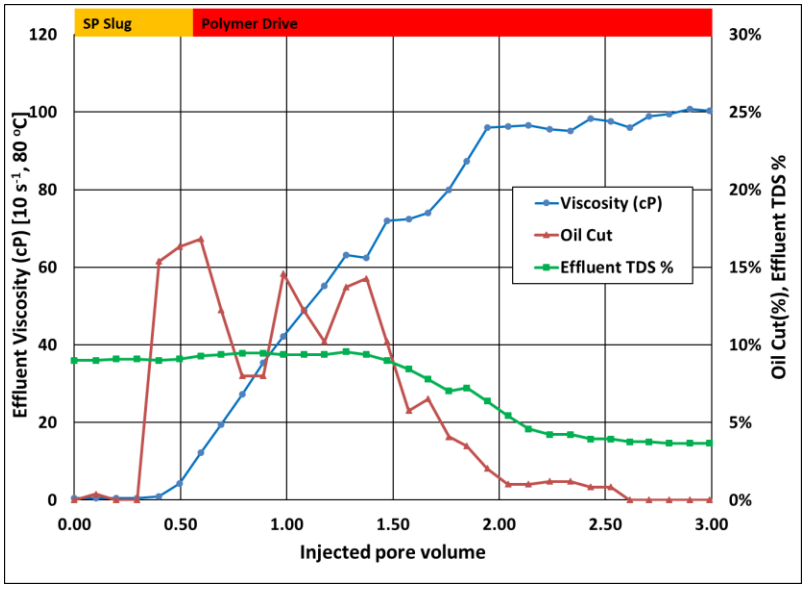

Figure 9.15. Effluent salinity, oil cut, and effluent viscosity for SP coreflood C2

9.2.4.1 Effect of Rock Wettability

Coreflood C3 was conducted in an outcrop limestone core, aged in crude oil at 90 ^{o}C for 24 months, to change the wettability of the core from water-wet to oil-wet (core properties listed in **Table 9.10**). This core was waterflooded before injection of the surfactant formulation A2. The detailed injection scheme followed in this experiment is shown in **Table 9.11**.

Table 9.10: Rock Properties for SP coreflood C3

Core Properties (Oil-wet)		**Indiana Limestone Oil Permeability**	
Diameter (cm)	3.77	**Whole Core (mD)**	450
Length (cm)	30.4	**Section 1 (mD)**	335
Mass (g)	775.4	**Section 2 (mD)**	487
Bulk Volume (mL)	339.4	**Section 3 (mD)**	538
Porosity	0.155	**Section 4 (mD)**	506
Area (cm^2)	11.16		
Pore Volume (mL)	52.5		
Soi	0.56		

Table 9.11: Injection sequence followed in SP coreflood C3

Fluid Injection Steps	**Pore Volumes**	**Chemical Composition**	**TDS (ppm)**
Waterflood (2 ft/D), pH ~ 6.6	3.5	Synthetic Injection Brine	92,336 ppm
SP Slug (1 ft/D) 32.6 cP at 80 ^{o}C (10 s^{-1}), pH ~ 6.6	0.6	0.5% C_{24}-35PO-40EO-COO^- + 0.25% C_{19-23} IOS + 0.25% C_{15-18} IOS + 0.25% Phenol-5EO + Formation Brine + Syn. Injection Brine + 5100 ppm AN125 VHM	79,000 ppm
Polymer Drive (1 ft/D) 39 cP at 80 ^{o}C (10 s^{-1}), pH ~ 8.0	2.5	Sea-Water Brine + 0.25% Phenol-5EO + 5100 ppm AN125 VHM	30,000 ppm

The initial oil saturation was 56% in coreflood C3. Waterflood was performed at 2 ft/D for 3.5 PV, until oil production stopped. The total oil recovery after waterflood was 63% OOIP and the residual oil saturation was 0.21. The injection rates were increased for a short period to estimate the water relative permeability at the waterflood residual. The high waterflood recovery was surprising in an oil-wet core because the oil-wetness was suggested by the significant increase in water relative permeability after waterflood by almost 4 times compared to corefloods C1 and C2. Nonetheless, there is a chance that at low oil saturations the core might not have been fully oil-wet and more like intermediate-wet, as suggested by high waterflood oil recovery.

The 3-component chemical formulation A2 (along with cosolvent) was used in this experiment to investigate the performance in Indiana limestone core. 0.6 PV of SP slug was injected at 1 ft/D followed by a single polymer drive of about 2.5 PV at 1 ft/D. **Figure 9.16** shows the oil recovery, the oil cut, and the remaining oil saturation as a function of PV injected. An oil bank was created by the SP slug that broke through early at about 0.3 PV (after chemical injection), an oil cut of about 20% was maintained until 1.2 PV of chemical injection. The additional oil produced due to SP flood was 92% ROIP. The total oil recovery at the end of the experiment was 96.8% OOIP and the residual oil saturation was about 0.01. The effluent viscosity measurements showed successful polymer transport during the experiment with almost 100% of the injected viscosity of polymer drive recovered at 2.2 PV of fluid injection. The pressure drops recorded during the experiment were consistent with the previous corefloods and final steady state pressure gradient of 3 psi/ft was observed at the end of the coreflood. The effluent salinity and viscosity

measurements along with oil cut are shown in **Figure 9.17**. The surfactant retention estimated during this experiment was about 0.25 mg/g of rock. The results showed that this surfactant formulation was very efficient in mobilizing the remaining oil after waterflood in an oil-wet core with similar retention compared to coreflood C2.

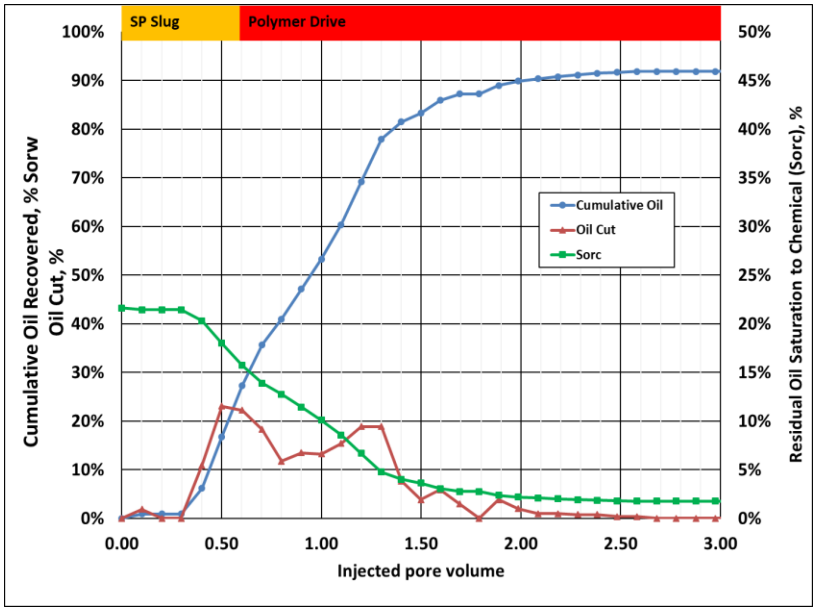

Figure 9.16. Oil recovery, oil cut, and remaining oil saturation for SP coreflood C3

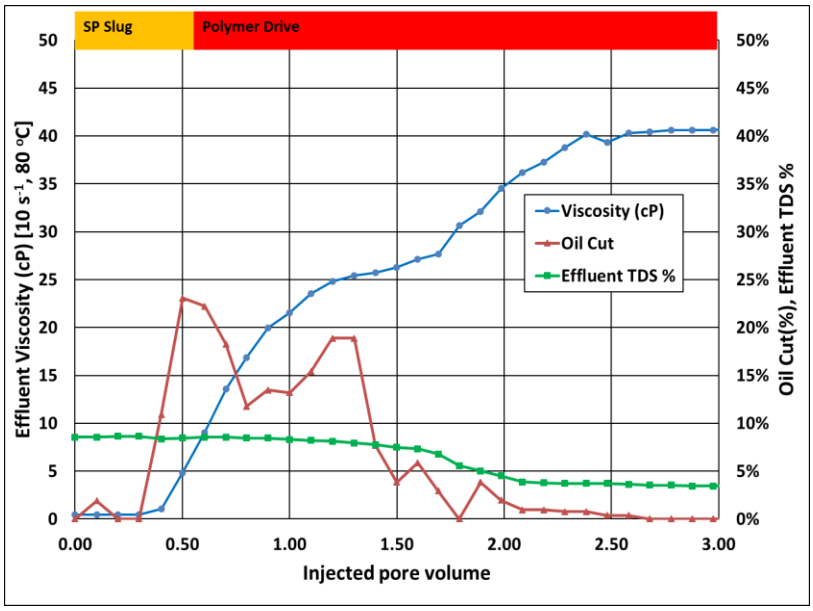

Figure 9.17. Effluent salinity, oil cut, and effluent viscosity for SP coreflood C3

9.2.4.2 Effect of Initial Oil Saturation

Coreflood C4 was conducted in an outcrop limestone core to investigate the effect of higher initial oil saturation (core properties listed in **Table 9.12**). This core was waterflooded before injection of the surfactant formulation A2. The detailed injection scheme followed in this experiment is shown in **Table 9.13**. As a part of the optimization process, the pH of the solutions injected were buffered around pH ~8.

Table 9.12: Rock Properties for SP coreflood C4

Core Properties (Water-wet)		Indiana Limestone Oil Permeability	
Diameter (cm)	3.77	**Whole Core (mD)**	417
Length (cm)	30.5	**Section 1 (mD)**	386
Mass (g)	772.6	**Section 2 (mD)**	353
Bulk Volume (mL)	340.5	**Section 3 (mD)**	452
Porosity	0.156	**Section 4 (mD)**	513
Area (cm^2)	11.16		
Pore Volume (mL)	53.0		
Soi	0.80		

Table 9.13: Injection sequence followed in SP coreflood C4

Fluid Injection Steps	Pore Volumes	Chemical Composition	TDS (ppm)
Waterflood (2 ft/D), pH ~ 8.2	3-3.5	Synthetic Injection Brine	92,336 ppm
SP Slug (1 ft/D) 46.3 cP at 80 ^oC (10 s^{-1}), pH ~ 8.2	0.6	0.5% C_{24}-35PO-40EO-COO^- + 0.25% C_{19-23} IOS + 0.25% C_{15-18} IOS + 0.25% Phenol-5EO + Formation Brine + Syn. Injection Brine + 5800 ppm AN125 VHM	79,000 ppm
Polymer Drive (1 ft/D) 49.7 cP at 80 ^oC (10 s^{-1}), pH ~ 7.5	2.5	Sea-Water Brine + 0.25% Phenol-5EO + 5800 ppm AN125 VHM	30,000 ppm

The initial oil saturation was 80.5% in coreflood C4 (obtained through vacuum saturation). Waterflood was performed at 2 ft/D for about 3.5 PV, until oil production stopped. The total oil recovery after waterflood was 51% OOIP and the residual oil saturation was 0.4. The injection rates were increased for a short period to estimate the water relative permeability at the waterflood residual at 80 ^oC. The higher initial oil saturation led to a higher residual oil saturation.

The 3-component chemical formulation A2 (along with cosolvent) was used in this experiment to investigate the performance in Indiana limestone core. 0.6 PV of SP slug was injected at 1 ft/D followed by a single polymer drive of about 2.5 PV at 1 ft/D. **Figure 9.18** shows the oil recovery, the oil cut, and the remaining oil saturation as a function of PV injected. An oil bank was created by the SP slug that broke through early at about 0.2 PV (after chemical injection), a maximum oil cut of about 50% was obtained and the oil production tail continued until 2 PV of chemical injection. The additional oil produced due to SP flood was 86% ROIP. The total oil recovery at the end of the experiment was 93% OOIP and the residual oil saturation was about 0.06. The effluent viscosity measurements showed successful polymer transport during the experiment with almost 100% of the injected viscosity of SP slug recovered at 1.5 PV of fluid injection. The pressure drops recorded during the experiment verified successful polymer transport with final steady state pressure gradient of 4 psi/ft at the end of the coreflood. The effluent salinity and viscosity measurements along with oil cut are shown in **Figure 9.19**. The surfactant retention estimated during this experiment was about 0.20 mg/g of rock. The results showed that this surfactant formulation was efficient in mobilizing the remaining oil after waterflood, but the tertiary recovery was lower compared to coreflood C2 and C3. This can be possibly explained by the inability to mobilize some trapped oil in the smaller pores (due to vacuum saturation method) whereas in coreflood C2 and C3 the oil resided primarily in the larger pores. Another important observation was due to pH buffering of all the solutions injected helped to reduce the retention of anionic surfactants in limestone cores during the experiment – an important optimization parameter for successful SP corefloods.

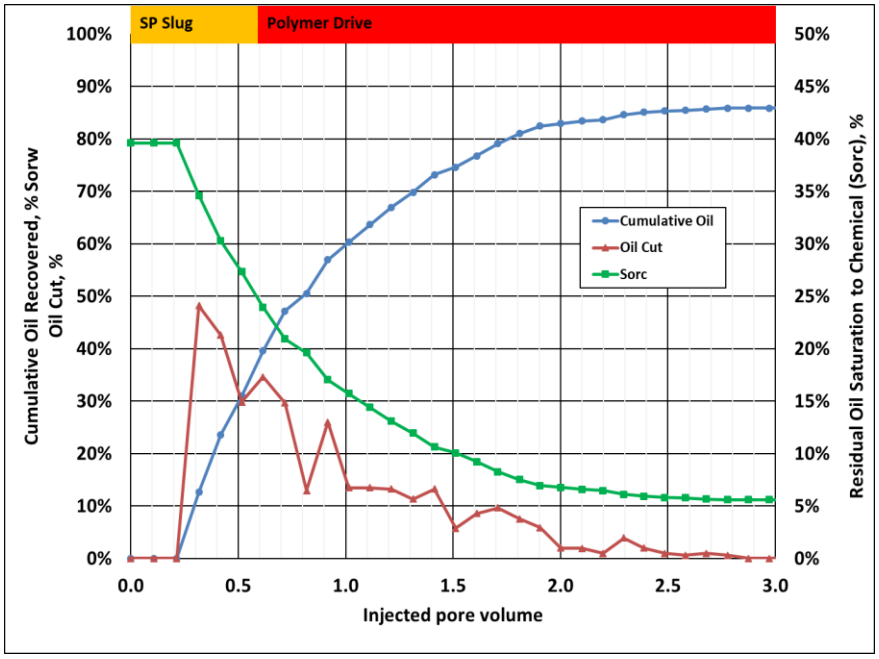

Figure 9.18. Oil recovery, oil cut, and remaining oil saturation for SP coreflood C4

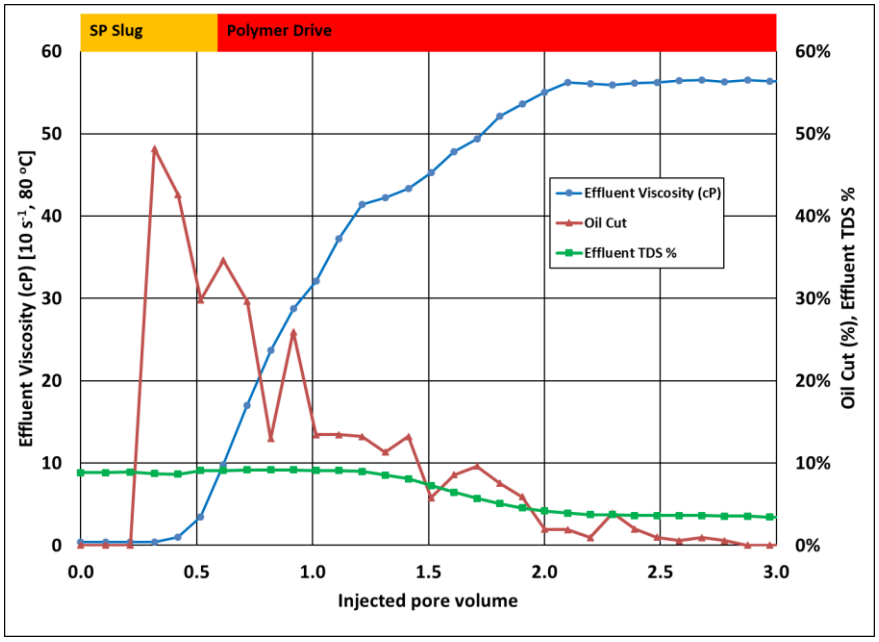

Figure 9.19. Effluent salinity, oil cut, and effluent viscosity for SP coreflood C4

9.2.4.3 Effect of Reduced Surfactant Concentration, Change in Salinity Gradient

Coreflood C5 was conducted in an outcrop limestone core to investigate the effect of reduced surfactant injection and a modified salinity gradient on oil production and surfactant retention (core properties listed in **Table 9.14**). The core was waterflooded before injection of the surfactant formulation A5. The detailed injection scheme followed in this experiment is shown in **Table 9.15**. The pH of the solutions injected were buffered around pH ~8.5.

Table 9.14: Rock Properties for SP coreflood C5

Core Properties (Water-wet)		**Indiana Limestone Oil Permeability**	
Diameter (cm)	3.77	**Whole Core (mD)**	751
Length (cm)	30.4	**Section 1 (mD)**	698
Mass (g)	769.2	**Section 2 (mD)**	538
Bulk Volume (mL)	339.4	**Section 3 (mD)**	1210
Porosity	0.15	**Section 4 (mD)**	741
Area (cm^2)	11.16		
Pore Volume (mL)	50.9		
Soi	0.805		

Table 9.15: Injection sequence followed in SP coreflood C5

Fluid Injection Steps	Pore Volumes	Chemical Composition	TDS (ppm)
Waterflood (2 ft/D), pH ~ 8.8	4	Synthetic Injection Brine	92,336 ppm
SP Slug (1 ft/D) 50.5 cP at 80 ^{o}C (10 s^{-1}), pH ~ 8.8	0.6	0.35% C_{24}-35PO-40EO-COO^{-} + 0.175% C_{19-23} IOS + 0.175% C_{15-18} IOS + 0.175% Phenol-5EO + Formation Brine + Syn. Injection Brine + 6000 ppm AN125 VHM	70,000 ppm
Polymer Drive 1 (1 ft/D) 50.7 cP at 80 ^{o}C (10 s^{-1}), pH ~ 8.7	1.0	Sea-Water Brine + 0.25% Phenol-5EO + 6000 ppm AN125 VHM	49,000 ppm
Polymer Drive 2 (1 ft/D) 62.4 cP at 80 ^{o}C (10 s^{-1}), pH ~ 7.8	1.6	Sea-Water Brine + 0.25% Phenol-5EO + 6000 ppm AN125 VHM	30,000 ppm

The initial oil saturation was 80.5% in coreflood C5 (obtained through vacuum saturation). Waterflood was performed at 2 ft/D for about 4.0 PV, until oil production stopped. The total oil recovery after waterflood was 55% OOIP and the residual oil saturation was 0.36. The injection rates were increased for a short period to estimate the water relative permeability at the waterflood residual.

The 3-component chemical formulation A5 (along with cosolvent) was used in this experiment to investigate the performance of surfactant reduction (25% by weight) and tapered polymer drive salinity in Indiana limestone core. 0.6 PV of SP slug was injected at 1 ft/D followed by polymer drive 1 at reduced salinity (70% of SP slug salinity) for about 1 PV at 1 ft/D. Finally, polymer drive 2 at a further reduced salinity was injected for about 1.6 PV at 1 ft/D until no oil was produced. **Figure 9.20** shows the oil recovery, the oil cut, and the remaining oil saturation as a function of PV injected. An oil bank was created by

the SP slug that broke through early at about 0.3 PV (after chemical injection), a maximum oil cut of about 27% was obtained (lower than that obtained in coreflood C4), the oil production tail continued until 2 PV of chemical injection and a second oil bank was observed with the injection of polymer drive 2 at reduced salinity after 2 PV of chemical injection. The additional oil produced due to SP flood was 81% ROIP. The total oil recovery at the end of the experiment was 91.4% OOIP and the residual oil saturation was about 0.07. The effluent viscosity measurements showed successful polymer transport during the experiment with almost 100% of the injected viscosity of SP slug recovered at 2 PV of fluid injection and 100% of the injected viscosity of PD2 recovered at 2.8 PV of fluid injection. The pressure drops recorded during the experiment were consistent with the viscosity of the fluids injected and the oil bank mobilization with final steady state pressure gradient of 3.5 psi/ft at the end of the coreflood. The effluent salinity and viscosity measurements along with oil cut are shown in **Figure 9.21**. The surfactant retention estimated during this experiment was about 0.20 mg/g of rock. The results showed that this surfactant formulation was efficient in mobilizing the remaining oil after waterflood even at lower amount of surfactant injected. Another possible explanation of similar performance with reduced surfactant injection could be due to the improved microemulsion behavior at lower surfactant concentrations (shown earlier in the phase behavior results). Also, an improved salinity gradient with tapered polymer drives was implemented during this coreflood to increase the residence time in Type III region during the coreflood and improve the performance of the chemical formulation. The second oil bank produced with

polymer drive 2 signifies transfer of the surfactants from the oil to the water phase, thus improving oil production and lowering surfactant retention.

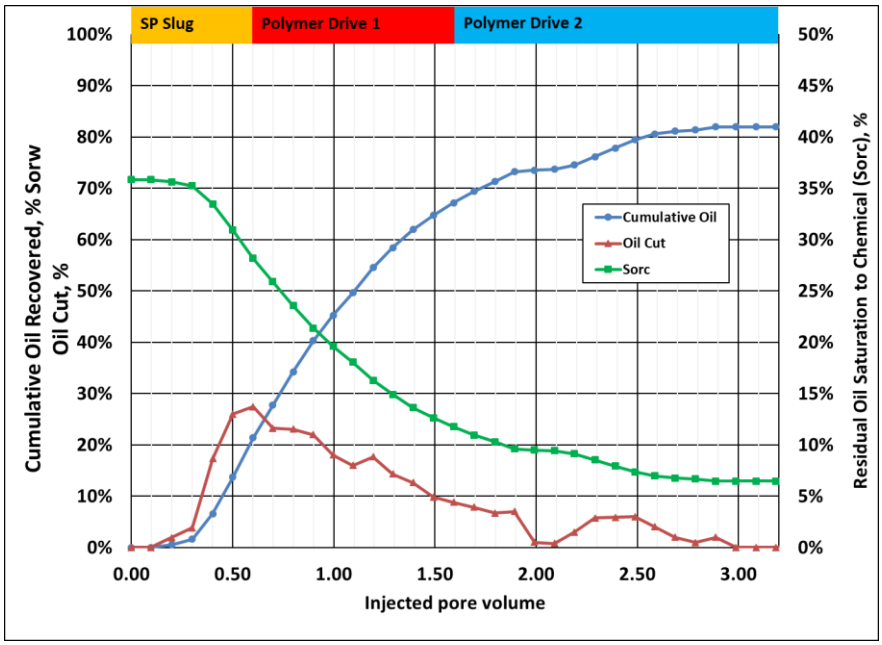

Figure 9.20. Oil recovery, oil cut, and remaining oil saturation for SP coreflood C5

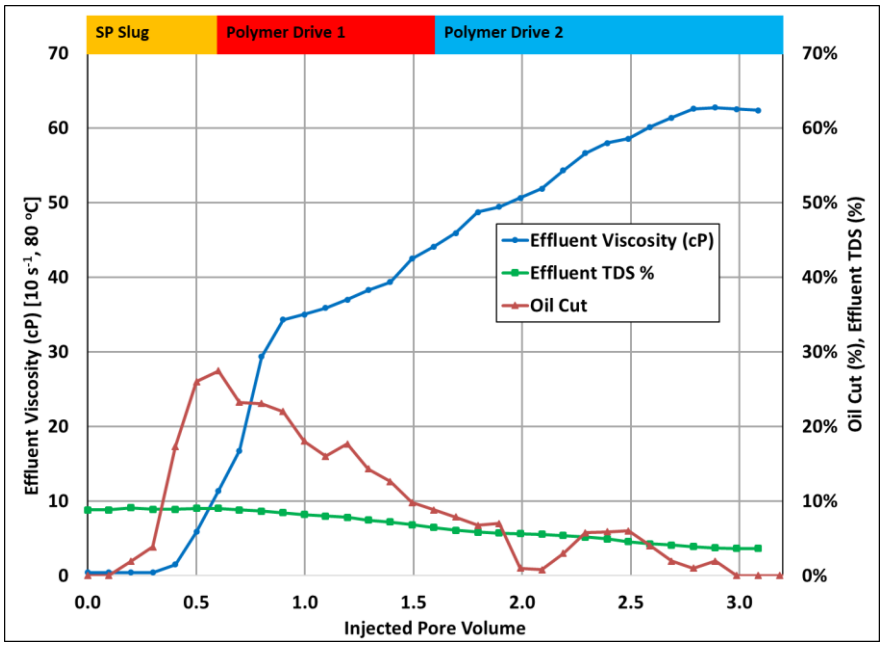

Figure 9.21. Effluent salinity, oil cut, and effluent viscosity for SP coreflood C5

9.2.4.4 Optimization Coreflood

Coreflood C6 was conducted in an outcrop limestone core to investigate the effect of further reduction of surfactant injection on oil production and surfactant retention (core properties listed in **Table 9.16**). The core was waterflooded before injection of the surfactant formulation A2. The detailed injection scheme followed in this experiment is shown in **Table 9.17**. The pH of the solutions injected were buffered around pH ~8.5.

Table 9.16: Rock Properties for SP coreflood C6

Core Properties (Water-wet)		**Indiana Limestone Oil Permeability**	
Diameter (cm)	3.78	**Whole Core (mD)**	348
Length (cm)	29.9	**Section 1 (mD)**	283
Mass (g)	764	**Section 2 (mD)**	292
Bulk Volume (mL)	335.5	**Section 3 (mD)**	409
Porosity	0.14	**Section 4 (mD)**	510
Area (cm^2)	11.22		
Pore Volume (mL)	47.8		
Soi	0.80		

Table 9.15: Injection sequence followed in SP coreflood C6

Fluid Injection Steps	**Pore Volumes**	**Chemical Composition**	**TDS (ppm)**
Waterflood (2 ft/D), pH ~ 8.8	4	Synthetic Injection Brine	92,336 ppm
SP Slug (1 ft/D) 49.9 cP at 80 ^oC (10 s^{-1}), pH ~ 8.8	0.6	0.5% C_{24}-35PO-40EO-COO^- + 0.25% C_{19-23} IOS + 0.25% C_{15-18} IOS + 0.25% Phenol-5EO + Formation Brine + Syn. Injection Brine + 6000 ppm AN125 VHM	79,500 ppm
Polymer Drive (1 ft/D) 72 cP at 80 ^oC (10 s^{-1}), pH ~ 8.7	1.0	Sea-Water Brine + 0.25% Phenol-5EO + 6000 ppm AN125 VHM	30,000 ppm

The initial oil saturation was 80% in coreflood C6 (obtained through vacuum saturation) and aged at 90 ^{o}C for 2 weeks. Waterflood was performed at 2 ft/D for about 4.0 PV, until oil production stopped. The total oil recovery after waterflood was 41% OOIP and the residual oil saturation was 0.47. The lower recovery during waterflood (compared to all the previous corefloods) can be attributed to altered wettability to mixed-wet and verifies our assumption on the requirement of sufficient initial oil saturation for effective wettability alteration from water-wet to oil-wet during aging process.

The 3-component chemical formulation A2 (along with cosolvent) was used in this experiment to investigate the performance of surfactant reduction (47% by weight compared to coreflood C4) and tapered polymer drive salinity in Indiana limestone core. 0.32 PV of SP slug was injected at 1 ft/D followed by polymer drive at reduced salinity for about 2.7 PV at 1 ft/D. **Figure 9.22** shows the oil recovery, the oil cut, and the remaining oil saturation as a function of PV injected. An oil bank was created by the SP slug that broke through early at about 0.4 PV (after chemical injection), a maximum oil cut of about 38% was obtained (lower than that obtained in coreflood C4 but higher than coreflood C5), the oil production tail continued until 3 PV of chemical injection. The additional oil produced due to SP flood was 64% ROIP. The total oil recovery at the end of the experiment was 79% OOIP and the residual oil saturation was about 0.17. The effluent viscosity measurements showed successful polymer transport during the experiment with 100% of the injected viscosity of SP slug recovered at 1.5 PV of fluid injection and 100% of the injected viscosity of PD recovered at 2.7 PV of fluid injection. The pressure drops recorded during the experiment were consistent with the viscosity of the fluids injected and

the oil bank mobilization with final steady state pressure gradient of 5 psi/ft at the end of the coreflood. The effluent salinity and viscosity measurements along with oil cut are shown in **Figure 9.23**. The surfactant retention estimated during this experiment was about 0.22 mg/g of rock since no surfactant was produced in the effluents. The results showed that the performance of this surfactant formulation was significantly lowered with reduction of total surfactant injected by 47%. This suggests that not enough surfactant was present in the core to satisfy the retention and mobilize the residual oil during the coreflood. Hence, this optimization coreflood provides some useful insight on the true estimation of surfactant retention (possibly >= 0.22 mg/grock based on injected surfactant mass) and also the efficiency of the surfactant formulation (in presence of high divalent ions) on incremental oil production during the coreflood based on sufficient injection of surfactant mass.

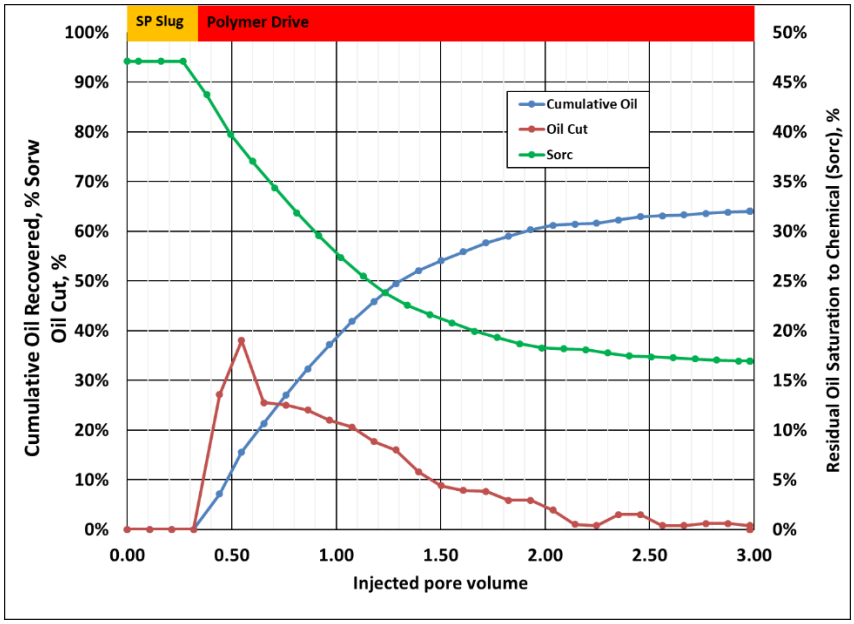

Figure 9.22. Oil recovery, oil cut, and remaining oil saturation for SP coreflood C6

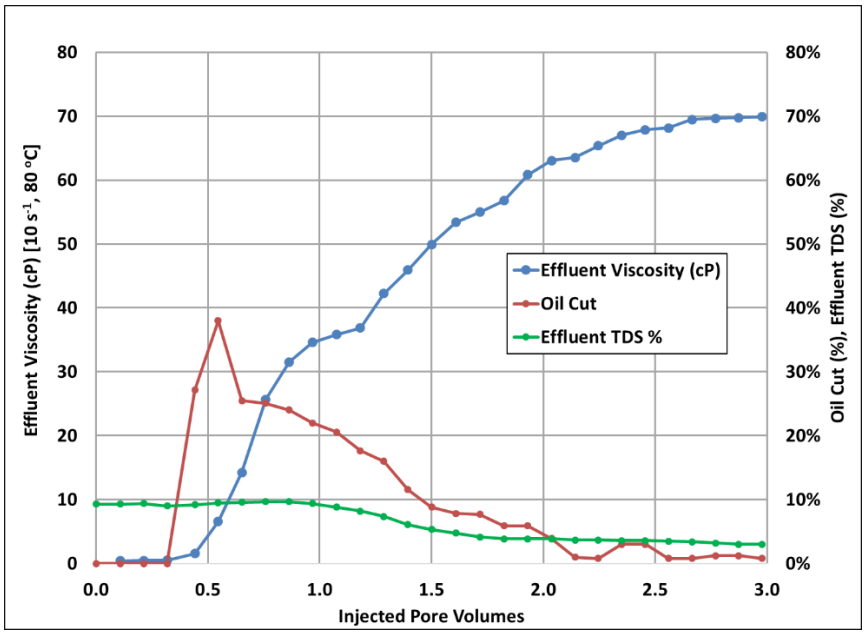

Figure 9.23. Effluent salinity, oil cut, and effluent viscosity for SP coreflood C6

9.3 CONCLUSIONS

This study addresses the challenges of developing ultra-low IFT surfactant-polymer formulations for high salinity (containing high concentration of divalent ions) and high temperature reservoirs. Detailed phase behavior experiments were performed to gain insight in the surfactant brine chemistry at this harsh conditions and possible mechanisms to improve the performance of the surfactant formulations without the use of any alkali. Additional experiments were performed to investigate the surfactant-brine-polymer compatibility and its effect on the performance of the chemical formulation during a coreflood. Single phase polymer flood and surfactant-polymer oil displacements were conducted in Indiana Limestone cores to understand the performance of the chemical formulations and necessary adjustments required to optimize the performance of the chemical floods. This study is unique in developing SP formulations (no alkali) for HTHS

carbonate reservoirs with only use of formation brine and synthetic sea water mix for phase behavior studies and coreflood experiments.

The following conclusions can be made:

- A carboxylate surfactant with a minimum of 30 EO groups and a large hydrophobe was necessary to make the chemical formulation tolerant to high concentrations of divalent ions. Optimization of the hydrophilic-lipophilic balance of the surfactant blends was key to obtaining an ultra-low IFT chemical formulation.
- The polymer increased the optimum solubilization ratio of the surfactant formulation slightly.
- Phase behavior experiments with lower surfactant concentrations, dilution experiments with SP slug - polymer drive and SP slug - injection brine are necessary experiments for robust design of SP floods in carbonates.
- Corefloods experiments showed promising incremental oil recovery over waterflood varying between 77 – 95% ROIP.
- Surfactant retentions during the corefloods were estimated to vary between 0.2 – 0.32 mg/g of rock.
- Total amount of injected surfactant mass should be optimized based on the reduction of performance of the surfactant formulation and cost.
- More optimization experiments can be performed to fine tune the performance of the chemical formulations, to reduce surfactant retentions and improve the performance of the SP technology in high salinity and high temperature carbonate reservoirs.

Chapter 10: Conclusions and Recommendations for Future Work

10.1 CONCLUSIONS

The major conclusions deduced from this study are summarized in this chapter. Foam EOR and chemical EOR processes like polymer (P), alkali surfactant polymer (ASP) and surfactant-polymer (SP) were successfully investigated for applications in challenging carbonate reservoirs (e.g., high temperature - high salinity conditions and low permeability formations). The challenges and benefits of each of these processes have been outlined in this chapter.

Foam is a promising tool to improve sweep efficiency in gas flooded reservoirs. Foam can reduce gas mobility by several orders of magnitude by increasing the apparent gas viscosity and reducing the relative permeability in the porous medium. The discontinuous gas bubbles in liquid lamellae are also effective in conformance control by blocking high permeability channels and diverting the injected fluids to lower permeability channels. Chapters 4 and 5 describe foam technology to improve oil recovery in oil-wet, low permeability carbonate reservoirs.

Chapter 4 focuses on developing foam formulations with anionic surfactants for improving oil recovery in oil-wet low permeability carbonates. Surfactant screening was performed through bulk tests like spontaneous imbibition, contact angle studies on calcite plates, and static foam tests (with and without crude oil) and foam flow experiments (in absence of crude oil) in porous media. Crude oils are typically detrimental to foam stability and negatively affect the foam strength as observed from the qualitative bulk foam tests.

The oil-film on the rock surfaces in an oil-wet carbonate presents a challenge for generation of strong in-situ foams. Hence, a synergistic approach of wettability alteration and foaming seemed to be beneficial for higher performance of these foaming formulations. Another challenge for foam stability was the low permeability of the carbonates that makes the entry pressures to be higher than the critical capillary pressure, thus collapsing the foam rapidly. Low interfacial tension (IFT) helps in lowering the entry pressure for the injected fluids thus increasing foam stability in tight formations. Hence, a combination of ultra-low IFT with wettability alteration and in-situ foaming seemed to be necessary for these challenging rock systems. In-situ foaming through alternating slug injection was investigated as a part of this study. Results showed that mobility reduction factors (compared to water flow) obtained in foam flow experiments, without crude oil, were low (less than 10 in most cases) in tight carbonate cores, signifying that no strong foam can be generated in such low permeability porous media and only coarse foam exists because of high limiting capillary pressure and high critical pressure gradient. Coreflood experiments showed improvement in oil recovery with smaller slug sizes due to better mixing of surfactant and gas in-situ and the results were in agreement with the trend that ultra-low IFT and wettability altering mechanisms are key to higher oil recovery for oil-wet carbonates. Chelating agents can be used in the presence of alkali and divalent ions from formation brine, the resulting calcite dissolution can result in severe formation damage. Hence, a better alternative is foam EOR processes, with the use of non-alkaline surfactant formulations that can prevent formation damage.

Chapter 5 focuses on the use of cationic surfactants, an alternative to anionic surfactants, in combination with zwitterionic surfactants to exploit foaming and wettability alteration properties in surfactant formulations. As established in the previous chapter, wettability alteration was found to be the most important mechanism to stabilize the foam in oil-wet porous media, and good foaming by itself was not very effective. Cationic surfactants showed good wettability altering capabilities and zwitterionic surfactants enhanced the foaming properties of the formulations developed. A positive correlation was obtained between the behavior of the foaming formulations in bulk tests to their performance in porous media, in absence and presence of crude oil. The performance of pre-generated foam through co-injection of surfactants and gas was investigated as part of this study. Results showed presence of weak foam in low permeability carbonate cores, thus verifying the results obtained in the previous chapter. This chapter also summarized the performance of the surfactant formulations after a secondary gasflood and after a waterflood. The efficiency of foam EOR process was estimated using tertiary recovery factors (TRFs) where the factors individually accounted for wettability altering and foaming capabilities of the formulation. On comparing the performances after a secondary gasflood and waterflood, the foaming formulations showed superior performance after a waterflood due to lower residual oil saturation and higher foam stability achieved at lower oil saturations. In summary, the results from Chapters 4 and 5 suggested that it is challenging to obtain strong foam in oil-wet low permeability porous medium and foam EOR processes result in two phase fluid flow where foam lamellae are intermittently stabilized by surfactants. This results in effective fluid diversion and improvement in sweep

efficiency for coreflood experiments performed in the lab scale, but their performance in a field scale with increased heterogeneity and complexity is still not clear. The uncertainties in the foam rheology and their mechanism of flow through challenging porous media makes it challenging for upscaling of foam EOR processes from lab scale to field scale. Thus, a more robust and effective chemical EOR technology, polymer flooding, that can be upscaled to field scale from laboratory studies with more confidence was investigated in the later chapters.

Injection of high molecular weight viscous polymers into low permeability carbonates is challenging due to injectivity issues from plugging of the reservoirs. Hence, mechanical degradation was used as a technique to modify the molecular weight distribution of these polymers to successfully inject into low permeability formations. It is beneficial to use shear degraded high molecular weight polymers compared to low molecular weight polymers to conserve viscosity and reduce the polymer concentration, thus making the process more economical. The polydispersity of the polymer molecules is the primary reason for plugging in the wide distribution of the pore network in carbonates, and mechanical degradation helps to reduce the polydispersity. The results from shear degradation process emphasized the importance of polymer molecular weight, type of monomers, brine salinity, shearing energy in terms of shear speed and shearing time in the mechanism of viscosity degradation and modification of polymer molecular weight. All the viscosity degradations measured at low shear rates suggested exponential decay with increase in shearing time in the blender. Master curves were established to predict the shear degraded viscosity for any given polymer stock in any given brine salinity which had good

agreement with measured viscosities from the rheometer. Also, a superimposed master curve was established for estimating the degradation of different polymers in varying brine salinities which can be helpful for understanding polymer rheology at various reservoir conditions in a laboratory scale. A combination of mechanical degradation along with aggressive filtration through small pore filter papers was investigated to develop a robust protocol to tailor the synthetic polymers for successful injection in low permeability carbonates. Dynamic light scattering (DLS) technique was used to qualitatively estimate the modifications in size distributions of the polymer samples after shear degradation and aggressive filtration. A robust approach of comparison between polymer size distribution from DLS and pore throat distribution from mercury injection capillary pressure (MICP) was suggested as an effective tool for qualification of polymer injection into tight formations. Single phase polymer injection experiments in porous media validated the robust method and the results can be used for upscaling to field scale applications.

A novel class of hydrophobically modified polyacrylamides, also known as associative polymers, were also investigated for injection potential in low permeability carbonates and their performances were compared to the conventional HPAM polymers under similar conditions. Associative polymers showed thermo-thickening effect at higher temperatures and higher salinities due to enhanced hydrophobic interactions between the monomers resulting in the formation of polymer networks. The critical polymer concentration for enhanced network formation was found to be dependent on polymer MW, polymer concentration, associative content, salinity of the brine and temperature. Higher salinity brines (with divalent ions) seemed to promote the polymer network formation, thus

increasing the bulk viscosities contrary to the behavior of coiled conventional polymers. Hence, this behavior of associative polymers can significantly improve upon the performance of HPAM polymers (sulfonated or conventional) in high salinity and high temperature carbonate reservoirs. Interaction between hydrophilic surfactants and hydrophobic monomers led to a reduction in polymer network formation, but still showed evidence of thermo-thickening behavior in moderate to higher salinities and can be used beneficially for chemical EOR applications. Results showed higher resistance to shear degradation for associative polymers compared to HPAM polymers and shear degradation was successfully applied to modify their molecular weight distribution to inject into low permeability carbonate reservoirs. The optimum shearing time in the blender was selected after comparison of the pore throat distribution from MICP and particle size analysis from DLS method, analogous to the method developed in the previous chapter. Based on the estimations from bulk viscosity, significantly higher resistance factors (RF) were obtained even after shear degradation of the polymer stock with reduction in polymer retention after mechanical degradation. The normalized resistance factors (RF*) with respect to bulk viscosity showed a positive correlation with polymer concentration, polymer molecular weight and associative content, and emphasized the apparent high viscosities generated for associative polymers in porous media flow. In summary, understanding the rheology of associative polymers in bulk and flow through porous media has the potential to change the future of polymer flooding in high salinity and high temperature carbonate reservoirs.

The next chapter focuses on the implementation of the polymer treatment protocol developed earlier for successful injection in low permeability carbonates. This novel

approach was combined with the development of ultra-low IFT surfactant formulations through phase behavior experiments for alkali-surfactant-polymer (ASP) and surfactant-polymer (SP) processes. An ultra-low IFT ASP formulation was developed in formation brine with a significant number of divalent ions by using a chelating agent and alkali but showed evidence of formation damage due to strong reaction of EDTA with limestone rocks, as suggested in Chapter 4 for low IFT foaming applications. Hence, an alternative ultra-low IFT SP formulation was developed in the similar formation brine. Coreflood experiments showed significantly high tertiary oil recovery in ASP and SP processes in low permeability carbonates. The surfactant retentions estimated for the ultra-low IFT formulations were between 0.3 and 0.4 mg/gm of rock for both ASP and SP techniques. This showed promising potential of SP technology for EOR applications in carbonate reservoirs with high saline brines.

The last chapter investigated the potential of SP techniques for high temperature and high salinity carbonate reservoirs. A systematic study of phase behavior experiments was performed to understand the surfactant brine chemistry under these harsh conditions and possible mechanisms to improve the performance of the surfactant formulations without the use of any alkali. This study incorporated a unique approach of performing phase behavior experiments and coreflood tests with the blending of sea-water and formation brine. Results obtained from phase behavior tests showed a requirement of a minimum of 30 EO groups in the carboxylate surfactant for higher tolerance to divalent ions and optimization of hydrophilic-lipophilic balance (HLB) is key for ultra-low IFT surfactant formulation. Presence of polymer in phase behavior experiments seemed to

improve the performance of the chemical system and requires more understanding of the underlying mechanism. Also, phase behavior experiments containing lower surfactant concentrations, dilution experiments with SP slug and polymer drive and SP slug and injection brine were necessary experiments for robust design of SP floods in carbonates with varying number of divalent ions. Coreflood experiments showed significantly high tertiary oil recovery after waterflood with surfactant retentions estimated between 0.2 and 0.32 mg/gm of rock, thus making the technology economically viable. Note, the surfactant retentions are negatively affected with higher divalent ions, higher temperature and lower permeability. More experiments can be performed to fine tune the performance of the chemical formulations, to reduce surfactant retentions and improve the performance of the SP technology in high salinity and high temperature carbonate reservoirs.

10.2 RECOMMENDATIONS FOR FUTURE WORK

Based on the experience and technical knowledge gained from this scope of work, the following future work is recommended.

1. Foam stability is known to decrease with decrease in crude oil viscosity. Hence, additional experiments need to be performed to investigate the effect of live oil on surfactant phase behavior experiments and their performance in coreflood experiments as foaming formulations. The performance with live oil would be a more realistic representation of these foam EOR processes in field scale.
2. A systematic study of different foam injection strategies for a similar chemical system would be interesting for more definitive conclusions on the most optimum foam injection method. Foam quality has a predominant role on foam behavior in porous

media and can be a good tuning parameter for optimization of foam EOR processes. Hence, comparison between in-situ foam and pre-generated foam can shed some useful light on the understanding.

3. Additional foam experiments need to be performed in low permeability formations for better understanding of foam behavior in challenging rock systems. A systematic study of varying surfactant concentration, foam quality, injection velocity, temperature and salinity need to be performed for a complete understanding of the foam mechanism. Also, effect of gas type on the performance of foam EOR processes needs to be explored.
4. Due to operational limitation of injection pressure in field scale applications, foam experiments in the lab scale needs to be focused on realistic injection rates and reasonable pressure drops for effective comparison of their performance from lab scale to field scale. Hence, additional oil recovery experiments are necessary with varying injection rates (or pressure drops) for better upscale from lab scale to field scale projects.
5. It would be interesting to compare the performance between foam EOR processes and polymer flooding processes in low permeability carbonates. Hence, coreflood experiments need to be performed with the same chemical system under similar reservoir conditions at similar injection rates with foam and polymer as the mobility control agents. The tertiary oil recovery, after secondary waterflood, would provide useful information on the benefits of the two processes. Finally, an economic analysis can be performed to estimate the applicability of each of these processes.

6. Polymer degradation experiments showed higher degradation rate in high salinity brines compared in DI. But higher salinity brines reduce the viscosity significantly and due to non-Newtonian behavior of the polymers definitive conclusions cannot be made. Hence, additional experiments should be performed with similar viscosity polymer solutions in DI and synthetic sea water to plot degradation with shearing time of the blender and understand the degradation mechanism in different salinity brines. Also, experiments with varying polymer concentration needs to be investigated to understand the effect on concentration on degradation mechanism.
7. It would be interesting to study the effect of varying shearing speeds as a continuation of this work to include into the dataset and possibly develop a master curve to capture the effect of shearing speeds on the degradation mechanism.
8. Upscaling of the laboratory blender experiments to field scale applications is necessary. Hence, capillary flow experiments with similar concentrations of polymer, as used in the blender treatment, in similar brine salinities would be helpful to translate the degradation mechanism in blender to shear rate (or flow rate) degradation in capillary flow. This information can be used to predict the viscosity degradations near well bore and flow through chokes and valves.
9. The novel associative polymers showed significant potential for application in high salinity and high temperature carbonate reservoirs. Additional experiments need to be performed to understand the polymer rheology in porous media, polymer network formation in presence of hydrophilic surfactants, and behavior of polymer rheology in

presence of crude oil. Oil recovery experiments needs to be performed to compare their performance with conventional HPAM polymers for chemical EOR processes.

10. Effect of shear degradation on viscosity degradation, reduced residual resistance factors and resistance factors in low permeability carbonates for associative polymers based on the molecular weight and associative content needs to be studied in detail. The results obtained can be useful in the optimization of polymer dosage based on polymer molecular weight and associative content.
11. Surfactant-polymer (SP) technology showed a high potential for high temperature and high salinity carbonate reservoirs. More phase behavior experiments can be performed to understand the surfactant formulation behavior based on HLB in presence of high divalent ions and also in presence of polymers. Additional coreflood experiments need to be performed to develop a robust design for successful SP processes and optimize the amount of chemical injection, thus making the process economical.

Abbreviation

IFT	Interfacial tension
FQ	Foam quality
OOIP	Original oil in place
EDTA	Ethylenediaminetetraacetic acid
HPLC	High performance liquid chromatography
ROIP	Residual oil in place
MRF	Mobility reduction factor
BPR	Back pressure regulator
WAG	Water alternating gas
SAG	Surfactant alternating gas
PV	Pore volume
WOR	Water-oil ratio
wt%	weight percent
ASP	Alkali Surfactant Polymer
SP	Surfactant Polymer
EPS	Ethylhexanol propoxy sulfate
IC	Ion chromatography
IOS	Internal olefin sulfonates
PS	Alcohol propoxy sulfate
ppm	parts per million
TSPC	Tristyrylphenol propoxy ethoxy carboxylate
MICP	Mercury Injection Capillary Pressure
DLS	Dynamic Light Scattering
RF	Resistance factor
RRF	Residual resistance factor
RK	Permeability reduction
TDS	Total dissolved solids
BT	Blending time (shearing time)

Nomenclature

∇p^{min}	Minimum pressure gradient
Pc*	Critical capillary pressure
γ	Surface tension
k_{rg}	Relative gas permeability
k_{ro}	Relative oil permeability
Nc	Capillary number
Rg	Radius of gyration
Rh	Hydrodynamic radius
$[\eta]$	Intrinsic viscosity
η_{sp}	Specific viscosity
β	Plugging parameter
σ	Solubilization ratio
η_{loss}	Viscosity loss
Γ	Decay constant
D	Diffusion coefficient
μ_{af}	Apparent foam viscosity
Sor_c	Residual oil saturation to chemical
$Sor_{w/g}$	Residual oil saturation to water-gas
$M_{w,ref}$	Reference molecular weight
tmix	Normalized shearing time
τ	Tortuosity
rh	Hydraulic radius
B	Bridging coefficient
S	Spreading coefficient
E	Entering coefficient
L	Lamella numer

References

Aarra, M. G., Ormehaug, P. A., Skauge, A., & Masalmeh, S. K. (2011, January). Experimental study of CO2-and methane-foam using carbonate core material at reservoir conditions. In SPE Middle East Oil and Gas Show and Conference. Society of Petroleum Engineers, SPE 141614-MS.

Abbas, G., Irawan, S., Kumar, S., & Elrayah, A. A. (2013). Improving oil well cement slurry performance using hydroxypropylmethylcellulose polymer. In *Advanced Materials Research* (Vol. 787, pp. 222-227). Trans Tech Publications.

Abidin, A. Z., Puspasari, T., & Nugroho, W. A. (2012). Polymers for enhanced oil recovery technology. *Procedia Chemistry*, *4*, 11-16.

Adibhatla, B., & Mohanty, K. K. (2008). Oil recovery from fractured carbonates by surfactant-aided gravity drainage: laboratory experiments and mechanistic simulations. SPE Reservoir Evaluation & Engineering, 11(01), 119-130.

Adkins, S., Liyanage, P. J., Arachchilage, P., Gayani, W. P., Mudiyanselage, T., Weerasooriya, U., & Pope, G. A. (2010, January). A New Process for Manufacturing and Stabilizing High-Performance EOR Surfactants at Low Cost for High-Temperature, High-Salinity Oil Reservoirs. In *SPE Improved Oil Recovery Symposium*. Society of Petroleum Engineers.

Almajid, M. M., & Kovscek, A. R. (2016). Pore-level mechanics of foam generation and coalescence in the presence of oil. *Advances in colloid and interface science*, *233*, 65-82.

Alvarez, J. O., Neog, A., Jais, A., & Schechter, D. S. (2014, April). Impact of Surfactants for Wettability Alteration in Stimulation Fluids and the Potential for Surfactant EOR in Unconventional Liquid Reservoirs. Proceeding of the SPE Unconventional Resources Conference. 1-3 April, The Woodlands, Texas, USA.

Anderson, W. G. (1987). Wettability literature survey-part 4: Effects of wettability on capillary pressure. *Journal of Petroleum Technology*, *39*(10), 1-283.

Andrianov, A., Farajzadeh, R., Mahmoodi Nick, M., Talanana, M., & Zitha, P. L. (2012). Immiscible foam for enhancing oil recovery: bulk and porous media experiments. Industrial & Engineering Chemistry Research, 51(5), 2214-2226.

Angarska, J. K., Tachev, K. D., Ivanov, I. B., Mehreteab, A., & Brose, G. (1997). Effect of magnesium ions on the properties of foam films stabilized with sodium dodecyl sulfate. *Journal of colloid and interface science*, *195*(2), 316-328.

Arnaudov, L., Denkov, N. D., Surcheva, I., Durbut, P., Broze, G., & Mehreteab, A. (2001). Effect of oily additives on foamability and foam stability. 1. Role of interfacial properties. *Langmuir*, *17*(22), 6999-7010.

Askarinezhad, R., Hatzignatiou, D. G., & Stavland, A. (2017, April). Associative Polymers as Enhanced Oil Recovery Agents in Oil-wet Formations-A Laboratory Approach. In IOR 2017-19th European Symposium on Improved Oil Recovery.

Austad, T., & Milter, J. (1997, January). Spontaneous imbibition of water into low permeable chalk at different wettabilities using surfactants. In International Symposium on Oilfield Chemistry. Society of Petroleum Engineers, SPE 37236-MS.

Awolayo, A.; Sarma, H.; & AlSumaiti, A. (2016). An experimental investigation into the impact of sulfate ions in smart water to improve oil recovery in carbonate reservoirs. Transport in Porous Media, 111(3), 649-668.

Basheva, E. S., Ganchev, D., Denkov, N. D., Kasuga, K., Satoh, N., & Tsujii, K. (2000). Role of betaine as foam booster in the presence of silicone oil drops. *Langmuir*, *16*(3), 1000-1013.

Bataweel, M. A., & Nasr-El-Din, H. A. (2011, January 1). Alternatives to Minimize Scale Precipitation in Carbonate Cores Caused by Alkalis in ASP Flooding in High Salinity/High Temperature Applications. Society of Petroleum Engineers. doi:10.2118/143155-MS

Beneventi, D., Carre, B., & Gandini, A. (2001). Role of surfactant structure on surface and foaming properties. *Colloids and Surfaces A: Physicochemical and Engineering Aspects*, *189*(1-3), 65-73.

Bennetzen, M. V., Gilani, S. F. H., Mogensen, K., Ghozali, M., & Bounoua, N. (2014, November). Successful polymer flooding of low-permeability, oil-wet, carbonate reservoir cores. In Abu Dhabi International Petroleum Exhibition and Conference. Society of Petroleum Engineers.

Bera, A., Ojha, K., & Mandal, A. (2013). Synergistic effect of mixed surfactant systems on foam behavior and surface tension. *Journal of Surfactants and Detergents*, *16*(4), 621-630.

Bergeron, V. (1997). Disjoining pressures and film stability of alkyltrimethylammonium bromide foam films. *Langmuir*, *13*(13), 3474-3482.

Bergeron, V., Fagan, M. E., & Radke, C. J. (1993). Generalized entering coefficients: a criterion for foam stability against oil in porous media. Langmuir, 9(7), 1704-1713.

Bird, R. B., Armstrong, R. C., & Hassager, O. (1987). Dynamics of polymeric liquids. Vol. 1: Fluid mechanics.

Blaker, T., Aarra, M. G., Skauge, A., Rasmussen, L., Celius, H. K., Martinsen, H. A., & Vassenden, F. (2002). Foam for gas mobility control in the Snorre field: the FAWAG project. *SPE Reservoir Evaluation & Engineering*, *5*(04), 317-323.

Boeije, C. S., & Rossen, W. R. (2013, April). Fitting foam simulation model parameters to data. In *IOR 2013-17th European Symposium on Improved Oil Recovery*.

Boud, D. C., & Holbrook, O. C. (1958). *U.S. Patent No. 2,866,507*. Washington, DC: U.S. Patent and Trademark Office.

Bourrel, M., & Chambu, C. (1983). The rules for achieving high solubilization of brine and oil by amphiphilic molecules. Society of Petroleum Engineers Journal, 23(02), 327-338, SPE 10676-PA.

Bourrel, M., & Schechter, R. S. (1988). Microemulsion and Related Systems, No. 30. Surfactant Science Ser.

Bratton, T., Canh, D. V., Van Que, N., Duc, N. V., Gillespie, P., Hunt, D., ... & Nelson, R. (2006). The nature of naturally fractured reservoirs. *Oilfield Review*, *18*(2), 4-23.

Broseta, D., Medjahed, F., Lecourtier, J., & Robin, M. (1995). Polymer adsorption/retention in porous media: effects of core wettability and residual oil. *SPE Advanced Technology Series*, *3*(01), 103-112.

Brownell, L. E., & Katz, D. L. (1947). Flow of fluids through porous media. 1. Single homogeneous fluids. *Chemical Engineering Progress*, *43*(10), 537-548.

Bullen, R. S., & Bratrud, T. F. (1976). Fracturing with foam. *Journal of Canadian Petroleum Technology*, *15*(02).

Caenn, R., Burnett, D. B., & Chilingarian, G. V. (1989). Polymer flooding. In *Developments in Petroleum Science* (Vol. 17, pp. 157-187). Elsevier.

Cao, F., Luo, H., & Lake, L. W. (2015). Oil-rate forecast by inferring fractional-flow models from field data with Koval method combined with the capacitance/resistance model. *SPE Reservoir Evaluation & Engineering*, *18*(04), 534-553.

Caram, Y., Bautista, F., Puig, J. E., & Manero, O. (2006). On the rheological modeling of associative polymers. Rheologica acta, 46(1), 45-57.

Carlisle, C., Al-Maraghi, E., Al-Saad, B., Britton, C., Fortenberry, R., & Pope, G. (2014, April 12). One-Spot Pilot Results in the Sabriyah-Mauddud Carbonate Formation in Kuwait Using a Novel Surfactant Formulation. Society of Petroleum Engineers. doi:10.2118/169153-MS

Carreau, P. J. (1972). Rheological equations from molecular network theories. *Transactions of the Society of Rheology*, *16*(1), 99-127.

Carro, S., Herrera-Ordonez, J., & Castillo-Tejas, J. (2010). On the evolution of the rate of polymerization, number and size distribution of particles in styrene emulsion polymerization above CMC. Journal of Polymer Science Part A: Polymer Chemistry, 48(14), 3152-3160.

Celis, M. T., Forgiarini, A., Briceno, M. I., & García-Rubio, L. H. (2008). Spectroscopy measurements for determination of polymer particle size distribution. Colloids and Surfaces A: Physicochemical and Engineering Aspects, 331(1-2), 91-96.

Chabert, M., Morvan, M., & Nabzar, L. (2012, January). Advanced Screening Technologies for the Selection of Dense CO2 Foaming. In SPE Improved Oil Recovery Symposium. Society of Petroleum Engineers, SPE 154147-MS.

Chambers, K. T., & Radke, C. J. (1990). *Micromodel foam flow study* (No. DOE/SF/00098-T17). California Univ., Berkeley, CA (USA). Dept. of Chemical Engineering.

Chandrasekhar, S., Sharma, H., Mohanty, K.K. (2018). Dependence of wettability on brine composition in high temperature carbonate rocks. Fuel (225): 573-587

Chang, H. L., Zhang, Z. Q., Wang, Q. M., Xu, Z. S., Guo, Z. D., Sun, H. Q., & Qiao, Q. (2006). Advances in polymer flooding and alkaline/surfactant/polymer processes as developed and applied in the People's Republic of China. Journal of petroleum technology, 58(02), 84-89.

Chang, S. H., & Grigg, R. B. (1998, January). Effects of foam quality and flow rate on co2-foam behavior at reservoir conditions. In *SPE/DOE Improved Oil Recovery Symposium*. Society of Petroleum Engineers.

Chilingar, G. V., & Yen, T. F. (1983). Some notes on wettability and relative permeabilities of carbonate reservoir rocks, II. *Energy Sources*, *7*(1), 67-75.

Chou, S. I., Vasicek, S. L., Pisio, D. L., Jasek, D. E., & Goodgame, J. A. (1992, January). CO2 foam field trial at north ward-estes. In *SPE Annual Technical Conference and Exhibition*. Society of Petroleum Engineers.

Cui, L., Ma, K., Puerto, M., Abdala, A. A., Tanakov, I., Lu, L. J., & Hirasaki, G. (2016). Mobility of ethomeen C12 and carbon dioxide (CO 2) foam at high temperature/high salinity and in carbonate cores. SPE Journal, 21(04), 1-151, SPE 179726-PA.

Dann, M. W., Burnett, D. B., & Hall, L. M. (1982, January). Polymer performance in low permeability reservoirs. In SPE Oilfield and Geothermal Chemistry Symposium. Society of Petroleum Engineers.

Das, A., Nguyen, N., Farajzadeh, R., Southwick, J. G., Vicent-Bonnieu, S., Khaburi, S., & Nguyen, Q. P. (2018, March). Laboratory Study of Injection Strategy for Low-Tension-Gas Flooding in High Salinity, Tight Carbonate Reservoirs. In SPE EOR Conference at Oil and Gas West Asia. Society of Petroleum Engineers, SPE 190348-MS.

Das, A., Nguyen, N., Alkindi, A., Farajzadeh, R., Azri, N., Southwick, J., Vicent-Bonnieu, S., Nguyen, Q. P. (2016, March). Low Tension Gas Process in High Salinity and Low Permeability Reservoirs. Society of Petroleum Engineers, SPE 179839-MS.

Davison, P., & Mentzer, E. (1982). Polymer flooding in North Sea reservoirs. *Society of Petroleum Engineers Journal*, *22*(03), 353-362.

Delamaide, E., Tabary, R., & Rousseau, D. (2014, March). Chemical EOR in low permeability reservoirs. In SPE EOR Conference at Oil and Gas West Asia. Society of Petroleum Engineers.

Delamaide, E., Zaitoun, A., Renard, G., & Tabary, R. (2014). Pelican Lake field: first successful application of polymer flooding in a heavy-oil reservoir. SPE Reservoir Evaluation & Engineering, 17(03), 340-354.

Denkov, N. D. (2004). Mechanisms of foam destruction by oil-based antifoams. Langmuir, 20(22), 9463-9505.

Derjaguin, B. (1940). On the repulsive forces between charged colloid particles and on the theory of slow coagulation and stability of lyophobe sols. *Transactions of the Faraday Society*, *35*, 203-215.

Dicksen, T., Hirasaki, G. J., & Miller, C. A. (2002, January). Conditions for foam generation in homogeneous porous media. In *SPE/DOE Improved Oil Recovery Symposium*. Society of Petroleum Engineers.

Doe, P. H., Moradi-Araghi, A., Shaw, J. E., & Stahl, G. A. (1987). Development and evaluation of EOR polymers suitable for hostile environments part 1: Copolymers of vinylpyrrolidone and acrylamide. *SPE Reservoir Engineering*, *2*(04), 461-467.

Dominguez, J. G., & Willhite, G. P. (1977). Retention and flow characteristics of polymer solutions in porous media. Society of Petroleum Engineers Journal, 17(02), 111-121.

Dong, P., Puerto, M., Ma, K., Mateen, K., Ren, G., Bourdarot, G., & Hirasaki, G. (2017, April). Low-interfacial-tension foaming system for enhanced oil recovery in highly heterogeneous/fractured carbonate reservoirs. In *SPE international conference on oilfield chemistry*. Society of Petroleum Engineers.

Driver, J. W. (2017). Tailoring polymer molecular weight distribution to pore size distribution using filtration and mechanical degradation (MS Thesis), UT Austin

Dupuis, G., Antignard, S., Giovannetti, B., Gaillard, N., Jouenne, S., Bourdarot, G., & Zaitoun, A. (2017, November). A New Thermally Stable Synthetic Polymer for Harsh Conditions of Middle East Reservoirs. Part I. Thermal Stability and Injection in Carbonate Cores. In SPE Abu Dhabi International Petroleum Exhibition & Conference. Society of Petroleum Engineers, SPE 188479-MS.

Dupuis, G., Rousseau, D., Tabary, R., Argillier, J. F., & Grassl, B. (2012). Hydrophobically modified sulfonated polyacrylamides for IOR: correlations between associative behavior and injectivity in the diluted regime. *Oil & Gas Science and Technology–Revue d'IFP Energies nouvelles*, *67*(6), 903-919.

Dupuis, G., Rousseau, D., Tabary, R., & Grassl, B. (2011). Flow of hydrophobically modified water-soluble-polymer solutions in porous media: New experimental insights in the diluted regime. Spe Journal, 16(01), 43-54.

Du Petrole, F., & Malmaison, F. R. (1990). Evaluation of reservoir wettability and its effect on oil recovery. In *Interfacial Phenomena in Petroleum Recovery* (p. 319). CRC Press Boca Raton, FL.

Enick, R. M., Olsen, D. K., Ammer, J. R., & Schuller, W. (2012, January). Mobility and Conformance Control for CO2 EOR via Thickeners, Foams, and Gels--A Literature Review of 40 Years of Research and Pilot Tests. In *SPE improved oil recovery symposium*. Society of Petroleum Engineers.

Ettinger, R. A., & Radke, C. J. (1992). Influence of texture on steady foam flow in Berea sandstone. SPE reservoir engineering, 7(01), 83-90, SPE 19688-PA.

Faisal, A., Bisdom, K., Zhumabek, B., Zadeh, A. M., & Rossen, W. R. (2009, January). Injectivity and gravity segregation in WAG and SWAG enhanced oil recovery. In *SPE Annual Technical Conference and Exhibition*. Society of Petroleum Engineers.

Falls, A. H., Thigpen, D. R., Nelson, R. C., Ciaston, J. W., Lawson, J. B., Good, P. A., & Shahin, G. T. (1994). Field test of cosurfactant-enhanced alkaline flooding. SPE Reservoir Engineering, 9(03), 217-223.

Falls, A. H., Hirasaki, G. J., Patzek, T. E. A., Gauglitz, D. A., Miller, D. D., & Ratulowski, T. (1988). Development of a mechanistic foam simulator: the population balance and generation by snap-off. *SPE reservoir engineering*, *3*(03), 884-892.

Falls, A. H., Musters, J. J., & Ratulowski, J. (1989). The apparent viscosity of foams in homogeneous bead packs. *SPE Reservoir Engineering*, *4*(02), 155-164.

Farajzadeh, R., Lotfollahi, M., Eftekhari, A. A., Rossen, W. R., & Hirasaki, G. J. H. (2015). Effect of permeability on implicit-texture foam model parameters and the limiting capillary pressure. *Energy & fuels*, *29*(5), 3011-3018.

Farajzadeh, R., Andrianov, A., & Zitha, P. L. J. (2009). Investigation of immiscible and miscible foam for enhancing oil recovery. *Industrial & Engineering Chemistry Research*, *49*(4), 1910-1919.

Farajzadeh, R., Andrianov, A., Krastev, R., Hirasaki, G. J., & Rossen, W. R. (2012). Foam–oil interaction in porous media: Implications for foam assisted enhanced oil recovery. *Advances in colloid and interface science*, *183*, 1-13.

Fletcher, A. J. P., & Morrison, G. R. (2008, January). Developing a Chemical EOR Pilot Strategy for a Complex, Low-Permeability Water Flood. In SPE Symposium on Improved Oil Recovery. Society of Petroleum Engineers.

Fortenberry, R., Kim, D. H., Nizamidin, N., Adkins, S., Arachchilage, G. W., Koh, H. S., & Pope, G. A. (2015). Use of cosolvents to improve alkaline/polymer flooding. *SPE Journal*, *20*(02), 255-266.

Frankema, W., van Bruijnsvoort, M., Tijssen, R., & Kok, W. T. (2002). Characterisation of core-shell latexes by flow field-flow fractionation with multi-angle light scattering detection. Journal of Chromatography A, 943(2), 251-261.

Friedmann, F., Chen, W. H., & Gauglitz, P. A. (1991). Experimental and simulation study of high-temperature foam displacement in porous media. *SPE reservoir engineering*, *6*(01), 37-45.

Fuseni, A. B., Julaih, A. H., Al-Aseeri, A. A., & AlSofi, A. M. (2017, March). Development and Evaluation of Foam-Based Conformance Control for a High Salinity and High Temperature Carbonate. *In SPE Middle East Oil & Gas Show and Conference*. Society of Petroleum Engineers.

Fuseni, A., Han, M., & Al-Aseeri, A. (2014, March). Evaluation of Foaming Agents for EOR Application in Carbonate Reservoirs. In *SPE EOR Conference at Oil and Gas West Asia*. Society of Petroleum Engineers.

Gaillard, N., Giovannetti, B., Leblanc, T., Thomas, A., Braun, O., & Favero, C. (2015, November). Selection of customized polymers to enhance oil recovery from high temperature reservoirs. In SPE Latin American and Caribbean petroleum engineering conference. Society of Petroleum Engineers, SPE 177073-MS.

Gaillard, N., Sanders, D. B., & Favero, C. (2010, January). Improved oil recovery using thermally and chemically protected compositions based on co-and ter-polymers containing acrylamide. In *SPE improved oil recovery symposium*. Society of Petroleum Engineers.

Gauglitz, P. A., Friedmann, F., Kam, S. I., & Rossen, W. R. (2002, January). Foam Generation in Porous Media. Society of Petroleum Engineers, SPE 75177-MS.

Gdanski, R. D. (1993). Experience and research show best designs for foam-diverted acidizing. *Oil and Gas Journal;(United States)*, *91*(36).

Ghosh, P., & Mohanty, K. K. (2019a). Study of surfactant alternating gas injection (SAG) in gas-flooded oil-wet, low permeability carbonate rocks. *Fuel*, *251*, 260-275.

Ghosh, P., Sharma, H., & Mohanty, K. K. (2019). ASP flooding in tight carbonate rocks. *Fuel*, *241*, 653-668.

Ghosh, P., & Mohanty, K. K. (2018). Novel application of cationic surfactants for foams with wettability alteration in oil-wet low-permeability carbonate rocks. SPE Journal, SPE 179598-PA.

Ghosh, P., Sharma, H., & Mohanty, K. K. (2018, September). Development of Surfactant-Polymer SP Processes for High Temperature and High Salinity Carbonate Reservoirs. In SPE Annual Technical Co nference and Exhibition. Society of Petroleum Engineers, SPE 191733-MS.

Ghosh, P., & Mohanty, K. K. (April, 2019b). Study of Surfactant-Polymer Flooding in High Temperature High Salinity Carbonate Rocks. Energy & Fuels, Accepted. 10.1021/acs.energyfuels.9b00407

Glover, C. J., Puerto, M. C., Maerker, J. M., & Sandvik, E. L. (1979). Surfactant phase behavior and retention in porous media. Society of Petroleum Engineers Journal, 19(03), 183-193, SPE 7053-PA.

Gogarty, W. B. (1967). Mobility control with polymer solutions. *Society of Petroleum Engineers Journal*, *7*(02), 161-173.

Green, D. W., & Willhite, G. P. (1998). Enhanced oil recovery (Vol. 6, pp. 143-154). Richardson, TX: Henry L. Doherty Memorial Fund of AIME, Society of Petroleum Engineers.

Guo, H., Faber, M. J., Buijse, M. A., & Zitha, P. L. (2011, January). A novel alkaline-surfactant-foam EOR process. In SPE Enhanced Oil Recovery Conference. Society of Petroleum Engineers, SPE 145043-MS.

Gupta, R., & Mohanty, K. (2010). Temperature effects on surfactant-aided imbibition into fractured carbonates. *SPE Journal*, *15*(03), 588-597.

Gupta, R., & Mohanty, K. (2010). Temperature effects on surfactant-aided imbibition into fractured carbonates. SPE Journal, 15(03), 588-597, SPE 110204-PA.

Hadjiiski, A., Tcholakova, S., Denkov, N. D., Durbut, P., Broze, G., & Mehreteab, A. (2001). Effect of oily additives on foamability and foam stability. 2. Entry barriers. *Langmuir*, *17*(22), 7011-7021.

Han, X., Zhang, G., Yu, J., Chen, Z., & Kurnia, I. (2018, April). An Investigation of Retention and Unusually High Apparent Viscosity of Hydrophobically Associative Polymer in Porous Media. In SPE Improved Oil Recovery Conference. Society of Petroleum Engineers.

Han, M., AlSofi, A., Fuseni, A., Zhou, X., & Hassan, S. (2013). Development of chemical EOR formulations for a high temperature and high salinity carbonate reservoir. In IPTC 2013: International Petroleum Technology Conference.

Han, M., Xiang, W., Zhang, J., Jiang, W., & Sun, F. (2006, January). Application of EOR technology by means of polymer flooding in Bohai Oilfields. In International Oil & Gas Conference and Exhibition in China. Society of Petroleum Engineers.

Haugen, A., Fernø, M. A., Graue, A., & Bertin, H. J. (2012). Experimental study of foam flow in fractured oil-wet limestone for enhanced oil recovery. *SPE Reservoir Evaluation & Engineering*, *15*(02), 218-228.

Haugen, Å., Mani, N., Svenningsen, S., Brattekås, B., Graue, A., Ersland, G., & Fernø, M. A. (2014). Miscible and immiscible foam injection for mobility control and EOR in fractured oil-wet carbonate rocks. *Transport in porous media*, *104*(1), 109-131.

He, L., Gang, C., & Guochen, S. (2007, January). Technical Breakthrough in PCPs' Scaling Issue of ASP Flooding in Daqing Oilfield. In SPE Annual Technical Conference and Exhibition. Society of Petroleum Engineers, SPE 109165-MS.

Healy, R. N., & Reed, R. L. (1977). Immiscible microemulsion flooding. *Society of Petroleum Engineers Journal*, *17*(02), 129-139.

Hinterwirth, H., Wiedmer, S. K., Moilanen, M., Lehner, A., Allmaier, G., Waitz, T., & Lämmerhofer, M. (2013). Comparative method evaluation for size and size-distribution analysis of gold nanoparticles. Journal of separation science, 36(17), 2952-2961.

Hirasaki, G. J., Miller, C. A., & Puerto, M. (2008). Recent advances in surfactant EOR. In SPE Annual Technical Conference and Exhibition. Society of Petroleum Engineers.

Hirasaki, G. J., Miller, C. A., Szafranski, R., Lawson, J. B., & Akiya, N. (1997, January). Surfactant/foam process for aquifer remediation. In *International symposium on oilfield chemistry*. Society of Petroleum Engineers.

Hirasaki, G. J., & Lawson, J. B. (1985). Mechanisms of foam flow in porous media: apparent viscosity in smooth capillaries. Society of Petroleum Engineers Journal, 25(02), 176-190, SPE 12129-PA.

Holm, L. W. (1968). The mechanism of gas and liquid flow through porous media in the presence of foam. *Society of Petroleum Engineers Journal*, *8*(04), 359-369.

Hourdet, D., L'alloret, F., & Audebert, R. (1997). Synthesis of thermoassociative copolymers. *Polymer*, *38*(10), 2535-2547.

Huang, B., Zhang, W., Xu, R., Shi, Z., Fu, C., Wang, Y., & Song, K. (2017). A Study on the Matching Relationship of Polymer Molecular Weight and Reservoir Permeability in ASP Flooding for Duanxi Reservoirs in Daqing Oil Field. Energies, 10(7), 951.

Huang, Y., & Sorbie, K. S. (1993). Scleroglucan behavior in flow through porous media: comparison of adsorption and in-situ rheology with xanthan. In SPE International Symposium on Oilfield Chemistry. Society of Petroleum Engineers, SPE 25173-MS.

Huh, C. (1979). Interfacial tensions and solubilizing ability of a microemulsion phase that coexists with oil and brine. Journal of Colloid and Interface Science, 71(2), 408-426.

Hunkeler, D., Nguyen, T. Q., & Kausch, H. H. (1996). Polymer solutions under elongational flow: 1. Birefringence characterization of transient and stagnation point elongational flows. Polymer, 37(19), 4257-4269.

Hutchins, R. D., & Miller, M. J. (2005). A circulating foam loop for evaluating foam at conditions of use. *SPE Production & Facilities*, *20*(04), 286-294.

Jabbar, M. Y., Al Sowaidi, A., Al Obeidli, A., Willingham, T. W., Britton, C., Adkins, S., & Teletzke, G. F. (2017, November). Chemical Formulation Design in High Salinity, High Temperature Carbonate Reservoir for a Super Giant Offshore Field in Middle East. In SPE Abu Dhabi International Petroleum Exhibition & Conference. Society of Petroleum Engineers, SPE 188604-MS.

Jang, S. H., Liyanage, P. J., Tagavifar, M., Chang, L., Upamali, K. A., Lansakara-P, D., & Pope, G. A. (2016, April). A systematic method for reducing surfactant retention to extremely low levels. In *SPE Improved Oil Recovery Conference*. Society of Petroleum Engineers.

Jennings, R. R., Rogers, J. H., & West, T. J. (1971). Factors influencing mobility control by polymer solutions. *Journal of Petroleum Technology*, *23*(03), 391-401.

Jensen, T., Kadhum, M., Kozlowicz, B., Sumner, E. S., Malsam, J., Muhammed, F., & Ravikiran, R. (2018, April). Chemical EOR Under Harsh Conditions: Scleroglucan As A Viable Commercial Solution. In *SPE Improved Oil Recovery Conference*. Society of Petroleum Engineers.

Jensen, J. A., & Friedmann, F. (1987, January). Physical and chemical effects of an oil phase on the propagation of foam in porous media. In SPE california regional meeting. Society of Petroleum Engineers, SPE 16375-MS.

Jones, S. A., Van Der Bent, V., Farajzadeh, R., Rossen, W. R., & Vincent-Bonnieu, S. (2016). Surfactant screening for foam EOR: Correlation between bulk and core-flood experiments. Colloids and Surfaces A: Physicochemical and Engineering Aspects, 500, 166-176.

Jones, M. A. (1966). Waterflood mobility control: a case history. Journal of Petroleum Technology, 18(09), 1-151.

Jouenne, S., Chakibi, H., & Levitt, D. (2018). Polymer stability after successive mechanical-degradation events. SPE Journal, 23(01), 18-33.

Jouenne, S., Heurteux, G., Hourcq, C., Joly, M., Questel, M., Levache, B. (2019, April). Universal Viscosifying Behavior of Acrylamide-based Polymers Used in EOR –

Application for QA/QC, Viscosity Predictions and Field Characterization. In 20th European Symposium on Improved Oil Recovery. EAGE

Jouenne, S., Chakibi, H., & Levitt, D. (2015, April). Polymer Stability Following Successive Mechanical Degradation Events. In *IOR 2015-18th European Symposium on Improved Oil Recovery*.

Kahrobaei, S., Vincent-Bonnieu, S., & Farajzadeh, R. (2017). Experimental study of hysteresis behavior of foam generation in porous media. Scientific Reports, 7(1), 8986.

Kalfoglou, G. (1977). U.S. Patent No. 4,016,932. Washington, DC: U.S. Patent and Trademark Office.

Kapetas, L., Bonnieu, S. V., Danelis, S., Rossen, W. R., Farajzadeh, R., Eftekhari, A. A., ... & Bahrim, R. K. (2016). Effect of temperature on foam flow in porous media. *Journal of Industrial and Engineering Chemistry*, *36*, 229-237.

Kato, H., Nakamura, A., Takahashi, K., & Kinugasa, S. (2012). Accurate size and size-distribution determination of polystyrene latex nanoparticles in aqueous medium using dynamic light scattering and asymmetrical flow field flow fractionation with multi-angle light scattering. Nanomaterials, 2(1), 15-30.

Kazempour, M., Manrique, E. J., Alvarado, V., Zhang, J., & Lantz, M. (2013). Role of active clays on alkaline–surfactant–polymer formulation performance in sandstone formations. Fuel, 104, 593-606.

Khatib, Z. I., Hirasaki, G. J., & Falls, A. H. (1988). Effects of capillary pressure on coalescence and phase mobilities in foams flowing through porous media. SPE reservoir engineering, 3(03), 919-926, SPE 15442-PA.

Kloet, M., Renkema, W. J., & Rossen, W. R. (2009, January). Optimal design criteria for sag foam processes in heterogeneous reservoirs. In *EUROPEC/EAGE conference and exhibition*. Society of Petroleum Engineers.

Koval, E. J. (1963). A method for predicting the performance of unstable miscible displacement in heterogeneous media. *Society of Petroleum Engineers Journal*, *3*(02), 145-154.

Kovscek, A. R., & Radke, C. J. (1993). Fundamentals of foam transport in porous media (No. DOE/BC-93000174). Lawrence Berkeley Lab., CA (United States).

Kovscek, A. R., Patzek, T. W., & Radke, C. J. (1994). Mechanistic prediction of foam displacement in multidimensions: A population balance approach. SPE 27789-MS, *SPE/DOE Improved Oil Recovery Symposium*, Tulsa. 17-20 April.

Kulawardana, E. U., Koh, H., Kim, D. H., Liyanage, P. J., Upamali, K., Huh, C., & Pope, G. A. (2012, January). Rheology and transport of improved EOR polymers under harsh reservoir conditions. In SPE improved oil recovery symposium. Society of Petroleum Engineers.

Kumar, S., & Mandal, A. (2017). Rheological properties and performance evaluation of synthesized anionic polymeric surfactant for its application in enhanced oil recovery. *Polymer*, *120*, 30-42.

Lake, L. W., & Venuto, P. B. (1990). A niche for enhanced oil recovery in the 1990s. Oil & Gas Journal, 88(17), 62-67.

Lara-Ceniceros, A. C., Rivera-Vallejo, C., & Jiménez-Regalado, E. J. (2007). Synthesis, characterization and rheological properties of three different associative polymers obtained by micellar polymerization. Polymer Bulletin, 58(2), 425-433.

Lawson, J. B., & Reisberg, J. (1980, January). Alternate slugs of gas and dilute surfactant for mobility control during chemical flooding. In *SPE/DOE enhanced oil recovery symposium*. Society of Petroleum Engineers.

Lee, H. O., Heller, J. P., & Hoefer, A. M. W. (1991). Change in apparent viscosity of CO2 foam with rock permeability. *SPE reservoir engineering*, *6*(04), 421-428.

Leonhardt, B., Ernst, B., Reimann, S., Steigerwald, A., & Lehr, F. (2014). Field testing the polysaccharide schizophyllan: results of the first year. In SPE Improved Oil Recovery Symposium. Society of Petroleum Engineers, SPE 169032-MS.

Levitt, D., Klimenko, A., Jouenne, S., Chamerois, M., & Bourrel, M. (2013, March). Overcoming design challenges of chemical EOR in high-temperature, high salinity carbonates. In SPE Middle East Oil and Gas Show and Conference. Society of Petroleum Engineers.

Levitt, D., Dufour, S., Pope, G. A., Morel, D. C., & Gauer, P. R. (2011, January). Design of an ASP flood in a high-temperature, high-salinity, low-permeability carbonate. In International Petroleum Technology Conference. International Petroleum Technology Conference.

Levitt, D., & Pope, G. A. (2008, January). Selection and screening of polymers for enhanced-oil recovery. In SPE Symposium on Improved Oil Recovery. Society of Petroleum Engineers.

Levitt, D., Jackson, A., Heinson, C., Britton, L. N., Malik, T., Dwarakanath, V., & Pope, G. A. (2006). Identification and evaluation of high-performance EOR surfactants. In SPE/DOE Symposium on Improved Oil Recovery. Society of Petroleum Engineers.

Li, R. F., Hirasaki, G. J., Miller, C. A., & Masalmeh, S. K. (2011, April). Wettability Alteration and Foam Mobility Control in a Layered 2-D Heterogeneous System. SPE 141462-MS in. In SPE International Symposium on Oilfield Chemistry.

Li, R. F., Hirasaki, G., Miller, C. A., & Masalmeh, S. K. (2012). Wettability Alteration and Foam Mobility Control in a Layered, 2D Heterogeneous Sandpack. SPE journal, 17(04), 1-207, SPE 141462-PA.

Li, S., Li, Z., & Li, B. (2011). Experimental study and application on profile control using high-temperature foam. *Journal of Petroleum Science and Engineering*, *78*(3-4), 567-574.

Li, Q., & Rossen, W. R. (2005, January). Injection strategies for foam generation in homogeneous and layered porous media. In *SPE annual technical conference and exhibition*. Society of Petroleum Engineers.

Liontas, R., Ma, K., Hirasaki, G. J., & Biswal, S. L. (2013). Neighbor-induced bubble pinch-off: novel mechanisms of in situ foam generation in microfluidic channels. *Soft Matter*, *9*(46), 10971-10984.

Liu, S., Zhang, D., Yan, W., Puerto, M., Hirasaki, G. J., & Miller, C. A. (2008). Favorable attributes of alkaline-surfactant-polymer flooding. SPE Journal, 13(01), 5-16, SPE 99744-PA.

Liu, Y., Grigg, R. B., & Bai, B. (2005, January). Salinity, pH, and surfactant concentration effects on CO2-foam. In *SPE International Symposium on Oilfield Chemistry*. Society of Petroleum Engineers.

Liyanage, P. J., Solairaj, S., Pinnawala Arachchilage, G., Linnemeyer, H. C., Kim, D. H., Weerasooriya, U., & Pope, G. A. (2012, January). Alkaline surfactant polymer flooding using a novel class of large hydrophobe surfactants. In *SPE Improved Oil Recovery Symposium*. Society of Petroleum Engineers.

Lu, J., Liyanage, P. J., Solairaj, S., Adkins, S., Arachchilage, G. P., Kim, D. H., & Pope, G. A. (2013). Recent technology developments in surfactants and polymers for enhanced

oil recovery. In International Petroleum Technology Conference. International Petroleum Technology Conference.

Lu, J., Goudarzi, A., Chen, P., Kim, D. H., Delshad, M., Mohanty, K. K., & Pope, G. A. (2014). Enhanced oil recovery from high-temperature, high-salinity naturally fractured carbonate reservoirs by surfactant flood. Journal of Petroleum Science and Engineering, 124, 122-131.

Lu, J., Liyanage, P. J., Solairaj, S., Adkins, S., Arachchilage, G. P., Kim, D. H., & Pope, G. A. (2014). New surfactant developments for chemical enhanced oil recovery. Journal of Petroleum Science and Engineering, 120, 94-101.

Lu, J., Britton, C., Solairaj, S., Liyanage, P. J., Kim, D. H., Adkins, S., & Pope, G. A. (2014). Novel large-hydrophobe alkoxy carboxylate surfactants for enhanced oil recovery. *SPE Journal*, *19*(06), 1-024.

Lyons, W. C., & Plisga, G. J. (2011). *Standard handbook of petroleum and natural gas engineering*. Elsevier.

Ma, K. (2013). Transport of surfactant and foam in porous media for enhanced oil recovery processes (Doctoral dissertation, Rice University).

Maerker, J. M. (1975). Shear degradation of partially hydrolyzed polyacrylamide solutions. *Society of Petroleum Engineers Journal*, *15*(04), 311-322.

Mahani, H., Keya, A. L., Berg, S., Bartels, W. B., Nasralla, R., & Rossen, W. R. (2015). Insights into the Mechanism of Wettability Alteration by Low-Salinity Flooding (LSF) in Carbonates. *Energy & Fuels*, *29*(3), 1352-1367.

Maia, A. M., Borsali, R., & Balaban, R. C. (2009). Comparison between a polyacrylamide and a hydrophobically modified polyacrylamide flood in a sandstone core. Materials Science and Engineering: C, 29(2), 505-509.

Makan, A. C., Spallek, M. J., du Toit, M., Klein, T., & Pasch, H. (2016). Advanced analysis of polymer emulsions: Particle size and particle size distribution by field-flow fractionation and dynamic light scattering. Journal of Chromatography A, 1442, 94-106.

Mamun, C. K., Rong, J. G., Kam, S. I., Liljestrand, H. M., & Rossen, W. R. (2002, January). Extending foam technology from improved oil recovery to environmental remediation. In *SPE Annual Technical Conference and Exhibition*. Society of Petroleum Engineers.

Manichand, R. N., & Seright, R. (2014). Field vs. laboratory polymer-retention values for

a polymer flood in the Tambaredjo field. *SPE Reservoir Evaluation & Engineering*, *17*(03), 314-325.

Mannhardt, K., Novosad, J. J., & Schramm, L. L. (2000). Comparative evaluation of foam stability to oil. SPE Reservoir Evaluation & Engineering, 3(01), 23-34, SPE 60686-PA.

Mansour, A. M., Al-Maamari, R. S., Al-Hashmi, A. S., Zaitoun, A., & Al-Sharji, H. (2014). In-situ rheology and mechanical degradation of EOR polyacrylamide solutions under moderate shear rates. *Journal of Petroleum Science and Engineering*, *115*, 57-65.

Martin, F. D. (1974, January). Laboratory investigations in the use of polymers in low permeability reservoirs. In Fall Meeting of the Society of Petroleum Engineers of AIME. Society of Petroleum Engineers.

Mast, R. F. (1972). Microscopic behavior of foam in porous media. SPE-3997-MS, *Fall Meeting of the Society of Petroleum Engineers of AIME*. San Antonio, 8-11 October.

Matthews, C. S. (1989). Carbon dioxide flooding. In *Developments in Petroleum Science* (Vol. 17, pp. 129-156). Elsevier.

Maubert, M., Jith Liyanage, P., Pope, G., Upamali, N., Chang, L., Ren, G., Morel, D. (2018, April 14). ASP Experiments in Indiana Limestone using NaOH to Reduce Surfactant Retention. Society of Petroleum Engineers. doi:10.2118/190187-MS

McGuire, P. L., & Stalkup, F. I. (1995). Performance analysis and optimization of the Prudhoe Bay miscible gas project. SPE Reservoir Engineering, 10(02), 88-93, SPE 22398-PA.

McGrath, J. G., Bock, R. D., Cathcart, J. M., & Lyon, L. A. (2007). Self-assembly of "paint-on" colloidal crystals using poly (styrene-co-N-isopropylacrylamide) spheres. *Chemistry of Materials*, *19*(7), 1584-1591.

Mohan, K., Gupta, R., & Mohanty, K. K. (2011). Wettability altering secondary oil recovery in carbonate rocks. *Energy & Fuels*, *25*(9), 3966-3973.

Montaron, B. (2005, October). Increasing Oil Recovery Factors: A Technical Challenge Key to Future World Energy Supply. In AFTP Conference, Paris.

Moradi-Araghi, A., & Doe, P. H. (1987). Hydrolysis and precipitation of polyacrylamides in hard brines at elevated temperatures. *SPE reservoir Engineering*, *2*(02), 189-198.

Morel, D. C., Jouenne, S., VERT, M., & Nahas, E. (2008, January). Polymer injection in deep offshore field: the Dalia Angola case. In SPE Annual Technical Conference and Exhibition. Society of Petroleum Engineers.

Morel, D. C., Vert, M., Jouenne, S., Gauchet, R. R. M., & Bouger, Y. (2010, January). First polymer injection in deep offshore field Angola: recent advances on Dalia/Camelia field case. In SPE annual technical conference and exhibition. Society of Petroleum Engineers.

Mungan, N., Smith, F. W., & Thompson, J. L. (1966). Some aspects of polymer floods. *Journal of Petroleum Technology*, *18*(09), 1-143.

Nelson, R. C., & Pope, G. A. (1978). Phase relationships in chemical flooding. *Society of Petroleum Engineers Journal*, *18*(05), 325-338.

Nelson, R. C., Lawson, J. B., Thigpen, D. R., & Stegemeier, G. L. (1984). Cosurfactant-enhanced alkaline flooding. In SPE Enhanced Oil Recovery Symposium. Society of Petroleum Engineers.

Nguyen, Q. P., Alexandrov, A. V., Zitha, P. L., & Currie, P. K. (2000, January). Experimental and modeling studies on foam in porous media: a review. In *SPE International Symposium on Formation Damage Control*. Society of Petroleum Engineers.

Nguyen, T. Q., & Kausch, H. H. (1988). Chain scission in transient extensional flow kinetics and molecular weight dependence. Journal of non-newtonian fluid mechanics, 30(2-3), 125-140.

Sheng, J. (2010). Modern chemical enhanced oil recovery: theory and practice. Gulf Professional Publishing.

Nikolov, A. D., Wasan, D. T., Huang, D. W., & Edwards, D. A. (1986, January). The effect of oil on foam stability: mechanisms and implications for oil displacement by foam in porous media. In *SPE annual technical conference and exhibition*. Society of Petroleum Engineers.

Noik, C. H., Delaplace, P. H., & Muller, G. (1995, January). Physico-chemical characteristics of polyacrylamide solutions after mechanical degradation through a porous medium. In *SPE International Symposium on Oilfield Chemistry*. Society of Petroleum Engineers.

Olajire, A. A. (2014). Review of ASP EOR (alkaline surfactant polymer enhanced oil recovery) technology in the petroleum industry: Prospects and challenges. Energy, 77, 963-982.

Orr, F. M., Heller, J. P., & Taber, J. J. (1982). Carbon dioxide flooding for enhanced oil recovery: Promise and problems. *Journal of the American Oil Chemists Society*, *59*(10), 810A-817A.

Ostwald, W. (1925). About the rate function of the viscosity of dispersed systems. *Kolloid Z*, *36*, 99-117.

Pandey, A., Suresh Kumar, M., Jha, M. K., Tandon, R., Punnapully, B., Kalugin, M. A., & Beliveau, D. (2012, January). Chemical EOR pilot in mangala field: results of initial polymer flood phase. In SPE Improved Oil Recovery Symposium. Society of Petroleum Engineers.

Panthi, K., Sharma, H., & Mohanty, K. K. (2016). ASP flood of a viscous oil in a carbonate rock. Fuel, 164, 18-27.

Panthi, K., Clemens, T., & Mohanty, K. K. (2016). Development of an ASP formulation for a sandstone reservoir with divalent cations. Journal of Petroleum Science and Engineering, 145, 382-391.

Patzek, T. W. (1996). Field applications of steam foam for mobility improvement and profile control. *SPE Reservoir Engineering*, *11*(02), 79-86.

Parkhurst, D. L., & Appelo, C. A. J. (2013). Description of input and examples for PHREEQC version 3--A computer program for speciation, batch-reaction, one-dimensional transport, and inverse geochemical calculations.

Parlar, M., Parris, M. D., Jasinski, R. J., & Robert, J. A. (1995, January). An experimental study of foam flow through Berea sandstone with applications to foam diversion in matrix acidizing. In SPE Western Regional Meeting. Society of Petroleum Engineers, SPE 29678-MS.

Prieditis, J., & Paulett, G. S. (1992, January). CO2-Foam Mobility Tests at Reservoir Conditions in San Andres Cores. In SPE/DOE Enhanced Oil Recovery Symposium. Society of Petroleum Engineers, SPE 24178-MS.

Pye, D. J. (1964). Improved secondary recovery by control of water mobility. *Journal of Petroleum technology*, *16*(08), 911-916.

Qi, P. (2018). The effect of polymer viscoelasticity on residual oil saturation (Doctoral dissertation), UT Austin

Ransohoff, T. C., & Radke, C. J. (1988). Mechanisms of foam generation in glass-bead packs. SPE reservoir engineering, 3(02), 573-585, SPE 15441-PA.

Raza, S. H., & Marsden, S. S. (1965, January). The flow of foam: I. Rheology and streaming potential. In *Fall Meeting of the Society of Petroleum Engineers of AIME*. Society of Petroleum Engineers.

Raza, S. H. (1970). Foam in porous media: characteristics and potential applications. Soc. Pet. Eng. J, 10, 328-336, SPE 2421-PA.

Reichenbach-Klinke, R., Stavland, A., Strand, D., Langlotz, B., & Brodt, G. (2016, March). Can associative polymers reduce the residual oil saturation? In SPE EOR Conference at Oil and Gas West Asia. Society of Petroleum Engineers.

Reichenbach-Klinke, R., Stavland, A., Langlotz, B., Wenzke, B., & Brodt, G. (2013, July). New insights into the mechanism of mobility reduction by associative type copolymers. In SPE Enhanced Oil Recovery Conference. Society of Petroleum Engineers.

Reichenbach-Klinke, R., Stavland, A., Zimmermann, T., Bittner, C., & Brodt, G. (2015, April). Associative Copolymers for Polymer Flooding-Structure-Performance Relationships in Porous Media. In IOR 2015-18th European Symposium on Improved Oil Recovery.

Reichenbach-Klinke, R., Zimmermann, T., Stavland, A., & Strand, D. (2018, April). Temperature-Switchable Polymers for Improved Oil Recovery. In SPE Norway One Day Seminar. Society of Petroleum Engineers.

Reichenbach-Klinke, R., Langlotz, B., Wenzke, B., Spindler, C., & Brodt, G. (2011, January). Associative copolymer with favorable properties for the application in polymer flooding. In SPE International Symposium on Oilfield Chemistry. Society of Petroleum Engineers.

Roehl, P. O., & Choquette, P. W. (Eds.). (1985). *Carbonate petroleum reservoirs*. Springer Science & Business Media.

Roof, J. G. (1970). Snap-off of oil droplets in water-wet pores. *Society of Petroleum Engineers Journal*, *10*(01), 85-90.

Rossen, W. R., Van Duijn, C. J., Nguyen, Q. P., Shen, C., & Vikingstad, A. K. (2010). Injection strategies to overcome gravity segregation in simultaneous gas and water injection into homogeneous reservoirs. *SPE Journal*, *15*(01), 76-90.

Rossen, W. R. (2000). Snap-off in constricted tubes and porous media. *Colloids and Surfaces A: Physicochemical and Engineering Aspects*, *166*(1-3), 101-107.

Rossen, W. R. (1996). Foams in enhanced oil recovery. *Foams: Theory, Measurements and Applications*, *57*, 413-464.

Rossen, W. R., & Gauglitz, P. A. (1990). Percolation theory of creation and mobilization of foams in porous media. AIChE Journal, 36(8), 1176-1188.

Rosen, M. J., & Dahanayake, M. (2000). Industrial utilization of surfactants: principles and practice. American Oil Chemists' Society.

Rossen, W. R. (1990). Minimum pressure gradient for foam flow in porous media: effect of interactions with stationary lamellae. *Journal of colloid and interface science*, *139*(2), 457-468.

Rossen, W. R., & Gauglitz, P. A. (1990). Percolation theory of creation and mobilization of foams in porous media. *AIChE Journal*, *36*(8), 1176-1188.

Sahni, V., Dean, R. M., Britton, C., Kim, D. H., Weerasooriya, U., & Pope, G. A. (2010, January). The role of co-solvents and co-surfactants in making chemical floods robust. In *SPE Improved Oil Recovery Symposium*. Society of Petroleum Engineers.

Sanchez, J. M., & Hazlett, R. D. (1992). Foam flow through an oil-wet porous medium: a laboratory study. SPE reservoir engineering, 7(01), 91-97, SPE 19687-PA.

Sandiford, B. B. (1964). Laboratory and field studies of water floods using polymer solutions to increase oil recoveries. *Journal of Petroleum Technology*, *16*(08), 917-922.

Sarsenbekuly, B., Kang, W., Fan, H., Yang, H., Dai, C., Zhao, B., & Aidarova, S. B. (2017). Study of salt tolerance and temperature resistance of a hydrophobically modified polyacrylamide based novel functional polymer for EOR. *Colloids and Surfaces A: Physicochemical and Engineering Aspects*, *514*, 91-97.

Satter, A., Iqbal, G. M., & Buchwalter, J. L. (2008). *Practical enhanced reservoir engineering: assisted with simulation software*. Pennwell Books.

Schramm, L. L. (1994). Foam sensitivity to crude oil in porous media. *ACS Advances in Chemistry Series*, *242*, 165-200.

Schramm, L. L., & Novosad, J. J. (1992). The destabilization of foams for improved oil recovery by crude oils: effect of the nature of the oil. Journal of Petroleum Science and Engineering, 7(1-2), 77-90.

Schramm, L. L., & Mannhardt, K. (1996). The effect of wettability on foam sensitivity to crude oil in porous media. *Journal of Petroleum Science and Engineering*, *15*(1), 101-113.

Schramm, L. L., & Wassmuth, F. (1994). Foams: basic principles. *Advances in chemistry series*, *242*, 3-3.

Seethepalli, A., Adibhatla, B., & Mohanty, K. K. (2004). Physicochemical interactions during surfactant flooding of fractured carbonate reservoirs. *SPE journal*, *9*(04), 411-418.

Seright, R. S., Fan, T., Wavrik, K. E., Wan, H., Gaillard, N., & Favéro, C. (2011, January). Rheology of a new sulfonic associative polymer in porous media. In *SPE International Symposium on Oilfield Chemistry*. Society of Petroleum Engineers.

Seright, R. S. (1983). The effects of mechanical degradation and viscoelastic behavior on injectivity of polyacrylamide solutions. Society of Petroleum Engineers Journal, 23(03), 475-485.

Shamsijazeyi, H., Hirasaki, G., & Verduzco, R. (2013). Sacrificial agent for reducing adsorption of anionic surfactants. In SPE International Symposium on Oilfield Chemistry. Society of Petroleum Engineers.

Shan, D., & Rossen, W. R. (2004). *Optimal Injection Strategies for Foam IOR. SPEJ 9 (2): 132–150*. SPE-75180-PA. DOI: 10.2118/75180-PA.

Sharma, H., Weerasooriya, U., Pope, G. A., & Mohanty, K. K. (2016). Ammonia-based ASP floods in carbonate cores containing gypsum. Fuel, 184, 362-370.

Sharma, H., Dufour, S., Arachchilage, G. W. P., Weerasooriya, U., Pope, G. A., & Mohanty, K. (2015). Alternative alkalis for ASP flooding in anhydrite containing oil reservoirs. Fuel, 140, 407-420.

Sharma, H. 2016. Study of Geochemical Interactions During Chemical EOR Processes. PhD Thesis, The University of Texas at Austin

Sharma, G., & Mohanty, K. (2013, April). Wettability Alteration in High-Temperature and High-Salinity Carbonate Reservoirs. Society of Petroleum Engineers. doi:10.2118/147306-PA

Sharma, H., Weerasooriya, U., Pope, G. A., Mohanty, K.K. (2016). Ammonia based ASP floods in carbonate rocks containing gypsum. Fuel (184): 362-370

Sharma, G., & Mohanty, K. (2013). Wettability alteration in high-temperature and high-salinity carbonate reservoirs. *SPE Journal*, *18*(04), 646-655.

Sharma, M. K., & Shah, D. O. (1985). Introduction to macro-and microemulsions.

Sharma, M. K., & Shah, D. O. (1989). Use of surfactants in oil recovery. In *Developments in Petroleum Science* (Vol. 17, pp. 255-315). Elsevier.

Sheng, J. J., Leonhardt, B., & Azri, N. (2015). Status of polymer-flooding technology. *Journal of Canadian Petroleum Technology*, *54*(02), 116-126.

Shi, J. X., & Rossen, W. R. (1998, January). Improved surfactant-alternating-gas foam process to control gravity override. In *SPE/DOE improved oil recovery symposium*. Society of Petroleum Engineers.

Shoaib, M., & Quadri, S. R. (2016, October). Evaluation of Scleroglucan for Polymer Flooding in High-Temperature, High-Salinity Carbonate Reservoir Conditions. In *EAGE Workshop on Petroleum Geochemistry in Operations and Production*.

Shutang, G., & Qiang, G. (2010). Recent progress and evaluation of ASP flooding for EOR in Daqing oil field. In SPE EOR Conference at Oil & Gas West Asia. Society of Petroleum Engineers.

Siddiqui, S., Talabani, S., Saleh, S. T., & Islam, M. R. (1997, January). A Laboratory Investigation of Foam Flow in Low-Permeability Berea Sandstone Cores. In SPE Production Operations Symposium. Society of Petroleum Engineers, SPE 37416-MS.

Singh, R., & Mohanty, K. K. (2014, April). Synergistic stabilization of foams by a mixture of nanoparticles and surfactants. In *SPE improved oil recovery symposium*. Society of Petroleum Engineers.

Singh, R., & Mohanty, K. K. (2015a). Foams Stabilized by In-Situ Surface-Activated Nanoparticles in Bulk and Porous Media. *SPE Journal*. http://dx.doi.org/10.2118/170942-PA

Singh, R., & Mohanty, K. K. (2015b). Synergy between Nanoparticles and Surfactants in Stabilizing Foams for Oil Recovery. *Energy & Fuels*, *29*(2), 467-479.

Singh, R. & Mohanty, K.K. (2016) Foams with Wettability-Altering Capabilities for Oil-Wet Carbonates: A Synergistic Approach, SPE 175027-PA, SPE Journal. DOI: 10.2118/175027-PA.

Sorbie, K. S. (2013). Polymer-improved oil recovery. Springer Science & Business Media.

Skauge, A., Aarra, M. G., Surguchev, L., Martinsen, H. A., & Rasmussen, L. (2002, January). Foam-assisted WAG: experience from the Snorre field. In *SPE/DOE Improved Oil Recovery Symposium*. Society of Petroleum Engineers.

Smith, C. L., Anderson, J. L., & Roberts, P. G. (1969, January). New diverting techniques for acidizing and fracturing. In *SPE California Regional Meeting*. Society of Petroleum Engineers.

Sorbie, K. S. (2013). *Polymer-improved oil recovery*. Springer Science & Business Media.

Sorbie, K. S., & Roberts, L. J. (1984, January). A model for calculating polymer injectivity including the effects of shear degradation. In SPE Enhanced Oil Recovery Symposium. Society of Petroleum Engineers.

Southwick, J. G., van den Pol, E., van Rijn, C. H., van Batenburg, D. W., Boersma, D., Svec, Y., & Raney, K. (2016). Ammonia as alkali for alkaline/surfactant/polymer floods. *SPE Journal*, *21*(01), 10-21.

Spirov, P., Rudyk, S., & Khan, A. (2012, January). Foam assisted WAG, snorre revisit with new foam screening model. In *North Africa Technical Conference and Exhibition*. Society of Petroleum Engineers.

Srivastava, M., & Nguyen, Q. P. (2010, January). Application of gas for mobility control in chemical EOR in problematic carbonate reservoirs. In *SPE Improved Oil Recovery Symposium*. Society of Petroleum Engineers.

Srivastava, M., Zhang, J., Nguyen, Q. P., & Pope, G. A. (2009, January). A Systematic Study of Alkali Surfactant Gas Injection as an Enhanced Oil Recovery Technique. In SPE Annual Technical Conference and Exhibition. Society of Petroleum Engineers, SPE 124752-MS.

Stalkup Jr, F. I. (1984). SPE Monograph Series (Second Printing), Henry L. *Doherty Memorial Fund of AIME, Society of Petroleum Engineers of AIME, New York–Dallas*.

Stalkup, F. I. (1983). Miscible Displacement, Monograph Volume 8, Henry L. *Doherty Series, SPE, Richardson, Texas*.

Stegemeier, G. L. (1997). Mechanisms of entrapment and mobilization of oil in porous media. *Improved oil recovery by surfactant and polymer flooding*, 55-91.

Strand, S., Standnes, D. C., & Austad, T. (2003). Spontaneous imbibition of aqueous surfactant solutions into neutral to oil-wet carbonate cores: Effects of brine salinity and composition. *Energy & fuels*, *17*(5), 1133-1144.

Strand, S., Høgnesen, E. J., & Austad, T. (2006). Wettability alteration of carbonates—Effects of potential determining ions (Ca^{2+} and SO_4^{2-}) and temperature. Colloids and Surfaces A: Physicochemical and Engineering Aspects, 275(1), 1-10.

Surguchev, L. M., & Hanssen, J. E. (1996, January). Foam application in North-sea reservoirs, I: design and technical support of field trials. In *SPE/DOE Improved Oil Recovery Symposium*. Society of Petroleum Engineers.

Szabo, M. T. (1975). Some aspects of polymer retention in porous media using a C14-tagged hydrolyzed polyacrylamide. Society of Petroleum Engineers Journal, 15(04), 323-337.

Taber, J. J., Martin, F. D., & Seright, R. S. (1997). EOR screening criteria revisited-Part 1: Introduction to screening criteria and enhanced recovery field projects. *SPE Reservoir Engineering*, *12*(03), 189-198.

Tagavifar, M., Herath, S., Weerasooriya, U. P., Sepehrnoori, K., & Pope, G. (2016, April). Measurement of microemulsion viscosity and its implications for chemical EOR. In *SPE Improved Oil Recovery Conference*. Society of Petroleum Engineers.

Talley, L. D. (1988). Hydrolytic stability of alkylethoxy sulfates. *SPE Reservoir Engineering*, *3*(01), 235-242.

Tang, G. Q., & Morrow, N. R. (1997). Salinity, temperature, oil composition, and oil recovery by waterflooding. *SPE Reservoir Engineering*, *12*(04), 269-276.

Tcholakova, S., Mitrinova, Z., Golemanov, K., Denkov, N. D., Vethamuthu, M., & Ananthapadmanabhan, K. P. (2011). Control of Ostwald ripening by using surfactants with high surface modulus. *Langmuir*, *27*(24), 14807-14819.

Teklu, T. W.; Alharthy, N.; Kazemi, H.; Yin, X.; Graves, R. M.; & AlSumaiti, A. M. (2014). Phase behavior and minimum miscibility pressure in nanopores. SPE Reservoir Evaluation & Engineering, 17(03), 396-403, SPE 168865-PA.

Teklu, T. W., Alameri, W., Graves, R. M., Kazemi, H., & AlSumaiti, A. M. (2016). Low-salinity water-alternating-CO2 EOR. Journal of Petroleum Science and Engineering, 142, 101-118.

Thielking, H., & Kulicke, W. M. (1996). On-line coupling of flow field-flow fractionation and multiangle laser light scattering for the characterization of macromolecules in aqueous solution as illustrated by sulfonated polystyrene samples. Analytical chemistry, 68(7), 1169-1173.

A Nadeeka Upamali, K., Liyanage, P. J., Cai, J., Lu, J., Jang, S. H., Weerasooriya, U. P., & Pope, G. A. (2016, April). New Surfactants and Co-Solvents Increase Oil Recovery and Reduce Cost. In *SPE Improved Oil Recovery Conference*. Society of Petroleum Engineers.

Vermolen, E., Van Haasterecht, M. J., Masalmeh, S. K., Faber, M. J., Boersma, D. M., & Gruenenfelder, M. A. (2011, January). Pushing the envelope for polymer flooding towards high-temperature and high-salinity reservoirs with polyacrylamide based ter-polymers. In *SPE middle east oil and gas show and conference*. Society of Petroleum Engineers.

Viken, A. L., Spildo, K., Reichenbach-Klinke, R., Djurhuus, K., & Skauge, T. (2017). Influence of Weak Hydrophobic Interactions on in Situ Viscosity of a Hydrophobically Modified Water-Soluble Polymer. Energy & Fuels, 32(1), 89-98.

Vikingstad, A. K., Skauge, A., Høiland, H., & Aarra, M. (2005). Foam–oil interactions analyzed by static foam tests. Colloids and Surfaces A: Physicochemical and Engineering Aspects, 260(1), 189-198.

Wang, L., & Mohanty, K. (2014). Enhanced oil recovery in gasflooded carbonate reservoirs by wettability-altering surfactants. *SPE Journal*, *20*(01), 60-69.

Wang, M., Ma, J., Chen, C., Lu, F., Du, Z., Cai, J., & Xu, J. (2012). Gold nanoparticles confined in the interconnected carbon foams with high temperature stability. *Chemical Communications*, *48*(84), 10404-10406.

Wang, D., Liu, C., Wu, W., & Wang, G. (2008, January). Development of an ultralow interfacial tension surfactant in systems with no-Alkali for chemical flooding. In SPE Symposium on Improved Oil Recovery. Society of Petroleum Engineers, SPE 109017-MS.

Wang, J., Zheng, Y., FENG, Y. J., & LUO, P. Y. (1999). A Novel Associative Polymer for EOR: Performance Properties. *Oilfield Chemistry*, *2*, 015.

Wang, J., Ayirala, S. C., AlSofi, A. M., Al-Yousef, A. A., & Aramco, S. (2018, March). SmartWater Synergy with Surfactant Polymer Flooding for Efficient Oil Mobilization in Carbonates. In SPE EOR Conference at Oil and Gas West Asia. Society of Petroleum Engineers, SPE 190334-MS.

Wang, D., Cheng, J., Yang, Z., Qun, L., Wu, W., & Yu, H. (2001, January). Successful field test of the first ultra-low interfacial tension foam flood. In SPE Asia Pacific Improved Oil Recovery Conference. Society of Petroleum Engineers, SPE 72147-MS.

Wang, L. K., & Langley, D. F. (1977). Identification and determination of ionic surface-active agents. Archives of environmental contamination and toxicology, 5(1), 447-456.

Wassmuth, F. R., Green, K., & Hodgins, L. (2005, January). Conformance control for miscible CO floods in fractured carbonates. In *Canadian international petroleum conference*. Petroleum Society of Canada.

Willhite, G. P. (1986). Waterflooding. SPE/Shell Textbook, Richardson, TX, p 1.
Olatunji, O. S. (2009). Effect of Reservoir Heterogeneity on Immiscible Foam Enhanced Oil Recovery. Delft University of Technology, p 55.

Winkel, E. S., Oweis, G. F., Vanapalli, S. A., Dowling, D. R., Perlin, M., Solomon, M. J., & Ceccio, S. L. (2009). High-Reynolds-number turbulent boundary layer friction drag reduction from wall-injected polymer solutions. Journal of Fluid Mechanics, 621, 259-288.

Witthayapanyanon, A., Phan, T. T., Heitmann, T. C., Harwell, J. H., & Sabatini, D. A. (2010). Interfacial properties of extended-surfactant-based microemulsions and related macroemulsions. Journal of surfactants and detergents, 13(2), 127-134.

Wreath, D. G. (1989). *A study of polymerflooding and residual oil saturation* (MS Thesis), UT Austin

Wu, Y., Mahmoudkhani, A., Watson, P., Fenderson, T. R., & Nair, M. (2012, January). Development of new polymers with better performance under conditions of high temperature and high salinity. In *SPE EOR conference at oil and gas West Asia*. Society of Petroleum Engineers.

Wu, Z., Cheng, T., Yu, J., & Yang, H. (2014). Effect of viscosity and interfacial tension of surfactant–polymer flooding on oil recovery in high-temperature and high-salinity reservoirs. Journal of Petroleum Exploration and Production Technology, 4(1), 9-16.

Wu, W. X., YAN, W., & LIU, C. D. (2007). Interfacial Activity of Sulfobetaine BS11 as Surfactant for EOR [J]. Oilfield Chemistry, 1, 013.

Xu, Q., & Rossen, W. R. (2004). Experimental Study of Gas Injection in Surfactant-Alternating-Gas Foam Process. *SPEREE 7 (6): 438–448*. SPE-84183-PA. DOI: 10.2118/84183-PA.

Yekeen, N., Manan, M. A., Idris, A. K., & Samin, A. M. (2017). Influence of surfactant and electrolyte concentrations on surfactant Adsorption and foaming characteristics. *Journal of Petroleum Science and Engineering*, *149*, 612-622.

Yousef, A. A., Al-Saleh, S. H., Al-Kaabi, A., & Al-Jawfi, M. S. (2011). Laboratory investigation of the impact of injection-water salinity and ionic content on oil recovery from carbonate reservoirs. SPE Reservoir Evaluation & Engineering, 14(05), 578-593.

Youyi, Z., Qingfeng, H., Guoqing, J., Desheng, M. A., & Zhe, W. A. N. G. (2013). Current development and application of chemical combination flooding technique. Petroleum Exploration and Development, 40(1), 96-103.

Yousef, A. A., Al-Saleh, S. H., Al-Kaabi, A., & Al-Jawfi, M. S. (2011). Laboratory investigation of the impact of injection-water salinity and ionic content on oil recovery from carbonate reservoirs. SPE Reservoir Evaluation & Engineering, 14(05), 578-593, SPE 137634-PA.

Youyi, Z., Zhang, Y., Jialing, N., Weidong, L. I. U., & Qingfeng, H. O. U. (2012). The research progress in the alkali-free surfactant-polymer combination flooding technique. Petroleum exploration and development, 39(3), 371-376.

Yousef, A.A., Al-Saleh, S., & Al-Jawfi, M.S. (2011). Smart waterflooding for carbonate reservoirs: Salinity and role of ions, SPE 141082-MS, SPE Middle East Oil & Gas Show and Conference, Bahrain, 25-28 September.

Yu, L., & Wardlaw, N. C. (1986). The influence of wettability and pore-throat size ratio on snap—off. *Journal of Colloid and Interface Science*, *109*(2), 461-472.

Yousef, A. A., Al-Saleh, S. H., Al-Kaabi, A., & Al-Jawfi, M. S. (2011). Laboratory investigation of the impact of injection-water salinity and ionic content on oil recovery from carbonate reservoirs. SPE Reservoir Evaluation & Engineering, 14(05), 578-593.

Zaitoun, A., Makakou, P., Blin, N., Al-Maamari, R. S., Al-Hashmi, A. A. R., & Abdel-Goad, M. (2012). Shear stability of EOR polymers. *Spe Journal*, *17*(02), 335-339.

Zaitoun, A., & Potie, B. (1983, January). Limiting conditions for the use of hydrolyzed polyacrylamides in brines containing divalent ions. In *SPE Oilfield and Geothermal Chemistry Symposium*. Society of Petroleum Engineers.

Zhang, G., & Seright, R. (2014). Effect of concentration on HPAM retention in porous media. *SPE Journal*, *19*(03), 373-380.

Zhang, T., Espinosa, D., Yoon, K. Y., Rahmani, A. R., Yu, H., Caldelas, F. M., & Milner, T. E. (2011, January). Engineered nanoparticles as harsh-condition emulsion and foam stabilizers and as novel sensors. In *Offshore Technology Conference*. Offshore Technology Conference.

Zhang, F. Y., Yang, G., Liu, Y. B., & Li, J. (2005). Development of chemical oil displacement agent for high temperature and high salinity reservoir. Advances in fine petrochemicals, 6(5), 8-11.

Zhang, Y., Yue, X., Dong, J., & Yu, L. (2000, January). New and effective foam flooding to recover oil in heterogeneous reservoir. In SPE/DOE Improved Oil Recovery Symposium. Society of Petroleum Engineers, SPE 59367-MS.

Zhang, D. L., Liu, S., Puerto, M., Miller, C. A., & Hirasaki, G. J. (2006). Wettability alteration and spontaneous imbibition in oil-wet carbonate formations. *Journal of Petroleum Science and Engineering*, *52*(1), 213-226.

Zhou, W., Zhang, J., Feng, G., Jiang, W., Sun, F., Zhou, S., & Liu, Y. (2008, January). Key technologies of polymer flooding in offshore oilfield of Bohai Bay. In SPE Asia Pacific Oil and Gas Conference and Exhibition. Society of Petroleum Engineers.

Zhu, Y., Hou, Q., Liu, W., Ma, D., & Liao, G. Z. (2012, January). Recent progress and effects analysis of ASP flooding field tests. In SPE Improved Oil Recovery Symposium. Society of Petroleum Engineers, SPE 151285-MS.